REPORT No. 244
GEOLOGICAL SURVEY OF JAPAN

MECHANICAL PROPERTIES OF JAPANESE TERTIARY SEDIMENTARY ROCKS UNDER HIGH CONFINING PRESSURES

By
Kazuo HOSHINO, Hitoshi KOIDE, Kazuo INAMI,
Shigeo IWAMURA & Shinobu MITSUI

GEOLOGICAL SURVEY OF JAPAN
Hisamoto, Kawasaki-shi, Japan
1972

552.5 : 551.78 : 53(52)

REPORT No. 244

GEOLOGICAL SURVEY OF JAPAN

Isamu KOBAYASHI, Director

Mechanical Properties of Japanese Tertiary Sedimentary Rocks under High Confining Pressures

By

Kazuo HOSHINO, Hitoshi KOIDE, Kazuo INAMI,
Shigeo IWAMURA & Shinobu MITSUI

CONTENTS

Mechanical Properties of Japanese Tertiary Sedimentary Rocks under High Confining Pressures

By

Kazuo HOSHINO*, Hitoshi KOIDE*, Kazuo INAMI*,
Shigeo IWAMURA** & Shinobu MITSUI***

Abstract

One hundred rocks from representative Tertiary sedimentary basins in Japan, most of which are fine- and medium-grained clastic rocks, ranging Pliocene to Oligocene in age, were deformed at confining pressures up to 2,500 kg/cm^2 at room temperature, in a strain rate of 10^{-4} to 10^{-6}/sec. All were tested under compression on dry cylindrical samples of 39.0 mm in length and 19.5 mm in diameter.

The results of experiments were tabulated in Table 4. The mechanical properties of sedimentary rocks have a wide range of value and are much influenced by lithological and geological factors. We tried to find relations among strength, confining pressure, deformational behavior, angle of fracture, strain at fracturing, failure type, porosity, grain size, axial shortening, sampled depth, elastic wave velocity, geologic age, stratigraphic level and tectonic environment.

The mode of deformation, angle of fracture, and strain at fracturing are related to the ratio of shearing stress to normal stress on the plane of fracture or to the ratio of the maximum strength to the confining pressure. The failure type corresponds almost to the deformational behavior, and the change among failure types seems to be continuous. The "visco-ductile" flow is observed in extreme porous rocks, possibly because the framework is crushed by higher pressure than formerly applied.

The strength of sedimentary rocks increases with diminution of porosity. Because of compaction, the rocks become, generally, stronger and less ductile with the sampled depth and with geologic age. The degree and effect of compaction, however, are much influenced by the lithofacies and tectonic history. The degree of strengthening with geologic age is the greatest in argillaceous rocks, greater in arenaceous rocks and less in pyroclastic rocks.

Among six areas studied, there exists an interesting contrast in deformational behavior and strength. The rocks in Joban and Miura are much more ductile and weaker than rocks in the other areas. The confining pressure of ductile–visco-ductile transition and degree of strengthening with geologic age, too, suggest that very lower compressive stress has been applied on the rocks in Joban and Miura than in the other areas.

* Geological Survey of Japan
** Tokyo Educational University
*** Kochi University

I. Introduction

This is a report on the mechanical properties of rocks which were deformed experimentally under various confining pressures in Geological Survey of Japan. The present report contains data on one hundred argillaceous, arenaceous, pyroclastic and volcanic rocks, which were systematically sampled from horizons ranging from Pliocene to Oligocene in representative Tertiary sedimentary basins in Japan.

The large variety of mechanical properties of sedimentary rocks increases the difficulty in the estimation of stability of rock mass and in the tectonophysical study of geological structure. Large amounts of systematic experiments are required to investigate the mechanical properties of the sedimentary rocks which are influenced by many factors. In 1962, a new research group for rock mechanics was organized in Geological Survey of Japan in view of the increasing importance of rock mechanics in the structural geology, engineering geology, mining engineering and geophysics. In 1965, the group had a high pressure rock deformation laboratory equipped with a set of triaxial testing apparatus. Since then, the authors, besides of their own subjects, have made an effort in order to add the experimental data on the Japanese rocks with the triaxial testing apparatus. Up to the present, the authors have finished experiments on one hundred representative Tertiary sedimentary rocks in Japan.

The first part of this report is a description of rocks studied, geological setting, apparatus and procedure of experiments. In the middle part, the results of experiments are summarized in the Table 4 followed by the figures of stress-strain curves and Mohr's envelops. In the last part, the authors tried to discuss relations among strength, mode of deformation, failure type, porosity, ages, among buried depth, etc.

The experimental study of the mechanical properties of the rocks under the condition deep in the earth crust has been done by a lot of workers.

GRIGGS (1942) summarized the results of experiments on rock deformation under high confining pressure and some other conditions in "Handbook of Physical Constant" of the Geological Society of America, before the last World War. The data and results of this kind of experimental work were re-summarized by HANDIN in 1966, in the revised edition of "Handbook of Physical Constant".

Between both years, a lot of works were made in this field. BRIDGMAN (1952) has made a few tests on rocks under extreme pressures to 30,000 kg/cm^2. E. C. ROBERTSON (1955) has done a triaxial test at pressures up to 4,000 kg/cm^2 on various kinds of rocks including limestone, marble, dolomite, slate, and granite to find a criterion of the strength of the rocks. From the end of 1950, we find, new experimental works on rock deformation from various aspects have been published one after another. HANDIN and his co-workers have made a series of experiments on the sedimentary rocks under high confining pressures; at room temperature (1957), at high temperature (1958), and with pore pressure tests (1963). Their studies cover six kinds of dolomite, five limestones, one marble, one anhydrite, five sandstones, one quartzite, four

shales, one siltstone, and one slate, and they are, it should be noted, the first systematic work on the sedimentary rocks. The scope of this study ranges up to 2,000 kg/cm^2 in confining pressure, 300 degree in temperature and 2,000 kg/cm^2 for pore pressure. HANDIN et al. have provided very interesting information about the state of the sedimentary rocks under different physical conditions in the crust such as strength, ductility, or fracturing. They first made the test up to the large strain; approximately 30%, that would be very important on geological problems of deformation. PATERSON (1958) has done a high pressure test on marble up to the confining pressure of 1,000 kg/cm^2, and provided an interesting result that there is a close relation between the behavior of deformation on the stress-strain curve and failure pattern. The publishment of "Rock Deformation" by the Geological Society of America (1960) was an epoch-making work in the research of experimental rock deformation, which includes very interesting and important 13 articles by 16 authors in various fields of rock mechanics. Among them, those concerning experimental study of rock properties in particular are by GRIGGS, TURNER, and HEARD on the high temperature test up to 800 degree of such rocks and minerals as peridotite, basalt, granite, marble, and quartz; MAXWELL on compaction and cementation of sand; BORG, FRIEDMAN, HANDIN, and HIGGS on nature of deformation of coarse-grained clastic rock- St. Peter sand; HEARD on the transition problem from brittle to ductile deformation using Solenhofen limestone; ROBERTSON on Creep of Solenhofen limestone; HANDIN, HIGGS, and O'BRIEN on torsion test on Yule marble.

We, then, see lots of recent experimental works. BRACE (1964) has made a study of brittle deformation on dolomite, diabase, and quartzite. MATSUSHIMA (1960) studied the deformation of some igneous rocks. MOGI (1964, 1965) has made high pressure tests on 12 kinds of rocks produced in Japan, which contain a diorite, a granite, a trachyte, two andesites, three dacite pumice tuffs, a sandstone, and two marbles. He has provided us some interesting observations concerning the change of deformational pattern as a function of confining pressure and strain hardening. MOGI (1966) and BYERLEE (1968) have given the additional experimental data for presenting discussions concerning the transition from brittle to ductile deformation and strength. HEARD (1963) has conducted high pressure tests at extremely low strain rate up to 10^{-8}/sec on Yule marble and showed an interesting results concerning the effects of strain rate to the ductile deformation of the marble. The DONATH's (1961, 1964) experimental work has provided the data on the effect of pre-existing fractures such as cleavage to the strength of rocks. BORG and HANDIN (1966) have made an experimental work on the deformation of crystalline rocks, 18 kinds of igneous and metamorphic rocks such as amphibolite, diabase, gabbro, pyroxenite, under confining pressure of 5,000 kg/cm^2 at temperature of 500 degree, up to strain of 32.2% at most. They described the change of failure characteristics such as kink bands and gliding in a crystal. PATERSON and WEISS (1968, 1969) have done a series of high pressure experimentation on phyllitic rocks under confining pressure of 5,000 kg/cm^2. They deformed the phyllite up to the strain of 70% at most and saw how kink bands, microfolding or other microstructural features are formed in much deformed rocks.

According to the previous works, we know many things for the scope, up to

5,000 kg/cm^2 of confining pressure, to 800° or more in temperature, up to 2,000 kg/cm^2 of pore pressure, and at strain rate between 10^{-2}/sec and 10^{-8}/sec. The results of different workers are consistent, and all rock specimens can be grouped into few categories as to mechanical properties under the above conditions, (HANDIN, 1966 p. 235).

However, questions still remain among the geologists; how about the effect of geological factors? Is there no variety among mechanical properties of sandstones from different places or in different geologic ages? We know that non-carbonate rocks diverge much in petrological properties. Is there no effect of grain size, grain-minerals, or porosity? HANDIN (1957, 1958) also noted as a result of the study of 23 kinds of sedimentary rocks that the clastic rocks such as sandstone and shale exhibit a considerable variety in mechanical properties under triaxial test, although carbonate rocks such as limestone and dolomite behave almost similarly. One of the authors noticed in a preliminary study (HOSHINO, 1967) that the Pennsylvanian "5,900-foot sand" shale, Eocene Green River shale and Cretaceous Muddy shale in the U. S. are similar in strength to Pliocene Nishiyama shale in Japan, and Cambrian Mettawee slate in the U. S. is about same in strength with Middle Miocene Funakawa shale in Japan.

From geological purpose, it is very important to know the mechanical properties of the rocks in terms of geological factors. Obviously, the previous available data were not sufficient in this point. This study intends to cover this area by making systematic experiments on the sedimentary rocks from several representative Tertiary sedimentary basins in Japan, most of which consist of fine- and medium-grained clastic rocks, ranging a few to nearly 50% in porosity.

Acknowledgements

The experiments are much owing to co-operation of the workers from the University of Tokyo, Tohoku University and Tokyo Educational University. The authors would like to thank Prof. Hideki IMAI of the University of Tokyo, Prof. Nobu KITAMURA of Tohoku University and Prof. Yukinori FUJITA of Tokyo Educational University for their courtesy and encouragement for it.

The authors are indebted to Drs. Shozaburo NAGUMO (now, Prof. at Earthquake Research Institute, University of Tokyo), Kiyoshi SEYA (now, Prof. at Okayama University), Konosuke SATO (now, Dowa Mining Co.), Masami HAYAKAWA (now, Prof. at Tokai University), Shun'ichi SANO, Junsuke CHUJO, Toshihiro KAKIMI, Shingoro IJIMA and Yasubumi ISHIWADA of the Geological Survey of Japan, whose understanding and encouragement for our research, much adventurous at an institution like the Geological Survey have been always behind us.

Discussions with Prof. Toshio KIMURA of Tokyo University, Prof. Shin KITAMURA, Dr. John HANDIN of Center for Tectonophysics, Texas A & M University and Prof. K. J. HSÜ of Swiss Federal Institute of Technology were very valuable.

II. The Rocks Studied

The one hundred rocks studied consist of 51 argillaceous, 31 arenaceous, twelve pyroclastic, and six volcanic rocks, (Table. 3). There are quite few carbonate rocks in Japanese Tertiary System. The seven representative sedimentary basins, where the samples were collected, are shown in Fig. 1. Detailed localities of each

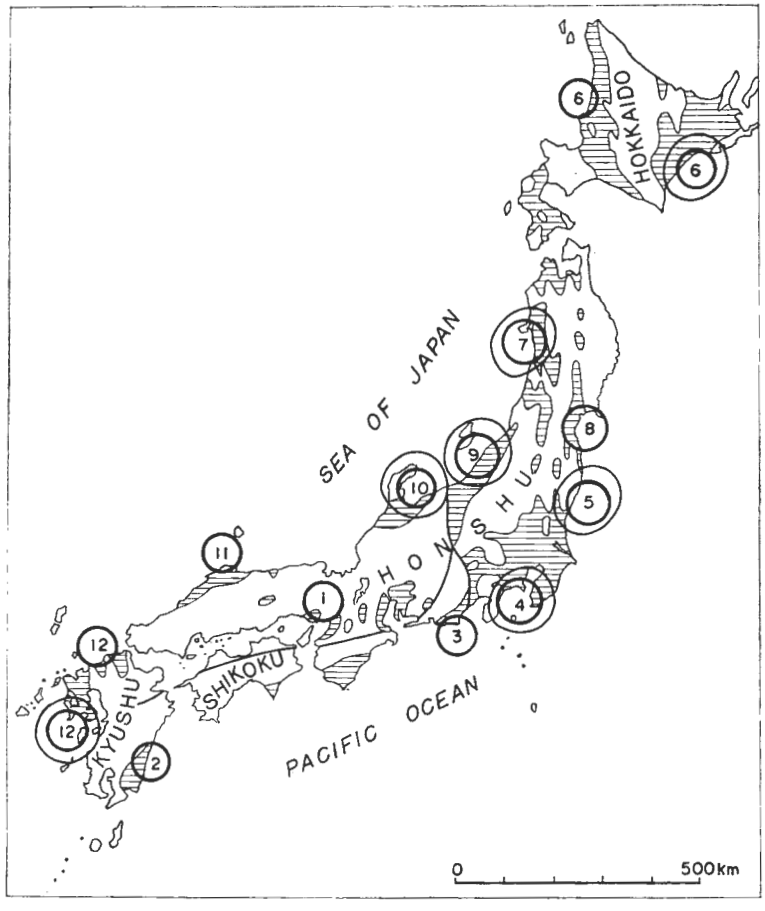

1. Kobe 2. Miyazaki 3. Shizuoka 4. Chiba 5. Joban coal field 6. Hokkaido
7. Akita 8. Sendai 9. Niigata 10. Toyama 11. Matsue 12. Northern Kyushu coal fields

Fig. 1 Cenozoic provinces. (after An outline of the Geology of Japan, Geol. Surv. Japan, 1969)

sample are in locality maps. The stratigraphic relation of the specimens is shown in Table 1. Since these Tertiary basins are without continuation each other, it is difficult to make exact correlation among these areas. There are still disagreements among the paleontologists about the correlation of some stratigraphic units of these basins. However, it is not a direct purpose of this report to discuss the correlation problem, and the problem of correlation may have little substantial meaning for the result of this report. Therefore, we do not intend to discuss the problem of correlation about Table 1, but we only mention this correlation was made mainly on a basis of CHINZEI's table (1967). The one hundred specimens are called with labo names in this report shown in Table 1 for convenience. In Table 2, lithology, geological formation, geological age, sampling locality, porosity, density, elastic wave velocity of each specimen are shown. The classification of the clastic rocks was done primarily upon a basis of average grain size. They were classified in this way; less than 3.9 micron is claystone, between 3.4 and 62.5 micron is siltstone, between 62.5 and 125 micron is very fine sandstone, between 125 and 250 micron is fine sand, between 250 and 500 micron is medium sandstone, and 500 micron to 2 mm is coarse sandstone. Claystone and siltstone were grouped in category of argillaceous rocks, while very fine to coarse sandstones were grouped as arenaceous rocks. Compact and hard claystone is called as shale. Five among 51 argillaceous rocks contain more or less tuffaceous material. Six among 30 arenaceous rocks are tuffaceous more or less. The volcanic rocks here studied are those that are found as sheets or lavas among the above-mentioned clastic rocks. Of six volcanic rocks, one is basalt, three are andesite and the rest two are liparite. Thirty-seven among 51 specimens in Akita and Niigata areas are from the nine exploratory wells for prospecting oil and gas. The depth of these core samples is shown in Table 2. The other 63 samples were collected from the surface exposures.

III. Apparatus and Procedure

The testing apparatus consists of a pressure vessel, loading press, and confining pressure system. A schematic diagram of the apparatus is shown in Fig. 2.

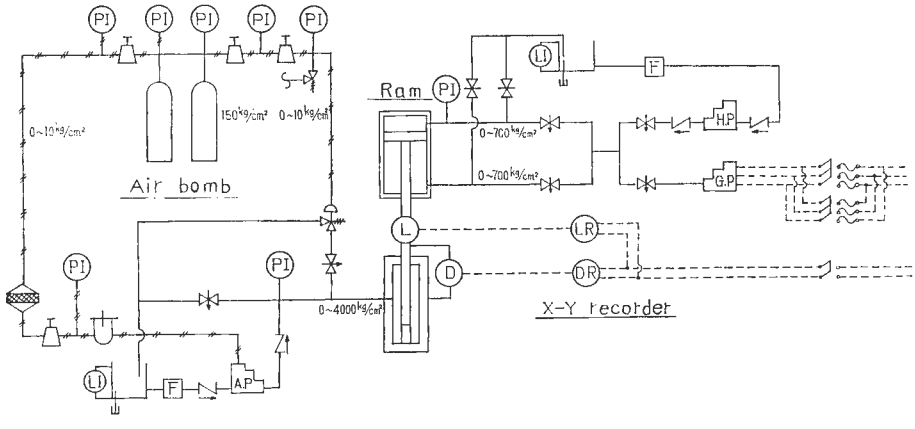

Fig. 2 Schematic diagram of testing apparatus.

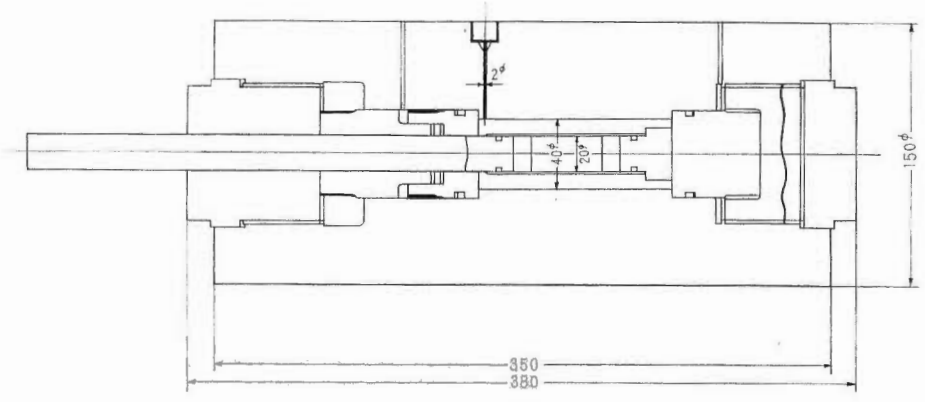

Fig. 3 Pressure vessel. (unit, mm)

The inside structure of the pressure vessel is shown in Fig. 3. The specimens were cored into a cylindrical form (39.0 mm long and 19.5 mm in diameter) and inserted in an annealed thin copper jacket. Because the copper jacket is thin and annealed before the test, its strength is negligible in comparison with that of the rock specimen and no correction is needed for the axial load sustained by the jacket. The specimen is finished within the accuracy of 1/500. This specimen and placers are placed to piston and anvil on each side. The O rings are put between the copper jacket and piston or anvil to prevent the flow of high pressure kerosene into the space between the inside of the copper jacket and the specimen. This piston-specimen assembly is shown in Fig. 4, and inserted in the pressure vessel as shown in Fig. 3. The inside of pressure vessel is filled with kerosene. The kerosene is given pressure by a pneumatic pump, capacity of which is 5,000 kg/cm^2. Confining pressure is applied by the kerosene from the outside of the copper jacket. In order to keep the confining pressure constant during deformation test, the pneumatic pump was equipped with specially designed regulator valves. By this equipment and with help of hand control in case when

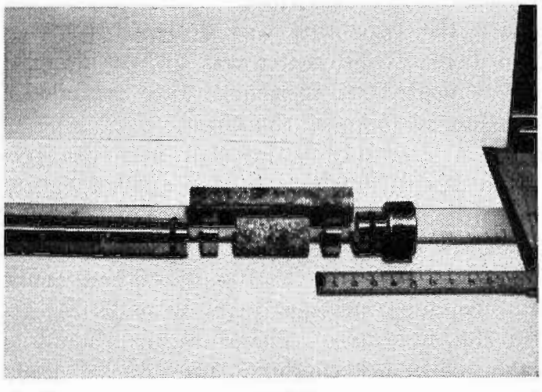

Fig. 4 Photograph of parts used for mounting test specimen.

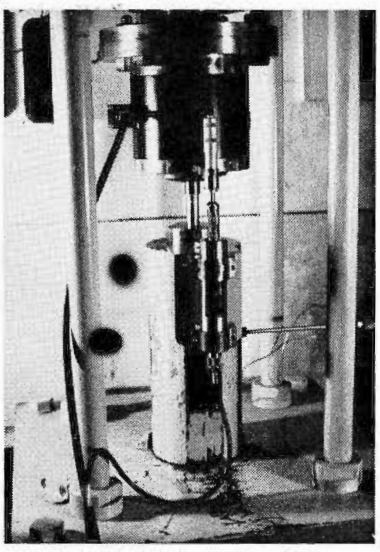

Fig. 5 Photograph of the vessel and frame.

the deformation goes rapidly near the breaking point or yielding point, we could keep the change of confining pressure within 1% of the fixed figure. The confining pressure was measured by Heise pressure gauge.

The loading press was equipped with 50 ton ram. The oil pressure to the ram was generated by 700 kg/cm^2 hand pump and a gear driven pump. The gear driven pump has a gear train of 10 : 1 gear reduction, and allow a variation in oil-flowing rate up to about 10^{-8}cm^3/sec. The screw piston in the gear driven pump is driven by a selector-gear. The gear driven pump permits each of the ten pumping rates and provides a range of loading rates from 10^{-1}/sec to 10^{-8}/sec. Because of the friction along the piston wall and different resistance to deformation of the specimen, the strain rate is different in each specimen and in stages of deformation. We used usually the 2nd, 3rd, and 4th gears. With these gears, we could make strain rate ranging 10^{-2} to 10^{-6}/sec. As shown in a recording chart (Fig. 6), strain rate is kept perfectly constant during the test with this pump. In case of the 3rd gear, strain rate is around 10^{-5}, and 10^{-4}/sec before and after the yielding, respectively. The hand pump was used in the beginning of the test only.

The load was measured with a load cell and the displacement of the specimen was measured with a differential transformer, which was fixed on the pressure vessel. Since the apparatus was designed for the deformation test of very large strain, the displacement meter was set outside of the pressure vessel. The load and displacement thus measured were recorded on a chart of a X–Y recorder. Fig. 6 gives an example of the chart.

The piston-specimen assembly is inserted into the pressure vessel. After the preparation for the test is finished, load is applied lightly by the hand pump. The piston is pushed into the vessel by the ram until the specimen assembly is seated. The curve on the chart then begins to rise, or load begins to be applied on the specimen (the mark "A" in the Fig. 6). Then, confining pressure is built up. The increase of confining pressure tends to make the piston upward because of the elongation of the specimen. Therefore we should apply the axial load corresponding to the increasing confining pressure so that the length of the specimen does not exceed the original length. When confining pressure attains

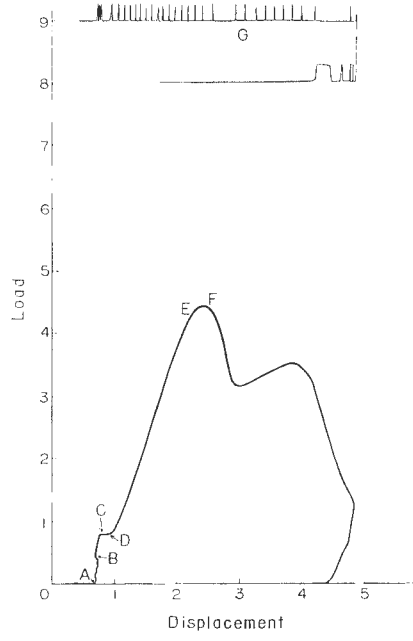

Fig. 6 Recording chart.

up to the value which we plan to make a test, it is stopped to increase. We continue further to press down the piston, but the axial load is kept constant for a while. Under this state, confining pressure and axial stress are equal, in other words, the specimen is under hydrostatic pressure (mark "C"). This state continues until the specimen again seats under the hydrostatic pressure. This point is marked "D" in the Figure. The specimen begins to be subjected to differential stress from this point.

The timer was set on the X-Y recorder. We can set four kinds of time interval; 0.5, 1.0, 5.0, and 10.0 minutes.

The curve recorded on the X-Y recorder thus obtained is load-displacement curve. The true shortening of specimen is obtained from the recorded displacement subtracting distortion of the apparatus. Shortening of specimen under hydrostatic pressure is calculated from displacement to the point "C". The strain under the differential stress is expressed as a percentage of specimen length reduced by the hydrostatic pressure. True stress is obtained from recorded value of load divided by cross-sectional areas of a specimen, under the assumptions that the deformation is homogeneous and that no volume change occurs by the differential stress. Fig. 7 is presented to show an example of corrected true stress-strain curve compared with the apparent stress-strain curve. The difference might be considerably large in case of ductile deformation at large strain. The assumption of no volume change means the rock material perfectly flows, and gives 0.5 as value of Poisson's ratio. We have no definite evidence for this assumption. Poisson's ratio for sandstone and shale is approximately 0.2 or nearly 0.1. Therefore **true** stress-strain curve should be

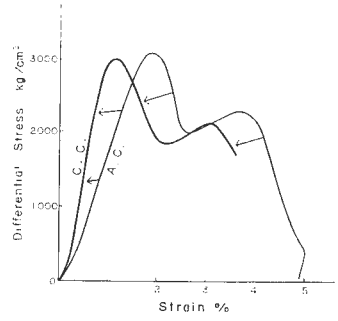

Fig. 7 An example of correction into true stress-strain curve. A. C. is the original curve on recording chart, and C.C. is corrected stress-strain curve.

between the corrected and apparent stress-strain curves.

All specimens tested are dry ones. However, they are exposed in atmosphere to dry naturally, so the pore contains a little water. All specimens of each rock are cored perpendicular to bedding. The specimens from a given rock are taken from the same stratigraphic layer to achieve maximum uniformity among the specimens.

After the experiment finished, some specimens were cut perpendicular to fracture, then thin section was made from the half part for microscopic studies.

IV. Results

IV. 1 Explanation of tables and definition of terms

The results of experiments are summarized in Table 4. The first column of the table gives the number for index and the second column gives the sample-name and sample-number. The samples of the same sample-name are collected from a uniform block. The lithology, geologic formation and localities of the samples can be read from Table 2. The stratigraphic positions are shown in Table 1. The porosity, density and elastic wave velocity are tabulated in Table 2.

The mode of deformation of each sample is summarized in Table 4. The confining pressure and axial shortening by the confining pressure are listed in the third and fourth columns, respectively. Following the form of J. HANDIN's table (1966) of stress-strain relationships of rocks and minerals, values of the differential stress at 1, 2, 5, and 10% longitudinal strain and ultimate strength are picked from the stress-strain curve and listed. Moreover, strain at fracturing, total strain, residual strain, strain rate, type of failure, angle of macrofracture, and mode of deformation are tabulated. In Fig. 10 to Fig. 219, stress-strain curve and Mohr envelope for each rock are illustrated. The Mohr envelopes were drawn as envelopes of Mohr stress circles which connect the confining pressures and ultimate strengths. In case the ultimate strength cannot be measured, they were drawn for 2%, 5%, or 10% strength.

Here brief explanation on each item used in Table 4 and the definition of some technical terms are described.

Axial shortening by confining pressure : This is a ratio of shortening of the specimen to the original length when it is subjected to the hydrostatic pressure equal to confining pressure, that is $\varepsilon_{cp}=\frac{l_0-l_p}{\varepsilon_0}$ where ε_{cp} is axial shortening, l_0 and l_p are lengths at atmospheric and hydrostatic pressures respectively. Volume compressibility β is given as 3 times as large as ε_{cp}, and therefore bulk modulus K is given by the following formula.

$$K=\frac{P}{3\varepsilon_{cp}} \qquad \cdots\cdots\cdots\cdots\cdots\cdots\cdots\cdots\cdots\cdots (4.1)$$

where P is confining pressure. However, it should be noted here that the accuracy of the calculation of the axial shortening is not so good because the determination of l_p includes two steps: one is reading of points A and C on the load-displacement curve (Fig. 6) and the other substracting the displacement by elastic distortion of the apparatus.

Strength : **Ultimate strength** is the maximum differential stress achieved during an experiment. Ultimate strength is read only when the stress-strain curve shows the maximum point. In brittle deformation, the point of maximum differential stress is very clear, and it is a point of fracturing in most cases. In very ductile and visco-ductile deformation, the stress-strain curves do not show the maximum point. In case ultimate strength cannot be determined, **the differential stresses at strain of 1, 2, 5 and 10 %** are taken to express the strength for convenience, and are called 1, 2, 5 and 10 % strength respectively in this report. **Yield strength** is the differential stress at the knee of the stress-strain curve. In this report, yield strength was not used. In many cases, it is usually difficult to decide a definite point as yielding "point", because of very gradual change of stress-strain curves from the linear to the flat part.

Strain at (macro)fracturing : This is a strain per cent at the point of ultimate strength. If the point of ultimate strength is not ascertained, this value is not recorded. The strain per cent thus determined is equal to the **ductility** defined by HANDIN (1957).

Total strain : This means the maximum strain per cent attained during an experiment.

Residual strain : This is a strain per cent when differential stress is reduced to zero under the confining pressure after the deformation test had stopped (point "F" in Fig. 6).

Strain rate : The strain rate were calculated for two parts of the stress-strain curve; one linear part, and the other so-called plastic region. As mentioned in previous pages, the oil for axial load is poured into the ram at a constant flow rate by the agency of the gear driven pump. Therefore, the strain rate of each specimen at different stage of deformation under different confining pressure would provide an information about the resistance of the rock-specimen against loading pressure. We see that the strain rate in the linear part is very constant, and that it is almost constant in the so-called plastic region.

Type of failure : GRIGGS and HANDIN (1960) described macroscopic deformation mechanism with classifying into three phenomena; extension fracture, faulting, and flow. We would like to classify the failure pattern into the next four groups simply upon a basis of macroscopic appearance, (Fig. 8). As con-

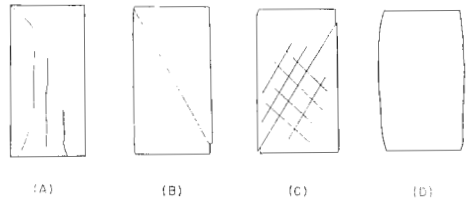

Fig. 8 Schematic diagram showing types of failure.

fining pressure increased up, the failure pattern changes in this succession without any exception.

(A) **Wedge fractures** : This is observed at atmospheric pressure or extremely low confining pressure. Fundamentally, this involves both the extension fractures and the faults defined by HANDIN (1966). At such low pressure, the fractures observed are a combination of extension and shear fractures. It is very rare that we find the specimen, in which extension fractures only are occurred. This might be partly due to the contact condition between the end of the specimen and the steel spacer, as suggested by BRACE (1964). However, this is not all of the cause. In microscopic studies of deformed specimen, some of the authors reported that most microfractures make angles of 0° to 45° with the axis of maximum compressive stress, and, in more detail, there are some preferred orientation; one nearly parallel, and the other ranging between 20° and 40° to the maximum compressive axis, (HOSHINO and KOIDE, 1970a). In the same report, it is shown that the deformation bands, in which lots of microfractures are concentrated, occur near the yield point and the macrofractures are formed along the deformation bands. It is probable that, under low confining pressure, most rocks are very brittle or brittle and the strain at fracturing is still small, which causes insufficient development of deformation bands. Therefore, the fractures might be formed by connection of the microfractures rather than by the connection of deformation bands, which would be resulted in the formation of the fractures ranging in angles of 0° to somewhat 10° or 20°.

(B) **Single shear fracture** : In this type, one or few fractures or deformation bands are observed in the only one direction of shear.

(C) **Network shear fractures** : In this type, shear fractures or deformation bands develop in the conjugate directions as if they exhibit network pattern. Single and network shear fractures are transitional, each other. In some cases, there are two peaks on the stress-strain curve, and two planes of shear are observed in these specimens. This is essentially single shear type, and the further increase of strain might cause to make out the other plane of shear. In most cases of single shear type, we find network pattern of deformation bands, if we examine it in the thin sections with a microscope. Under the microscope, the deformation bands, concentrated zones of microfractures, are observed in conjugate directions at both brittle and ductile cases (KOIDE and HOSHINO, 1967;

HOSHINO and KOIDE, 1970). The interval of deformation bands is wide in brittle case, while narrow in ductile case.

(D) **Flow** : This denotes the failure without any macroscopic fracture. This includes **uniform flow** defined by HANDIN (1966).

Angle of macroscopic fractures : This is the angle between the conjugate fractures and expressed as 2θ. For wedge fractures, the largest angle of fracture is measured as θ, and the value was doubled. In single shear pattern, the value θ was measured and doubled.

Mode of deformation : The mode of deformation was classified as Fig. 9 on a basis of the patterns of stress-strain curve.

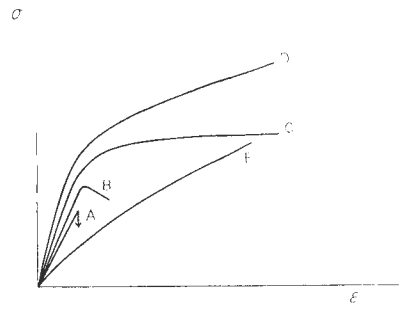

Fig. 9 Schematic diagram showing behavior of deformation.

(A) **Very brittle behavior** : This is characterized by a sudden occurrence of macrofractures with an abrupt drop of stress-strain curve. The stress-strain curve is kept almost linear up to the fracturing point.

(B) **Brittle behavior** : This is characterized by a rather rapid occurrence of macrofractures soon after the yield point and the following moderate drop of stress-strain curve.

(C) **Transitional behavior** : This is characterized by a nearly horizontal stress-strain curve after the yield point.

(D) **Ductile behavior**: This is characterized by a stress-strain curve without any drop after the yield point.

(E) **Visco-ductile behavior** : This is a rather conventional term, and refers to such stress-strain relation that the stress-strain curve goes upward monotonously without any indication of yield point. As far as the record of our experiment is concerned, the strain rate seems nearly constant regardless to increasing differential stress.

In all cases, visco-ductile behavior is observed next to ductile behavior, when confining pressure is increased. In porous rocks, visco-ductile behavior is found even at moderately low confining pressure (Figs. 58, 59, 153 and so on.)

Table 1 Stratigraphic position of the samples.

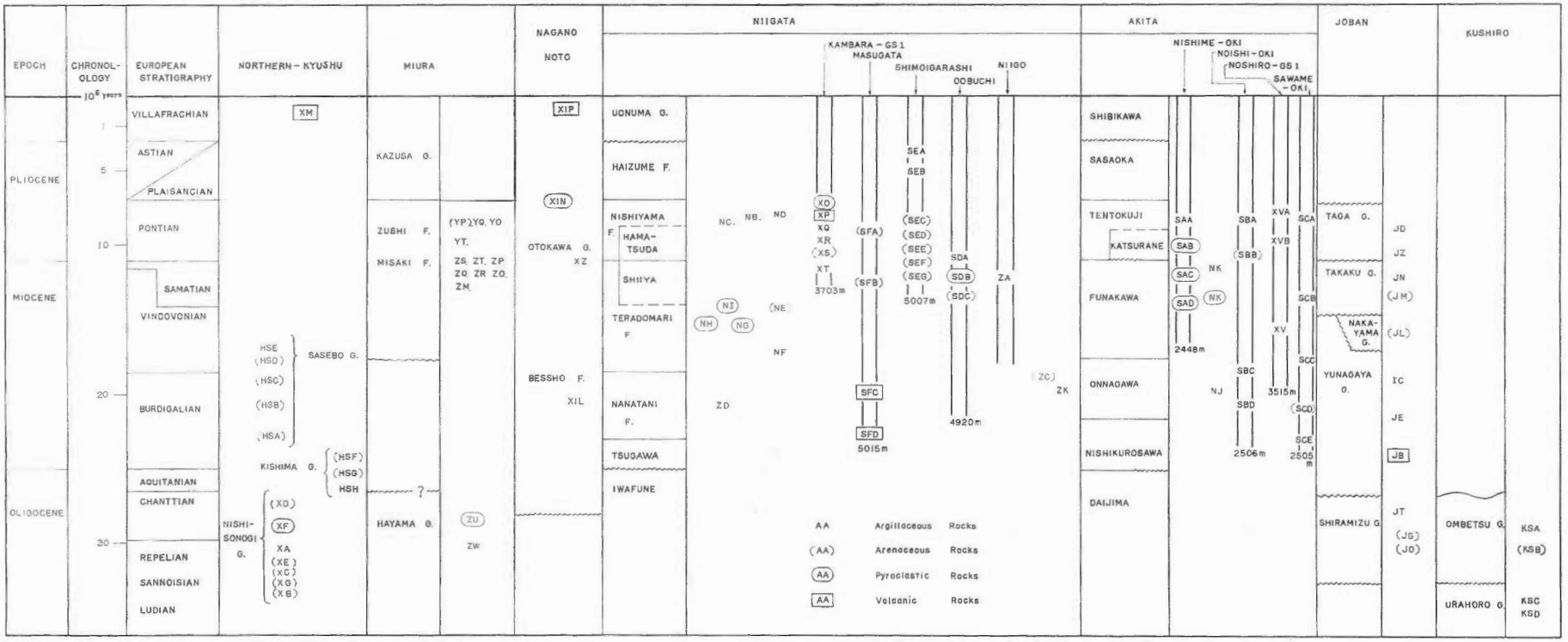

Table 2 Lithology, geologic formations, age, localities, porosity, density and wave velocity of the samples.
(d) : measured at dry condition. The other values with no symbols are measured at naturally wet condition.

Area	Number for index	Labo. name	Lithofacies	Formation	Age	Locality	Porosity (%)	Density (g/cm³)	Wave velocity (km/sec) Compressive	Shear
Kushiro (Hokkaido)	S1	KSA	grey hard shale	Charo f. Ombetsu g.	upper Oligocene	Charo, Shiranuka-machi	19.7	2.12	3.06	2.07
	S2	KSB	grey, well sorted fine sandstone	Ohmagari f. Ombetsu g.	〃	〃	5.34	2.58	3.83	2.34
	S3	KSC	grey hard shale	Shakubetsu f. Urahoro g.	middle Oligocene	Ohmagari, Shiranuka-machi	3.98	2.62	5.04	2.77
	S4	KSD	medium sandstone	〃	〃	〃	6.40	2.51	3.20	2.24
Joban (Fukushima Pref.)	S5	JD	grey siltstone	Taga g.	lower Pliocene	Kitagama, Hirono-machi	55.3	1.15	1.06(d)	0.73(d)
	S6	JZ	grey siltstone	〃	〃	Hadeya, Hirono-machi	58.6	1.09	0.98(d)	0.66(d)
	S7	JN	grey siltstone with grains of pumice	Shimotakaku, Takaku g.	lower Pliocene to upper Miocene	Shimotakaku, Iwaki City	63.9	1.08	1.87(d)	1.29(d)
	S8	JM	fine sandstone with grains of pumice	Numanouchi, Takaku g.	〃	〃	55.9	1.39	2.35(d)	1.37(d)
	S9	JL	grey, well sorted fine sandstone	Nakayama g.	upper Miocene	〃	—	—	—	—
	S10	IC	tuffaceous claystone	Honya f. Yunagaya g.	middle Miocene	Misawa, Kashima-machi	—	—	—	—
	S11	JE	grey siltstone	Mizunoya f. Yunagaya g.	〃	Irimikosen, Naraha-machi	—	—	—	—
	S12	IB	grey siltstone	〃	〃	Shimoasagai, Iwaki City	—	—	—	—

Area	Number for index	Labo. name	Lithofacies	Formation	Age	Locality	Porosity (%)	Density (g/cm³)	Wave velocity (km/sec) Compressive	Shear
	S13	JB	reddish liparite	Taki f. Yunagaya g.	lower Miocene	Shimokitaba, Hirono-machi	22.8	1.85	3.09	1.86
	S14	JT	grey claystone	Shirasaka f. Shiramizu g.	upper Oligocene	Furudate, Iwaki City	18.1	2.25	3.17	1.80
	S15	JG	grey, fine sandstone	Asagai f. Shiramizu g.	〃	Shimodera, Naraha-machi	—	—	—	—
	S16	JO	grey, medium sandstone	Iwaki f. Shiramizu g.	〃	Yumoto-yonko, Iwaki City	30.3	1.87	1.81	1.25
	S17	XVA	grey claystone	upper Tentokuji f.	lower Pliocene	Noshiro GS-1 Well Noshiro City depth 1001m	32.5	1.93	1.61(d	1.24(d
	S18	XVB	grey siltstone	lower Tentokuji f.	〃	〃 depth 1802m	33.6	1.90	2.11(d	1.22(d
	S19	XV	grey claystone	Funakawa f.	upper Miocene	〃 depth 3200m	12.3	2.29	3.74	2.39
	S20	SAA	pale brown yellowish siltstone	upper Tentokuji f.	lower Pliocene	Nishime-oki Well off Nishime-mura depth 501m	47.0	1.94	1.98	—
Akita Pref.	S21	SAB	sandy tuff	lower Tentokuji f.	〃	〃 depth 994m	36.2	2.03	1.68	—
	S22	SAC	〃	upper Funakawa f.	upper Miocene	〃 depth 506m	38.6	2.03	2.39	—
	S23	SAD	pale grey tuff	upper Funakawa f.	〃	〃 depth 1811m	26.5	2.17	3.01	—
	S24	SBA	pale grey	upper Tentokuji f.	lower Pliocene	Noishi-oki Well off Noishi, Kotohama-mura depth 601m	60.5	1.28	1.19(d	0.73(d

	S25	SBB	tuffaceous fine sandstone	lower Tentokuji f.	〃	〃 depth 1008m	55.2	1.74	1.70(d)	0.83(d)
	S26	SBC	grey shale	Onnagawa f.	lower Miocene	〃 depth 1801m	26.3	2.22	3.02(d)	1.70(d)
	S27	SBD	black, hard shale	〃	〃	〃 depth 2100m	0.0	2.75	6.22(d)	0.86(d)
	S28	SCA	grey siltstone	upper Tentokuji f.	lower Pliocene	Sawame-oki Well off Minehama-mura depth 900m	47.0	1.87	1.935	1.250
	S29	SCB	grey claystone	Funakawa f.	upper Miocene	〃 depth 1702m	34.2	2.08	2.810	1.665
	S30	SCC	grey shale	Onnagawa f.	lower Miocene	〃 depth 2000m	29.2	2.16	2.790	1.535
	S31	SCD	glauconite bearing fine sandstone	〃	〃	〃 depth 2232m	—	—	—	—
	S32	SCE	grey claystone	Nishikurozawa f.	〃	〃 depth 2503m	25.0	2.23	2.460	1.595
	S33	NJ	black shale	Onnagawa f.	〃	Onnagawa, Oga Peninsula	1.81	2.71	5.48	3.51
	S34	NK	pale yellowish brown claystone	Funakawa f.	upper Miocene	Funakawa, Oga Peninsula	60.1	1.20(d)	1.65(d)	1.05(d)
	S35	NL	white acidic tuff	〃	〃	Nampeizawa, Oga Peninsula	39.7	1.59(d)	2.00(d)	1.50(d)
Yamagata Pref.	S36	ZK	ZK_a : black shale ZK_b : reddish tuff and shale	Aosawa f.	lower Miocene	Yawata-machi	21.28	2.10	—	—
	S37	ZC	tuffaceous pale green fine sandstone	Nanatani f.	〃	Nanatani, Kanazuka, Kitakambara	8.60	2.45	5.54(d) 4.76	2.85(d)

Area	Number for index	Labo. name	Lithofacies	Formation	Age	Locality	Porosity (%)	Density (g/cm³)	Wave velocity (km/sec) Compressive	Shear
	S38	NF	tuff and claystone	lower Teradomari f.	middle Miocene	Nozumibashi, Teradomari-machi	15.56	2.22	2.87	2.07
	S39	NE	medium sandstone	upper Teradomari f.	〃	Hamano, Teradomari-machi	30.5	1.88(d)	1.67(d)	1.09(d)
	S40	ZA	grey claystone	Shiiya f.	upper Miocene	Niigō NT-2 Well Toyosaka machi depth 3052m	6.86	2.38	—	—
	S41	NB	grey siltstone	Haizume-Nishiyama f.	lower Miocene	Yoita-machi	48.4	1.50(d)	1.67(d)	0.99(d)
Niigata Pref.	S42	NC	grey siltstone	Nishiyama f.	〃	Izumozaki-machi	63.8	1.12(d)	1.77(d)	1.08(d)
	S43	ND	grey siltstone	Nishiyama f.	〃	Urase, Nagano City	44.3	1.63(d)	1.56(d)	1.04(d)
	S44	NG	pumice tuff	upper Teradomari f.	middle Miocene	Hozumi, Izumozaki-machi	17.9	2.23(d) 2.27	2.29	1.52
	S45	NH	fine-grained white tuff	upper Teradomari f.	〃	Katsumi, Izumozaki-machi	—	—	—	—
	S46	NI	coarse pumice tuff	〃	〃	Ishiji, Nishiyama-machi	15.6	2.45 2.42(d)	2.38	1.44
	S47	ZD	black shale	Nambayama f.	lower Miocene	West of Aotanamba-yama, Takata City	10.9	2.46 2.44(d)	3.37	2.30
	S48	SDA	grey claystone	Shiiya f.	upper Miocene	Ōbuchi Well depth 2036m Toyosaka-machi, Kita-kambara	23.4	2.32	2.82	—
	S49	SDB	white fine tuff	〃	〃	〃 depth 2485m	25.1	1.95(d) 2.10	1.33(d) 2.72	0.97(d)

S50	SDC	fine sandstone with coal material lamina	〃	〃	〃 depth 3585m	11.2	2.53	3.07	—
S51	SEA	yellowish grey siltstone	Haizume f.	upper Pliocene	Shimoigarashi Well depth 1001m Kamishinei-machi, Niigata City	38.9	2.09	2.30	—
S52	SEB	grey siltstone	〃	〃	〃 depth 1507m	35.4	2.17	1.88	—
S53	SEC	yellowish brown fine sandstone	Nishiyama f.	lower Pliocene	〃 depth 2522m	25.8	1.79(d) 2.37	0.71(d) 2.80	0.49(d) —
S54	SED	grey tuffaceous sandstone	〃	〃	〃 depth 3515m	18.3	2.47	2.09	—
S55	SEE	pale greenish medium sandstone	〃	〃	〃 depth 3999m	23.9	2.36	2.35	—
S56	SEF	fine-medium sandstone	Shiiya f.	upper Miocene	〃 depth 4500m	17.7	2.12(d) 2.40	1.33(d) 1.82	0.98(d) —
S57	SEG	medium sandstone	〃	〃	〃 depth 5000m	14.4	2.22(d)	1.88(d)	—
S58	SFA	greenish grey medium sandstone	Nishiyama f.	lower Pliocene	Masugata Well depth 2501m Katahigashi-mura, Nishi-kambara	16.42	2.38	1.920	—
S59	SFB	grey fine-medium sandstone	Shiiya f.	upper Miocene	〃 depth 4006m	—	2.23	3.600	—
S60	SFC	white liparite	Nanatani f.	lower Miocene	〃 depth 4510m	—	2.15	3.710	2.235
S61	SFD	andesite	Tsugawa f.	〃	〃 depth 5000m	8.5	2.57	3.520	1.695

Area	Number for index	Labo. name	Lithofacies	Formation	Age	Locality	Porosity (%)	Density (g/cm³)	Wave velocity (km/sec) Compressive	Shear
	S62	XQ	grey claystone	lower Nishiyama f.	upp r Miocene	Kambara GS-1 Well depth 2405m Wanou-machi, Naka-kambara	20.40	2.18	2.43	1.77
	S63	XR	〃	Hamatsuda f.	〃	〃 depth 2700m	7.0	2.53	—	—
	S64	XT	grey, hard shale	Shiiya f.	〃	〃 depth 3514m	11.05	2.26	3.36	2.23
	S65	XS	greenish grey medium sandstone	lower Hamatsuda f.	〃	〃 depth 3365m	—	—	—	—
	S66	XO	white, fine tuff	Nishiyama f.	lower Pliocene	〃 depth 2097m	—	—	—	—
	S67	XP	hornblende andesite	〃	〃	〃 depth 2313m	10.74	2.26	4.28	2.32
Noto Peninsula (Ishikawa)	S68	XZ	grey siltstone	Mushizaki f.	upper Miocene	Nanao-1 Well depth 122m Nanao City	58.7	1.63	—	—
Nagano Pref.	S69	XIL	black shale	Bessho f.	lower Miocene	Matsushiro-machi, Nagano City	2.56	2.67 2.64(d)	5.13 4.81(d)	—
	S70	XIN	tuff	—	Pleistocene	Mt. Kimyo-san, Matsushiro-machi, Nagano City	7.76	2.45 2.37(d)	4.50 4.36(d)	—
	S71	XIP	andesite	—	〃	Mt. Minakami-yama, Matsushiro-machi, Nagano City	16.38	2.14 1.97(d)	3.07 3.07(d)	—
	S72	YP	very coarse volcanic black sandstone	Ikego f.	lower Pliocene ～ upper Miocene	Yokosuka City	33.1	1.74 1.74(d)	2.61 2.54(d)	1.51(d

	S73	YQ	grey siltstone	Ikego f.	〃	〃	43.0	1.60 1.59 (d)	2.26 2.52(d)	1.56(d)
	S74	YO	grey claystone	〃	〃	〃	36.6	1.85 1.87 (d)	1.77 1.78(d)	1.22(d)
	S75	YT	siltstone with tuff-lamina	〃	〃	〃	46.5	1.53	2.30	—
	S76	ZM	coarse siltstone	Misaki f.	upper Miocene	Kenzaki, Miura City	43.2	1.91	1.81	1.12
	S77	ZO	grey siltstone including fine sand grains	〃	〃	Tōriya, Miura City	42.7	1.60	1.88	1.11
	S78	ZP	grey claystone with sand-lamina	〃	〃	Jōgashima, Miura City	30.2	1.75	1.58	1.69
Miura Peninsula (Kanagawa Pref.)	S79	ZQ	pale brown siltstone bearing medium sand	〃	〃	Miura City	40.3	1.44	1.87	1.44
	S80	ZR	grey siltstone	〃	〃	Miura City	45.1	1.63	1.92	1.53
	S81	ZS	fine sand bearing siltstone	〃	〃	Moroiso, Miura City	43.4	1.64	2.29	1.26
	S82	ZT	medium sand bearing siltstone	〃	〃	Aburatsubo, Miura City	41.2	1.72	2.36	1.30
	S83	ZU	tuffaceous siltstone	Hayama g.	upper Oligocene	Takeyama, Zushi City	36.3	1.67	3.00	1.79
	S84	ZW	grey tuff	〃	〃	Shibazaki, Zushi City	36.3	1.99	3.31	1.70
	S85	XA	hard black shale	Tokuman f. Nishisonogi g.	middle Oligocene	Ohshima-machi, Nishisonogi	2.15	2.56	5.58	3.35

Area	Number for index	Labo. name	Lithofacies	Formation	Age	Locality	Porosity (%)	Density (g/cm³)	Wave velocity (km/sec) Compressive	Shear
Northern Kyushu (Nagasaki Pref.)	S86	XB	grey medium sandstone	Maze f. Nishisonogi g.	middl· Oligocene	Chshima-machi, Nishisonogi	2.89	2.50	3.86	2.59
	S87	XC	〃	〃	〃	〃	6.2	2.66	5.27	2.90
	S88	XD	greenish grey tuffaceous coarse sandstone	Shioda f. Nishisonogi g.	upper Miocene	〃	—	—	—	—
	S89	XE	grey medium sandstone	Maze f. Nishisonogi g.	middle Oligocene	〃	12.30	2.56	4.67	2.71
	S90	XF	greenish grey tuff and claystone	Yuridake f. Nishisonogi g.	〃	〃	3.11	2.43	5.58	3.39
	S91	XG	grey medium sandstone	Maze f. Nishisonogi g.	〃	〃	2.40	2.63	4.30	2.95
	S92	XM	hypersthene olivine basalt	—	Pleistocene	Ohtawa, Saikai-mura	—	2.74	5.05	2.98
	S93	HSA	reddish brown medium sandstone	Ainoura f. Sasebo g.	lower Miocene	Nishikawachi, Hokusho coal field	6.52	2.43	3.46	2.32
	S94	HSB	grey fine sandstone	Yunoki f. Sasebo g.	〃	Kosaza-machi, Hokusho coal field	10.20	2.36	2.83	1.95
	S95	HSC	white medium sandstone	Sechihara f. Sasebo g.	〃	Hiratayama, Hokusho coal field	12.72	2.18	2.88	1.75
	S96	HSD	pale brown fine sandstone	Fukui f. Sasebo g.	〃	Kaze Hokusho coal field	13.2	2.33(d)	2.43	1.39
	S97	HSE	hard black shale	Kaze f. Sazebo g.	lower-middle Miocene	〃	3.21	2.63	4.16	2.76

S98	HSF	reddish, very fine sandstone	Funakawa f. Kishima g.	upper Oligocene	Furukawa, Hokusho coal field	3.85	2.62	4.60	2.76
S99	HSG	coarse, hard sandstone	Kuroishi f. Kishima g.	〃	Kuroishi, Hokusho coal field	4.06	2.61	4.25	2.42
S100	HSH	black hard shale	Mikaeri f. Kishima g.	〃	〃	5.13	2.55	4.60	3.27

Table 3 Number of the tested rocks.

Area	Argillaceous	Arenaceous	Pyroclastic	Volcanic	Total
Kushiro, Hokkaido	2	2			4
Joban	7	4		1	12
Akita	13	2	4		19
Niigata (Yamagata)	13	11	5	3	32
Nagano (Noto)	2		1	1	4
Northern Kyushu	3	11	1	1	16
Miura	11	1	1		13
	51	31	12	6	100

Table 4 E perimental results.

Types of failure : W ; wedge type, S ; single shear type, N ; network shear type, F ; flow (no macroscopic fractures). Behavior of deformation : V.B ; very brittle, B ; brittle, T ; transitional, D ; ductile, V.D ; visco-ductile. P ; strain rate after the yield point. θ ; angle of fracture to the direction of maximum compression. 2θ ; angle between conjugate shear fractures. P ; Strain rate for plastic region.

Number for index	Rock		Confining pressure (kg/cm²)	Axial shortening at confining pressure	Differential stress (kg/cm²) at strain 1 (%)	2 (%)	5 (%)	10(%)	Ultimate strength (kg/cm²)
S 1	K S A	5	1	0	410	1190			1290
S 2	K S B	9	1	0	710				800
		15	500	5.64×10^{-3}	1850	2820	1840		2930
		10	1000	8.72×10^{-3}	2300	3630	3190	3030	3800
		14	1500	8.98×10^{-3}	1920	3290	4180		4660
		13	2000	7.71×10^{-3}	2370	3660	4820		4900
S 3	K S C	3	1	0	1250				1710
		9	500	2.56×10^{-3}	1950	2900			2920
		10	1000	3.08×10^{-3}	2260	4000			4200
		1	1500	7.70×10^{-3}	2540	4230	4380		4930
S 4	K S D	7	1	0	570				760
		4	200		1520				1850
		2	500	5.13×10^{-3}	1930	2760	2160		2880
		9	1000	6.66×10^{-3}	1470	2730	3700		3730
		11	1200	7.18×10^{-3}	1890	3570	4620	4170	4620
		12	1500	8.98×10^{-3}	2020	4080	5600	4910	5600
S 5	J D	3	1	0	50				52
		13	50	0.003	50	85	120	145	
		10	200	0.021	65	90	170	263	
S 6	J Z	7	1	0	20				21
		3	50	0.003	26	58	100	126	
		1	100		37	64	109	156	
		10	200	0.033	45	84	149	219	
S 7	J N	1	1	0	90	107			123
		5	100	0.016	100	140	193	231	
		6	300	0.023	90	156	253	380	
S 8	J M	3	1	0	96				97
		6	50	0.002	128	169	200	230	

Ductility-strain at macro-fracturing (%)	Total strain (%)	Residual strain (%)	Strain rate (/sec)	Type of failure	Angle of macro-fractures θ	Angle of macro-fractures 2θ	Behavior of deformation	Remarks
2.32				W	7°, 8°	15°	V. B	
1.11				W	8°	16°	V. B	
2.60	6.85	6.30		S	31°, 34°	65°	B	
2.7	10.7	10.0		S, N	31°, 33° 37°, 38°	69°	B	double peaks
5.0	9.0	8.3		S	30°~38°	69°	B	
6.2	6.8	5.9		F	40°, 39°	79°	T	
1.23				W	18°	36°	V. B	
1.8				S	18°, 19°	37°	V. B	
2.2				S	26°, 24°	50°	V. B	
3.5				S	29°, 29°	58°	B	
1.3				W	12°	24°	V. B	
1.8				S	21°, 26°	47°	B	
3.0	5.1	4.9		S	29°, 27°	56°	B	
4.2	8.0	7.3		S	30°, 30°	60°	B	
5.0				S, N	36°, 36° 24°, 23°	72°~ 47°	B	
5.2	14.2	13.8		S, N	28° 32°	55° 64°	B	
1.4	1.4		1.1×10^{-4}	W		40°	B	
	14.53	14.28	1.3×10^{-4}	F			D	
	19.10	18.5	1.3×10^{-4}	F			D~V. D	
1.1	1.6			W	12°, 8°	20°	B	
	14.8	14.4	1.7×10^{-4}	F			D	
	17.3	17.0	1.3×10^{-4}	F			D	
	9.4	9.3	1.3×10^{-4}	F			D~V. D	
0.6	5.2	4.1		W	19°, 25°	44°	B	
	9.6	9.4	1.3×10^{-4}	S	31°, 21°	52°	D	
	10.4	10.2	1.1×10^{-4}	F			D~V. D	
1.1	1.2		3.3×10^{-5}	S	13°, 22°	35°	B	
	15.5	14.9	1.7×10^{-5} 1.3×10^{-4}P	F			D	

Number for index	Rock		Confining pressure (kg/cm²)	Axial shortening at confining pressure	Differential stress (kg/cm²) at strain 1 (%)	2 (%)	5 (%)	10(%)	Ultimate strength (kg/cm²)
		4	100	0.005	138	179	240	290	
S 9	J L	1	1	0	111				140
		2	100	0.058	124	190	257	310	
		5	200	0.008	124	191	281	379	
S10	I C	1	1		106	230			246
		2	55	0.020	154	338	533		533
		4	100	0.025	200	359	600		620
		5	200	0.012	228	400	683	787	797
		6	300	0.011	228	418	861	1050	1057
S11	J E	2	1		50	76			83
		3	100	0.006	50	83	150	217	
		8	200	0.003	50	93	183	273	
S12	I B	3	1		46	107			120
		1	50		117	171	228	244	
		2	100		205	236	276	292	
S13	J B	1	1		768				785
		2	500	0.006	1000	1793			2524
		3	1000	0.009	1000	1793	2960	3190	3280
		4	1500	0.014	1000	1793	3420	4195	4200
S14	J T	5	1	0	638				790
		3	100	0.024	776				1220
		4	200	0.002	1100				1508
		2	300	0.003	931	1600			1790
		1	1000	0.007	776	1433	2207	2300	2350
		6	1500	0.016	1100	1767	2732	3086	3100
		8	2000	0.014	931	1600	2638	3293	3414
S15	J G	10	1	0	161				240
		11	300	0.009	552	800	865	838	866
		9	500	0.010	600	893	1049	1083	1100
		12	1000	0.017	400	627	1083	1566	
S16	J O	1	1	0	130				131

Ductility-strain at macro-fracturing (%)	Total strain (%)	Residual strain (%)	Strain rate (/sec)	Type of failure	Angle of macro-fractures θ	Angle of macro-fractures 2θ	Behavior of deformation	Remarks
	14.0	13.8		F			D	
1.4	1.4		1.1×10^{-4}	W	12°, 22° 20°	44°	V. B	
	14.4	14.2	1.3×10^{-4}	F			D	
	19.4	18.8	1.3×10^{-4}	F			D	
2.5	2.5		1.4×10^{-4}	W			V. B	
5.0	5.0		1.1×10^{-4}	S	22°, 15°	37°	B	
5.8	5.8		9.7×10^{-5}	S	31°, 29°	60°	B	
8.5	20.0	18.8	1.3×10^{-4}P	N			T	
11.2	21.1	19.3	1.3×10^{-4}P	F			T	
3.3	(3.3)	0	1.5×10^{-4}	S	28°, 29°	57°	B	
	19.2	18.6	1.2×10^{-4}	F			V. D	
	21.15	20.40	9.6×10^{-5}	F			V. D	
2.3	(2.3)		1.9×10^{-4}	W	10°～28°	56°	B	
	16.6		1.4×10^{-4}	F			D	
	18.6			F			D	
1.2	(1.2)		6.7×10^{-5}	W	5°～15°	30°	V. B	
4.0	(4.0)			S	22°, 23°	45°	B	
7.8	17.4	15.5	9.7×10^{-5} 1.2×10^{-4}P	N	25°, 25°	50°	T	
11.0	16.3	14.2		N		60°	T	
1.3	(1.3)		5.4×10^{-5}	W	3°～12°	24°	V. B	
1.9	(1.9)		5.3×10^{-5}	S	23°, 22°	45°	V. B	
1.5	2.7	1.8	5.3×10^{-5}	S	23°	46°	V. B	
3.0			8.3×10^{-5}	S		56°	B	
8.3				S			T	
11.0	19.05	17.9	1.03×10^{-4} 1.09×10^{-4}P	F			T	
14.7	18.5	17.8	1.05×10^{-4}	F			T	
1.4	(1.4)		4.7×10^{-5}	S		40°	V. B	
5.2	14.6	13.9	1.3×10^{-4}	F			T	
14.0	18.2	18.0	4.4×10^{-5} 1.3×10^{-4}P	F			T～D	
	13.0	12.3	1.2×10^{-4}	F			V. D	
1.1	(1.1)			S		50°	B	

Number for index	Rock		Confining pressure (kg/cm²)	Axial shortening at confining pressure	Differential stress (kg/cm²) at strain 1 (%)	2 (%)	5 (%)	10(%)	Ultimate strength (kg/cm²)
		9	100	0.003	172	233	266	313	
		8	200	0.008	253	307	387	480	
		2	300	0.010	253	307	413	560	
		7	500	0.014	152	253	447	714	
S17	XVA	3	1		43	48			70
		4	500	0.045	44	125	333	558	
		8	1000	0.048	47	165	433	870	
		1	1500	0.087	225	429	987	1730	2085
S18	XVB	6	1		154				160
		2	500	0.043	114	228	476	743	
		3	1000	0.040	184	336	743	1192	
		8	1500	0.060	320	596	1120	1360	1370
S19	XV	2	1		638				1460
		1	500	0.0006	1121	2390			2685
		3	1000	0.0010	1214	2495	3425		3440
		6 7	1500	0.0011 0.0010	1460	2640	4150		4185
		5	2000	0.0012	1460	2677	4468	4830	4882
		14	2500	0.0010	1596	2885	4710	5595	5605
S20	SAA	2	1	0					61.2
		4	300	0.020	118.4	208.1	416.3	563.2	
		5	600	0.033	65.3	126.5	306.1	620.4	
		6	1000	0.057	171.4	330.6	746.9	1224.4	
		7	1500	0.077	355.1	571.4	1118.4	1367.3	
S21	SAB	1	1	0	60				117
		3	600	0.015	190	347	641	927	
		4	1000	0.016	190	355	734	1282	
		6	1500	0.043	190	355	806	1476	
S22	SAC	1	1	0	81				137
		2	300	0.013	121	226	415	625	
		3	1000	0.041	218	379	794	1403	

Ductility-strain at macro-fracturing (%)	Total strain (%)	Residual strain (%)	Strain rate (/sec)	Type of failure	Angle of macro-fractures θ	Angle of macro-fractures 2θ	Behavior of deformation	Remarks
	16.4	16.2	$1.3\times10^{-4}P$	F			D	
	13.2	12.9	8.9×10^{-5} $1.3\times10^{-4}P$	F			D	
	8.3	8.3	$1.2\times10^{-4}P$	F			D	
	9.5	9.1	$1.3\times10^{-4}P$	F			V. D	
1.4	2.7	2.5	1.1×10^{-4}	W, S		36°～44°	B	
	18.2	17.9	$1.36\times10^{-4}P$	F			V. D	
	18.5			F			V. D	
15.8	17.8		$1.28\times10^{-4}P$	F			T	
1.1	(1.2)	1.6		W	19°～17°	38°	B	
	18.3	17.1	$1.32\times10^{-4}P$	F			V. D	
	21.7	20.4		F			V. D	
10.5	13.8	13.6	$1.21\times10^{-4}P$	F			V. D	
1.7	(1.7)		5.7×10^{-6}	W			V. B	
2.5	(2.5)		5.5×10^{-6}	S		46°	B	
4.7	6.4	4.4	5.5×10^{-6}	S		58°	B	double peaks
5.4	5.4		5.4×10^{-6}	S		64°	B	
8.2	13.8	11.7	5.4×10^{-6} $8.3\times10^{-6}P$	N			B～T	
10.5	14.7	13.1	5.3×10^{-6} $1.4\times10^{-5}P$	F			T	
0.7	(0.7)			W	15°	30°	B	
	16.8	17.2	1.22×10^{-4}	F			V. D	
	17.8	17.8	1.23×10^{-4}	F			V. D	
		16.8	1.12×10^{-4}	F			V. D	
	13.4	13.4	1.12×10^{-4}	F			V. D	
1.9	(1.9)			S	20°, 30°	50°	B	
	19.1	19.0	1.22×10^{-4}	F			V. D	
	20.6	20.5	1.50×10^{-4}	F			V. D	
	17.15	17.15	1.17×10^{-4}	F			V. D	
1.9	(1.9)			W			B～T	
	18.8	18.8	1.22×10^{-4}	F			V. D	
	17.4	17.1	1.15×10^{-4}	F			V. D	

Number for index	Rock		Confining pressure (kg/cm²)	Axial shortening at confining pressure	Differential stress (kg/cm²) at strain 1 (%)	2 (%)	5 (%)	10(%)	Ultimate strength (kg/cm²)
S 23	S A D	1	1	0	156	173			329
		2	300	0.011	247	453	774	984	
		3	600	0.010	288	514	988	1547	
		4	1000	0.0059	350	650	1494	2374	
		7	1500	0.026	527	852	1523	2654	
S 24	S B A	1	1	0	34				40
		2	200	0.024	44	67	137	220	
		3	500	0.062	93	140	290	470	
		4	1000	0.073	160	290	554		
		5	1500	0.089	240	413	610		
S 25	S B B	2	1		51	105	198	260	
		3	500	0.012	98	182	366	612	
		5	1000	0.034	183	311	671		
S 26	S B C	2	200	0.0013	582	1043			1122
		3	500	0.0044	830	1362	1562	1500	1572
		4	1000	0.010	712	1255	1935	2285	
		5	1500	0.012	846	1426	2445	3080	
		6	2000	0.015	894	1455	2532	3500	
S 27	S B D	1	1						1750
		3	500	0.003					6500
S 28	S C A	1	1		89	171			207
S 29	S C B	1	1		230				240
		2	200	0.005	234	447	606	613	
		3	500	0.010	256	467	700		
		4	1000	0.022	230	421	824		
		5	1500	0.040	327	586	1058		
S 30	S C C	1	1		226	460			504
		2	200	0.006	293	560			610
		3	500	0.009	363	787	1356	1358	1404
		6	1000	0.016	466	884	1740	2008	2022
		7	2000		700	1372	2365		

Ductility-strain at macro-fracturing (%)	Total strain (%)	Residual strain (%)	Strain rate (/sec)	Type of failure	Angle of macro-fractures θ	Angle of macro-fractures 2θ	Behavior of deformation	Remarks
1.85	(1.85)		6.94×10^{-5}	W	13°, 22°	35°	B	
	18.8	18.8	1.23×10^{-4}	F			T	
	19.3	19.1	1.18×10^{-4}	F			D	
	18.7	17.9	1.11×10^{-4}	F			D	
	16.4	15.5	1.04×10^{-4}	F			V. D	
1.3		(1.5)		S	27°, 23°	50°	B	
	12.0	10.7	1.29×10^{-4}	F			V. D	
	14.2	11.8	1.27×10^{-4}	F			V. D	
	6.9	6.5	1.20×10^{-4}	S	20°, 19°	39°	D	
	8.5	7.9	1.24×10^{-4}	S	28°, 29°	57°	D	
	13.0	12.9		W	12°	24°	B	
	12.8	12.2	1.19×10^{-4}	F			V. D	
	8.1	7.5	1.18×10^{-4}	F			V. D	
2.8	3.4	2.4		S	24°, 24°	48°	B	
3.7	13.3	11.8	7.0×10^{-5} 1.31×10^{-4}P	N	29°, 30° 35°	59°	T	
	14.9	13.0	1.05×10^{-4}	F			D	
	12.6	10.5	9.8×10^{-5}	F			D	
	11.4	10.7	9.5×10^{-5}	F			D	
1.0			1.11×10^{-5}	W		30°	V. B	
1.1			1.90×10^{-5}	S	28°	56°	V. B	
2.9	2.9			W	32°	64°	B	
1.0	1.7		7.0×10^{-5}	W	25°, 24°	49°	B	
	10.7	9.6	7.5×10^{-5} 1.23×10^{-4}P	N	32°, 31°	63°	T	
	6.0	5.2	1.11×10^{-4}	F			D	
	7.9	7.4	1.11×10^{-4}	F			D	
	8.1	7.5	1.15×10^{-4}	F			D	
2.2		2.9	8.4×10^{-5}	W	18°	36°	B	
2.2	5.1	4.8	9.2×10^{-5}	W	19°	38°	B	
6.7	10.3	9.0	1.15×10^{-4}	S	31°, 34°	65°	T	
11.0	18.4	16.8	1.17×10^{-4}	F			T	
	7.6						D	

Number for index	Rock		Confining pressure (kg/cm²)	Axial shortening at confining pressure	Differential stress (kg/cm²) at strain 1 (%)	2 (%)	5 (%)	10(%)	Ultimate strength (kg/cm²)
S31	SCD	1	1	0	562				616
		2	200	0.0005	788				1328
S32	SCE	1	1		318				422
		5	1000		534	882	1226	885	1260
		8	1500		669	1062	1865	2443	
S33	NJ	5	1	0	3327	3547			3853
		3	500	0.0015	4060	5947			6120
		6	1000	0.0021	5587				7273
		4	1500	0.0036	5587	8080			8200
		12	2000	0.0038	5587	8100			9287
S34	NK	10	1	0	45	50			50
		2	100	0.010	50	65	120		
		9	300	0.018	35	65	170	330	
S35	NL	2	1	0	170	286			290
		3	500	0.013	289	400	780	1130	
		6	1000	0.023	318	550	1014	1672	
		4	1500	0.044	318	550	1250	2220	
		5	2000	0.075	420	735	1640	2780	
S36	ZK_b	1	1						513
	ZK_a	2	500	0.0048	1220	2125			2340
	ZK_a	4	1000	0.0068	1220	2157			2910
	ZK_b	3	1500	0.0090	1999	3610			4760
	ZK_b	6	2000	0.0082	2122	3790	5185		
	ZK_a	5	2500	0.011	576	2042	3767	4827	
S37	ZC	1	1	0					970
		5	500	0.0018	2804				4050
		8	1000	0.0030	2862				4120
		6	1500	0.0048	2517	3952	4668	4908	4915 4980
S38	NF	1	1		470				710
		5	1000	0.0092	850	1450	2100	2340	2340
		6	1500	0.0125	850	1530	2600	2970	2980

Ductility-strain at macro-fracturing (%)	Total strain (%)	Residual strain (%)	Strain rate (/sec)	Type of failure	Angle of macro-fractures θ	Angle of macro-fractures 2θ	Behavior of deformation	Remarks
1.1	6.9	6.7		W	27°	54°	V. B	
1.45	9.8	9.0	1.35×10^{-4}P	S	32°, 31°	63°	V. B	
1.2	(1.2)			W	18°, 20°	38°	B	
6.4	11.3		9.01×10^{-5}	N	30°, 31° 45°, 45°	61°~ 90°	T	
	26.3	24.8	1.09×10^{-4}	F			D	
1.2			2.50×10^{-5}	W	1°~10°	20°	V. B	
1.6			2.42×10^{-5}	S	16°	32°	V. B	
1.7			2.36×10^{-5}	S	15°~16°	32°	B	
2.2			2.62×10^{-5}	S	14°~16.5°	33°	B	
3.3				S	24°~25°	49°	B	
2.0	2.0			S	26°, 23°	49°	B	
	9.2		1.2×10^{-4}P	F			D	
	11.2		1.2×10^{-4}	F			V. D	
2.1	2.1		6.7×10^{-5}	W	5°~18°	36°	B	
	17.5	17.1		F			V. D	
	19.9	19.1	1.16×10^{-4}	F			V. D	
	13.9	12.2	1.09×10^{-4}	F			V. D	
	15.9	14.0	1.06×10^{-4}	F			V. D	
0.8	1.07			W	1°~20°	40°	V. B	
2.8	3.7	2.1	5.6×10^{-5}	S	20°~22°	44°	B	
4.13	10.2	8.2	6.7×10^{-5}	S	29°~30°	60°	B	
4.07	8.2	6.6	4.5×10^{-5}	N	22°, 25° 26°	50°	B	
	6.2	4.0		N	38°	76°	T	
	15.2	13.2	7.3×10^{-5}	F			V. D	
0.8	0.8			W	15°~16°	31°	V. B	
1.6	1.6		3.4×10^{-5}	S	34°. 36° 32°	67°	V. B	
1.9	6.5		2.9×10^{-5} 1.4×10^{-4}P	S	31°, 30°	61°	B	
10.1 14.0	18.8		6.7×10^{-5} 8.6×10^{-5}P	N	32°, 30° 33°, 36°	62° 69°	T	double peaks
1.5	1.77		6.7×10^{-5}	W	1°~21°	42°	V. B	
9.6	18.2	17.2		N	32°, 34°	66°	T	
10.8	17.0	16.5	8.3×10^{-5} 1.1×10^{-4}P	N	36°	72°	T	

Number for index	Rock		Confining pressure (kg/cm²)	Axial shortening at confining pressure	Differential stress (kg/cm²) at strain 1 (%)	2 (%)	5 (%)	10(%)	Ultimate strength (kg/cm²)
		7	2000	0.0148	690	1210	2280	3210	
S 39	N E	4	1		95				137
		6	200	0.0079	248	400	437		437
		1	300	0.0099	292	508	719		
		5	500	0.012	315	580	796		
S 40	Z A	5	1		380				470
		4	500	7.52×10^{-3}	490	810	1150		1180
		1	1000	1.25×10^{-2}	550	970	1430	1400	1470
		2	1500	1.69×10^{-2}	550	1050	1650	1750	1750
		3	2000	1.99×10^{-2}	550	1050	1820		
S 41	N B	3	1		48				50
		8	200	1.95×10^{-2}	87	137	226		
		4	500	2.83×10^{-2}	24	61	223	503	
S 42	N C	7	1		34	50			52
		3	200	4.32×10^{-2}	71	123	226		
		4	300	4.43×10^{-2}	30	64	137	262	
		1	500	7.62×10^{-2}	71	123	242	425	
S 43	N D	5,7	1		54				88
		10	100	8.92×10^{-3}	90	144	282		
		8	200	1.08×10^{-2}	105	162	270	428	
S 44	N G	1	1						233
S 45	N H	1	1		439.1				709.4
		2	500	5.3×10^{-3}	753.3	1239.8	1584.4		1630
		3	1000	5.58×10^{-3}	868.2	1304.1	1817.5	2317.5	2427
		4	1500	1.01×10^{-2}	868.2	1689.1	2263.5	3016.8	3268
		5	2000	1.01×10^{-2}	476.3	1047.3	2118.2	3371.6	
S 46	N I	1	1						253
		2	500	3.06×10^{-3}	862	1253	1562		
		3	1000	5.3×10^{-3}	869	1259	1960	2263	
		5	1500	6.65×10^{-3}	657	1172	2246	3104	
S 47	Z D	5	1	0	980				1170

Ductility-strain at macro-fracturing (%)	Total strain (%)	Residual strain (%)	Strain rate (/sec)	Type of failure	Angle of macro-fractures θ	Angle of macro-fractures 2θ	Behavior of deformation	Remarks
	16.4	15.0	9.9×10^{-4}	F			V. D	
1.5			8.3×10^{-5}	W	17°, 19°	36°	B	
3.4	8.3		1.2×10^{-4}P	F			T	
	9.0		1.5×10^{-4}P	F			D	
				F			D	
1.4			9.35×10^{-5}	W	17°, 9°	26°	V. B	
4.2	9.6	8.1	9.26×10^{-5} 12.4×10^{-5}P	F			T	
7.2	9.7	8.0	10.7×10^{-5} 12.4×10^{-5}P	F			T	
9.3	11.8	10.4	9.53×10^{-5} 12.6×10^{-5}P	F			D	
	7.1	5.8	11.5×10^{-5}	F			D	
1.1				S	15°, 16°	31°	V. B	
	9.5	9.5	1.30×10^{-4}	F			D	
	12.4	12.4	1.27×10^{-4}	F			V. D	
2.6	(4.2)		1.40×10^{-4}	S	24°, 23° max	47°	T	
	7.5	7.5	1.32×10^{-4}	F			D	
	16.8	16.8	1.29×10^{-4}	F			V. D	
	16.3	16.2	1.29×10^{-4}	F			V. D	
1.6			1.055×10^{-4}	S	25°, 23° 22°, 21°	58° 43°	V. B	
	5.7		1.19×10^{-4}	F			V. D	
	17.1	16.7	1.75×10^{-4}				V. D	
1.2			6.7×10^{-5}	W	7°	14°	B	
1.6				S	21°, 22°	43°	V. B	
	8.75	8.4	1.03×10^{-4} 1.30×10^{-4}P	S	32°	(64°)	T	
13.4	20.25	19.8	1.10×10^{-4}	S	35°	70°	T	
15.4	19.4	18.3	1.07×10^{-4}	S	37°, 34°	71°	T	
	17.0	16.2	9.67×10^{-5}	F	(40°)	(80°)	V. D	
0.4				S	17°, 22°	39°	V. B	
	8.8	8.6	5.55×10^{-5} 1.27×10^{-4}P	F			D	
	12.2	11.7	1.02×10^{-4}	F			V. D	
	12.0	11.3	9.76×10^{-5}	F			V. D	
1.2			6.7×10^{-5}	W		18°	V. B	

Number for index	Rock		Confining pressure (kg/cm²)	Axial shortening at confining pressure	Differential stress (kg/cm²) at strain 1 (%)	2 (%)	5 (%)	10(%)	Ultimate strength (kg/cm²)
		4	500	0.0038	1580	2520			3300
S48	SDA	1	1	0	186				342
		2	200	4.10×10^{-3}	254	492	650	643	672
S49	SDB	1	1	0	114	435			442
		2	200	4.62×10^{-3}	542	841	895	813	959
		4	1000	1.79×10^{-2}	550	1102	1578	1549	1605
S50	SDC	1	1	0	51	136			279
		2	200	1.23×10^{-2}	245	578	813	782	823
S51	SEA	1	1	0	64				100
		2	200	0.0079	102	176	305	418	
		3	500	0.029	102	183	412	643	
		4	1000	0.060	186	329	674	1108	
		5	1500	0.068	203	413	922	1523	
S52	SEB	1	1	0	94	165			199
S53	SEC	1	1	0	34	27			47
		2	200	0.011	170	334	411	479	
		3	500	0.013	131	269	471	758	
		4	1000	0.026	131	269	602	1046	
		5	1500	0.046	236	441	910	1665	
		6	2000	0.050	303	653	1440	2706	
S54	SED	1	1	0	61	141			242
		2	200	0.015	259	578	915		946
		3	500	0.018	364	774	1178	1238	1238
		4	1000	0.022	488	925	1521	1750	1757
		5	1500	0.031	391	825	1548	1934	1941
		6	2000	0.032	522	994	1852	2287	2288
S55	SEE	1	1	0	57				100
		2	200	0.0088	461	773	729	682	789
		3	500	0.0067	588	955	994	1062	
		4	1000	0.019	595	962	1246	1583	
		5	1500	0.021	428	762	1278	1964	

Ductility-strain at macro-fracturing (%)	Total strain (%)	Residual strain (%)	Strain rate (/sec)	Type of failure	Angle of macro-fractures		Behavior of deformation	Remarks
					θ	2θ		
3.1			7.9×10^{-5}	W		50°	V. B	
1.9	4.5	3.8	6.55×10^{-5}				B	
5.8	13.7	12.75	1.27×10^{-4}	F			T	
1.98	2.8	2.2	6.65×10^{-5}	W	13°, 8°	21°	V. B	
3.33	10.4	9.7	8.33×10^{-5} 1.39×10^{-4}P	S	36°, 34°	70°	T	
7.25	14.0	13.5	8.70×10^{-5} 1.28×10^{-4}P	F			T	
3.4	5.0	4.0	8.83×10^{-5}	S	16°, 16°	32°	B	
5.9	16.2	16.7	1.03×10^{-4} 1.33×10^{-4}P	F	38°(40°)	78°	T	
1.7	4.2	3.5	1.4×10^{-4}	W	17°～18° 25°	35°～ 50°	B	
	13.5	13.0	1.3×10^{-4}	F			V. D	
	13.8	13.4	1.2×10^{-4}	F			V. D	
	13.4	12.9	1.14×10^{-4}	F			V. D	
	13.6	13.0	1.1×10^{-4}	F			V. D	
2.4	(2.4)		1.1×10^{-4}	W	16°	32°	B	
1.5	4.8	4.5	1.4×10^{-4}	W			B	
	14.0	13.5	9.5×10^{-5} 1.3×10^{-4}P	F			T	
	14.13	13.5	1.2×10^{-4}	F			V. D	
	14.0	13.5	1.2×10^{-4}	F			V. D	
	13.5	12.9	1.1×10^{-4}	F			V. D	
	12.1	11.9	1.0×10^{-4}	F			V. D	
2.9	(2.9)		1.3×10^{-4}	W	18°, 22°	40°	B	
4.3	11.5	10.8	9.7×10^{-5}	S	36°, 34°	70°	B	
7.0	13.5	12.6	1.2×10^{-4}P	F			T	
11.1	14.8	14.0	1.2×10^{-4}P	F			T	
10.3	13.9	13.2	1.1×10^{-4}P	F			T	
10.2	14.7	13.9	1.1×10^{-4}P	F	45°	(90°)	T	
1.57	(1.6)		1.1×10^{-4}	S	20°, 19°	39°	B	
2.6	11.3	11.0	9.3×10^{-5} 1.4×10^{-4}P	F			T	
	13.5	12.8	6.3×10^{-5} 1.2×10^{-4}P	F			T	
	13.5	12.7	8.7×10^{-5} 1.2×10^{-4}P	F			D	
	14.4	13.6	1.1×10^{-4}	F			V. D	

Number for index	Rock		Confining pressure (kg/cm²)	Axial shortening at confining pressure	Differential stress (kg/cm²) at strain 1 (%)	2 (%)	5 (%)	10(%)	Ultimate strength (kg/cm²)
		6	2000	0.028	428	762	1460	2448	
S56	S E F	1	1	0	47	210			220
		2	200	0.0013	658	1160	877		1160
		3	500	0.0069	732	1580	1604	1512	1634
		4	1000	0.014	1064	1780	2072	2282	2283
		5	1500	0.019	896	1332	1867	2346	
		6	2000	0.020	896	1662	2535	3336	
S57	S E G	1	1	0	228				595
		3	500	0.0054	870	1670	1398		1742
		4	1000	0.0097	1240	2000	2265		2280
		5	1500	0.012	1240	1930	2504	2458	2512
		6	2000		1240	1789	2062	2258	
S58	S F A	2	200	0.016	135	220	303		317
		3	500	0.023	135	270	472	681	
		4	1000	0.030	216	398	769	1358	
		5	1500	0.042	280	532	1079		
S59	S F B	1	1		403				460
		2	200	0.00056	635	1030	904		1058
		3	500	0.0047	1062	1462	1605	1540	1622
		4	1000	0.011	922	1462	2000	2140	2162
		5	1500	0.013	535	1253	2266	2793	2800
		6	2000	0.023	922	1638	2734	3294	3330
S60	S F C	1	1		927				1230
		3	500	0.0052	2320	2790	2540		2873
		4	1000	0.059	2450	3723	3827		3703
		5	1500		1240	2227	3457	3897	3773
S61	S F D	1	1		515				573
		3	500	0.0070	912	1492			1533
S62	X Q	3	1		332				362
		16	300	0.0020	465	880			970
		2	500	0.0065	498	1037	1302		1312

Ductility-strain at macro-fracturing (%)	Total strain (%)	Residual strain (%)	Strain rate (/sec)	Type of failure	Angle of macro-fractures θ	Angle of macro-fractures 2θ	Behavior of deformation	Remarks
	14.45	13.55	1.1×10^{-4}				V. D	
2.0			1.1×10^{-4}	S	11°～17°	34°	V. B	
2.06	11.3	10.6	7.4×10^{-5}	S	37°, 39° 45°, 33°	78°	B	
3.2	13.5	12.8	7.0×10^{-5} 1.3×10^{-4}P	F		80°	T	
10.6	14.1	13.1	6.3×10^{-5} 1.2×10^{-4}P	F			D	
	12.7	11.8	1.0×10^{-4}	F			V. D	
	13.1	12.2	9.6×10^{-3}	F			V. D	
1.92				W	9°～17°	34°	V. B	
2.54	12.56	11.62	6.9×10^{-5}	S	27°～30°	58°	B	
4.15	9.30	7.62	6.0×10^{-5} 1.4×10^{-4}P	F	37°～40°	80°	T	
4.9	13.70	12.32	5.8×10^{-5} 1.3×10^{-4}P	F	40°	80°	T	
	14.6	13.74		F	42°	84°	D	
6.1	7.5	7.2	1.25×10^{-4}	F			V. D	
	15.65	15.15	1.27×10^{-4}	F			V. D	
	14.7	13.96	1.14×10^{-4}	F			V. D	
	9.8	9.2	1.05×10^{-4}	F			V. D	
1.1			4.58×10^{-5}	W	23°	46°	V. B	
2.6			7.62×10^{-5}	S	31°(33°)	64°	B	
4.4	11.9	10.9	8.8×10^{-5} 1.3×10^{-4}P	F	(38°)	(76°)	T	
8.5	13.5	12.3	1.22×10^{-4} 1.21×10^{-4}P	F	(40°)	(80°)	T	
10.3	15.5	14.8	1.00×10^{-4} 1.19×10^{-4}P	F			T	
11.4	13.5	12.3	9.82×10^{-5} 1.13×10^{-4}P	F			D	
1.5			6.66×10^{-5}	W	13°	26°	V. B	
1.6			8.35×10^{-5}	S	30°, 23°	53°	B	
3.0	6.9	5.9	6.9×10^{-5} 1.00×10^{-4}P	N	33°, 28° 23°, 35°	60°	T	
11.7	13.5	12.5	8.15×10^{-5} 1.16×10^{-4}P	N	27°, 37° 31°, 32°	64°	T	
1.15			7.67×10^{-5}	W	15°	30°	V. B	
2.25	4.0	3.3	8.34×10^{-5}	S	29°, 35°	64°	B	
1.2	1.9	1.3		W	15°, 17°	34°	B	
2.9	4.3	4.0	8.2×10^{-6}	S	38°	76°	B	
3.75	8.1	7.3	8.9×10^{-6} 1.4×10^{-5}P	N	33°, 36°	69°	T	

Number for index	Rock		Confining pressure (kg/cm²)	Axial shortening at confining pressure	Differential stress (kg/cm²) at strain 1 (%)	2 (%)	5 (%)	10(%)	Ultimate strength (kg/cm²)
		8	1000	0.0070	664	1123	1727	1834	1860
S63	XR	2	1		570	700			760
		17	200	0.00010	1480	1690			1780
		12	400		1270	1730	1220		1740
		1	500	0.0041	1100	1630	1500		1730
		19	600	0.0023	1270	1800	1760		2040
		14	600	0.0064	1270	1800	2020	1980	2030
		13	800	0.0018	960	1580	1820		1870
		15	800	0.0048	1270	2000	2170	2000	2210
		8	1000	0.0082	1270	1900			2190
		10	1000	0.0090	1270	1800	2210	2150	2250
		9	1200	0.0080	1270	2040	2740	2760	2800
		11	1500	0.011	1270	2040	2940	3190	3200
		7	2000	0.012	1270	2040	3000		
S64	XT	1	1		926				1532
		9	500	2.56×10^{-3}	1347	2710	2239		2980
		4	1000	7.80×10^{-3}	1514	2842			3899
		2	1500	8.82×10^{-3}	1347	2441	4108	3987	4172
		5	2000	1.44×10^{-2}	1347	2710	4360	4704	4704
		8	2500	1.781×10^{-2}	1431	2747	5185	5727	5758
S65	XS	1	1		66	157	144		302
		3	500	1.61×10^{-2}	216	426	639	915	1108
		4	1000	2.82×10^{-2}	210	305	689	1111	
		5	1500	2.40×10^{-2}	180	446	1000	1767	
S66	XO	1	1		834				1126
		2	500	4.19×10^{-3}	1470	2815	3762	3311	3841
		3	1000	8.84×10^{-3}	1252	2483	4291	5278	5411
		5	1500	1.15×10^{-2}	1060	2318	5113		
S67	XP	1	1						960
		3	500	1.4×10^{-3}	1706	2659	2398		2660
		4	1000	9.06×10^{-3}	2575	4241	3886		5000

Ductility-strain at macro-fracturing (%)	Total strain (%)	Residual strain (%)	Strain rate (/sec)	Type of failure	Angle of macro-fractures θ	Angle of macro-fractures 2θ	Behavior of deformation	Remarks
11.7	20.6		9.1×10^{-6} 1.2×10^{-5}P	N	37°, 33°	70°	T	
1.4				S	22°	40°	V. B	
1.5	3.2		3.6×10^{-5}	S	26°, 30°	56°	B	
2.6	5.8		6.3×10^{-5}	S	32°, 30°	62°	B	
2.5	5.8	5.0		S	32°	64°	B	
3.0	10.1	9.1	4.8×10^{-5} 1.8×10^{-4}P	S		70°	B	
3.7	13.3	12.6	4.5×10^{-5} 2.1×10^{-4}P	N	35°, 37°	72°	T	
4.4	9.7	9.2	6.3×10^{-5} 1.2×10^{-4}P	N	37°, 24°	61°	T	
3.0	17.2	16.6	4.2×10^{-5} 1.3×10^{-4}P	N	36°, 28° 45°, 35°	64°~ 80°	T	
4.5	4.8	3.9	4.1×10^{-5}	F			T	
3.8	13.0	12.1	5.4×10^{-5} 1.2×10^{-4}P	F			T	
6.3	10.7	9.9	7.8×10^{-5} 1.45×10^{-4}P	F			T	
9.2	9.8	9.2	5.6×10^{-5} 1.2×10^{-4}P	F			T~D	
	7.5	6.9	8.1×10^{-5}	F			D	
1.6			8.21×10^{-5}	W	8°, 7°	15°	V. B	
2.4			10.0×10^{-5}	S	11°, 18° 21°	39°	V. B	
3.4			11.7×10^{-5}	S	28°, 21°	49°	B	
6.5	11.9	7.2		S	29°, 31°	60°	T	
6.5	13.1	10.6	9.16×10^{-5} 11.3×10^{-5}P	S	30° 40°	60°~ 70°	T	
7.2	12.5	10.5	8.78×10^{-5} 10.4×10^{-5}P	N	43°, 44° 38°	(82°)	T	
2.1			8.04×10^{-5}	S	15°	30°	B	
14.9	15.6	14.5	12.0×10^{-5} 12.5×10^{-5}P	F			T~D	
	15.1	14.2	11.4×10^{-5}	F			V. D	
	14.7	13.7	12.1×10^{-5}	F			V. D	
1.3			6.67×10^{-5}	W	26°, 15°	41°	V. B	
6.0	14.2	12.9	8.89×10^{-5} 12.5×10^{-5}P	N	27°, 34°	63°	T	
11.8	15.1	12.9	9.05×10^{-5} 12.6×10^{-4}P	N	37°, 32°	69°	T	
	6.0		12.9×10^{-5}	F			V. D	
0.6			5.0×10^{-5}	W	28°, 20°	48°	V. B	
1.9			7.92×10^{-5}	N	32°, 30°	62°	V. B	
2.9			11.7×10^{-5}	N	30°, 34°	64°	B	

Number for index	Rock		Confining pressure (kg/cm²)	Axial shortening at confining pressure	Differential stress (kg/cm²) at strain 1 (%)	2 (%)	5 (%)	10(%)	Ultimate strength (kg/cm²)
		5	1500	7.11×10^{-3}	2575	4365	5525		5719
		11	2000	1.53×10^{-3}	2776	5204	6883		6965
S68	XZ	2	1		16	33	59		60
		24	300	0.0017	28	50	105		
		3	500	0.0058	34	69	175		
S69	XIL	1	1		1200	1923			2010
		5	500	0.0020	2633	3910	2013		4247
		10	1000	0.0018	2733	5207	3410		5207
		7	2000	0.0044	3833	6850	5847	4467	7467
S70	XIN	1	1		300				440
		3	500	0.0018	1080	1713	2027		2073
		7	1000	0.0036	1580	2493	2980		3167
		6	1500	0.0069	1400	2540	4167	4163	4373
		10	2000	0.0096	1400	2540	4413	4850	4867
S71	XIP	1	1		134	127	94		134
		3	500	0.0031	1137	1853	1913		1973
		6	1000	0.0062	1739	3579	3856		4130
		7	1500	0.010	1003	1605	2582	3421	
		9	2000	0.013	1064	1706	2893	4010	
S72	YP	7	1						120
		8	1000	0.029	303	415			442
		6	1500	0.027	374	534			548
S73	YQ	1	1		205				290
		7	500	0.022	93	152	311	450	
		6	1000	0.035	170	311	612	958	
		9	1500	0.050	208	374	785	1356	
S74	YO	10	1		170				212
		1	500	0.0024	126	230	431	628	
		4	1000	0.0058	83	150	328	628	
		9	1500	0.0072	142	277	617	1040	
S75	YT	1	1						155

Ductility-strain at macro-fracturing (%)	Total strain (%)	Residual strain (%)	Strain rate (/sec)	Type of failure	Angle of macro-fractures θ	Angle of macro-fractures 2θ	Behavior of deformation	Remarks
3.3				N	31°～34° 37°	70°	B	
4.4	10.1	18.3	7.42×10^{-5} 7.34×10^{-5}P	N	40°	80°	B	
5.7	6.9	5.1	9.1×10^{-5}P	S	32°, 37°	69°	B	
	7.0		1.1×10^{-4}P	F			V. D	
	7.2		1.3×10^{-4}P	F			V. D	
1.6			3.33×10^{-5}	W		22°	V. B	
1.7			2.96×10^{-5}	S	28°, 25°	53°	B	
2.0			3.25×10^{-5}	S	29°	58°	B	
2.3			2.64×10^{-5}	S		68°	B	
0.5			4.17×10^{-5}	W	25°	45°	V. B	
3.1	7.6	6.6	5.47×10^{-5} 1.37×10^{-4}P	S	30°	60°	T	
6.0	9.7	8.65	6.86×10^{-5} 1.33×10^{-4}P	S	33°, 30°	63°	T	
6.3	11.6	10.25	5.33×10^{-5} 1.33×10^{-4}P	S	34°	68°	T	
8.6	15.5	14.5	5.58×10^{-5} 1.24×10^{-4}P	F	47°	(84°)	T	
0.6			4.17×10^{-5} 1.22×10^{-4}P	W	13°, 13°	26°	B	
3.5	7.6	6.4	6.25×10^{-5} 1.29×10^{-4}P	S	32°, 30°	62°	B	
3.2	5.7	4.4	4.12×10^{-5} 1.29×10^{-4}P	N	31°, 32°	63°	B	
	16.3	15.1	1.09×10^{-4}	S	32°	64°	V. D	
	13.0	11.6	1.02×10^{-4}	S	11°	22°	V. D	
0.7				W	22°	44°	V. B	
1.23	3.10	3.02	1.2×10^{-4}	F			T	
1.67	4.60	4.43	1.2×10^{-4}	F			T	
1.4			7.8×10^{-5}	W	27°, 18°	54°	V. B	
	21.9	20.8	2.5×10^{-4}	F			V. D	
	10.7	10.1	1.0×10^{-4}	F			V. D	
	13.9	13.0	1.1×10^{-4}	F			V. D	
1.3			7.2×10^{-5}	S	21°, 26°	47°	V. B	
	19.0			F			V. D	
	17.60	15.8	2.3×10^{-4}	F			V. D	
	17.0	14.8	2.2×10^{-4}	F			V. D	
0.9			6.0×10^{-5}	W	36°	(72°)	V. B	

Number for index	Rock		Confining pressure (kg/cm²)	Axial shortening at confining pressure	Differential stress (kg/cm²) at strain 1 (%)	2 (%)	5 (%)	10(%)	Ultimate strength (kg/cm²)
		5	500	0.0018	81	127	292	500	
		4	1000	0.0058	208	364	754	1233	
		6	1500		208	415	983	1788	
S76	ZM	1	1		190				200
		5	1						
		6	20	0.0014	252	322	267		322
		7	50	0.0017	219	287	330		331
		8	100	0.0019	235	335	417	440	440
		9	300	0.0050	235	364	550	696	
		2	500	0.014	135	236	464		
		3	1000	0.037	134	261	595	1030	
		4	1500	0.055	194	368	887	1632	
S77	ZO	1	1						142
		6	500	0.010	122	163	327	584	
		3	1000	0.042	188	339	714	1237	
		4	1500	0.067	163	339	918	1665	
S78	ZP	1	1		320				324
		2	500	0.010	260	426	678	945	
		3	1000	0.031	183	325	692	1134	
		4	1500	0.051	260	478	969	1599	
S79	ZQ	1	1						80
		2	500	0.021	98	179	379	670	
		3	1000	0.080	223	393	786	1286	
		4	1500	0.088	170	330	902	1696	
S80	ZR	1	1						80
		2	500	0.036	53	101	285	592	
		3	1000	0.082	206	395	860	1570	
		4	1500	0.091	232	443	1013	1930	
S81	ZS	1	1						125
		2	500	0.026	101	180	441	705	
		3	1000	0.030	163	295	700	1247	

Ductility-strain at macro-fracturing (%)	Total strain (%)	Residual strain (%)	Strain rate (/sec)	Type of failure	Angle of macro-fractures θ	Angle of macro-fractures 2θ	Behavior of deformation	Remarks
	17.5		1.2×10^{-4}	F			V. D	
	13.0	12.2	1.2×10^{-4}	F			V. D	
	17.0			F			V. D	
1.3			8.7×10^{-5}	W	21° 22°	44°	V. B	
			7.2×10^{-5}	W	11°, 12°	23°	V. B	
1.86	6.1	5.8	1.2×10^{-4}	W	17°, 16° 18°	34°	B	
4.74	7.0	6.9		S	37°	74°	T	
11.00	18.7	18.5		F			T	
	22.4	21.7		F			D	
	5.7	5.4	1.06×10^{-4}	F			V. D	
	19.5	18.5	1.2×10^{-4}	F			V. D	
	16.2	15.6	1.04×10^{-4}	F			V. D	
0.8			5.3×10^{-5}	S	24°, 22°	46°	V. B	
	21.6	20.7	1.2×10^{-4}	F			V. D	
	18.3	17.1	1.1×10^{-4}	F			V. D	
	17.4	16.4	1.2×10^{-4}	F			V. D	
1.05				W	16°(33°)	32°(66°)	V. B	
	16.9	15.2		F			V. D	
	16.8	16.0		F			V. D	
	19.2			F			V. D	
0.8	2.4	2.1	6.7×10^{-5}	W	8°	16°	V. B	
	19.3	18.5	1.2×10^{-4}	F			V. D	
	13.5	13.2	1.2×10^{-4}	F			V. D	
	14.1	13.8	1.2×10^{-4}	F			V. D	
0.9	1.4	1.1	6.0×10^{-5}	W	21° 29°	58°	V. B	
	21.0	20.2	1.24×10^{-4}	F			V. D	
	16.0	15.1		F			V. D	
	13.6	12.8	1.19×10^{-4}	F			V. D	
0.9	1.5	1.3	5.5×10^{-5}	S	31°	62°	V. B	
	19.0	18.3	1.24×10^{-4}	F			V. D	
	14.3	13.5	1.14×10^{-4}	F			V. D	

Number for index	Rock		Confining pressure (kg/cm²)	Axial shortening at confining pressure	Differential stress (kg/cm²) at strain 1 (%)	2 (%)	5 (%)	10(%)	Ultimate strength (kg/cm²)
		4	1500	0.089	189	352	903	1736	
S82	ZT	1	1						80
		1	500	0.026	72	129	321	691	
		2	1000	0.060	108	209	546	1044	
		3	1500	0.064	161	313	876	1715	
S83	ZU	1	1		660				690
		2	500	0.0033	802	1302	1788	1865	1890
		3	1000	0.0097	712	1233	2017	2521	2985
		1	1500	0.011	354	694	1510	2465	
S84	ZW	1	1		718				935
		2	500	0.0033	976	1559			1814
		3	1000	0.0064	976	1664	2644	2922	2949
		1	1500	0.011	976	1664	3024	3728	3735
S85	XA	1	1	0	2667	3127			3510
		5	500	0.77×10^{-3}	3367	5470			5763
		6	1000	1.03×10^{-3}	4567	7453			7667
		39	1500	5.44×10^{-3}	1800	6200			9500
S86	XB	2	1	0	333				467
		3	500	1.54×10^{-3}	750	2150			2517
		5	1000	2.31×10^{-3}	848	2635			3500
		10	1500	8.87×10^{-3}	1700	4000			4833
S87	XC	6	1	0	1099				1150
		1	500	1.19×10^{-3}	2177	2909			2980
		3	1000	4.04×10^{-3}	2953	3836	3547		4040
		1	1500	5.93×10^{-3}	3190	4073	4276	4039	4310
		55	2000	5.59×10^{-3}	3405	4224	5078	4909	5172
		7	2500	2.77×10^{-3}	3526	4397	5767	5789	
S88	XD	2	1	0					1517
		1	1000	4.21×10^{-3}	2700	4530	3910		4966
		8	1500	3.72×10^{-3}	3060	5410	5500		5767
		3	2000	5.56×10^{-3}	3060	5250	6500		6634

Ductility-strain at macro-fracturing (%)	Total strain (%)	Residual strain (%)	Strain rate (/sec)	Type of failure	Angle of macro-fractures θ	Angle of macro-fractures 2θ	Behavior of deformation	Remarks
	16.6	15.7	1.32×10^{-4}	F			V. D	
0.6	4.2	3.8	5.7×10^{-5}	W	17°	34°	V. B	
	15.6	15.0	1.16×10^{-4}	F			V. D	
	17.4	17.0	1.27×10^{-4}	F			V. D	
	15.2	14.3	1.16×10^{-4}	F			V. D	
1.1			6.2×10^{-5}	W	28°	56°	V. B	
7.8	12.9	11.4	1.10×10^{-4}	S	28°, 30°	58°	T	
18.2	22.0	20.6		N	31°～33° 43°～45°	68°～88°	T	
	19.0	18.4	1.04×10^{-4}	F	(38°)	(76°)	V. D	
1.27			5.3×10^{-5}	W	16°	32°	V. B	
3.2	4.7	3.5	8.3×10^{-5} 1.2×10^{-4}P	S	27°, 28°	55°	B	
8.5	12.2	10.6	6.7×10^{-5} 1.2×10^{-4}P	S	32°, 31°	63°	T	
10.65	16.7			F	(38°, 40°)	(78°)	T	
1.2				W	7°, 8°	15°	V. B	4th gear
1.6			4.29×10^{-5}	S	16°, 15°	31°	V. B	
1.8			3.91×10^{-5}	S	17°	33°	V. B	
3.0				S	15°, 23°	38°	V. B	
1.2			4.34×10^{-5}	S		48°	V. B	
2.58	4.7	3.7	7.28×10^{-5} 8×10^{-5}P	S		70°	B	
3.82	6.6	5.1	4.35×10^{-5} 1.15×10^{-4}P	S		74°	B	
3.61	8.9		9.64×10^{-5} 9.17×10^{-5}P	S		78°	B	
1.0			3.7×10^{-5}	W		37°	V. B	
1.6			4.1×10^{-5} 1.5×10^{-4}P	S	28°	54°	B	
3.2	8.22	7.45	2.8×10^{-5} 1.2×10^{-4}P	S	33°	66°	B	
3.8	10.58	9.96	2.8×10^{-5} 2.8×10^{-4}P	N	35°, 30°	75°	T	
	16.52	15.27	2.5×10^{-5} 1.31×10^{-4}P	F			T	
	16.13	15.1	2.5×10^{-5} 1.18×10^{-4}P	F			D	
0.7			1.67×10^{-5}	W		50°	V. B	
3.0	9.2	7.8	9.08×10^{-5} 11.7×10^{-5}P	N		71°	B	
3.9	9.5		7.12×10^{-5} 9.95×10^{-5}P	N		74°	B	
4.2	9.5		8.89×10^{-5} 10.1×10^{-5}P	N		74°	B	

Number for index	Rock		Confining pressure (kg/cm²)	Axial shortening at confining pressure	Differential stress (kg/cm²) at strain 1 (%)	2 (%)	5 (%)	10(%)	Ultimate strength (kg/cm²)
S 89	X E	**1**	1	0	417				867
		13	1000	2.05×10^{-3}	1210	2897			4000
		6	2000	5.74×10^{-3}	920	3133	5333		5567
S 90	X F	2	1	0	1197				1478
		63	500	5.3×10^{-3}	2334	2759			3010
		64	1000	7.18×10^{-3}	3010	2759	4181		4358
		53	2000	7.2×10^{-3}	3177	5030	5957	5853	5977
S 91	X G	1	1		833				933
		4	1000	5.95×10^{-5}	2492				3533
		18	2000	8.05×10^{-3}	1000	3300			5866
S 92	X M	3	1						1400
		5	500	1.38×10^{-3}					3166
		6	1000	6.65×10^{-3}					4300
S 93	H S A	2	1		700				700
		3	500	0.0026	1553	2916	1943		2975
		4	1000	0.0062	2333	3756	3193	3217	3885
		5	1500	0.0082	2816	4490	4477	4173	4654
S 94	H S B	2	1		562				664
		3	500	0.0054	1351	2184	1756	1873	2245
		4	1000	0.0054	1388	2462	2920	2659	2945
		5	1500	0.0072	1472	2669	3843	3512	3840
S 95	H S C	1	1		444				450
		5	500	0.0013	875	1492	1478	1448	1530
		4	1000	0.0059	1034	1646	1875	2148	
S 96	H S D	2	1		387				498
		3	500	0.0051	1017	1733	1743	1733	1900
		4	1000	0.0098	1350	2290	2649	2533	2340
		5	1500	0.012	1350	2526	2803	2649	2963
S 97	H S E	1	1		1308				1773
		2	500	0.00062	2458	3385			3421
		3	1000	0.0022	2736	4472			4532

Ductility–strain at macro-fracturing (%)	Total strain (%)	Residual strain (%)	Strain rate (/sec)	Type of failure	Angle of macro-fractures θ	Angle of macro-fractures 2θ	Behavior of deformation	Remarks
1.35			5.42×10^{-5}	S	20°, 21°	41°	V. B	
3.84	7.1	5.9	5.28×10^{-5} 12.1×10^{-5}P	S	30°, 33°	63°	B	
6.64	11.8	10.2	7.41×10^{-5} 9.60×10^{-5}P	S	35°, 37°	72°	T	
1.45			3.38×10^{-5}	W		14°	V. B	
1.55				S		52°	B	
2.8	7.6	6.4		N	35°, 30°	65°	T	
5.45	15.7	14.1	6.68×10^{-5} 11.2×10^{-5}P	N		75°	T～D	
1.0			2.85×10^{-5}	S		60°	V. B	
1.82	1.6		5.93×10^{-5}	S		60°	V. B	
4.55	8.4	6.8	8.09×10^{-5} 8.95×10^{-5}P	S	30°, 32°	62°	B	
0.88			3.66×10^{-5}	W		38°	V. B	
2.3			7.28×10^{-5}	N	27°, 26°	53°	B	
2.6	6.4	5.7	7.18×10^{-5} 9.80×10^{-5}P	N	30°, 33°	63°	B	
1.0	2.4	2.1	3.4×10^{-5}	W	12°(18°)	30°	V. B	
2.26	6.3		4.4×10^{-5} 1.3×10^{-4}P	S	25°～26° 35°～34°	51° 69°	B	double peaks
2.47	11.6		3.8×10^{-5} 1.3×10^{-4}P	N	29°～27° 30°～34°	56° 64°	B	double peaks
2.93	12.7		3.4×10^{-5} 1.4×10^{-4}P	N	41°～39° 39°～40°	80°	T	
1.2	2.6			W	20°, 21°	41°	B	
2.54	13.6	13.0	4.6×10^{-5} 1.4×10^{-4}P	S	36°, 37°, 28°, 39°	64° 71°	B	double peaks
4.34	11.6	10.5	5.0×10^{-5} 1.4×10^{-4}P	S	34°, 33°	67°	T	
5.22	12.4	11.2	5.6×10^{-5} 1.4×10^{-4}P	S	34°, 28°	62°	T	
1.0	1.9	1.6	2.6×10^{-5}	W	26°, 25°	41°	V. B	
2.5	14.0	13.4	5.8×10^{-5} 1.3×10^{-4}P	F	40°	(80°)	T	
	14.4	13.6	5.8×10^{-5} 1.3×10^{-4}P	F			D	
1.3	2.2	1.9					V. B	
3.0	10.6	11.0	6.0×10^{-5} 1.3×10^{-4}P	S	31° 33°, 32°	62° 65°	B	
4.0	13.6	12.8	5.4×10^{-5} 1.3×10^{-4}P	F		(84°)	T	
3.1	10.9	9.4	4.4×10^{-5} 1.2×10^{-4}P	F			T	
1.2	3.4	3.0	3.4×10^{-5}	W	0°～14°	28°	V. B	
1.85	4.0	3.5	3.4×10^{-5}	S	13°, 21°	34°	V. B	
2.2	4.8	4.4	2.8×10^{-5}	S	22°, 24°	46°	V. B	

Number for index	Rock		Confining pressure (kg/cm²)	A ial shortening at confining pressure	Differential stress (kg/cm²) at strain 1 (%)	2 (%)	5 (%)	10(%)	Ultimate strength (kg/cm²)
		4	1500	0.0043	3294	5092			5582
		5	2000	0.0059	3395	5234	5753		6368
S98	HSF	1	1		1600				1740
		2	500	0.0019	2253	3780			3800
		3	1000	0.0025	2913	5093			5363
		4	1500	0.0025	3440	6100			6660
		5	2000	0.0046	1847	5333	6167		7273
S99	HSG	1	1		800				1100
		2	500	0.0028	1367	2294	1894	2243	2323
		3	1000	0.0049	1867	5500			5898
		4	1500	0.0077	1867	4917			6277
		5	2000	0.0098	1550	4467			6633
S100	HSH	2	1		800				1567
		3	500	0.00064	2250				3533
		4	1000	0.0033	1967	4100			4110
		5	1500	0.0057	2250	5500			5867
S87	XC	29	1						1071
		26	500	1.19×10^{-3}	2254	2050			2907
		107	500	3.84×10^{-3}	2589 2101	3222			3223
		52	1000	5.7×10^{-3}	2769	3887	3279		4009
		9	1000	9.4×10^{-3}	2829	3860			3923
		14	1000	4.4×10^{-3}	3124 2798	3201			4143
		34	1500	7.0×10^{-3}	2487 2509	3770	4308		4309
		39	1500	9.1×10^{-3}	2415	3962	4573		4585

Ductility-strain at macro-fracturing (%)	Total strain (%)	Residual strain (%)	Strain rate (/sec)	Type of failure	Angle of macro-fractures θ	Angle of macro-fractures 2θ	Behavior of deformation	Remarks
3.1	9.5	9.4	3.0×10^{-5}	S	32°, 30°	62°	B	
4.1		13.2	3.4×10^{-5} 1.2×10^{-4}P	S	33°, 31°	64°	B	double fractures
1.1	1.1		2.3×10^{-5}	W	15°	30°	V. B	
2.16	4.6	3.7	2.9×10^{-5}	S	22°, 26° (21°)	43°～47°	V. B	
2.67	6.0	5.4	3.0×10^{-5}	S	28°, 25°	53°	V. B	
2.70	11.4		3.0×10^{-5}	S	33°, 34°	67°	V. B	
3.5	9.9		3.2×10^{-5}	S	33°, 36°	69°	B	
1.24	1.24		5.0×10^{-5}	W	17°, 19°	36°	V. B	
2.14	12.0	11.0	5.4×10^{-5} 1.3×10^{-4}P	S	22°, 19° 36°, 30°	41° 66°	V. B	double peaks
2.22	2.22		3.2×10^{-5}	S	25°, 25°	50°	V. B	
2.97			3.4×10^{-5}	S	30°, 31°	61°	V. B	
3.64			3.2×10^{-5}	S	30°, 34°	64°	V. B	
1.44	1.44		5.0×10^{-5}	W	22°, 22°	44°	V. B	
1.76			3.2×10^{-5}	S	22°, 23° (25°)	46°	V. B	
2.05			3.4×10^{-5}	S	24°, 28°	52°	V. B	
2.44			3.0×10^{-5}	S	30°, 28°	58°	V. B	
0.73			2.7×10^{-6}	W			V. B	4th gear
1.53	2.85	2.40	3.5×10^{-6} 1.2×10^{-5}P	S	25°	50°	B	4th gear Repeated Load
1.99	2.18		3.7×10^{-6}				B	4th gear
2.67	6.51		2.7×10^{-6} 1.3×10^{-5}P	S	32°	64°	B	4th gear
2.47	3.07	2.36	2.8×10^{-5} 6.6×10^{-5}P	S	32°	64°	B	Hand Pump Repeated Load
2.51	4.24	3.30	6.7×10^{-6} 3.7×10^{-5}P	S	33°	66°	B	4th gear
4.97	8.54	7.61	3.7×10^{-6} 1.3×10^{-5}P	F			T	4th gear
5.21	6.37	5.49	3.3×10^{-6} 1.1×10^{-5}P				T	4th gear

IV. 2 Argillaceous rocks

Oligocene argillaceous rocks

Tested specimens are XA(S85) : Tokuman shale, Nishisonogi group, northwestern Kyushu ; HSH(S100) : Mikaeri shale, Kishima group from Nagasaki Prefecture ; ZW (S84) : Hayama group siltstone ; JT (S14) : Shirasaka shale, Shiramizu group, Joban ; KSA(S1) : Charo shale and KSC(S3) : Shakubetsu shale from Kushiro, Hokkaido. Except Hayama siltstonea nd Shirasaka shale, they all are hard black shale. Tokuman shale is very brittle up to 1500kg/cm^2 of confining pressure and has strength more than 9000 kg/cm^2 at 1500 kg/cm^2 confining pressure. The three shales from northern and southern ends in Japan, HSH(S100), KSA(S1), and KSC(S3) are quite similar in behavior of deformation and strength. These three are very brittle at 1 or 1000 kg/cm^2 confining pressure, and brittle at 500 to 1500kg/cm^2 confining pressure. They have ultimate strength about 1500 and 5000kg/cm^2 at 1 and 1500kg/cm^2 confining pressures, respectively. The fracture of the above four shales exhibits clearly wedge type and sharp single shear of small angle through every confining pressure. Comparing with these hard shale from Kyushu and Hokkaido, the argillaceous rocks from the basins along the Pacific coast are more ductile and weak. Shirasaka shale and Hayama siltstone are brittle up to 500kg/cm^2 confining pressure and they turn into transitional behavior at 1000 kg/cm^2. At 1500 and 2000 kg/cm^2 of confining pressures, both do not produce fracture, although the tests were continued up to strain 17% and up to more than 20%. Hayama siltstone, grey, well sorted, 36.3% in porosity, exhibits single shear fracture type at 500 kg/cm^2. At 1000 kg/cm^2, it also forms single shear with a faint trace of network deformation bands (PL.3). In Fig. 22, relation between ultimate strength and confining pressure of six Oligocene rocks are shown.

Lower Miocene argillaceous rocks

As the argillaceous rocks as old as Burdigalian stratigraphic units, we have two groups ; the first group consists of different formations among Yunagaya group, Joban coal field; and the other consists of samples of Onnagawa horizon in Nagano, Niigata, Yamagata and Akita Prefectures in northeastern Honshu. In addition, a shale from Nishikurozawa formation that is immediately below the Onnagawa in stratigraphic section is taken into this units.

Honya claystone, IC(S10) from Yunagaya group is a little tuffaceous. It is very porous and ductile rocks. At 200 kg/cm^2 confining pressure, it becomes transitional and exhibits network failure type. At 300 kg/cm^2, it produces no fracture. Two Mizunoya siltstones, JE (S11) and IB (S12) are also very ductile and weak. However, mode of stress-strain curves is a little different. JE (S11) shows visco-ductile behavior at 100 and 200 kg/cm^2 confining pressures, while IB (S12) does transitional behavior at 50 and 100 kg/cm^2 confining pressures. Both flow at extremely low confining pressure, less than 50 or 100 kg/cm^2. It seems unreasonable that Honya claystone is stronger and more brittle than Mizunoya siltstone, which is older than Honya in stratigraphic section. Possibly, this is due to the petrological characteristic of Honya claystone, that is, which is more compact, finer grained and less porous than Mizunoya siltstone.

Argillaceous rocks from the northeastern Honshu are generally much stronger and more brittle than those from the Joban area. Bessho shale, XIL (S69) which is also a typical black shale of Onnagawa horizon but a little porous, is very

brittle up to 500 kg/cm^2 confining pressure. Aosawa shale, ZK (S36), more porous, presents more ductile behavior. ZK (a) consists of black shale. It is brittle at 500 and 1000 kg/cm^2 confining pressures, but has less strength than Bessho and Nambayama shales, ZD(S47), (Fig.49). At 2500 kg/cm^2 confining pressure it becomes perfectly ductile and flows. ZK (b) consists of shale and tuff at the other end. This presents a different mode of stress-strain curves. It is more brittle in mode of deformation than ZK (a), while it tends to make network fracture type in part of tuff material than shaly part, (PL.7). NJ(S33), SBD(S27), SBC(S26), and SCC(S30) are shale belonging to Onnagawa formation in Akita Prefecture. They are from the same stratigraphic unit and show similar outlook in lithology. However, they differ in strength and ductility. In Figs. 33,34,35 and 36, stress-strain curves of 4 shales are shown. The difference might be resulted mainly from porosity. NJ(S33) and SBD(S27) are little porous about 2% at most, while SBC (S26) and SCC(S30) have porosity around 25 and 30%. The former two are very brittle and strong, while the later two are extremely ductile and weak. SBC(S26) and SCC(S30)are transitional as low as 500 kg/cm^2 confining pressure, and show ductile behavior above 1500 kg/cm^2. They are almost similar to Honya claystone of Joban area in strength and mode of deformation.

SCE (S32) was taken from Nishikurosawa formation, dated in the lower part of Burdigalian, and the oldest shale among the samples described in this section. It is again strange that SCE(S32) is the weakest and most ductile among the above-mentioned Onnagawa shales. The porosity is 25.0%, which is about the same as those of SBC (S26) and SCC(S30). The reason might be reduced to a particular stratigraphic position, in which SCE(S32) had been placed. SCE(S32) is found as thin bed between thick basaltic pyroclastic rocks. Possibly, some effect of surrounding thick volcanic material upon the petrological characteristics of the shale is a cause of weak and ductile property of this sample.

Upper Miocene argillaceous rocks

There are one sample from Sasebo group, northwestern Kyushu, seven from the middle part of Miura peninsula, southern Kwanto, one from Takaku group in Joban, one from Otokawa group in Noto peninsula, Ishikawa Prefecture, three from Shiiya formation in Niigata, one from Teradomari formation in Niigata, and two from Funakawa formation in Akita Prefecture, as argillaceous rocks in this geological age.

Kase shale, HSE(S97), that is tight, hard shale from Sasebo group, Kyushu, is very brittle up to 1000 kg/cm^2 confining pressure. Up to 2000 kg/cm^2 confining pressure it is brittle. The fracture type is sharp single shear fracture at all confining pressures except for atmospheric pressure.

The seven siltstones from Misaki formation, Miura group, have been collected within the thickness of about 800 m in stratigraphic columnar section. They are siltstone(Zp(S78) only is finer grained, thus termed claystone), and some: ZT (S82), ZS(S81), and ZQ (S79); include fine sand of volcanic origin. The porosity ranges between 40 and 45% except one, ZP(S78), which has porosity of 30.2%. They all have similar stress-strain curve at 1, 500, 1000 and 1500 kg/cm^2 confining pressures. At atmospheric pressure, they are brittle and the fractures are wedge type. However, at higher confining pressure than 500 kg/cm^2, they exhibit visco-ductile behavior. In order to study the transition of deformational behavior in more detail, the experiments were done of ZM (S76) at lower confining pressures.

In Fig. 59, the results are shown. Here, a typical transition from brittle, to ductile and to visco-ductile, is clearly presented as a function of confining pressure. At 1 and 20kg/cm^2, it is brittle, and, at 50 and 100 kg/cm^2, it shows transitional behavior. At 300 kg/cm^2, it turns into ductile behavior. Then, it becomes visco-ductile behavior at higher confining pressures than 500 kg/cm^2. In Fig. 60, a sketch shows the outlook of deformed specimens. At 20 and 50 kg/cm^2' s specimens, it is seen something like shear fractures, but, at 100 kg/cm^2 and more, no fracture is observed. The seven Misaki formation rocks have a similar strength versus confining pressure relation, that is, they are approximately 1500 kg/cm^2, 1000kg/cm^2, 800 kg/cm^2 and 200k g/cm^2 in 10% or ultimate strength at 1500, 1000, 500, and 1 kg/cm^2 confining pressures, respectively.

Mushizaki claystone from Otokawa group,X Z(S68) and Takaku group siltstone, JN (S68) are very porous, ranging 60 and 63% in porosity, and weaker than Misaki formation siltstone, as shown in Fig. 81. They are more visco-ductile than Misaki siltstone. JN(S7) shows ductile behavior at 100 kg/cm^2 confining pressure, which is observed at 300 kg/cm^2 on ZM(S76)'s stress-strain curve.

As for argillaceous rocks from Akita-Niigata province, effect of porosity on strength and deformational behavior is quite clear. Shiiya formation shale, XT (S64)and Funakawa formation shale, XV(S19), are 11 or 12% in porosity, and both show similar stress-strain relation each other, (Figs. 71 and 77). They arev ery brittle, brittle and transitional at 1, 500 and 1000 or 1500 (XV), and 1500 (XT), 2000 and 2500 kg/cm^2 confining pressures, respectively. Fracture types are also similar: wedge at atmospheric pressure, shear at 500, 1000 and 1500 kg/cm^2, and, at more than 2000kg/cm^2, network fracture or faint ductile fault. Teradomari formation shale, NF(S38) has porosity of 15.6% and is a little tuffaceous. It is transitional as early as 1000 kg/cm^2, and at 2000 kg/cm^2 it becomes visco-ductile behavior. At transitional stages, it presents good network fracture pattern. ZA (S40), one of Shiiya formation claystones is nearly equal to NF(S38) in porosity. However, deformational behavior is much more ductile. It is transitional as early as 500 kg/cm^2 confining pressure. It is interesting that ZA (S40) is more ductile at low confining pressure than NF(S38), while NF is more visco-ductile at high pressure than ZA. ZA (S40) does not produce fracture at more than 500 kg/cm^2 confining pressure. SDA(S48), Shiiya formation claystone and SCB(S29), Funakawa formation claystone are next to ZA(S40) in porosity and ductility. They are transitional at 200 kg/cm^2 confining pressure, and weaker than ZA(S40). They have network fracture (SCB), or no fracture (SDA) at 200 kg/cm^2.

Lower Pliocene argillaceous rocks

The tested samples, that belong to lower Pliocene, contain three from the upper part of Miura group, Miura peninsula, two from Taga group in Joban area, five from Nishiyama and Hamatsuda formations in Niigata, and six from Tentokuji formation in Akita Prefecture.

About the lower Pliocene argillaceous rocks, strong effect of porosity on strength and ductility is observed, too. Most samples range between 30 and 60% in porosity. Two Hamatsuda shales, XQ(S62) and XR(S63) have smaller porosity. XQ has porosity of 20.4% and XR has 7.0%.

XR(S63) is a black shale, and contains thin patch of silty sand. This impurity in material caused a little irregular stress-strain relation among the specimens deformed even at the same confining pressure,(Fig.98). It is brittle up to 500kg/cm^2,

and, between 600 and 1200 kg/cm², it shows transitional behavior. Under 500 kg/cm² confining pressure, failure type is single shear. In transitional behavior, fracture of network type will occur if the strain goes beyond 10 or 13%. At less strain than those %, no fracture is produced. XQ(S62) is more porous, more ductile and weaker than XR(S63). It becomes transitional at 500 kg/cm² confining pressure. It produced single shear fracture in the test of 8% total strain at 500 kg/cm² confining pressure. At 1000 kg/cm² confining pressure, it did not produce fracture although the total strain attained up to 20% in this test.

The remaining 14 kinds of samples show similar strength versus confining pressure relation, regardless the areas collected (Fig.112). These rocks are Zushi formation siltstones or claystone, YQ(S73), YT(S75), YO(S74); Taga siltstones, JD(S5), JZ(S6); Nishiyama siltstones, NC(S42), NB(S41), ND(S43); Tentokuji siltstones, NK(S34), SAA(S20), SBA (S24), SCA(S28), XVA(S17), XVB(S18). They show visco-ductile behavior as early as 500 kg/cm² confining pressure. SBA (S24) becomes visco-ductile at 200 kg/cm². NK(S34) turns visco-ductile at 100 kg/cm², and both JZ(S6) and JD(S5) seem to become visco-ductile at 50 kg/cm². Other rocks have not been tested in detail between 1 and 500 kg/cm². However such changes of behavior as the samples JZ, JD, NK, and SBA, are probably common in the other rocks. Therefore, it might be correct that very porous lower Pliocene argillaceous rocks, ranging 30 and 60% in porosity, behave visco-ductile at a confining pressure between 50 or 100 kg/cm².

Upper Pliocene argillaceous rocks

Two samples of Haizume formation, Niigata Prefecture were tested. They are grey siltstones, 35 or 40% in porosity. SEA (S51) becomes visco-ductile at 200 kg/cm² confining pressure. We have no data between 1 and 200 kg/cm². SEB (S52) was tested at atmospheric pressure only.

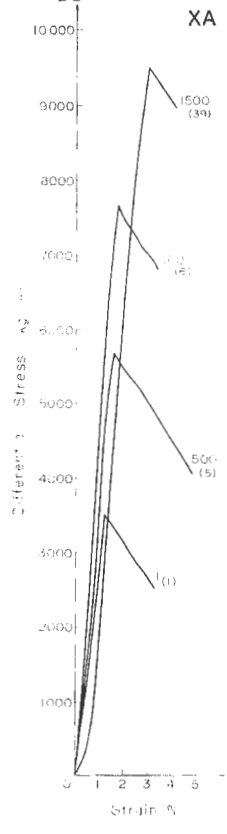

Fig. 10 Stress-strain curve for Tokuman shale, XA(S85). The numbers in the figure denote confining pressures in kg/cm². The sample numbers are enclosed with parentheses.

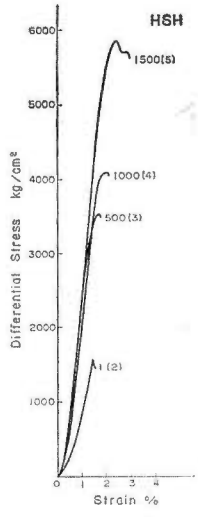

Fig. 11 Stress-strain curve for Mikaeri shale, HSH(S100).

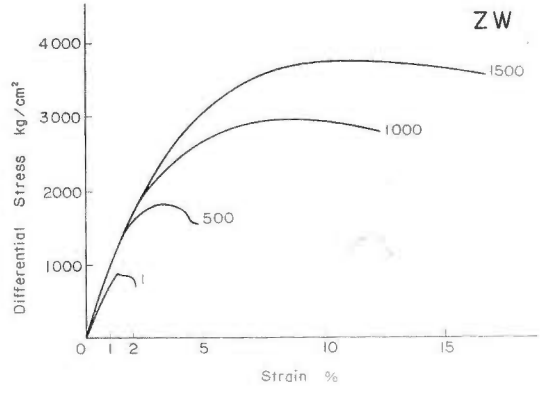

Fig. 12 Stress-strain curve for Hayama group siltstone, ZW(S84).

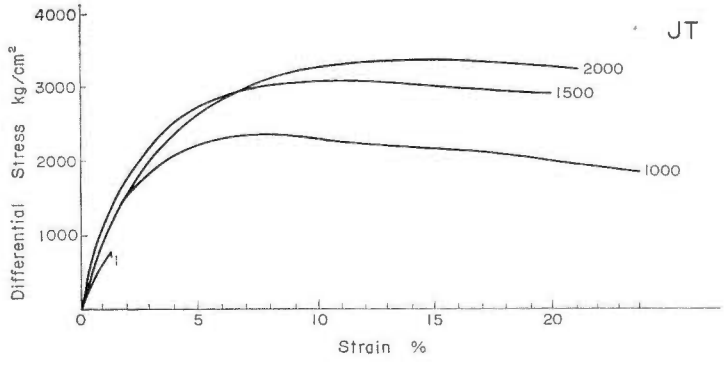

Fig. 13 Stress-strain curve for Shirasaka shale, JT(S14).

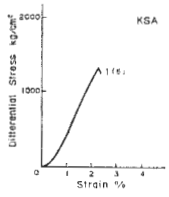

Fig. 14 Stress-strain curve for Charo shale, KSA(S1).

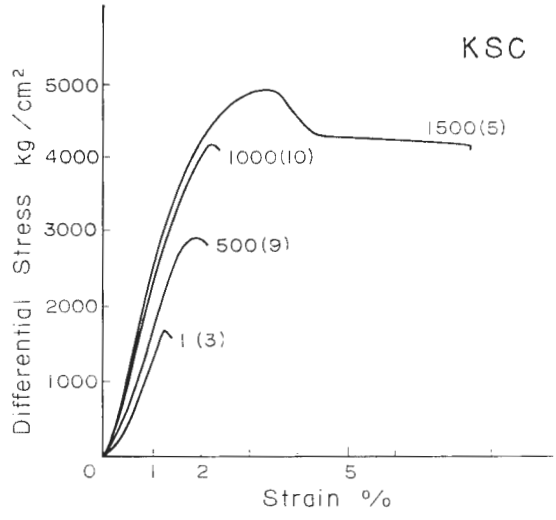

Fig. 15 Stress-strain curve for Shakubetsu shale, KSC(S3).

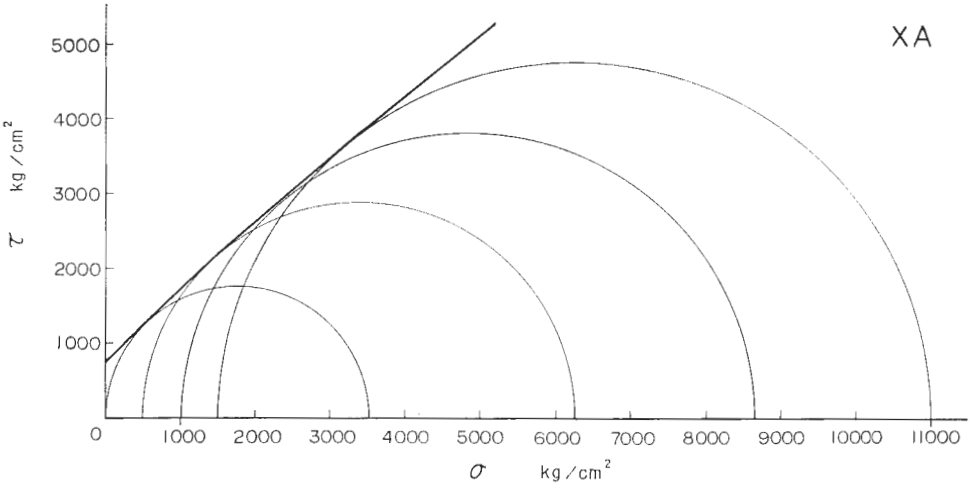

Fig. 16 Mohr envelope curve for Tokuman shale, XA(S85).
σ is normal stress, τ is shearing stress. In case of no remark, Mohr's stress circles were constructed from ultimate strength in the following figures with no remarks.

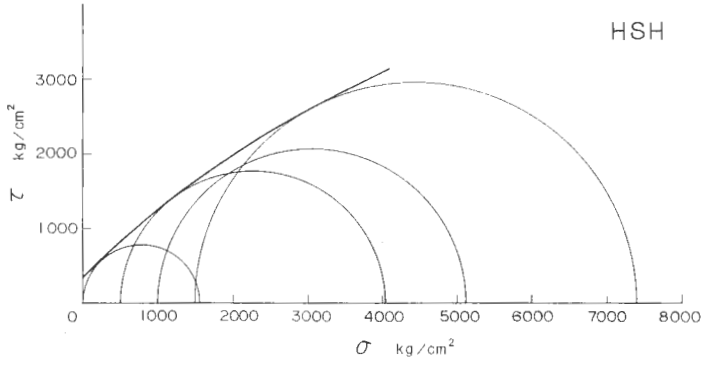

Fig. 17 Mohr envelope curve for Mikaeri shale, HSH(S100).

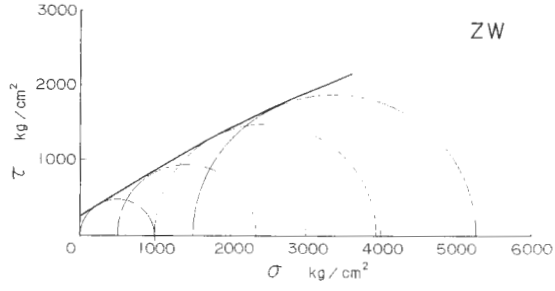

Fig. 18 Mohr envelope curve for Hayama group siltstone, ZW(S84).

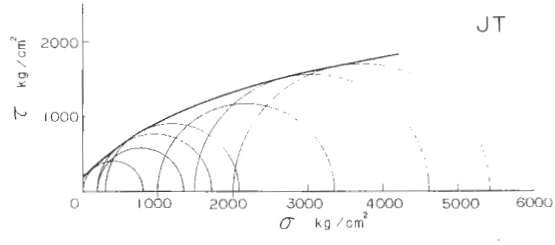

Fig. 19 Mohr envelope curve for Shirasaka shale, JT(S14).

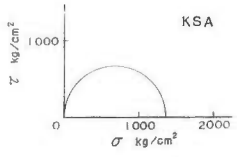

Fig. 20 Mohr envelope curve for Charo shale, KSA(S1).

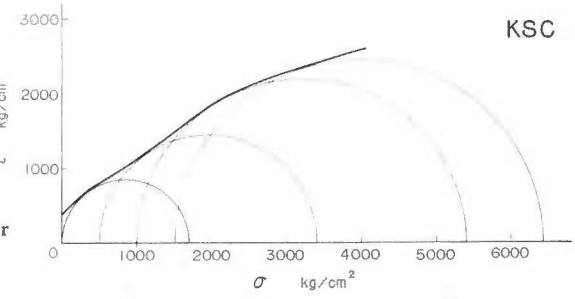

Fig. 21 Mohr envelope curve for Shakubetsu shale, KSC(S3).

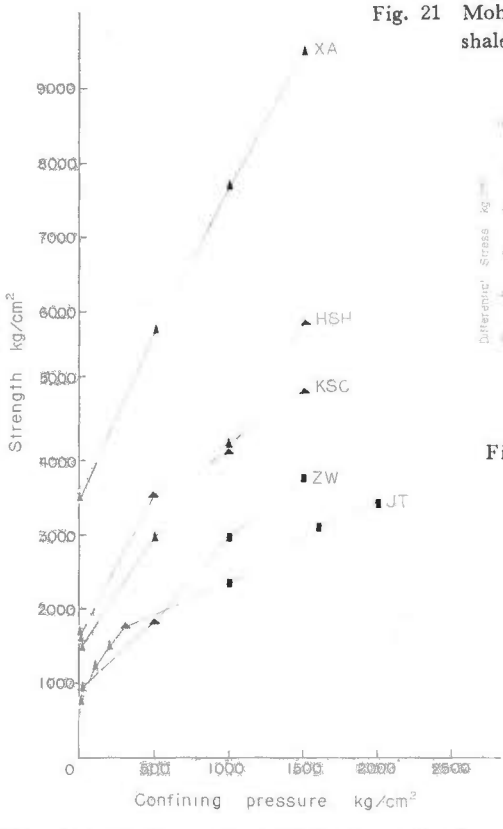

Fig. 22 Strength versus confining pressure for Oligocene argillaceous rocks, XA, HSH, ZW, JT, KSA, KSC. All points show ultimate strength. ▮, ▲, ▌ indicate very brittle, brittle, and transitional behavior, respectively.

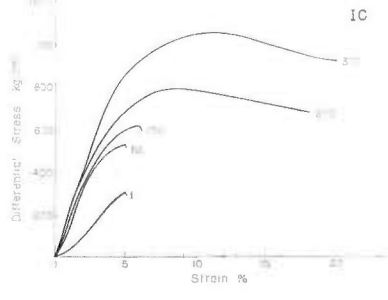

Fig. 23 Stress-strain curve for Honya claystone, IC(S10).

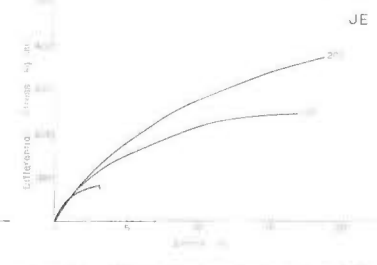

Fig. 24 Stress-strain curve for Mizunoya siltstone, JE(S11).

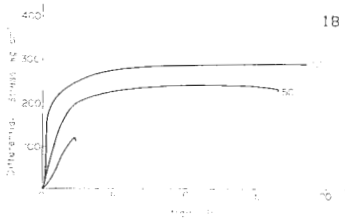

Fig. 25 Stress-strain curve for Mizunoya siltstone, IB(S12).

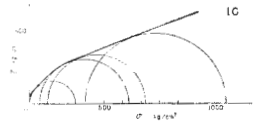

Fig. 26 Mohr envelope curve for Honya claystone, IC(S10).

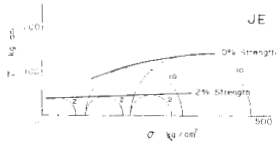

Fig. 27 Mohr envelope curve for Mizunoya siltstone, JE(S11). 2 and 10 % strength.

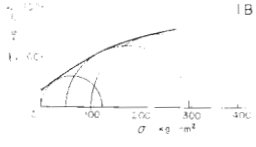

Fig. 28 Mohr envelope curve for Mizunoya siltstone, IB(S12).

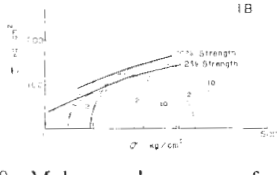

Fig. 29 Mohr envelope curve for Mizunoya siltstone, IB(S12). 2 and 10 % strength.

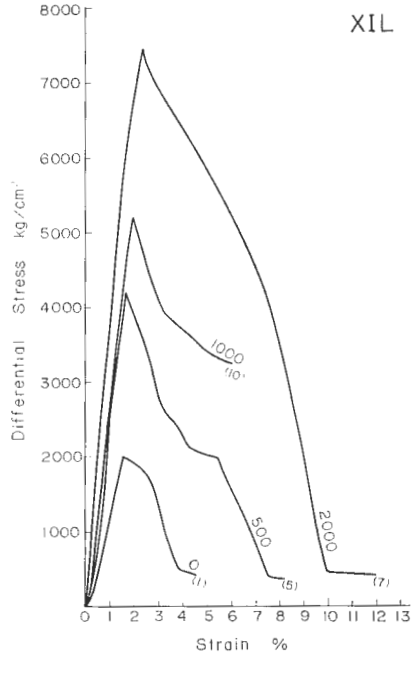

Fig. 30 Stress-strain curve for Bessho shale, XIL(S69).

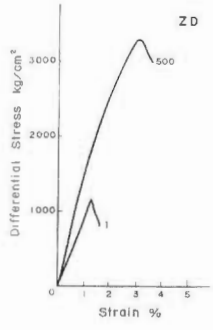

Fig. 31 Stress-strain curve for Nambayama shale, ZD(S47).

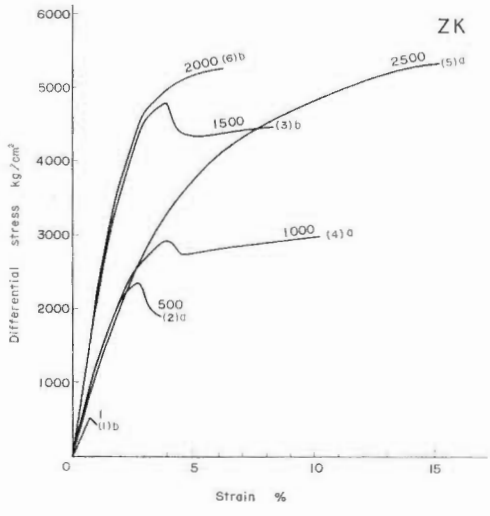

Fig. 32 Stress-strain curve for Aosawa shale, ZK(S36). (a) for black shale specimen, (b) for shale and tuff specimen.

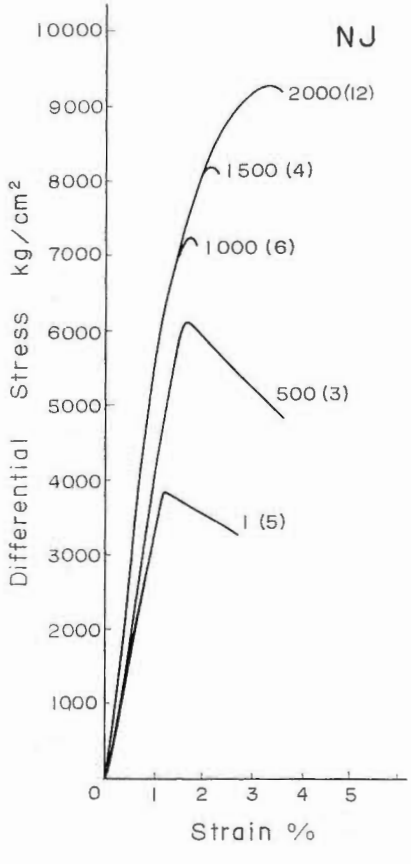

Fig. 33 Stress-strain curve for Onnagawa shale (1), NJ(S33).

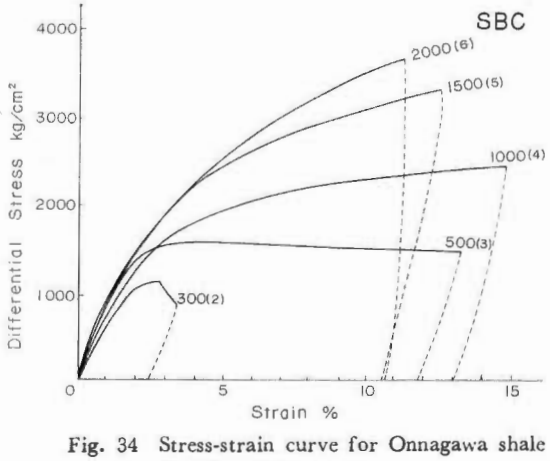

Fig. 34 Stress-strain curve for Onnagawa shale (2), SBC(S26).

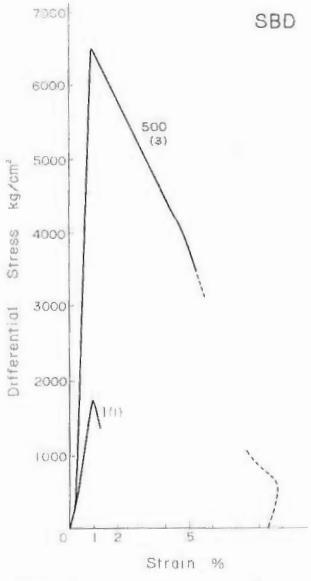

Fig. 35 Stress-strain curve for Onnagawa shale (3), SBD(S27).

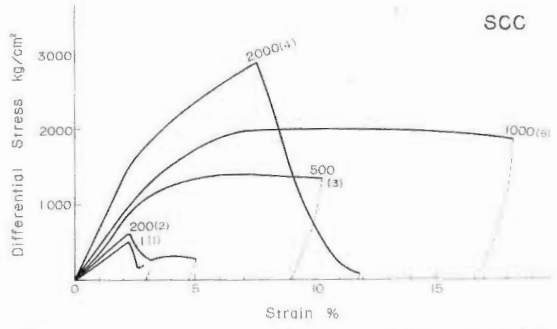

Fig. 36 Stress-strain curve for Onnagawa shale (4), SCC(S30).

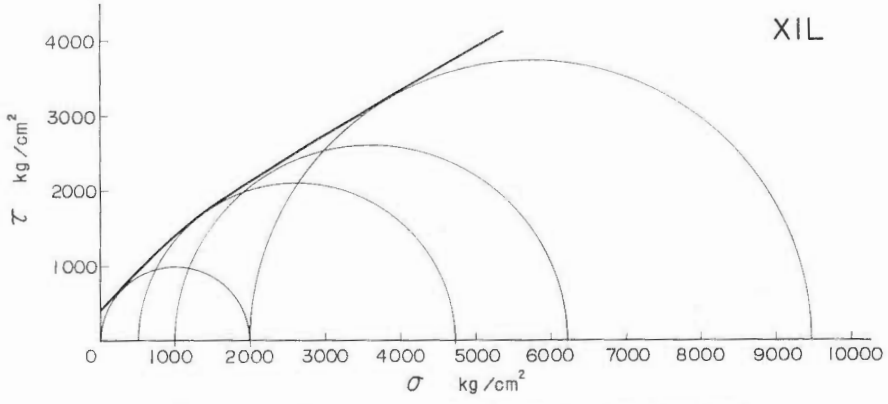

Fig. 37 Mohr envelope curve for Bessho shale, XIL(S69).

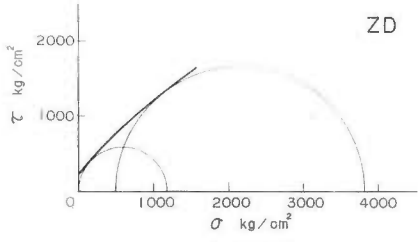

Fig. 38 Mohr envelope curve for Nambayama shale, ZD(S47).

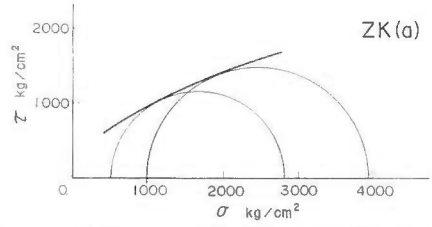

Fig. 39 Mohr envelope curve for Aosawa shale, ZK(a)(S36), black shale part.

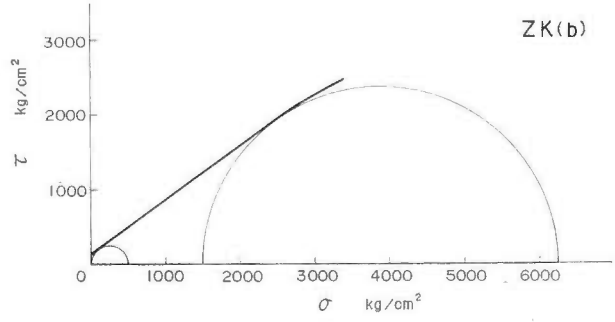

Fig. 40 Mohr envelope curve for Aosawa shale, ZK(b)(S36), shale and tuff part.

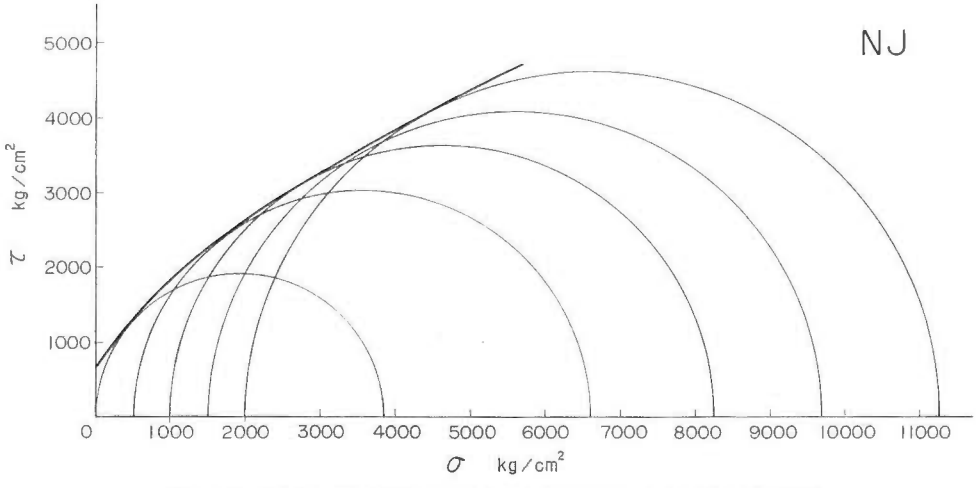

Fig. 41 Mohr envelope curve for Onnagawa shale (1), NJ(S33).

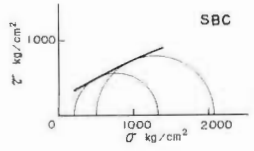

Fig. 42 Mohr envelope curve for Onnagawa shale (2), SBC(S26).

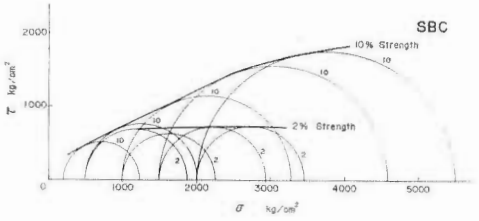

Fig. 43 Mohr envelope curve for Onnagawa shale (2), SBC(S26). 2 and 10 % strength.

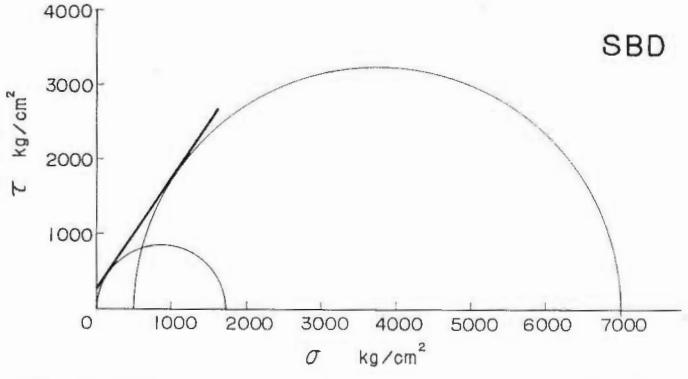

Fig. 44 Mohr envelope curve for Onnagawa shale (3), SBD(S27).

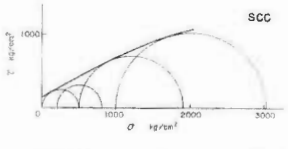

Fig. 45 Mohr envelope curve for Onnagawa shale (4), SCC(S30).

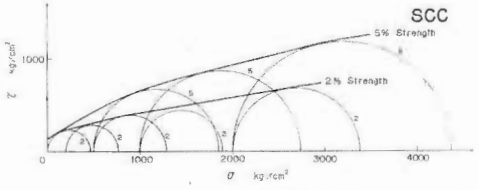

Fig. 46 Mohr envelope curve for Onnagawa shale (4), SCC(S30). 2 and 5 % strength.

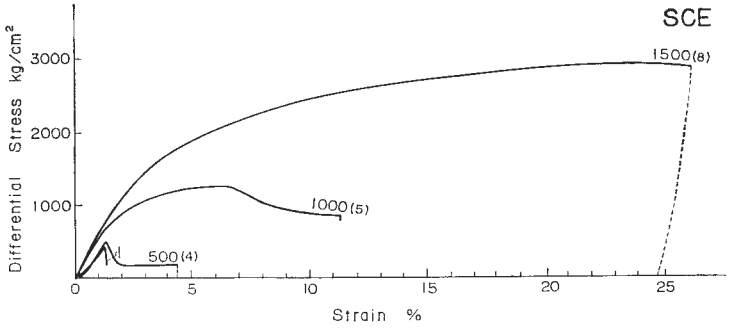

Fig. 47 Stress-strain curve for Nishikurosawa shale, SCE(S32).

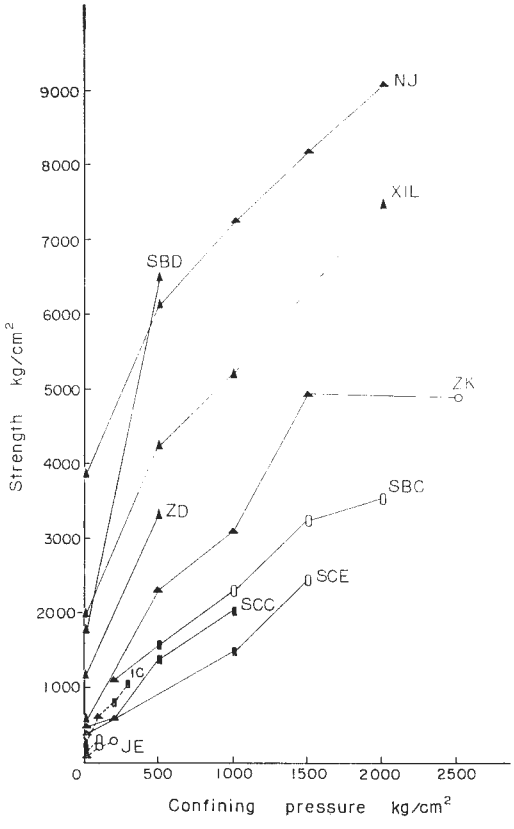

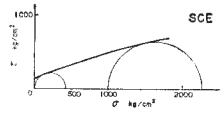

Fig. 48 Mohr envelope curve for Nishikurosawa shale, SCE(S32).

Fig. 49 Strength versus confining pressure for lower Miocene argillaceous rocks, IC, JE, IB, XIL, ZD, ZK, NJ, SCC, SEC, SBD, and SCE. Marks; ▲, ▲, ▌, 0, ○ indicate very brittle, brittle, transitional, ductile and visco-ductile behavior respectively. Solid mark represents maximum strength and open mark represents 10 % strength. Dotted lines indicate rocks of Unagaya group.

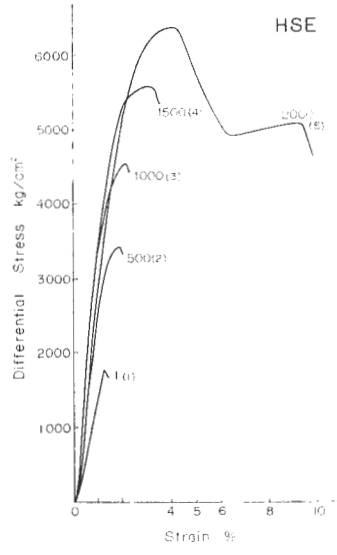

Fig. 50 Stress-strain curve for Kase shale, HSE(S97).

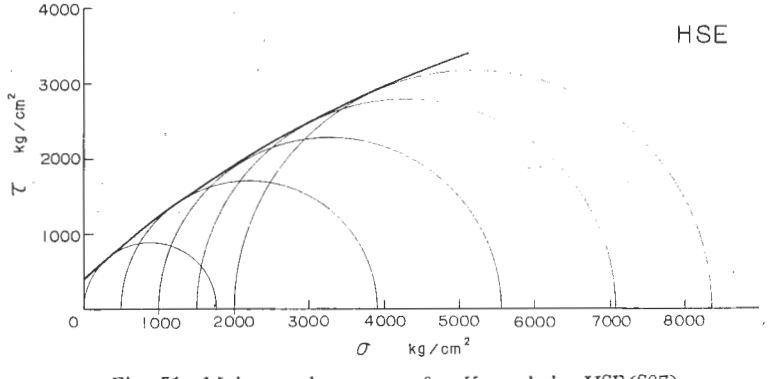

Fig. 51 Mohr envelope curve for Kase shale, HSE(S97).

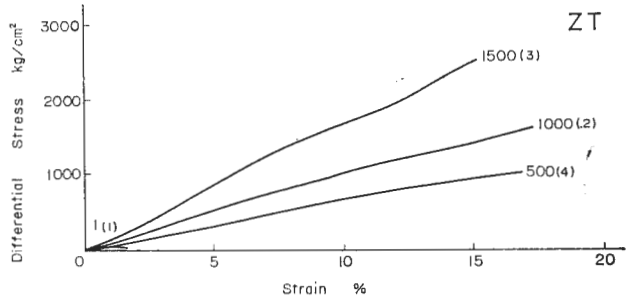

Fig. 52 Stress-strain curve for Misaki formation siltstone (1), ZT(S82).

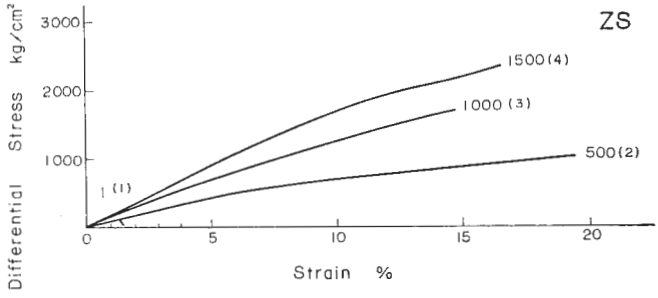

Fig. 53 Stress-strain curve for Misaki formation siltstone(2), ZS(S81).

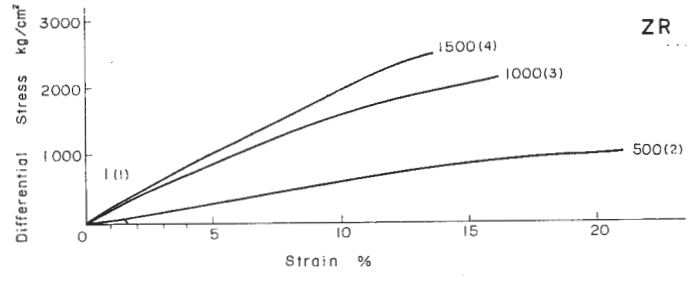

Fig. 54 Stress-strain curve for Misaki formation siltstone(3), ZR(S80).

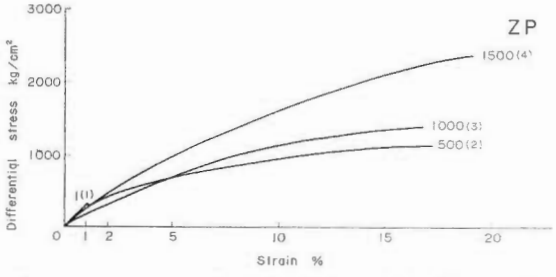

Fig. 55 Stress-strain curve for Misaki formation siltstone(4), ZP(S78).

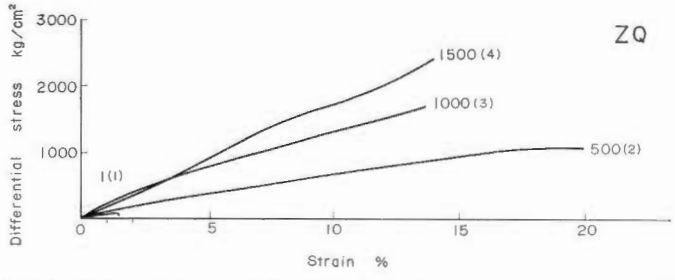

Fig. 56 Stress-strain curve for Misaki formation siltstone(5), ZQ(S79).

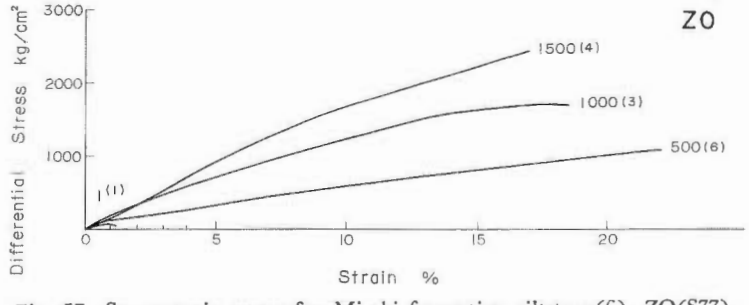

Fig. 57 Stress-strain curve for Misaki formation siltstone(6), ZO(S77).

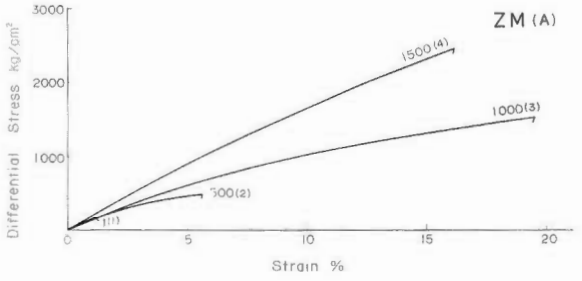

Fig. 58 Stress-strain curve for Misaki formation siltstone(7), ZM(S76) at high confining pressures.

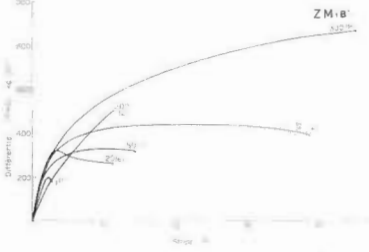

Fig. 59 Stress-strain curve for Misaki formation siltstone(7), ZM(S76) at low confining pressures.

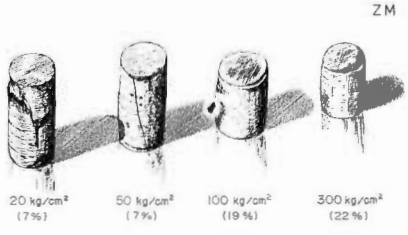

Fig. 60 Sketch showing specimens of ZM (S76) deformed at low confining pressures.

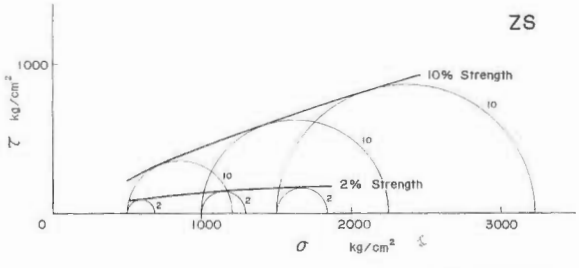

Fig. 61 Mohr envelope curve for Misaki formation siltstone(2), ZS(S81). 2 and 10 % strength.

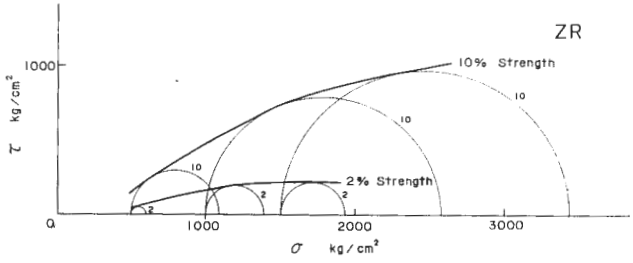

Fig. 62 Mohr envelope curve for Misaki formation siltstone(3), ZR(S80). 2 and 10 % strength.

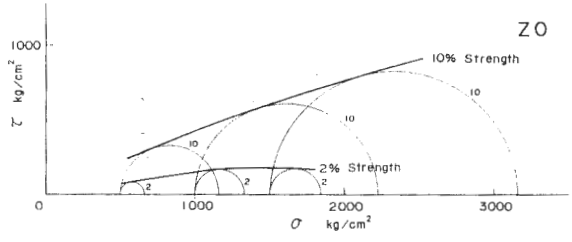

Fig. 63 Mohr envelope curve for Misaki formation siltstone(6), ZO(S77). 2 and 10 % strength.

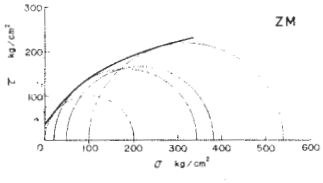

Fig. 64 Mohr envelope curve for Misaki formation siltstone(7), ZM(S76).

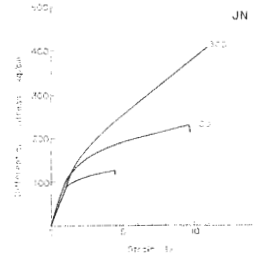

Fig. 65 Stress-strain curve for Takaku group siltstone, JN(S7).

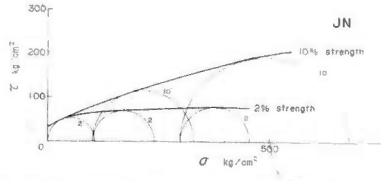

Fig. 66 Mohr envelope curve for Takaku group siltstone, JN(S7). 2 and 10% strength.

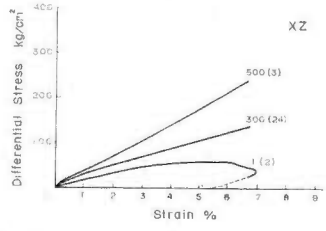

Fig. 67 Stress-strain curve for Mushizaki claystone, XZ(S68).

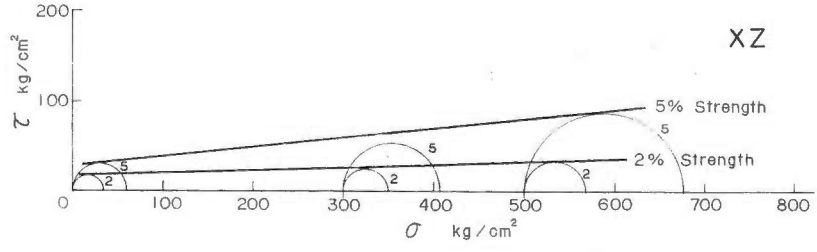

Fig. 68 Mohr envelope curve for Mushizaki claystone, XZ(S68). 2 and 5% strength.

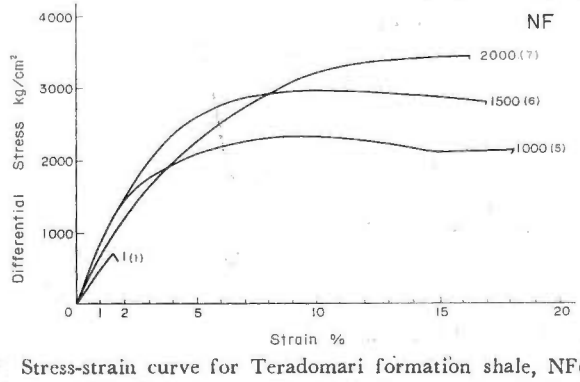

Fig. 69 Stress-strain curve for Teradomari formation shale, NF(S38).

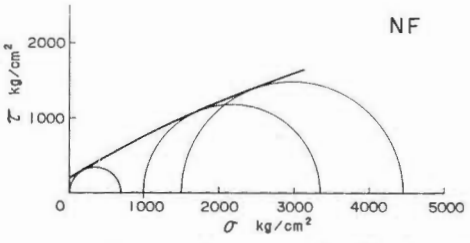

Fig. 70 Mohr envelope curve for Teradomari formation shale, NF(S38).

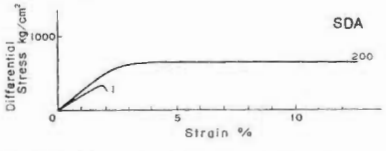

Fig. 72 Stress-strain curve for Shiiya formation claystone (1), SDA(S48).

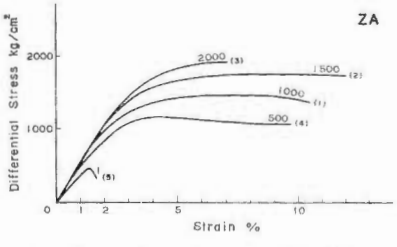

Fig. 73 Stress-strain curve for Shiiya formation claystone (2), ZA(S40).

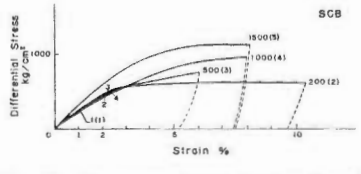

Fig. 75 Stress-strain curve for Funakawa formation claystone, SCB(S29).

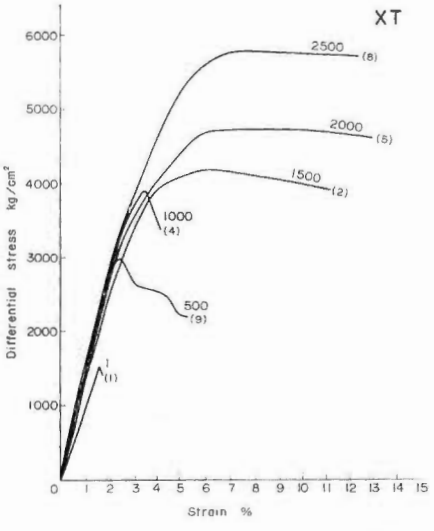

Fig. 71 Stress-strain curve for Shiiya formation shale, XT(S64).

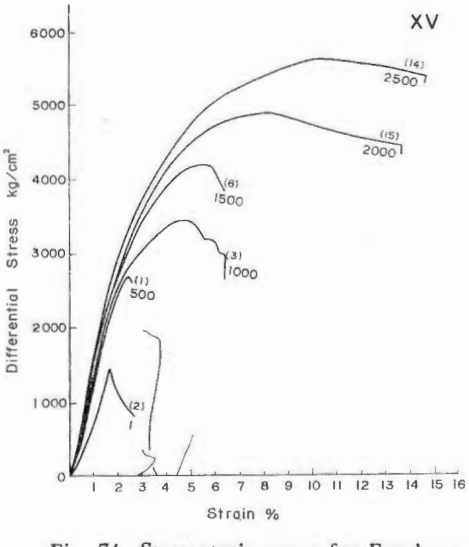

Fig. 74 Stress-strain curve for Funakawa formation shale, XV(S19).

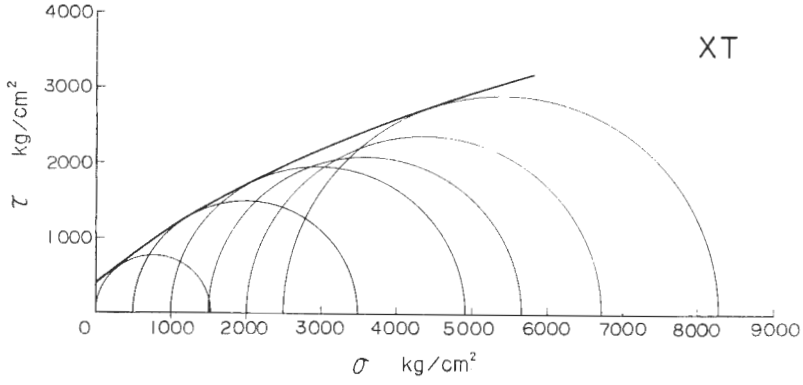

Fig. 76 Mohr envelope curve for Shiiya formation shale, XT(S64).

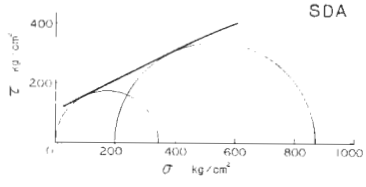

Fig. 77 Mohr envelope curve for Shiiya formation claystone (1), SDA(S48).

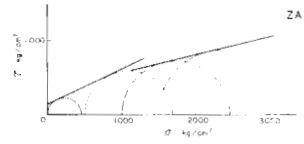

Fig. 78 Mohr envelope curve for Shiiya formation claystone (2), ZA(S40).

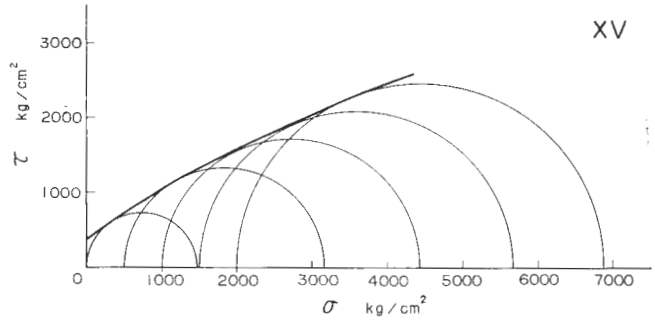

Fig. 79 Mohr envelope curve for Funakawa formation shale, XV(S19).

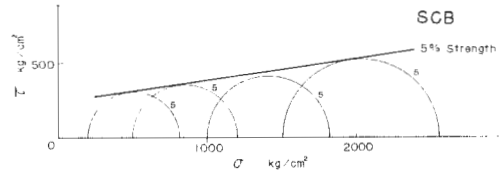

Fig. 80 Mohr envelope curve for Funakawa formation claystone, SCB(S29). 5 % strength.

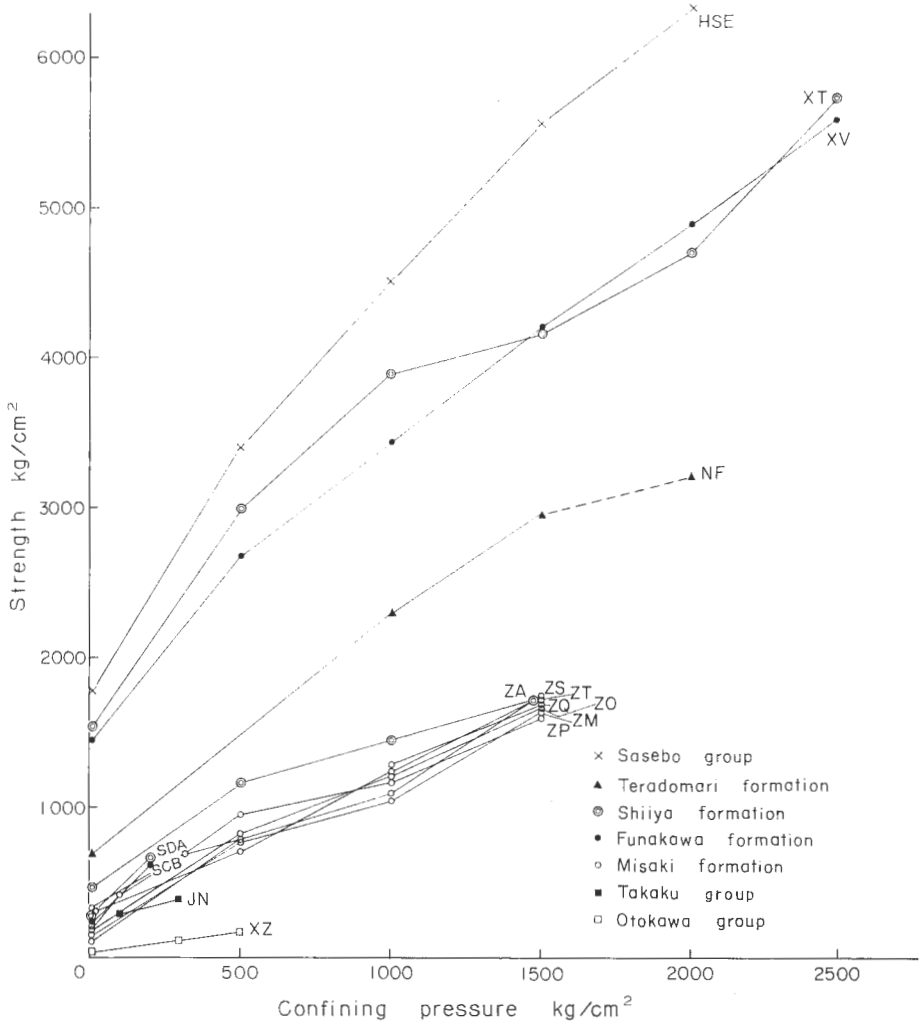

Fig. 81 Strength versus confining pressure for upper Miocene argillaceous rocks, HSE, ZT, ZS, ZP, ZQ, ZO, ZM, JN, XZ, NF, XT, SDA, ZA, XV, and SCB. The points show ultimate or 10 % strength.

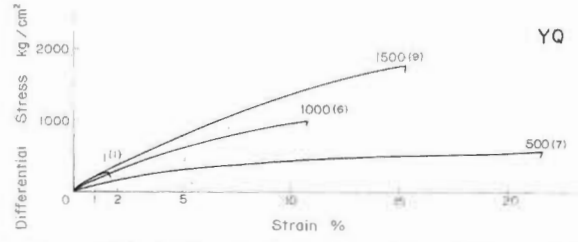

Fig. 82 Stress-strain curve for Zushi formation siltstone (1), YQ(S73).

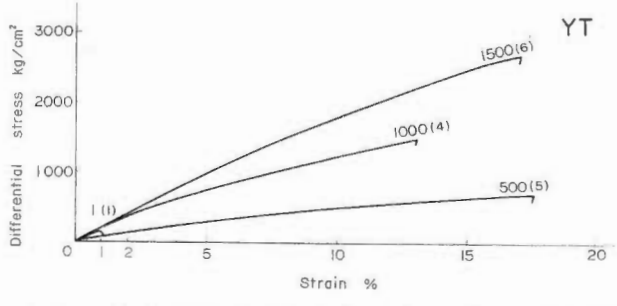

Fig. 83 Stress-strain curve for Zushi formation siltstone (2), YT(S75).

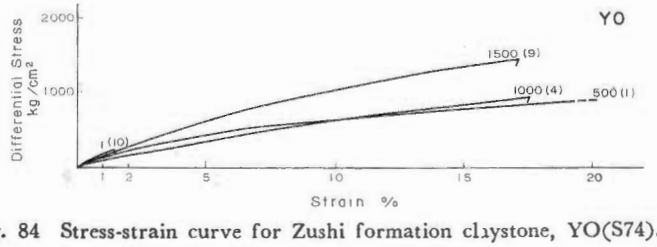

Fig. 84 Stress-strain curve for Zushi formation claystone, YO(S74).

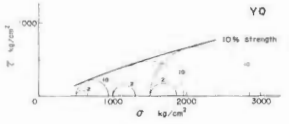

Fig. 85 Mohr envelope curve for Zushi formation siltstone (1), YQ(S73). 2 and 10 % strength.

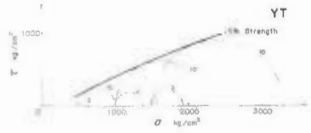

Fig. 86 Mohr envelope curve for Zushi formation siltstone (2), YT(S75). 2 and 10% strength.

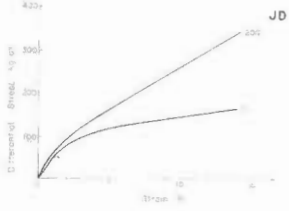

Fig. 87 Stress-strain curve for Taga siltstone (1), JD(S5).

Fig. 88 Stress-strain curve for Taga siltstone (2), JZ(S6).

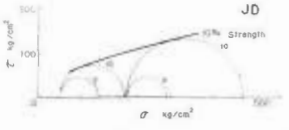

Fig. 89 Mohr envelope curve for Taga siltstone (1), JD(S5). 2 and 10 % strength.

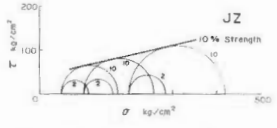

Fig. 90 Mohr envelope curve for Taga siltstone (2), JZ(S6). 2 and 10 % strength.

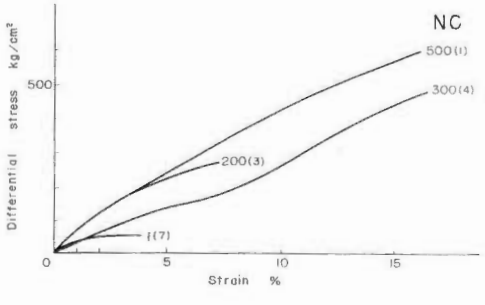

Fig. 91 Stress-strain curve for Nishiyama siltstone (1), NC(S42).

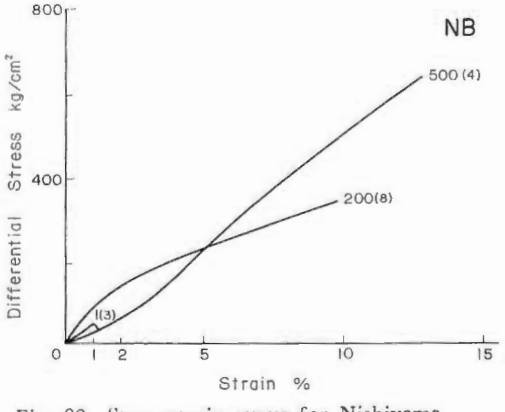

Fig. 92 Stress-strain curve for Nishiyama siltstone (2), NB(S41).

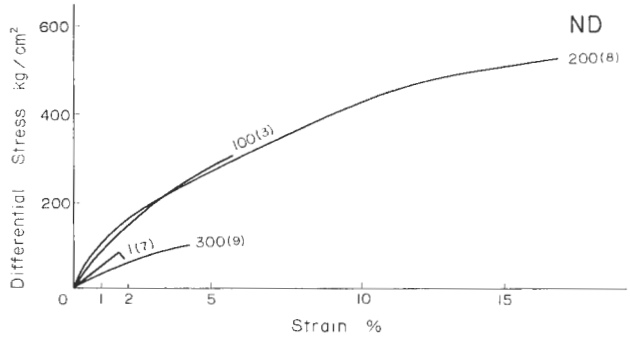

Fig. 93 Stress-strain curve for Nishiyama siltstone (3), ND(S43).

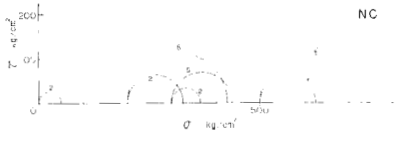

Fig. 94 Mohr envelope curve for Nishiyama siltstone (1), NC(S42). 2 and 5 % strength.

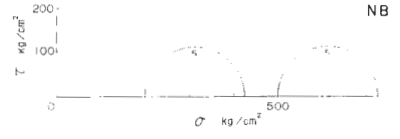

Fig. 95 Mohr envelope curve for Nishiyama siltstone (2), NB(S41). 5 % strength.

Fig. 96 Mohr envelope curve for Nishiyama siltstone (3), ND(S43). 2 % strength.

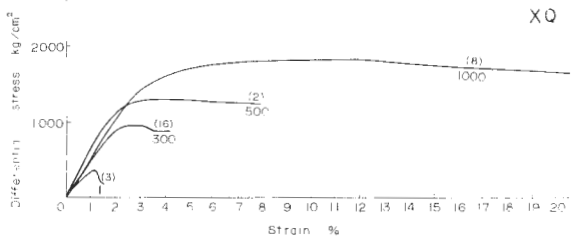

Fig. 97 Stress-strain curve for Hamatsuda claystone (1), XQ(S62).

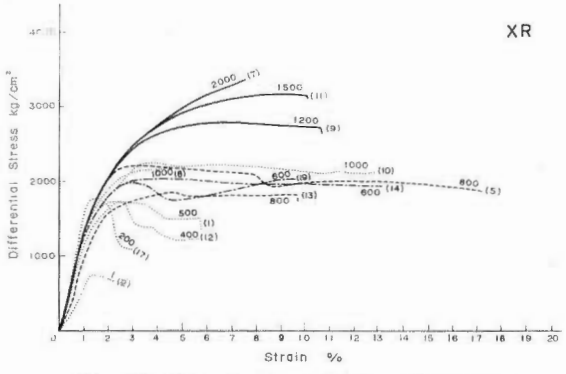

Fig. 98 Stress-strain curve for Hamatsuda claystone (2), XR(S63).

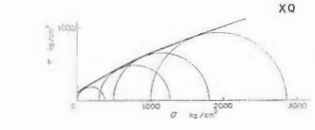

Fig. 99 Mohr envelope curve for Hamatsuda claystone (1), XQ(S62).

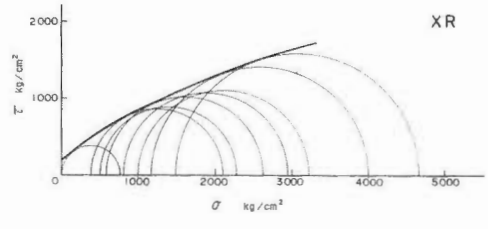

Fig. 100 Mohr envelope curve for Hamatsuda claystone (2), XR(S63).

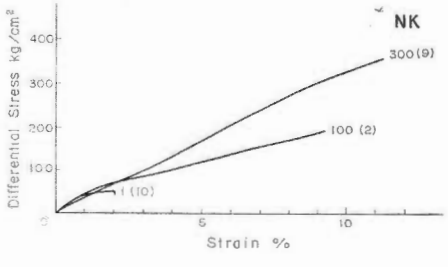

Fig. 101 Stress-strain curve for Tentokuji siltstone (1), NK(S34).

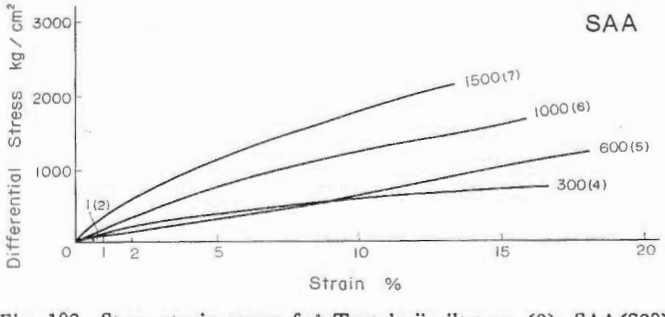

Fig. 102 Stress-strain curve for Tentokuji siltstone (2), SAA(S20).

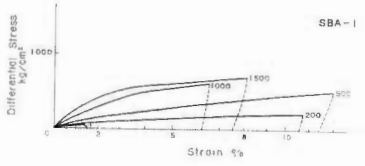

Fig. 103 Stress-strain curve for Tentokuji siltstone (3), SBA(S24).

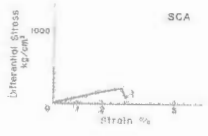

Fig. 104 Stress-strain curve for Tentokuji siltstone (4), SCA(S28).

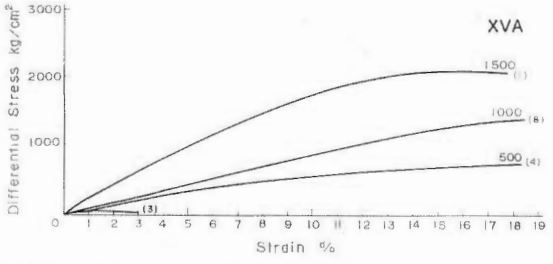

Fig. 105 Stress-strain curve for Tentokuji siltstone (5), XVA(S17).

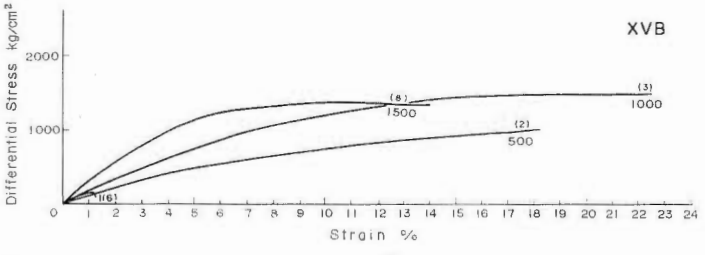

Fig. 106 Stress-strain curve for Tentokuji siltstone (6), XVB(S18).

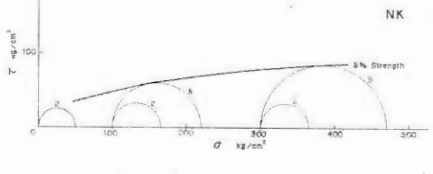

Fig. 107 Mohr envelope curve for Tentokuji siltstone (1), NK(S34). 2 and 5 % strength.

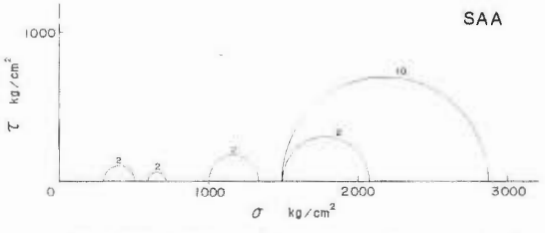

Fig. 108 Mohr envelope curve for Tentokuji siltstone (2), SAA(S20). 2 and 10 % strength.

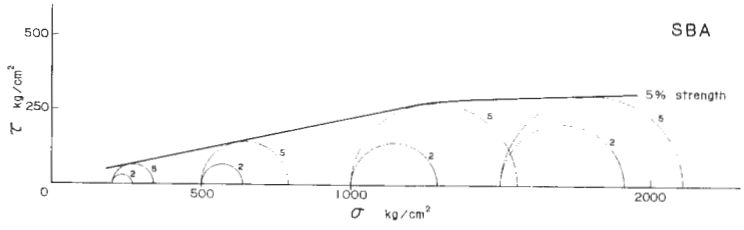

Fig. 109 Mohr envelope curve for Tentokuji siltstone (3), SBA(S24). 2 and 5 % strength.

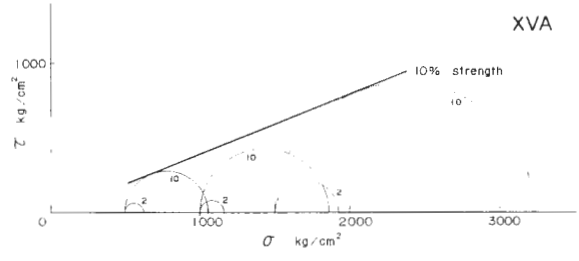

Fig. 110 Mohr envelope curve for Tentokuji siltstone (5), XVA(S17). 2 and 10 % strength.

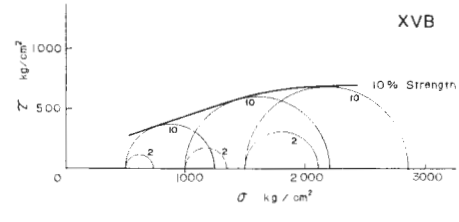

Fig. 111 Mohr envelope curve for Tentokuji siltstone (6), XVB(S18). 2 and 10 % strength.

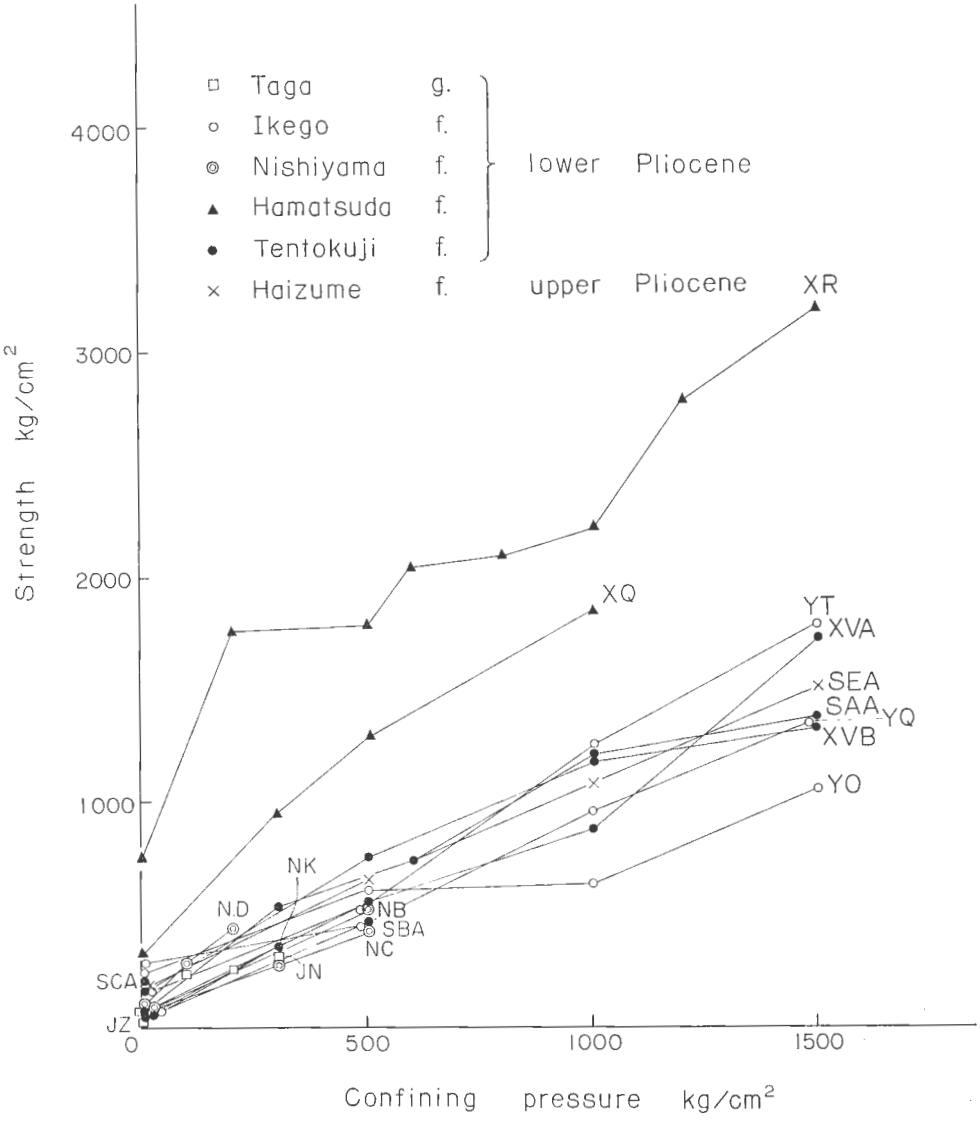

Fig. 112 Strength versus confining pressure for Pliocene argillaceous rocks, YQ, YO, YT, JD, JZ, NC, NB, ND, XQ, XR, SAA, SBA, SCA, XVA, XVB, and NK. The points show ultimate or 10% strength.

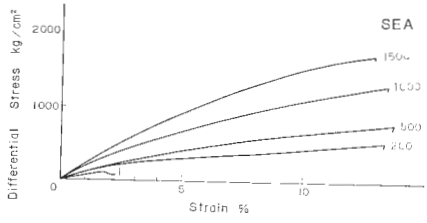

Fig. 113 Stress-strain curve for Haizume formation siltstone (1), SEA(S51).

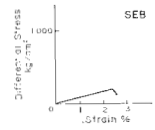

Fig. 114 Stress-strain curve for Haizume formation siltstone, SEB(S52).

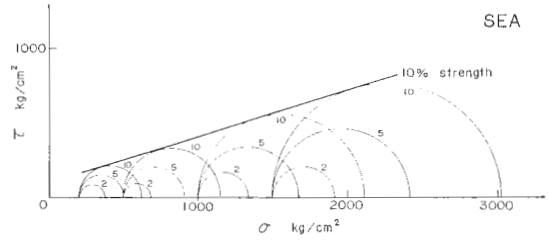

Fig. 115 Mohr envelope curve for Haizume formation siltstone (1), SEA(S51). 2, 5 and 10% strength.

IV. 3 Arenaceous rocks

Oligocene arenaceous rocks

In the Oligocene arenaceous rocks tested, there are two rocks HSF (S98) and HSG(S99)from Kishima group, northwestern Kyushu; five, XD(S88), XE(S89), XC (S87), XG(S91), and XB(S86) from Maze formation, Nishisonogi group, northwestern Kyushu; two KSB (S2) and KSD(S4) from Ombetsu and Urahoro groups, Kushiro, Hokkaido; two, JG(S15) and JO(S16) from Shiramizu group, Joban coal field.

Fig. 182 shows a relation between strength and confining pressure of the Oligocene arenaceous rocks. This Figure indicates that strength-confining pressure relation for Kishima, Nishisonogi, Ombetsu, and Urahoro groups is almost similar, while that for Shiramizu group is considerably different from those of the other groups. Among Kishima, Nishisonogi, Ombetsu, and Urahoro groups, Kishima group is the strongest. Nishisonogi, Ombetsu, and Urahoro groups have nearly the same strength. Since Nishisonogi, Ombetsu, and Urahoro groups are considered approximately the same in geological age, the above result is quite acceptable from geological point. However, Kishima group shows larger strength than Nishisonogi group, although the former is stratigraphically younger than the latter. The reason is possibly due to its small porosity. The porosity of the samples from Kishima group is about 4.0%, and those of Maze sandstones are 3 to 12%. The porosities of Ombetsu and Urahoro groups are 5 or 6%. The porosity of JO(S16), Iwaki sandstone, Shiramizu group, is 30%. Therefore, the difference among the strength-confining pressure relation for arenaceous rocks might be reduced mostly to effect of porosity as well as in case of argillaceous rocks.

HSF (S98) and HSG (S99) from Kishima group are very brittle up to 1000 or 1500 kg/cm^2 confining pressure and brittle to 2000 kg/cm^2. The fractures are sharp cut single shear fractures. Five samples of Maze sandstones were collected from the layer of about 300 m in thickness and the rock materials are quite similar. They are grey medium sandstones ranging 1.0 to 0.3 mm in the greatest grain size. The sorting of grains is quite well. They are very brittle or brittle to 1000 or 1500 kg/cm^2. They present very brittle behavior at atmospheric confining pressure, brittle behavior with clear cut single shear at 500 and 1000 kg/cm^2, and turned into transitional behavior having conjugate shear fractures making an angle of 75 degrees at 1500 kg/cm^2. At 2000 kg/cm^2, there are still transitional, without fracture, and, at 2500 kg/cm^2, they become ductile and are not accompanied with any fractures. The rocks from Hokkaido, KSB(S2) and KSD(S4), behave similarly as Maze sandstones, but a little more brittle. They are brittle up to 1500 kg/cm^2 confining pressure. At 2000 kg/cm^2, KSB(S2) seems to be changed into transitional behavior without fracture.

The sandstones from Joban area, JO(S16) and JG(S15) are very ductile. JO (S16), Iwaki sandstone, becomes ductile and produced no fracture. JG(S15), Asagai sandstone, is transitional above 300 kg/cm^2 confining pressure without fracture.

Lower Miocene arenaceous rocks

Six lower Miocene arenaceous rocks from Sasebo group, northwestern Kyushu and Onnagawa-Nanatani formation, Niigata-Akita province, show almost similar strength-confining pressure relation, (Fig. 183). The strengths are approximately between 5000 and 3000 kg/cm^2, 4000 and 2000 kg/cm^2, 3000 and 1400 kg/cm^2, and 1000 and 500 kg/cm^2 at 1500, 1000, 500 and 1 kg/cm^2 confining pressures, respectively. Four rocks from Sasebo group are collected according to the stratigraphic order from below, HSA(S93), Ainoura formation sandstone; HSB(S94), Yunoki formation sandstone; HSC (S95), Sechibaru formation sandstone; and HSD(S96), Fukui formation sandstone. The strength and ductility decrease according to this stratigraphic order except the case of HSD(S96). HSA(S93) is brittle up to 1500 kg/cm^2 confining pressure and has strength 3885 kg/cm^2 at 1000 kg/cm^2 pressure. HSB(S94) is also brittle to 1500 kg/cm^2 but the strength at 1000 kg/cm^2 is 2945 kg/cm^2. HSC (S95) and HSD(S96) are changed almost to transitional behavior at 500 kg/cm^2. HSC(S95) turns into ductile at 1000 kg/cm^2. HSD(S96) is a little stronger than HSC(S95), although the former is younger than the latter in the stratigraphic order.

ZC(S37), Nanatani formation sandstone, collected from the northern part of Niigata, is brittle up to 1000 kg/cm^2, at which it produces single shear fracture inclined at an angle of 30 degree. At 1500 kg/cm^2, it changed to transitional behavior and made conjugate shear fractures of 31° or 40° in angle. SCD(S31), Onnagawa formation sandstone from Akita shows very brittle behavior at 1 and 200kg/cm^2.

Upper Miocene and Lower Pliocene arenaceous rocks

The rocks in this section include one of Teradomari formation, four of Shiiya formation, five of Hamatsuda formation, one of Tentokuji formation (the above eleven rocks are from Akita-Niigata province); two from Takaku and Nakayama groups in Joban area; and one from Zushi formation in southern Kwanto area.

Among the rocks in this section, those from the Joban and Kwanto areas are more ductile and weaker in strength, similarly to the case of argillaceous rocks

(Fig. 184). Among the rocks from Akita-Niigata area, Shiiya formation sandstones are the strongest, Hamatsuda formation sandstones are next, and Teradomari and Tentokuji formation sandstones are the weakest. Shiiya sandstones, SFB(S59), SEF (S56), SEG(S57), and SDC(S50) are transitional at 200 (SFB, SDC) or 500 (SEF) or 1000 kg/cm^2(SEG) confining pressure. They did not produce any fracture under transitional and ductile behavior. Hamatsuda sandstones, SEC(S53), SED(S54), SEF (S55), SFA(S58) and XS(S65) are more visco-ductile. They become transitional as early as 200kg/cm^2 except SED(S54), which is transitional at 500kg/cm^2, and turn into visco-ductile at 500 (SFA, SEC and XS),or 1500 (SEE) kg/cm^2 confining pressure. SED (S54) only keeps transitional behavior until 2000 kg/cm^2. The Hamatsuda sandstones are not accompanied by fracture under transitional behavior. The ultimate or 10% strengths of Hamatsuda sandstones are between 1800 and 1400 kg/cm^2, and 1000 and 500 kg/cm^2 at 1500 and 200 kg/cm^2 confining pressures, respectively. The Tentokuji sandstone, SBB(S25), behaves visco-ductile from 1 to 1000 kg/cm^2 confining pressure. Teradomari formation sandstone, NE(S39), is very ductile, too. It becomes transitional at 200 kg/cm^2 and ductile at 300 and 500 kg/cm^2 confining pressures. The more ductile behavior and weaker strength of SBB(S25) and NE(S39) are attributed to the larger porosity. The porosity of NE(S39) and SBB(S25) are 30 and 55% respectively, while those of other rocks of the same age range between 10 and 25%.

JM(S8), Takaku sandstone and JL(S9), Nakayama sandstone are very ductile. They become ductile possibly at 50 kg/cm^2 (JM) or a little more. Zushi sandstone, YP(S72), is very weak, but shows somewhat brittle behavior. It is brittle at 1000 and 1500 kg/cm^2 confining pressures. JM(S8) and JL(S9) are around 400 kg/cm^2 or a little weaker at 200 kg/cm^2 confining pressure .YP(S72) is the weakest in strength; 550 kg/cm^2 and 440 kg/cm^2 at 1500 and 1000 kg/cm^2 confining pressures, respectively. The above three sandstones flow under all confining pressures tested except atmospheric pressure.

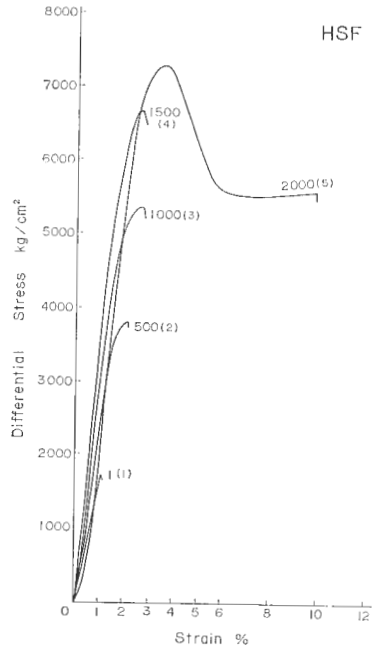

Fig. 116 Stress-strain curve for Furukawa sandstone, HSF(S98).

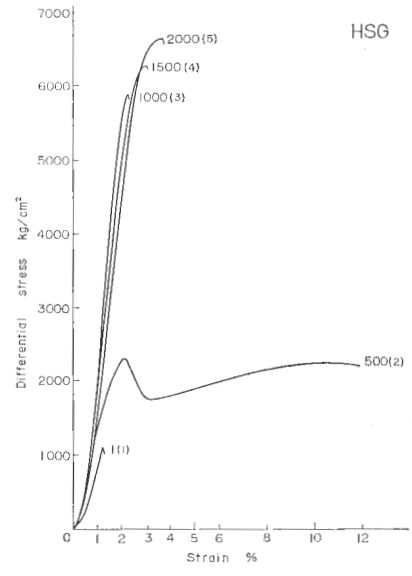

Fig. 117 Stress-strain curve for Kuroishi sandstone, HSG(S99).

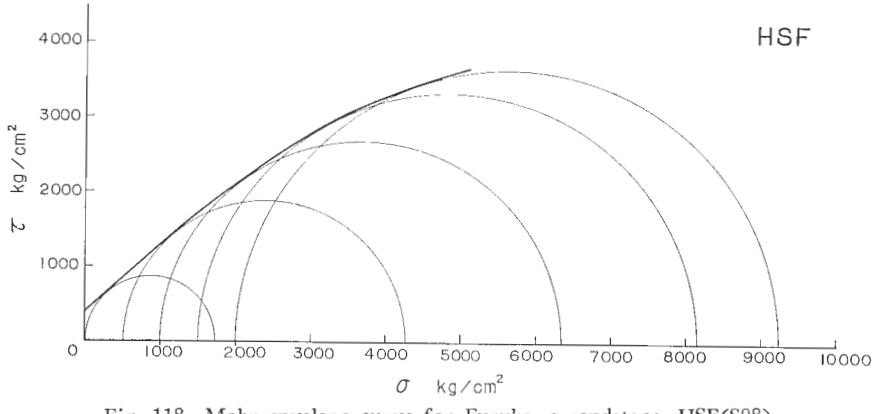

Fig. 118 Mohr envelope curve for Furukawa sandstone, HSF(S98).

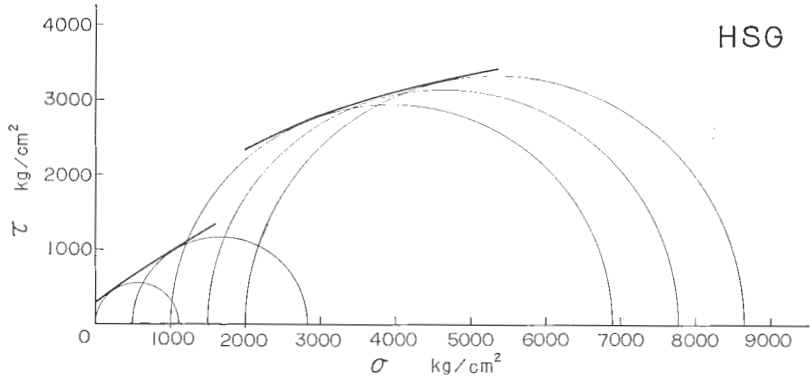

Fig. 119 Mohr envelope curve for Kuroishi sandstone, HSG(S99).

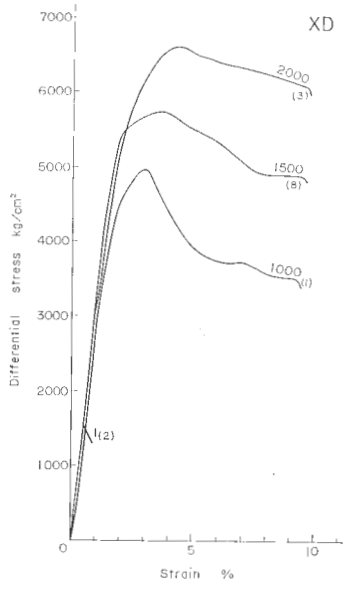

Fig. 120 Stress-strain curve for Maze sandstone (1), XD(S88).

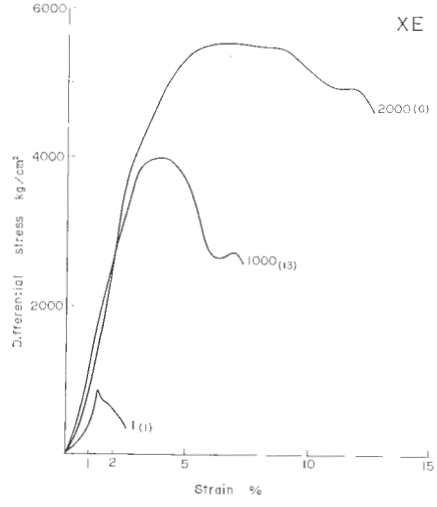

Fig. 121 Stress-strain curve for Maze sandstone (2), XE(S89).

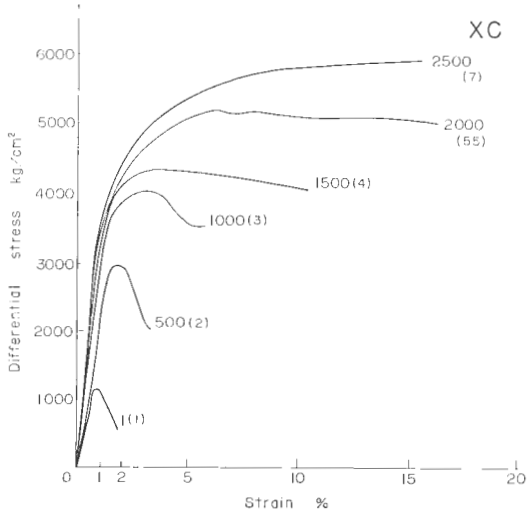

Fig. 122 Stress-strain curve for Maze sandstone (3), XC(S87).

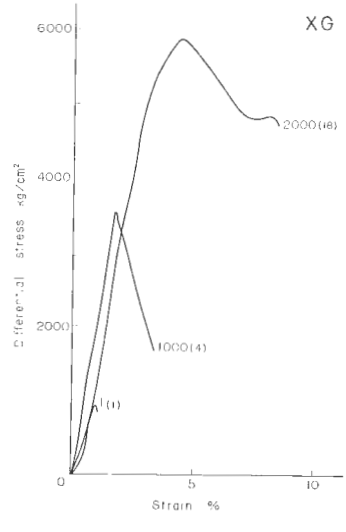

Fig. 123 Stress-strain curve for Maze sandstone (4), XG(S91).

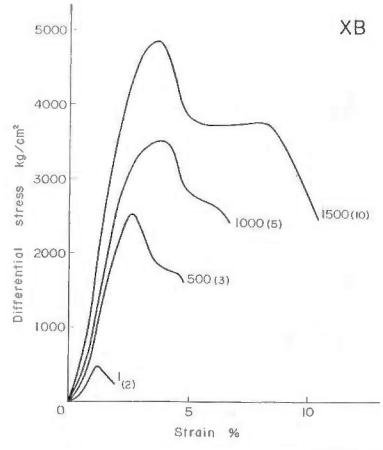

Fig. 124 Stress-strain curve for Maze sandstone (5), XB(S86).

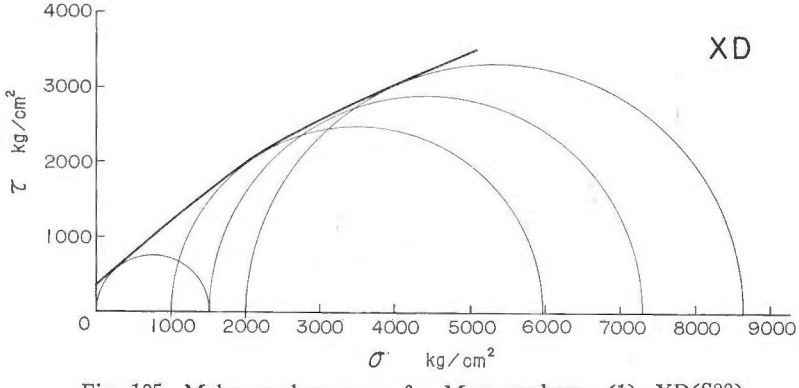

Fig. 125 Mohr envelope curve for Maze sandstone (1), XD(S88).

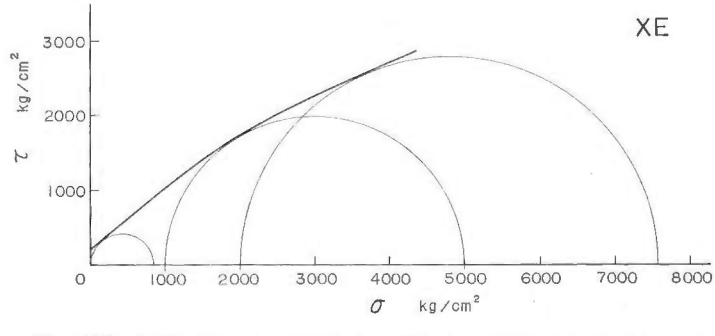

Fig. 126 Mohr envelope curve for Maze sandstone (2), XE(S89).

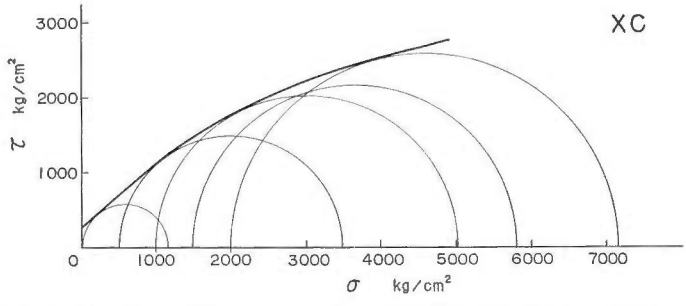

Fig. 127 Mohr envelope curve for Maze sandstone (3), XC(S87).

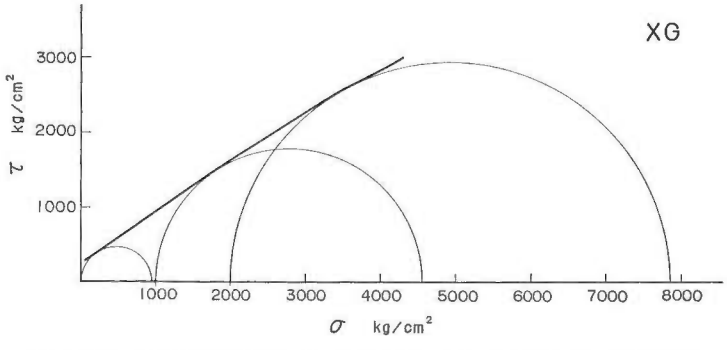

Fig. 128 Mohr envelope curve for Maze sandstone (4), XG(S91).

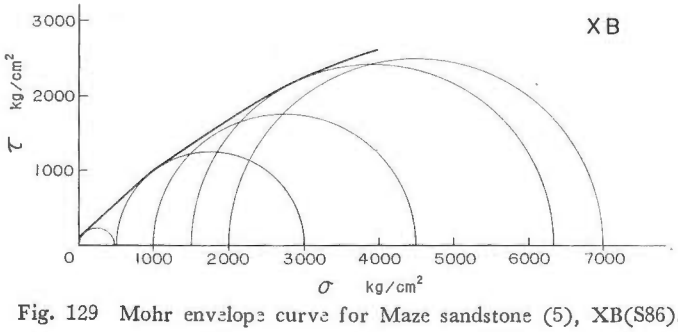

Fig. 129 Mohr envelope curve for Maze sandstone (5), XB(S86).

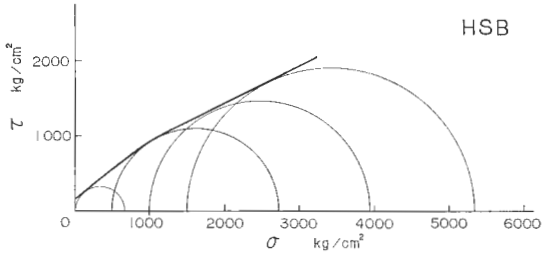

Fig. 139 Mohr envelope curve for Yunoki formation sandstone, HSB(S94).

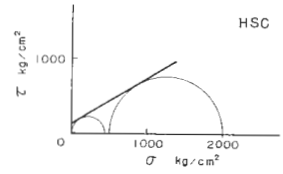

Fig. 140 Mohr envelope curve for Sechibaru formation sandstone, HSC(S95).

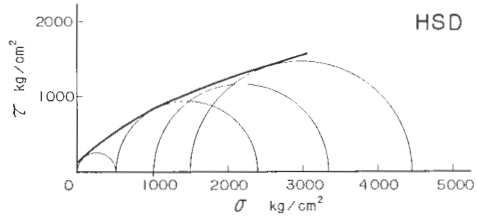

Fig. 141 Mohr envelope curve for Fukui formation sandstone, HSD(S96)

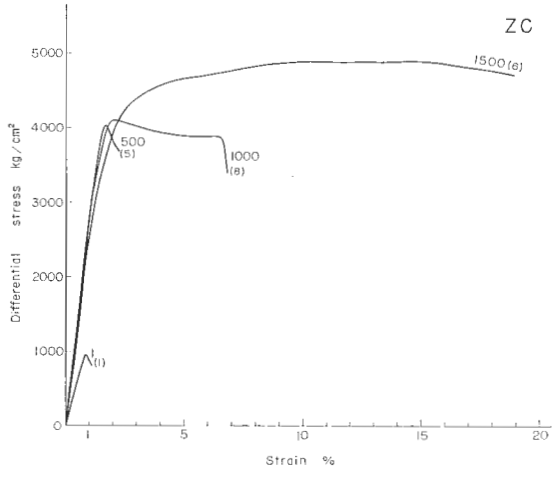

Fig. 142 Stress-strain curve for Nanatani formation sandstone, ZC(S37).

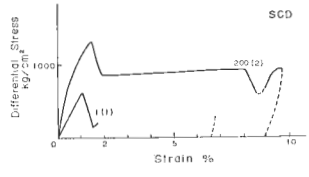

Fig. 143 Stress-strain curve for Onnagawa formation sandstone, SCD(S31).

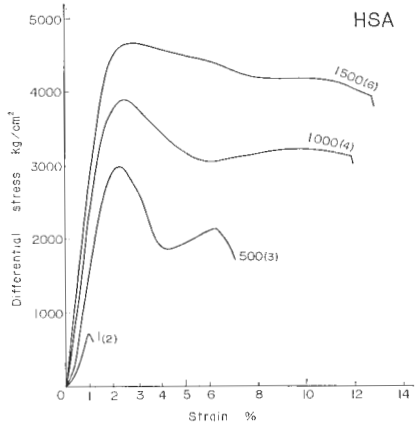

Fig. 134 Stress-strain curve for Ainoura formation sandstone, HSA(S93).

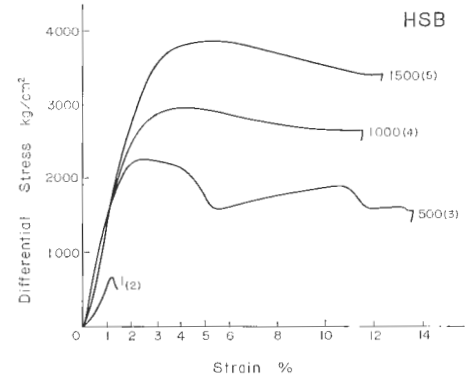

Fig. 135 Stress-strain curve for Yunoki formation sandstone, HSB(S94).

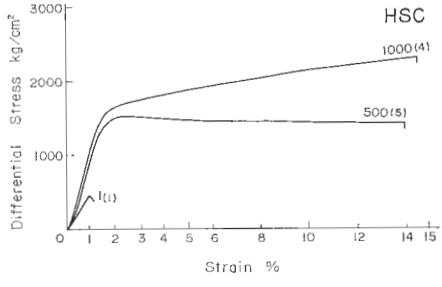

Fig. 136 Stress-strain curve for Sechibaru formation sandstone, HSC(S95).

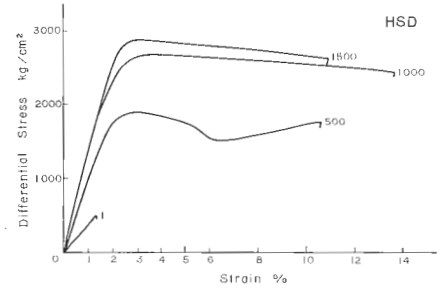

Fig. 137 Stress-strain curve for Fukui formation sandstone, HSD(S96).

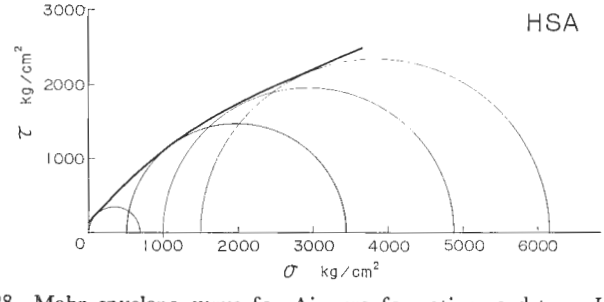

Fig. 138 Mohr envelope curve for Ainoura formation sandstone, HSA(S93).

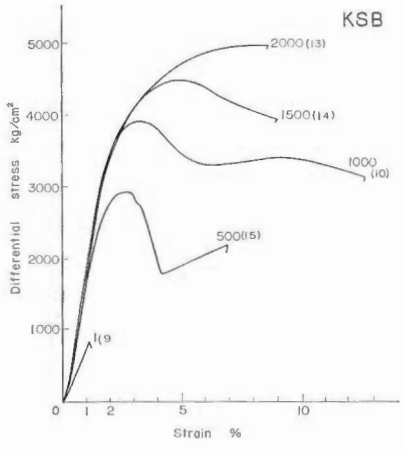

Fig. 130 Stress-strain curve for Ohmagari sandstone, KSB(S2).

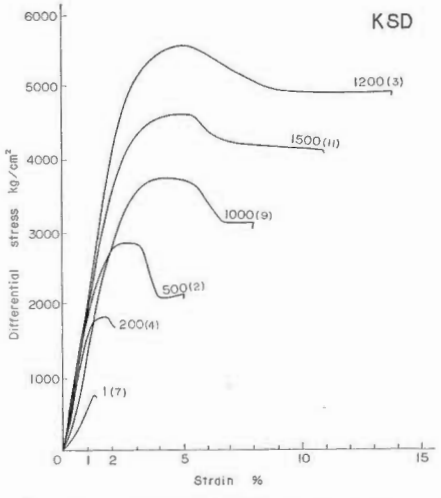

Fig. 131 Stress-strain curve for Shakubetsu sandstone, KSD(S4).

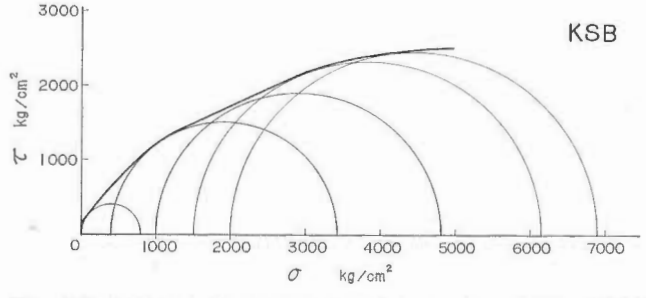

Fig. 132 Mohr envelope curve for Ohmagari sandstone, KSB(S2).

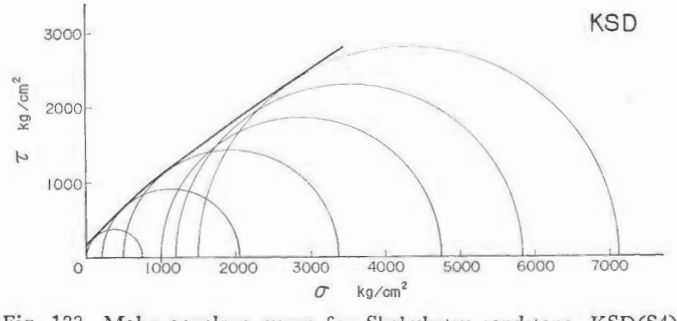

Fig. 133 Mohr envelope curve for Shakubetsu sandstone, KSD(S4).

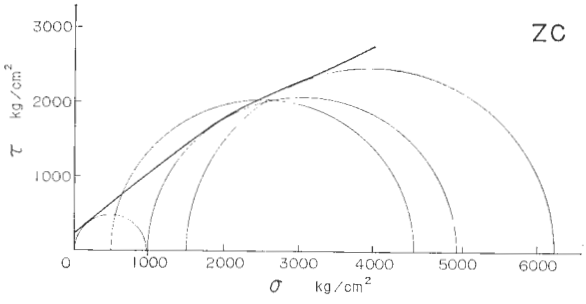

Fig. 144 Mohr envelope curve for Nanatani formation sandstone, ZC(S37).

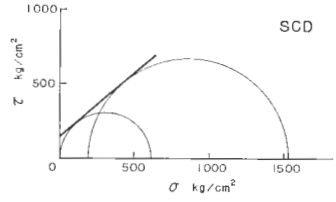

Fig. 145 Mohr envelope curve for Onnagawa formation sandstone, SCD(S31).

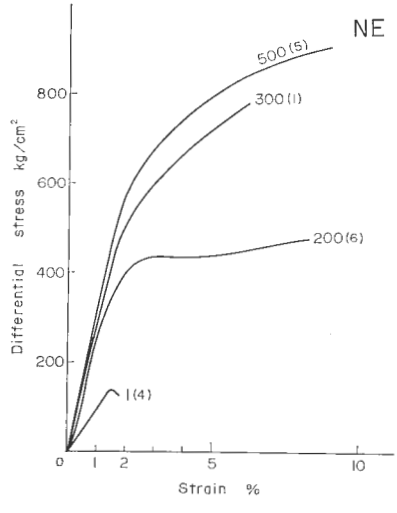

Fig. 146 Stress-strain curve for Teradomari sandstone, NE(S39).

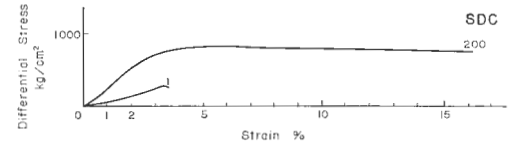

Fig. 147 Stress-strain curve for Shiiya sandstone (1), SDC(S50).

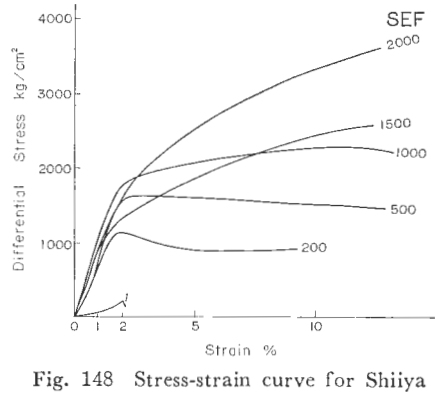

Fig. 148 Stress-strain curve for Shiiya sandstone (2), SEF(S56).

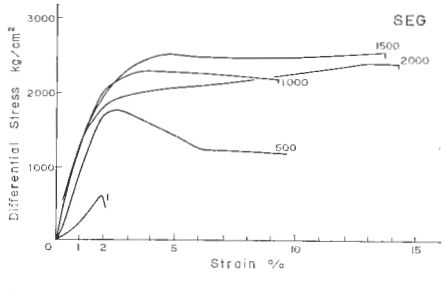

Fig. 149 Stress-strain curve for Shiiya sandstone (3), SEG(S57).

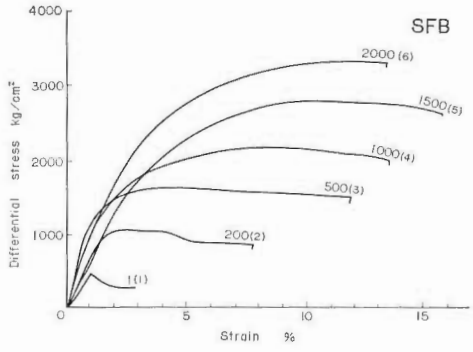

Fig. 150 Stress-strain curve for Shiiya sandstone (4), SFB(S59).

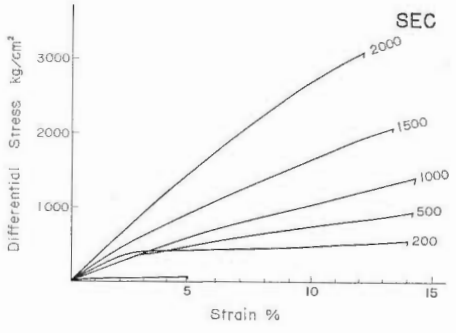

Fig. 151 Stress-strain curve for Hamatsuda sandstone (1), SEC(S53).

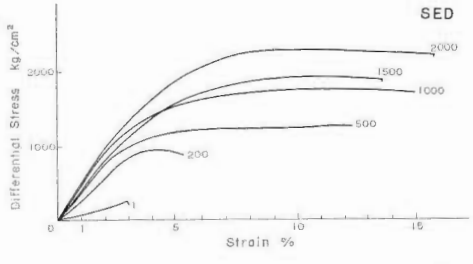

Fig. 152 Stress-strain curve for Hamatsuda sandstone (2), SED(S54).

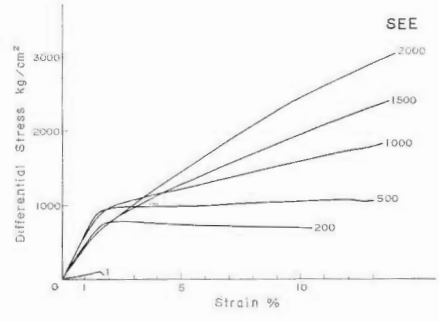

Fig. 153 Stress-strain curve for Hamatsuda sandstone (3), SEE(S55).

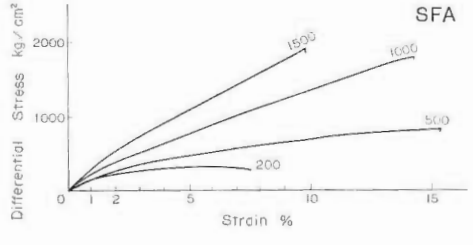

Fig. 154 Stress-strain curve for Hamatsuda sandstone (4), SFA(S58).

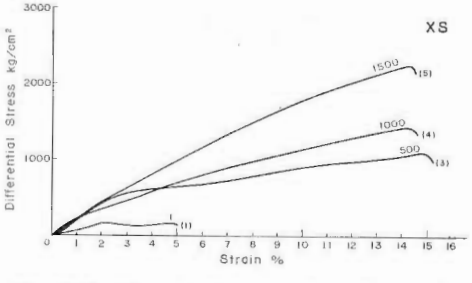

Fig. 155 Stress-strain curve for Hamatsuda sandstone (5), XS(S65).

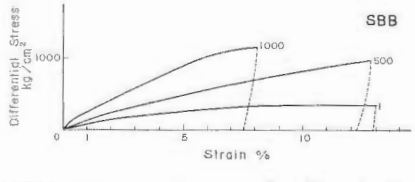

Fig. 156 Stress-strain curve for Tentokuji sandstone, SBB(S25)

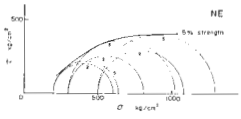

Fig. 157 Mohr envelope curve for Teradomari sandstone, NE(S39). 2 and 5 % strength.

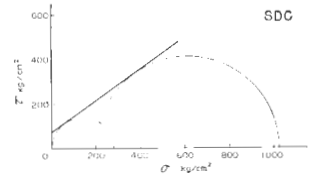

Fig. 158 Mohr envelope curve for Shiiya sandstone (1), SDC(S50).

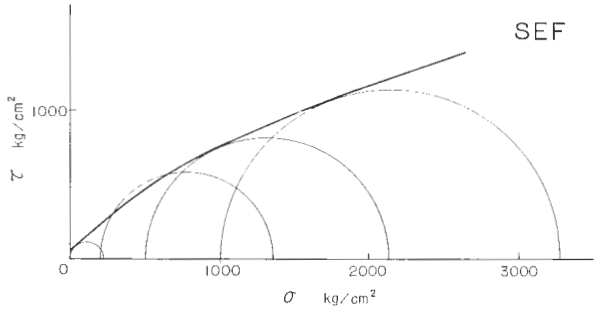

Fig. 159 Mohr envelope curve for Shiiya sandstone (2), SEF(S56).

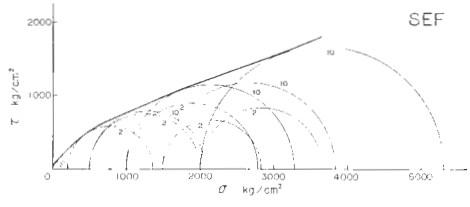

Fig. 160 Mohr envelope curve for Shiiya sandstone (2), SEF(S56). 2 and 10 % strength.

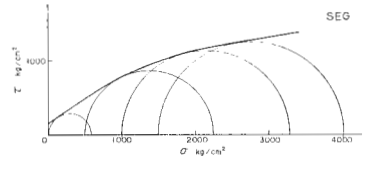

Fig. 161 Mohr envelope curve for Shiiya sandstone (3), SEG(S57).

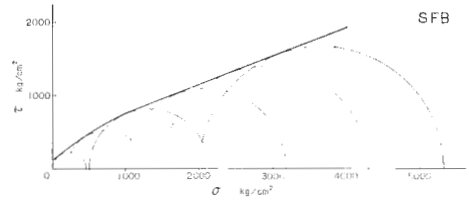

Fig. 162 Mohr envelope curve for Shiiya sandstone (4), SFB(S59).

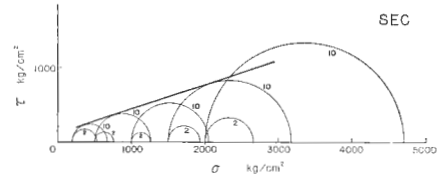

Fig. 163 Mohr envelope curve for Hamatsuda sandstone (1), SEC(S53). 2 and 10 % strength.

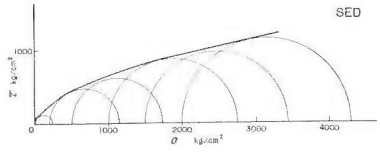

Fig. 164 Mohr envelope curve for Hamatsuda sandstone (2), SED(S54).

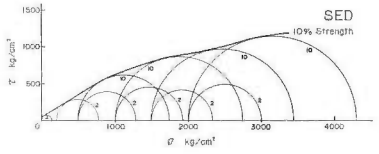

Fig. 165 Mohr envelope curve for Hamatsuda sandstone (2), SED(S54). 2 and 10 % strength.

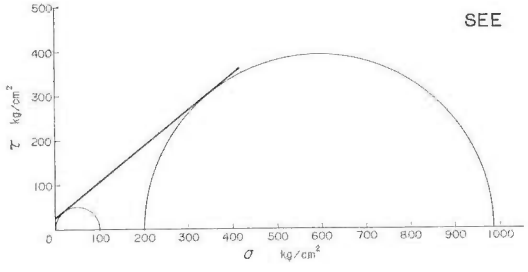

Fig. 166 Mohr envelope curve for Hamatsuda sandstone (3), SEE(S55).

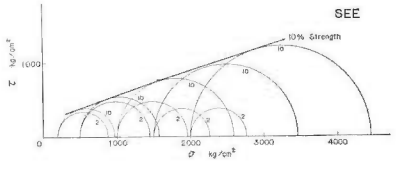

Fig. 167 Mohr envelope curve for Hamatsuda sandstone (3), SEE(S55). 2 and 10 % strength.

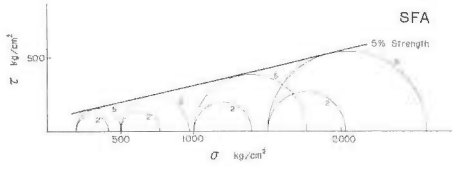

Fig. 168 Mohr envelope curve for Hamatsuda sandstone (4), SFA(S58). 2 and 10 % strength.

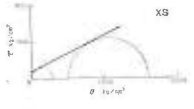

Fig. 169a Mohr envelope curve for Hamatsuda sandstone (5), XS(S69).

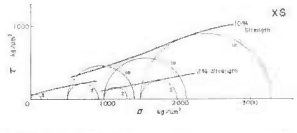

Fig. 169b Mohr envelope curve for Hamatsuda sandstone (5), XS(S69). 2 and 10 % strength.

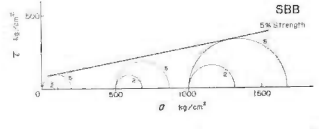

Fig. 170 Mohr envelope curve for Tentokuji sandstone, SBB(S25). 2 and 5 % strength.

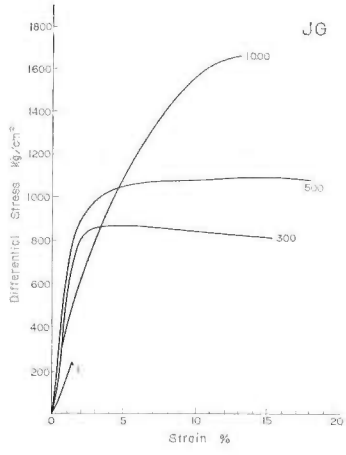

Fig. 171 Stress-strain curve for Asagai sandstone, JG(S15).

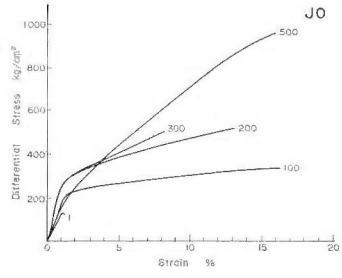

Fig. 172 Stress-strain curve for Iwaki sandstone, JO(S16).

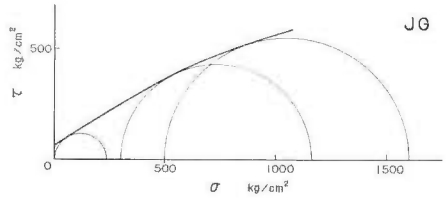

Fig. 173 Mohr envelope curve for Asagai sandstone, JG(S15).

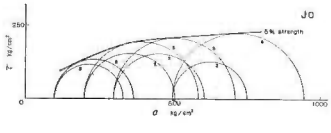

Fig. 174 Mohr envelope curve for Iwaki sandstone, JO(S16). 2 and 5 % strength.

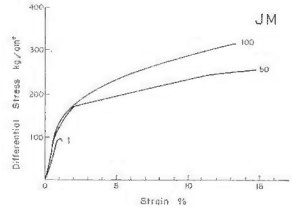

Fig. 175 Stress-strain curve for Takaku group sandstone, JM(S8).

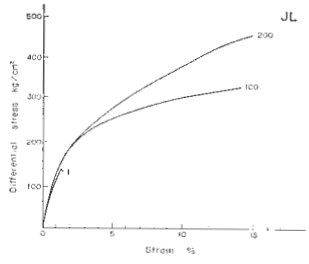

Fig. 176 Stress-strain curve for Nakayama sandstone, JL(S9).

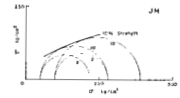

Fig. 177 Mohr envelope curve for Takaku group sandstone, JM(S8). 2 and 10 % strength.

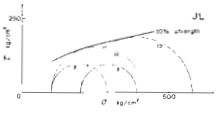

Fig. 178 Mohr envelope curve for Nakayama sandstone, JL(S9). 2 and 10 % strength.

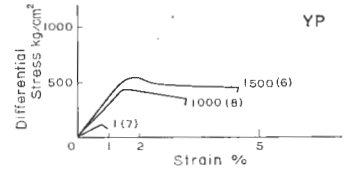

Fig. 179 Stress-strain curve for Zushi formation sandstone, YP(S72).

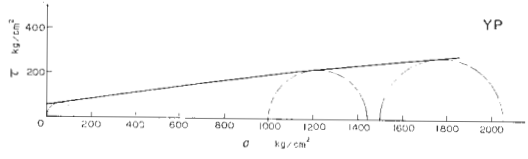

Fig. 180 Mohr envelope curve for Zushi formation sandstone, YP(S72).

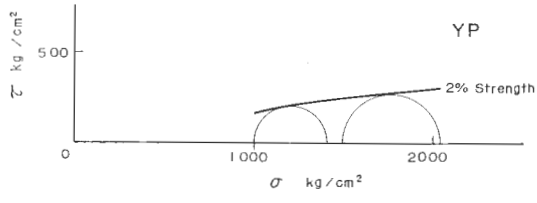

Fig. 181 Mohr envelope curve for Zushi formation sandstone, YP(S72). 2 % strength.

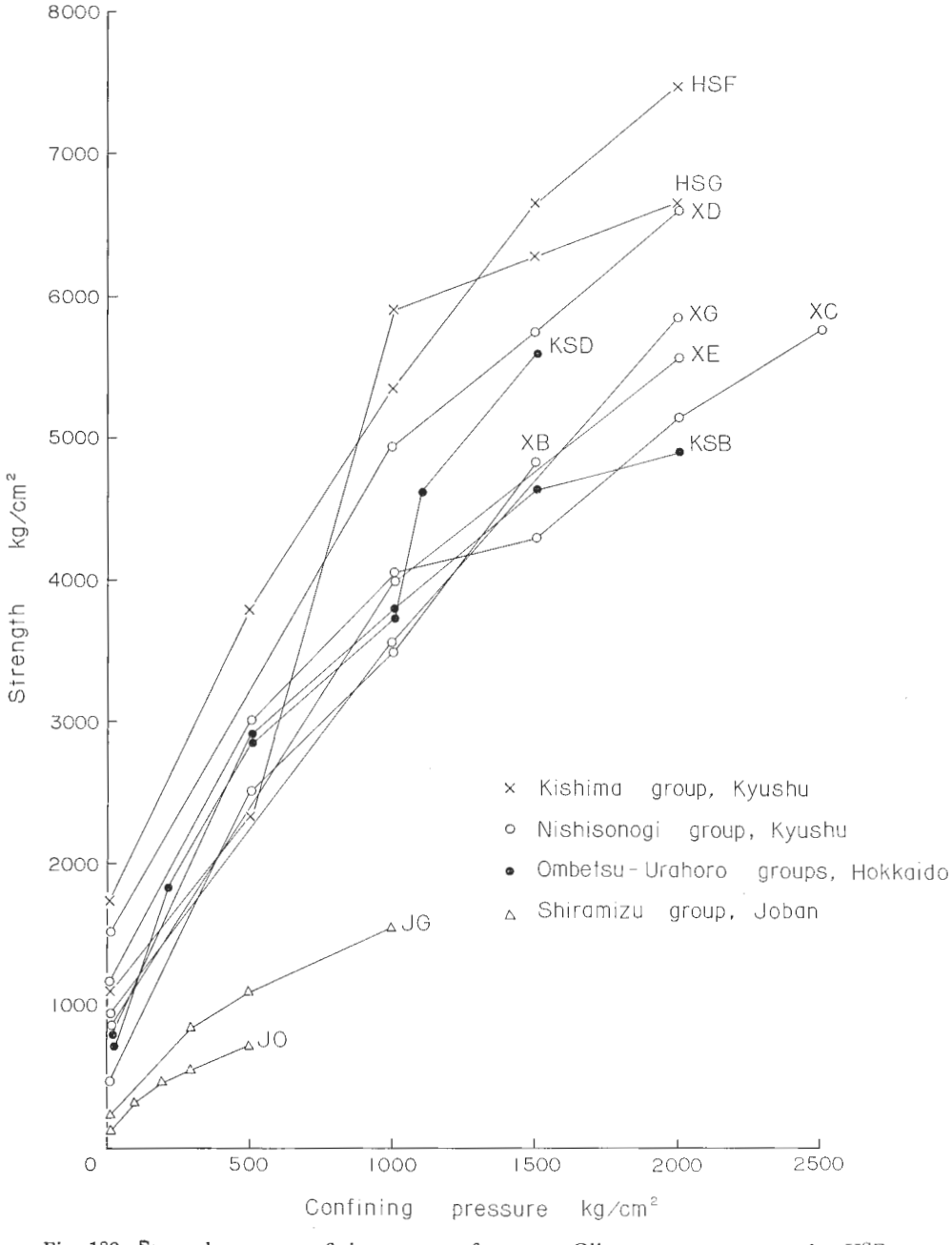

Fig. 182 Strength versus confining pressure for upper Oligocene arenaceous rocks, HSF, HSG, XD, XE, XC, XG, XB, KSB, KSD, JG, and JO.
×, Kishima group sandstones: ○, Nishisonogi group sandstones: ●, Ombetsu-Urahoro group sandstones: △, Shiramizu group sandstones.
The points of strength show ultimate or 10 % strength.

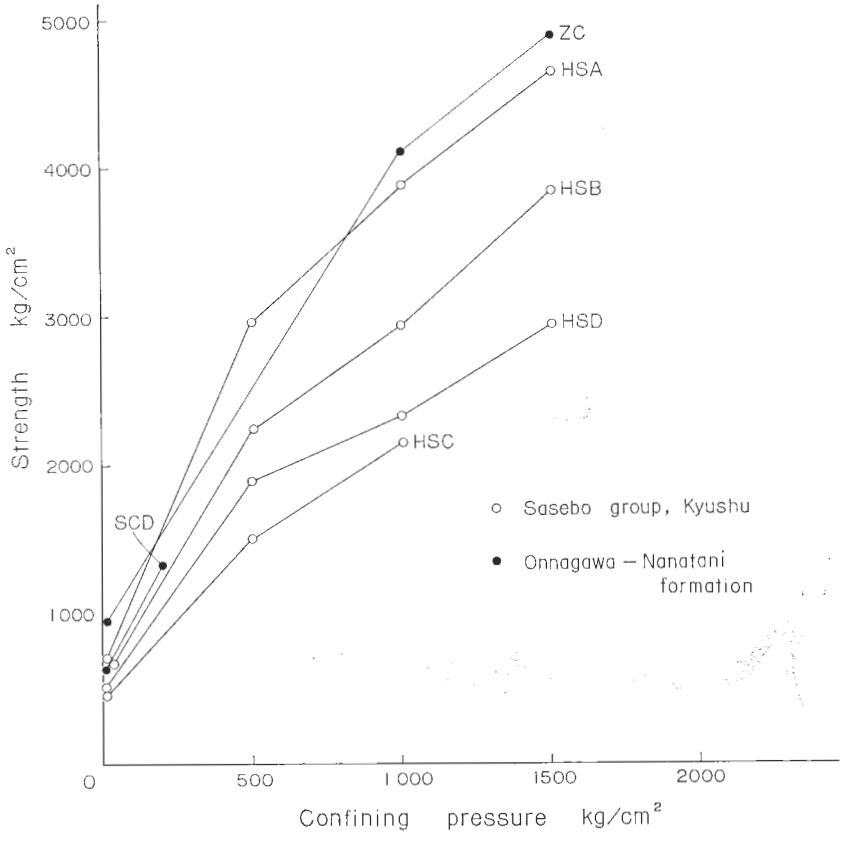

Fig. 183 Strength versus confining pressure for lower Miocene arenaceous rocks, ZC, SCB, HSA, HSB, HSC, and HSD. ○, Sasebo group sandstones: ●, Onnagawa-Nanatani formation sandstones. The points of strength show ultimate or 10% strength.

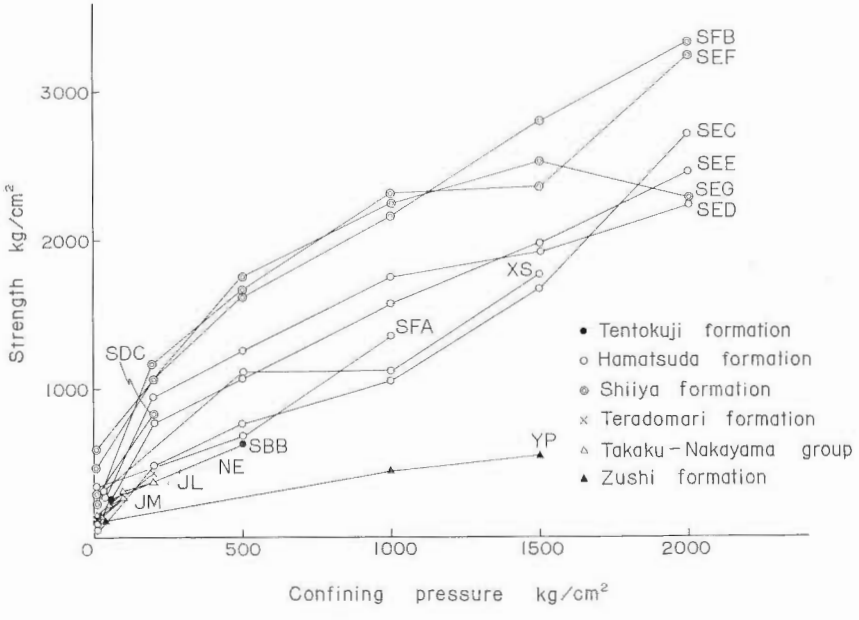

Fig. 184 Strength versus confining pressure for upper Miocene to lower Pliocene arenaceous rocks, NE, SDC, SEF, SEG, SFB, SEC, SED, SEE, SFA, XS, SBB, JM, JL, and YP. ●, Tentokuji formation sandstones: ○, Hamatsuda formation sandstones: ◎, Shiiya formation sandstones: ×, Teradomari formation sandstones: △, Takaku-Nakayama group sandstones: ▲, Zushi formation sandstone. The points of strength show ultimate and 10% strength.

IV. 4 Pyroclastic rocks

Fig. 207 denotes the relation between strength and confining pressure of the tested pyroclastic rocks. It also seems, that porosity is the most important factor to determine the strength and ductility. Three rocks, XO(S66), Nishiyama formation tuff; XF(S90), Uridake formation tuff, Nishisonogi group; and XIN(S70), Kimyozan tuff from Matsushiro, Nagano Prefecture, are less than 10% in porosity. These rocks are the most brittle among tested twelve pyroclastic rocks (NG(S44), Hozumi tuff of Teradomari formation, was deformed at atmospheric pressure only). XO (S66) and XF(S90) become transitional at 1000 kg/cm^2 and XIN (S70) becomes transitional at 500 kg/cm^2. XO(S66) and XF(S90), both fine-grained compact tuff, tend to make network type fracture. XO(S66) produces conjugate shear fractures at 500 kg/cm^2 in brittle behavior (or nearly transitional). XF (S90) presents a typical network in the part that contains much tuffaceous materials. In the above rocks, an effect of grain size upon strength and ductility is also an important factor. XO(S66) is the most fine-grained, XF(S90) is next and XIN(S70) is medium sand-grained.

ZU(S83), Hayama group tuff has the porosity of 36.3%, but it is very fine-grained. NH(S45), Katsumi tuff of Teradomari formation, is very fine sand-grained tuff with the porosity of 14.0%. ZU(S83) and NH(S45) are next strong and brittle. They become transitional at 500 kg/cm^2 and turn into visco-ductile at 1500 kg/cm^2 (ZU) or 2000 kg/cm^2 (NH). ZU(S83), finer-grained tuff, is found with network type of fractures at 500 kg/cm^2 under transitional behavior, while NH(S45), a little coarser-grained tuff, presents single shear fracture from 500 to 1500 kg/cm^2 confining pressure. SDB(S49), Shiiya formation tuff, SAD (S23), Funakawa formation tuff, NI (S35), Nampeizawa tuff, SAC(S22), Nanakura tuff, and SAB, Tentokuji formation tuff, are fine to coarse sand-grained tuff with porosity ranging from approximately 40 to 16%. They are visco-ductile at low confining pressure. SAD(S23) is visco-ductile behavior at 600 kg/cm^2 and others are visco-ductile approximately at 300 kg/cm^2.

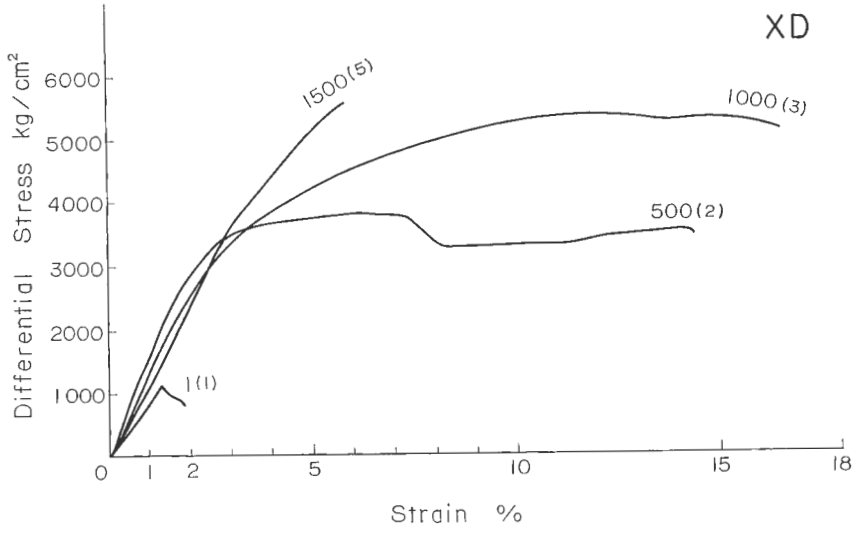

Fig. 185 Stress-strain curve for Nishiyama formation tuff, XO(S66).

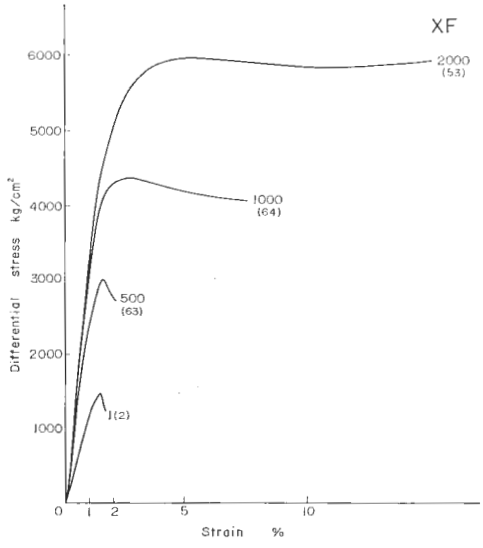

Fig. 186 Stress-strain curve for Uridake formation tuff, XF(S90).

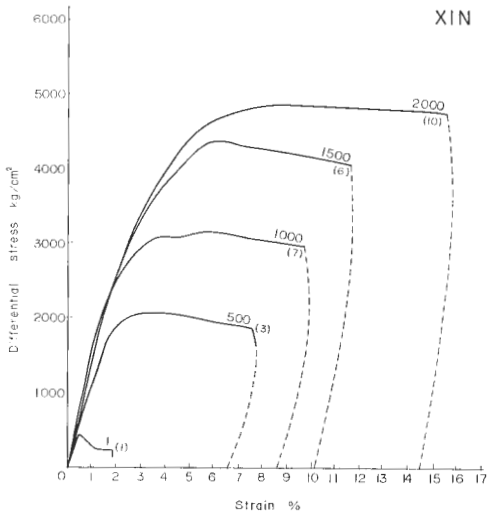

Fig. 187 Stress-strain curve for Kimyozan tuff, XIN(S70).

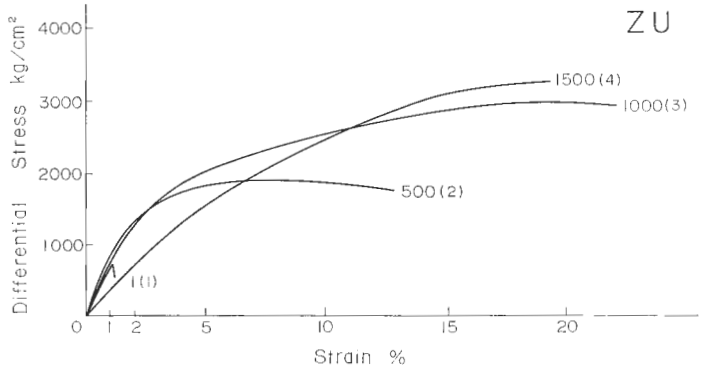

Fig. 188 Stress-strain curve for Hayama group tuff, ZU(S83).

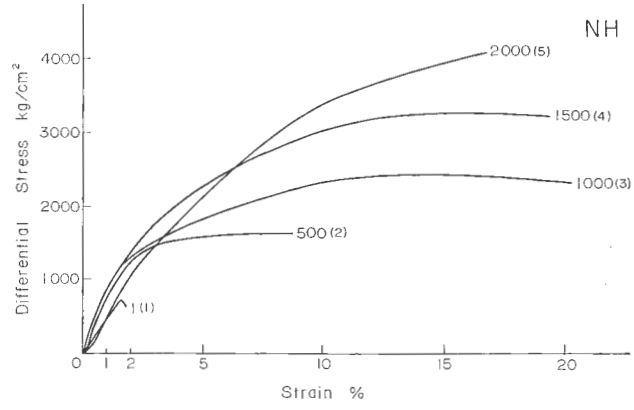

Fig. 189 Stress-strain curve for Katsumi tuff, Teradomari formation, NH(S45).

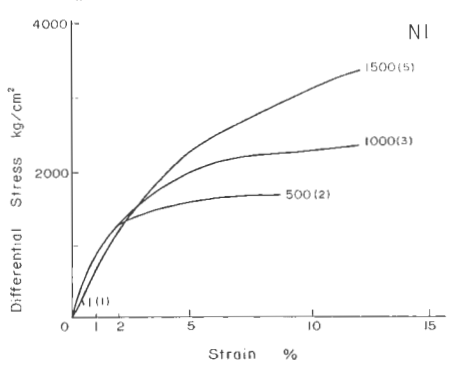

Fig. 190 Stress-strain curve for Gomoto tuff, Teradomari formation NI(S46).

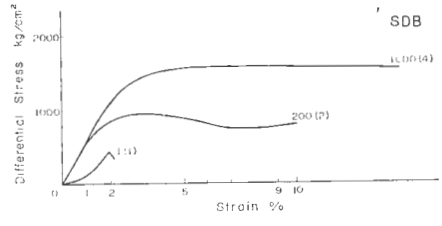

Fig. 191 Stress-strain curve for Shiiya formation tuff, SDB(S49).

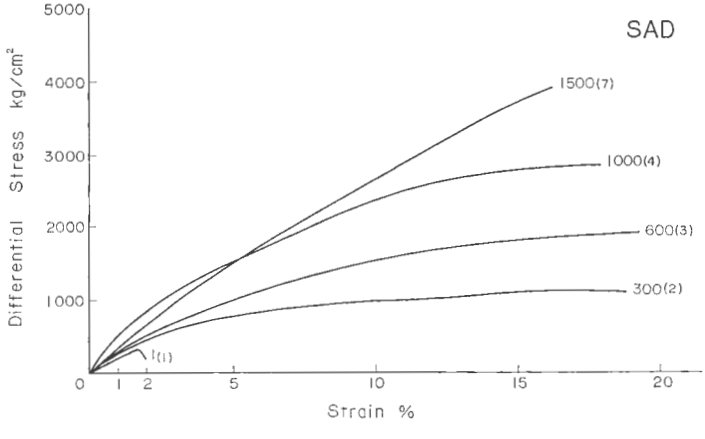

Fig. 192 Stress-strain curve for Funakawa formation tuff (1), SAD(S23).

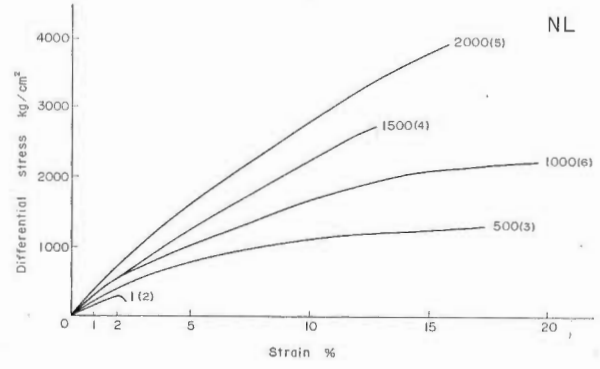

Fig. 193 Stress-strain curve for Nampeizawa tuff, Funakawa formation (2), NL(S35).

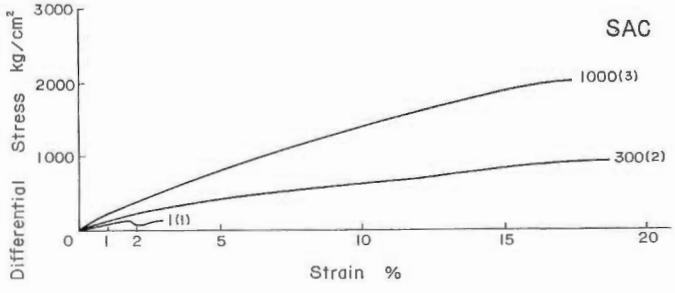

Fig. 194 Stress-strain curve for Nanakura tuff, Funakawa formation (3), SAC(S22).

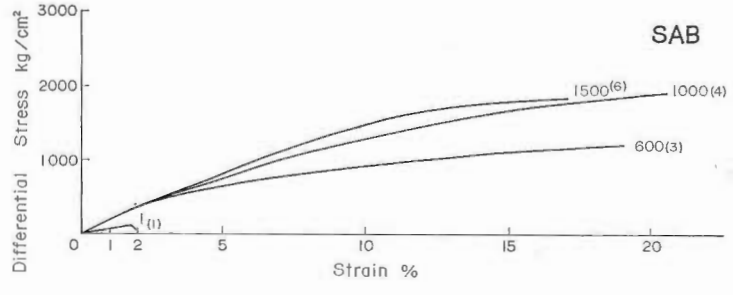

Fig. 195 Stress-strain curve for Tentokuji formation tuff, SAB(S21).

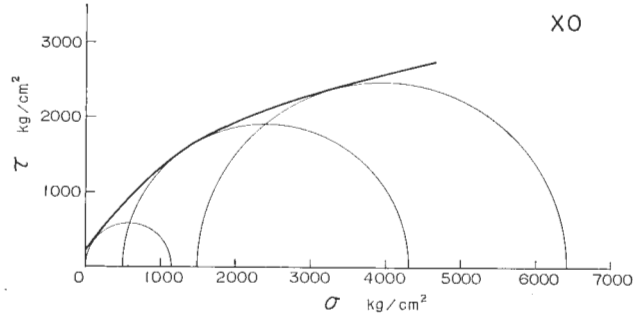

Fig. 196 Mohr envelope curve for Nishiyama formation tuff, XO(S66).

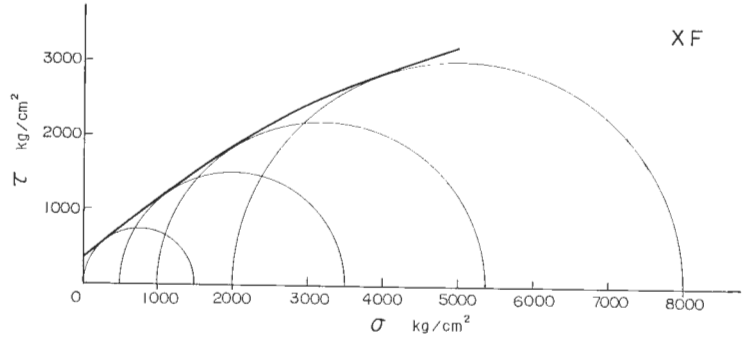

Fig. 197 Mohr envelope curve for Uridake formation tuff, XF(S90).

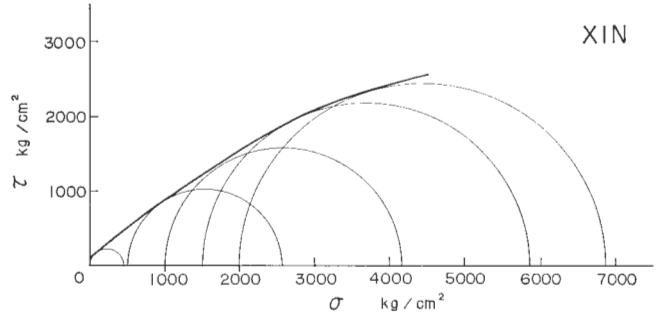

Fig. 198 Mohr envelope curve for Kimyozan tuff, XIN(S70).

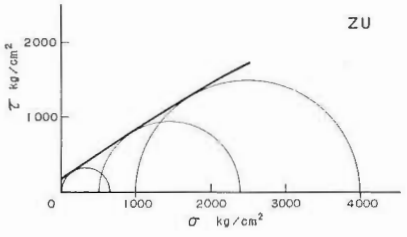

Fig. 199 Mohr envelope curve for Hayama group tuff, ZU(S83).

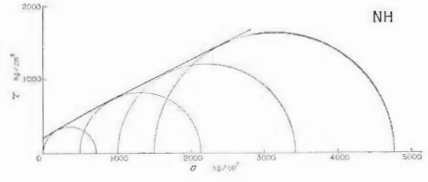

Fig. 200 Mohr envelope curve for Katsumi tuff, NH(S45).

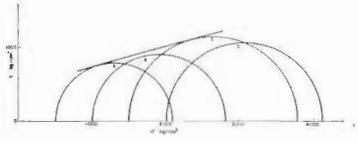

Fig. 201 Mohr envelope curve for Katsumi tuff, NH(S45). 5% strength.

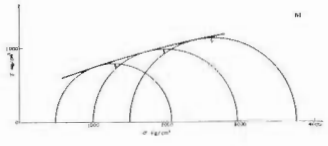

Fig. 202 Mohr envelope curve for Gomoto tuff, NI(S46). 5 % strength.

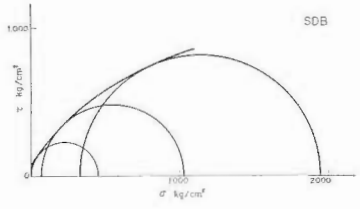

Fig. 203 Mohr envelope curve for Shiiya formation tuff, SDB(S49).

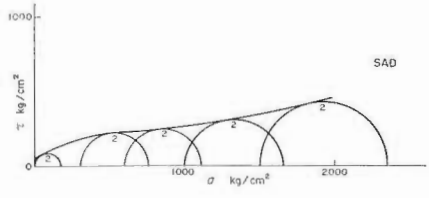

Fig. 204 Mohr envelope curve for Funakawa formation tuff (1), SAD(S23). 2 % strength.

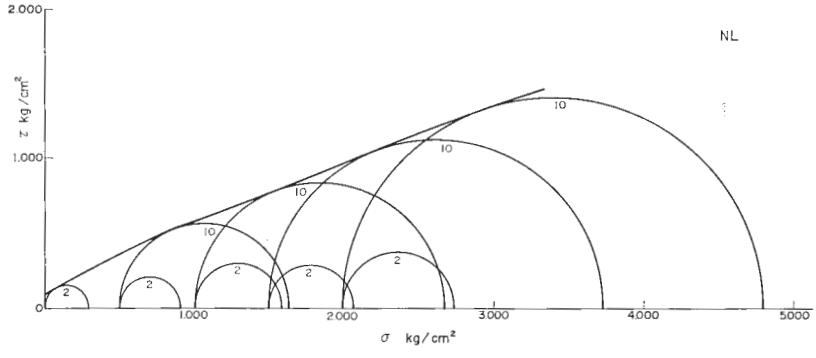

Fig. 205 Mohr envelope curve for Nampeizawa tuff, NL(S35). 2 and 10 % strength.

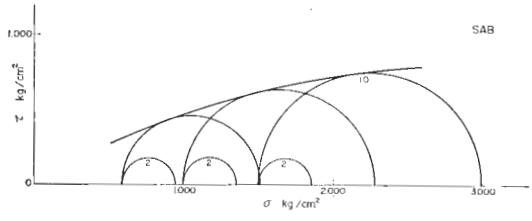

Fig. 206 Mohr envelope curve for Tentokuji formation tuff, SAB(S21). 2 and 10 % strength.

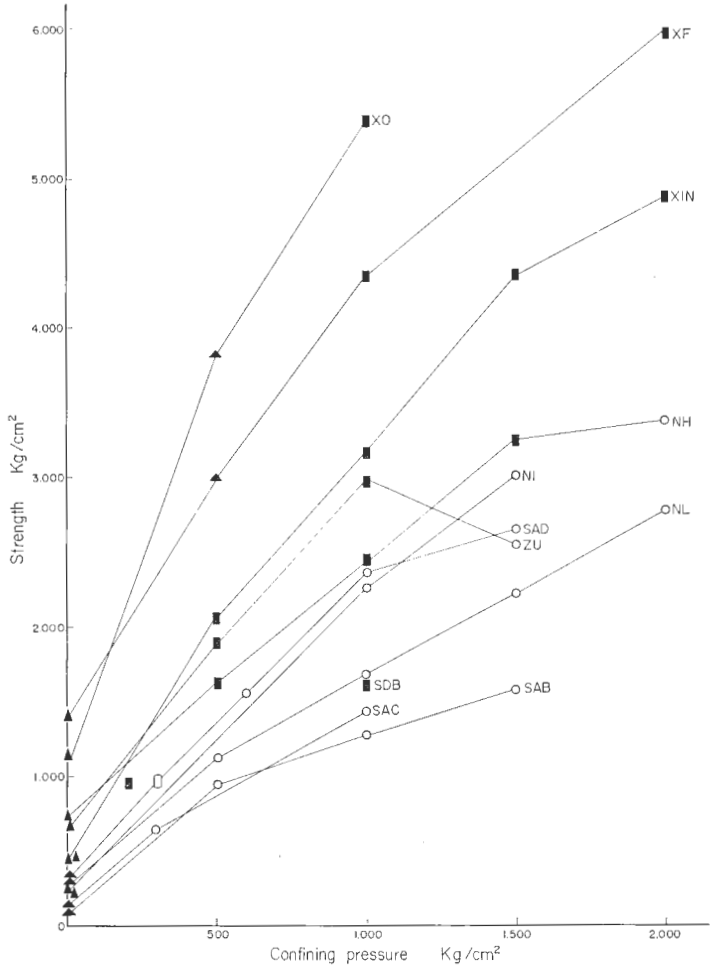

Fig. 207 Strength versus confining pressure for pyroclastic rocks, XO, XF, XIN, ZU, NH, NI, SAD, NL, SAC, and SAB. ▮, very brittle behavior: ▲, brittle behavior: ▮, transitional behavior: ○, ductile behavior: ○, visco-ductile behavior. Solid mark is ultimate strength, and open mark is 10% strength.

IV. 5 Volcanic rocks

Because volcanic rocks were experimented incidentally, the tested rocks here are limited to a kind of sheets or lava flows that are found among the clastic sedimentary rocks in the studied area. The tested rocks contain one basalt, three andesites, and two liparites.

Ohtawa basalt, XM(S92), is upper Pliocene basalt that develops over a wide area in northwestern Kyushu. It is brittle up to 1000 kg/cm^2 (Fig. 209). It produces network fractures at 500 and 1000 kg/cm^2.

Among the andesites, XP(S67), Nishiyama formation andesite, is the most brittle and strongest. This is brittle up to 2000 kg/cm^2 confining pressure, and its strength is about 7000 kg/cm^2 and 5000 kg/cm^2 at 2000 and 1000 kg/cm^2 confining pressures, respectively. Of this rock, produced fractures are of network type from 500 to 2000 kg/cm^2. Other two andesites show different curves. Minagamiyama andesite, XIP(S71), is brittle up to 1000 kg/cm^2. However, at 1500 and 2000 kg/cm^2, it becomes visco-ductile. Tsugawa formation andesite, SFD(S61) is a loose cemented, dirty andesite. It belongs stratigraphically to green tuff horizon. The tested pressures are 1 and 500 kg/cm^2 only. As far as up to the tested pressures, it is brittle. XIP(S71) tends to be of network type under brittle behavior (1000kg/cm^2).

Liparite samples show visco-ductile behavior comparatively. Taki liparite, JB (S13) becomes transitional at 1000 kg/cm^2. Nanatani formation liparite, SFC(S60) is transitional at 1000 kg/cm^2, too. SFC(S60) shows a similar change as XIP(S71). At 1500 kg/cm^2, it seems to be more visco-ductile. JB (S13) shows network type fractures at 1000 and 1500 kg/cm^2. SFC(S60) shows network type fractures at 1000 and 1500 kg/cm^2.

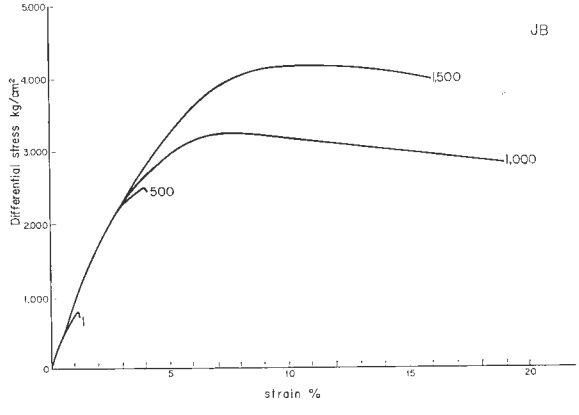

Fig. 208 Stress-strain curve for Taki formation liparite, JB(S13).

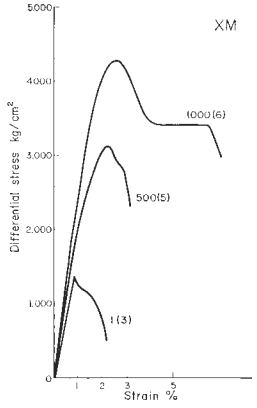

Fig. 209 Stress-strain curve for Ohtawa basalt, XM(S92).

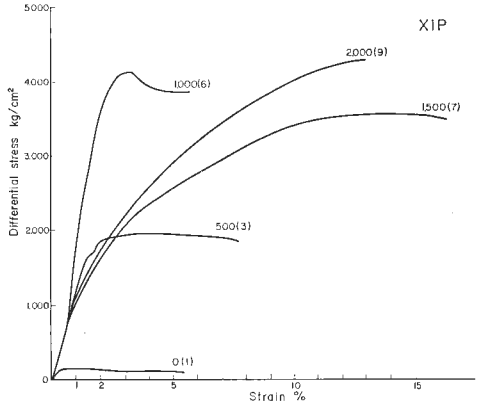

Fig. 210 Stress-strain curve for Minagamiyama andesite, XIP(S71).

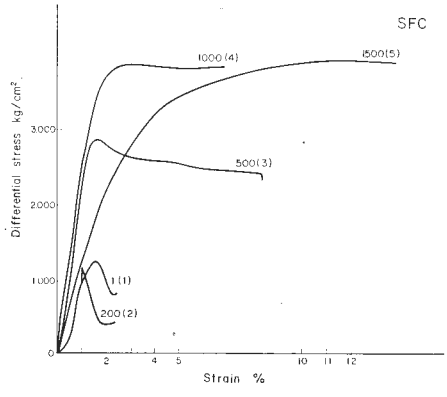

Fig. 211 Stress-strain curve for Nanatani formation liparite, SFC(S60).

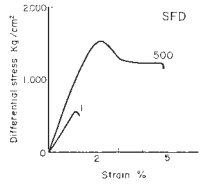

Fig. 212 Stress-strain curve for Tsugawa formation andesite, SFD(S61).

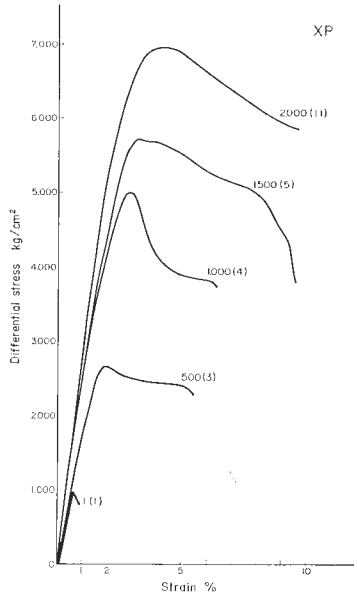

Fig. 213 Stress-strain curve for Nishiyama formation andesite, XP(S67).

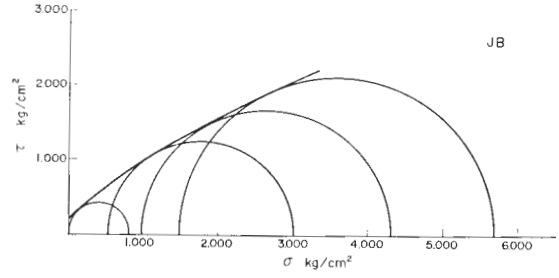

Fig. 214 Mohr envelope curve for Taki formation liparite, JB(S13).

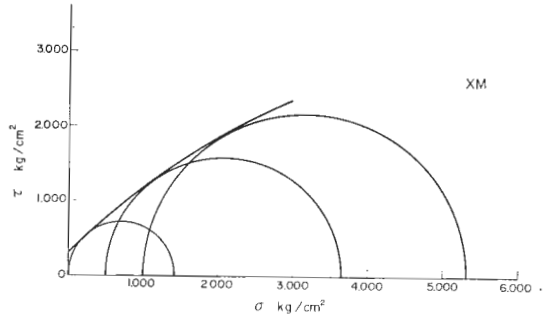

Fig. 215 Mohr envelope curve for Ohtawa basalt, XM(S92).

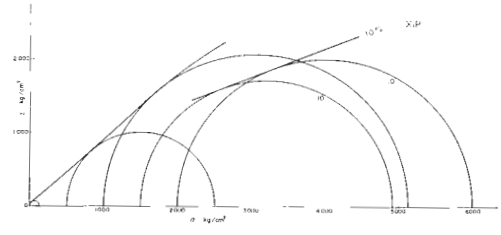

Fig. 216 Mohr envelope curve for Minagamiyama andesite, XIP(S71). Ultimate and 10 % strength.

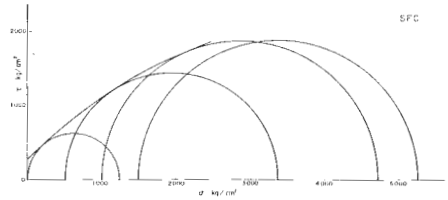

Fig. 217 Mohr envelope curve for Nanatani formation liparite, SFC(S60).

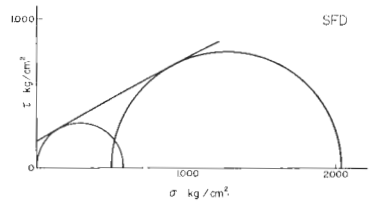

Fig. 218 Mohr envelope curve for Tsugawa formation andesite, SFD(S61).

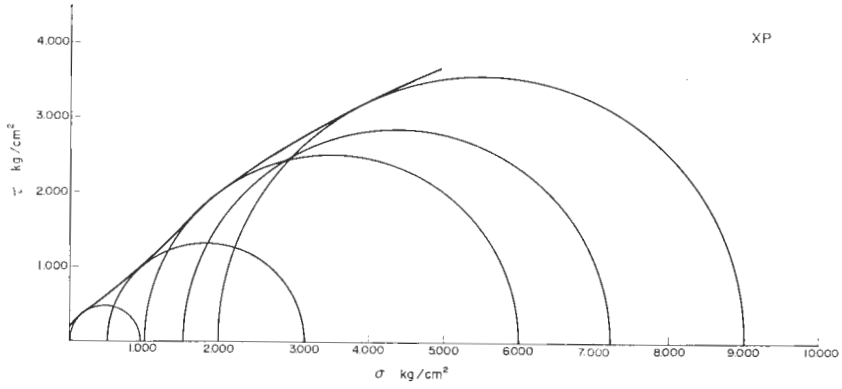

Fig. 219 Mohr envelope curve for Nishiyama formation andesite, XP(S67).

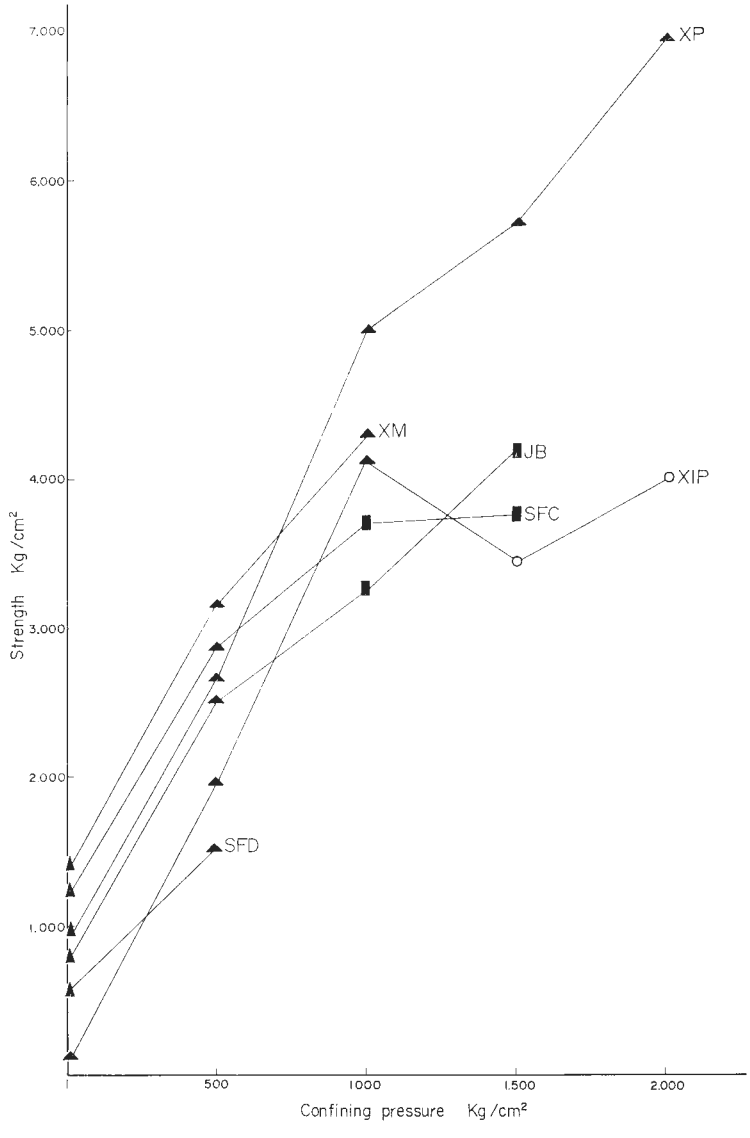

Fig. 220 Strength versus confining pressure for volcanic rocks, JB, XM, XIP, SFC, SFD, and XP. ▲, very brittle behavior : ▲, brittle behavior : ▌, transitional behavior : □, ductile behavior : ○, visco-ductile behavior. Solid mark is ultimate strength and open mark is 10% strength.

V. Discussion

V. 1 Deformational behavior and strength

It has been known that the rocks are brittle at low confining pressure, and as confining pressure increases, the behavior of deformation becomes ductile (ROBERTSON, 1955 ; HANDIN and HAGER, 1957 ; PATERSON, 1958 ; MOGI, 1966). MOGI (1966) found out a simple rule of transition from brittle to ductile behaviors. BYERLEE (1968) clarified the rule further. BYERLEE's work is based upon the observation that, in brittle behavior, the stress-strain curve shows remarkable stress drop after the yielding, while, in ductile behavior, the stress strain curve shows no visible stress drop. According to this basis, BYERLEE calculated the frictional force along the fracture plane. BYERLEE showed that an almost linear relationship exists between normal stress and shear stress along the fracture planes thus determined, and that this line is closely agreeable with the boundary line between brittle and ductile behaviors in cases of silicate and carbonate rocks.

In order to study the transition from brittle to ductile, we also based on the frictional hypothesis. However, the method is different from BYERLEE's method. BYERLEE calculated normal and shearing stress along the already produced planes. Moreover, he used a conventional method in the calculation. He put the fracture angle θ as 30 degree for all cases. However, we tried to find out the initial friction along the macrofracture-planes when the macrofracture is about to be formed. MOGI(1964) and etc indicated that the angle of macroscopic fracture is not constant, but increases as confining pressure increases. we, also, obtained the result that this relation is varid for all tested rocks, (Figs. 251, 252, 253, and 254).

When an ultimate point is clearly shown on the stress-strain curve, it is probable that macrofracturing occurred at the ultimate point. Normal and shearing stresses along the fracture plane inclining θ to compressional axis are given by the next equation.

$$\tau=\frac{1}{2}(\sigma_1-\sigma_3)\sin 2\theta \cdots\cdots (5.1)$$

$$\sigma=\frac{1}{2}(\sigma_1+\sigma_3)-\frac{1}{2}(\sigma_1-\sigma_3)\cos 2\theta \cdots\cdots (5.2)$$

where $\sigma_1-\sigma_3$ is ultimate strength, and σ_3 is confining pressure. Compressional stress is taken positive.

we obtained σ_1 and σ_3 from the experimentation and θ by measuring the deformed specimens. Precise measurement of the angle is something difficult. It was measured as carefully as possible so that the figures obtained can represent an average value of the fracture of a specimen. The measured angle is shown in Table 4. The calculation was made for the test, in which the point of ultimate strength is known on stress-strain curve. The points indicated by the calculated τ and σ are usually below the points determined from Mohr envelope (points P, Q, R in Fig. 221). The results for argillaceous, arenaceous, pyroclastic, and volcanic rocks are shown in Fig. 222, 223, 224 and 225, respectively. On each point determined on the $\sigma-\tau$ co-ordinates, the mark showing the mode of deformation is drawn. We find in these figures that a simple curve separates very brittle and brittle marks from transitional and ductile marks. This, line is called the boundary from brittle to ductile. The inclination of boundary line is approximately 0.8 for τ/σ at low

pressure, and 0.65 for τ/σ at high pressure for argillaceous rocks. For arenaceous rocks, τ/σ along the boundary lines is a little high, that is 0.8 and 0.7 at low and high pressures, respectively. Pyroclastic rocks show the highest value of τ/σ, that is, 1.02 or 1.03 at low and high pressures, respectively. For volcanic rocks, the ratio τ/σ lies between pyroclastic and arenaceous rocks, 0.9 to 0.75 from low to high pressure. Fig. 226 shows the boundary lines from brittle to ductile for four kinds of rocks for comparison. The line showing friction along already fractured plane for carbonate and silicate rocks by BYERLEE is shown in the same diagram for reference.

It is very interesting that transition from brittle to ductile is closely related to the ratio τ/σ. The ratio is not the same for all kinds of rocks, but differs among the kinds of rocks. The ratio τ/σ is related to the internal frictional force along the fracture planes at the fracturing. The above results indicate that brittle fracturing requires more shearing stress under the same normal stress to make fracture than in ductile behavior. In Fig. 226, it is indicated that, for the same τ/σ, argillaceous rcoks are the most brittle, arenaceous rocks are next brittle, volcanic rocks are next, and pyroclastic rocks are the most ductile.

The transition from ductile to visco-ductile behavior is expressed by a simple relation, too. In Figs. 227 to 230, the transition lines on confining pressure-strength co-ordinates for argillaceous, arenaceous, pyroclastic and volcanic rocks respectively are shown. As shown in Fig. 232, argillaceous rocks are the least visco-ductile, especially at high confining pressure, arenaceous rocks are next visco-ductile. Pyroclastic and volcanic rocks are more visco-ductile than the former two. Pyroclastic rocks are more visco-ductile at low confining pressure and less visco-ductile at high confining pressure than volcanic rocks.

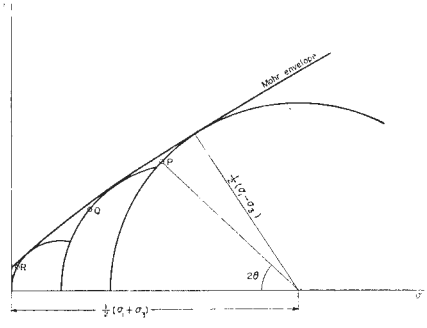

Fig. 221 A diagram showing how to find the respective points P, Q, R, and so on, from the measured angle 2θ and principal stresses σ_1 and σ_3 on a σ–τ co-ordinate.

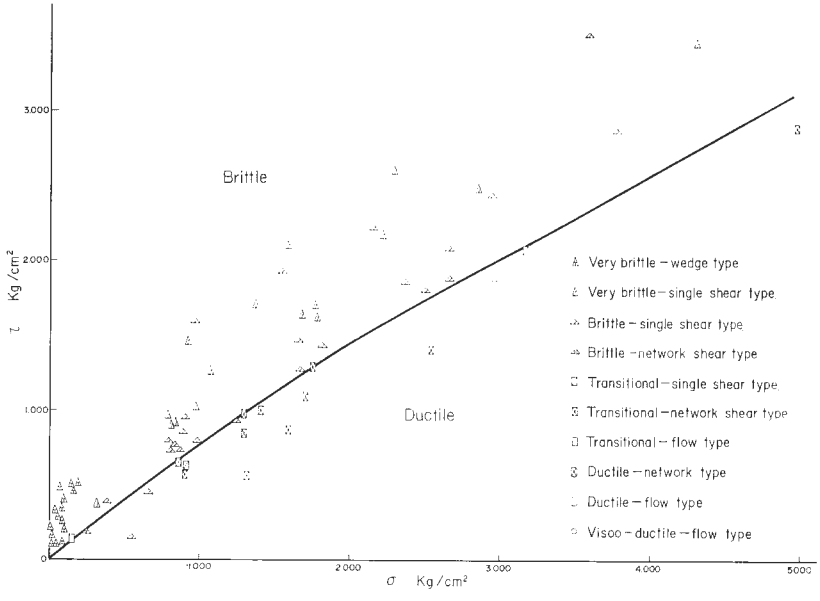

Fig. 222 Deformational behavior for argillaceous rocks plotted on σ–τ co-ordinate.

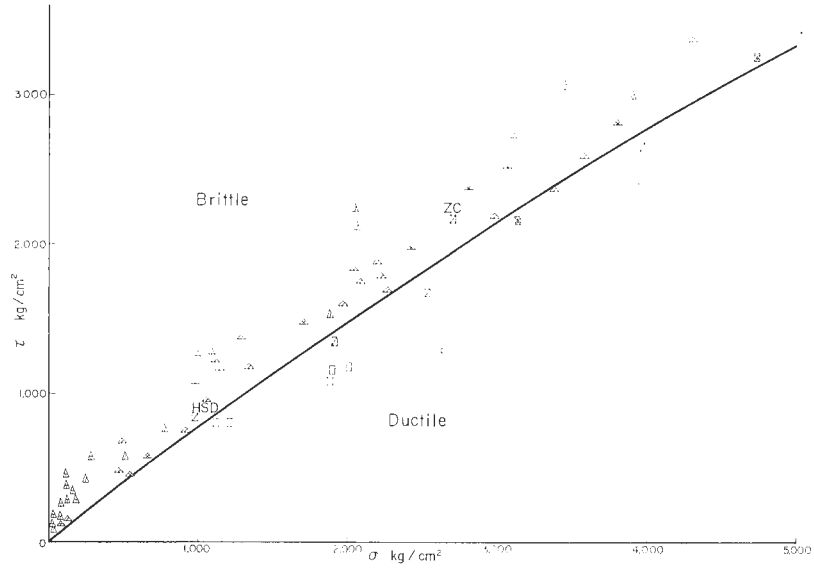

Fig. 223 Deformational behavior for arenaceous rocks plotted on σ–τ co-ordinate. The marks are the same as Fig. 222.

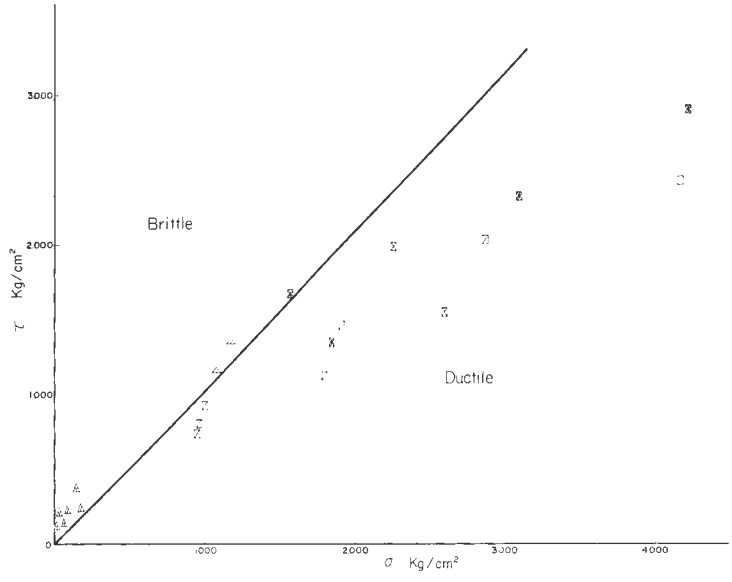

Fig. 224 Deformational behavior for pyroclastic rocks plotted on σ–τ co-ordinate. The marks are the same as Fig. 222.

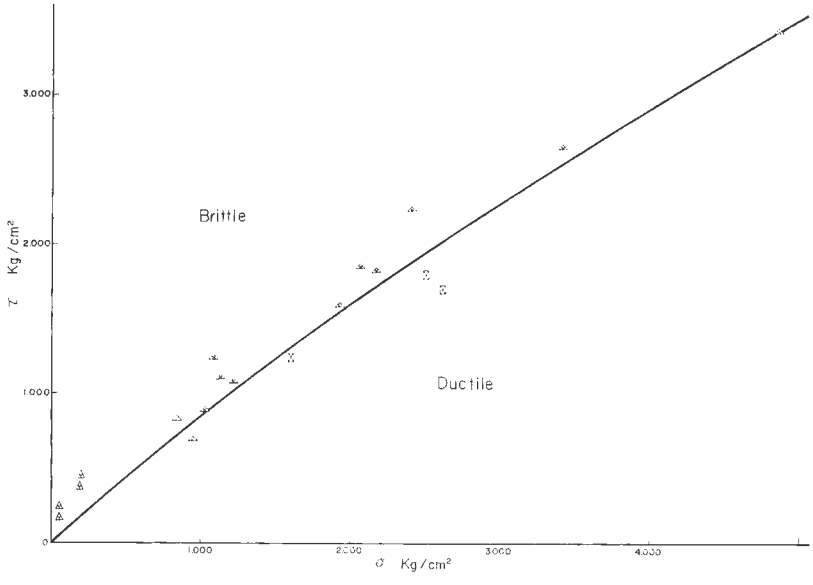

Fig. 225 Deformational behavior for volcanic rocks plotted on σ–τ co-ordinate. The marks are the same as Fig. 222.

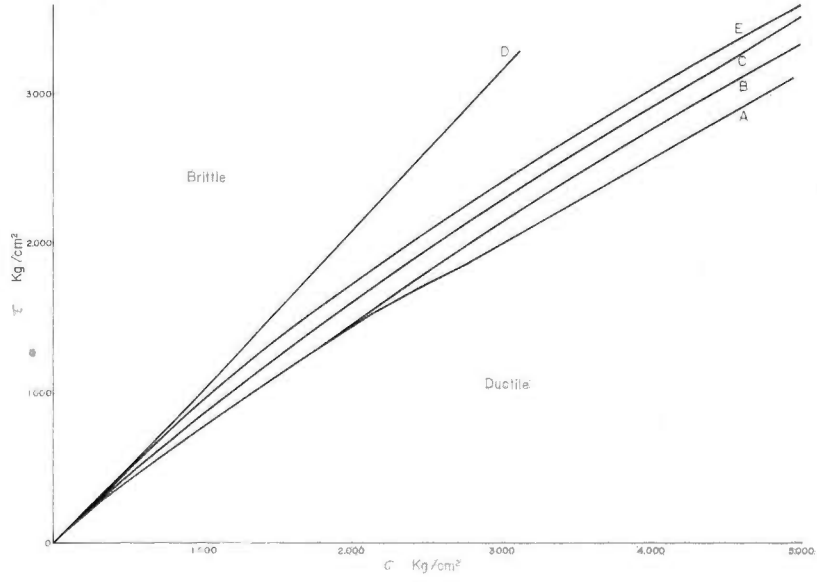

Fig. 226 The boundary lines from very brittle and brittle behaviors to transitional and ductile behaviors for each kind of rocks. A, for argillaceous rocks; B, for arenaceous rocks; C, for volcanic rocks; and D, for pyroclastic rocks. E is the line for the friction along pre-existed fracture plane of carbonate and plutonic rocks cited from BYERLEE(1968).

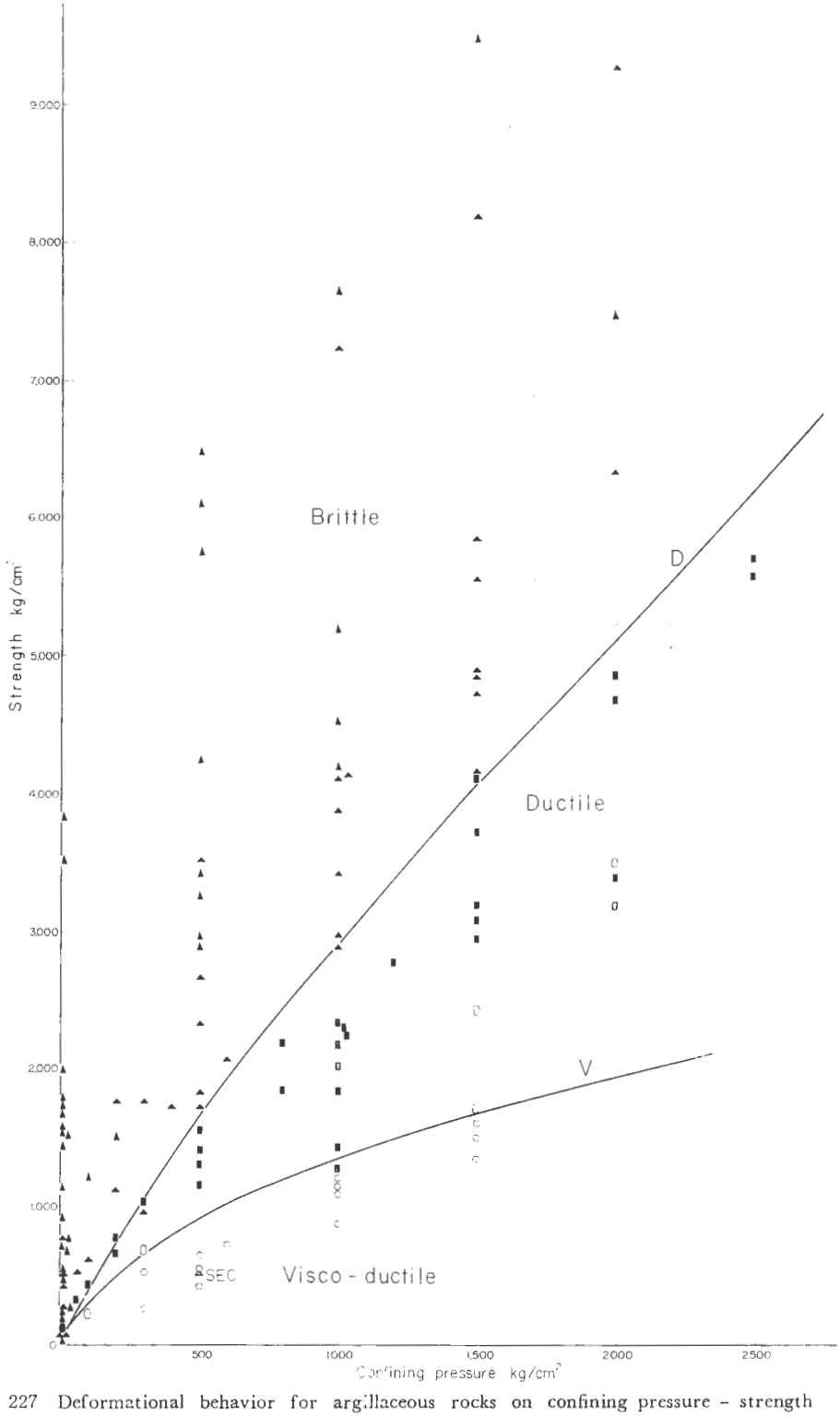

Fig. 227 Deformational behavior for argillaceous rocks on confining pressure – strength co-ordinate. The line D is the boundary from brittle to ductile calculated from the line in Fig. 222. The line V is the boundary for transition between transitional and ductile, and visco-ductile behaviors. The marks are the same as Fig. 220.

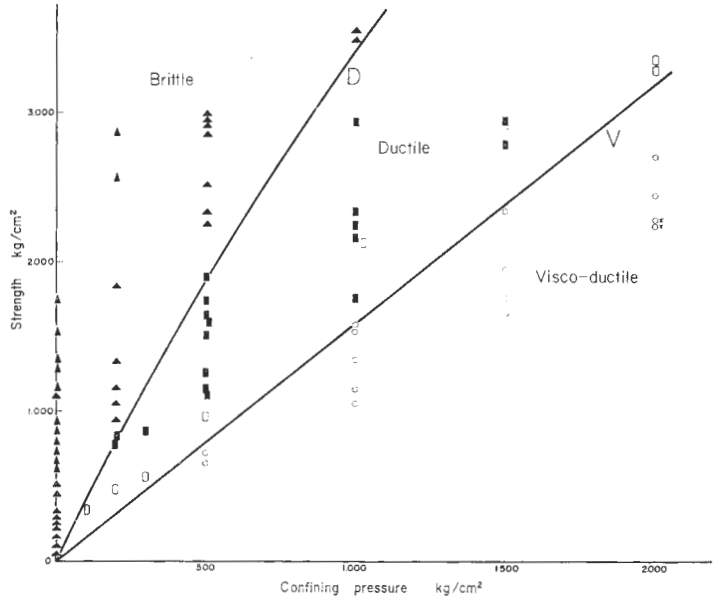

Fig. 228 Deformational behavior and transitional lines for arenaceous rocks. The marks are the same as Figs. 220 and 227.

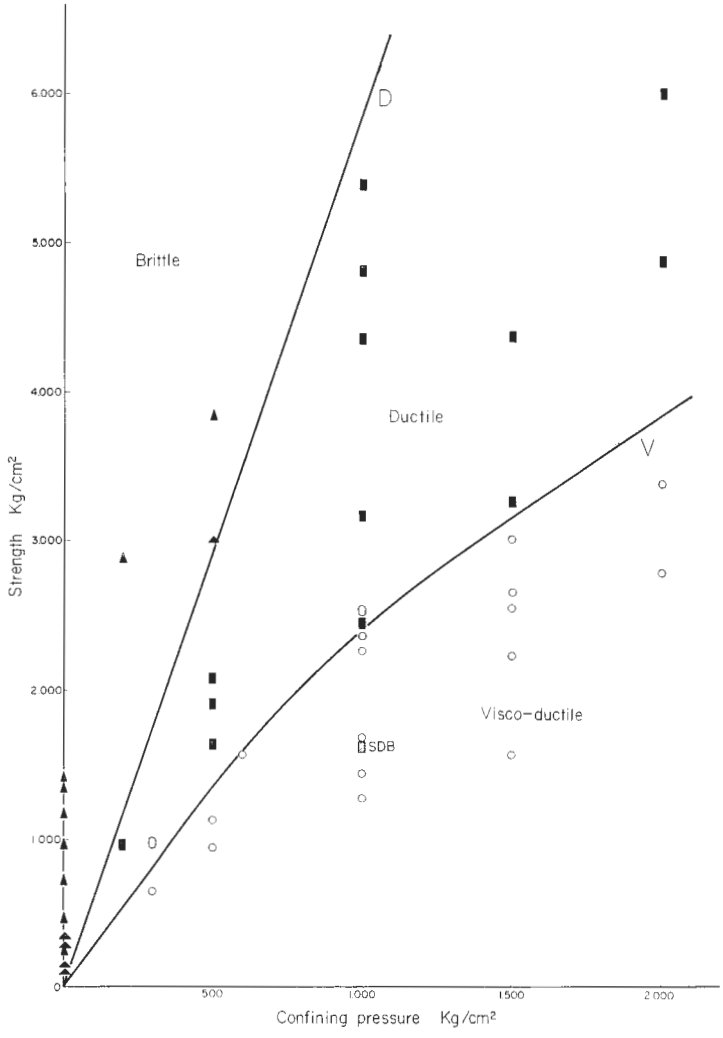

Fig. 229 Deformational behavior and transitional lines for pyroclastic rocks. The marks are the same as Figs. 220 and 227.

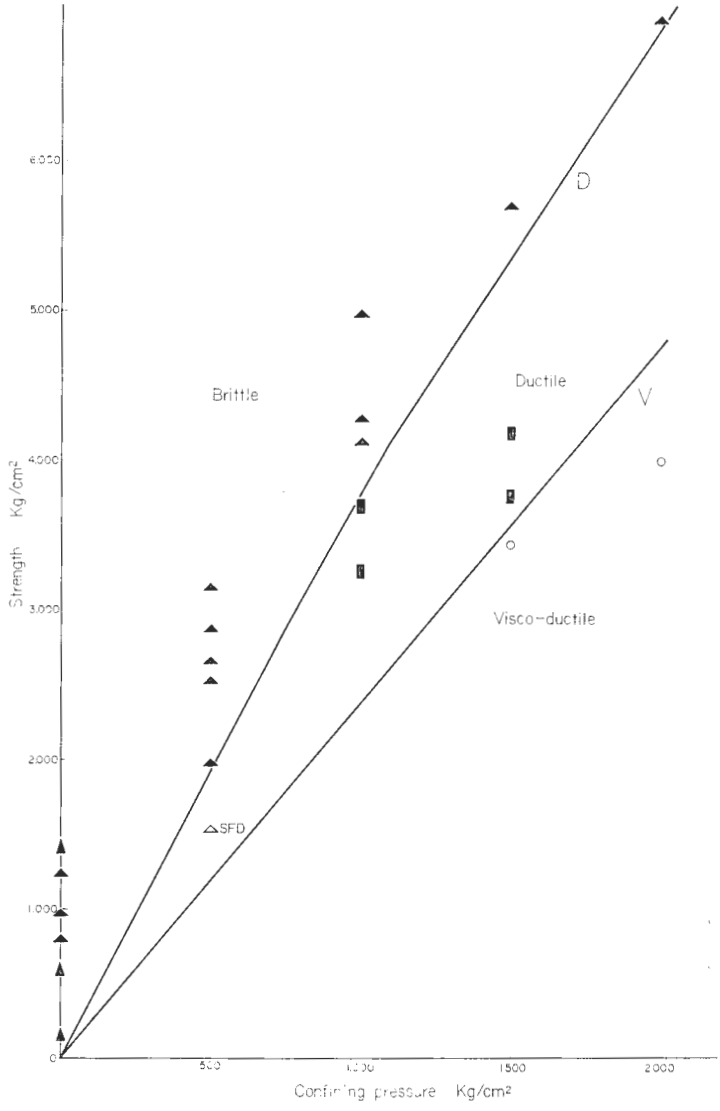

Fig. 230 Deformational behavior and transitional lines for volcanic rocks. The marks are the same as Figs. 220 and 227.

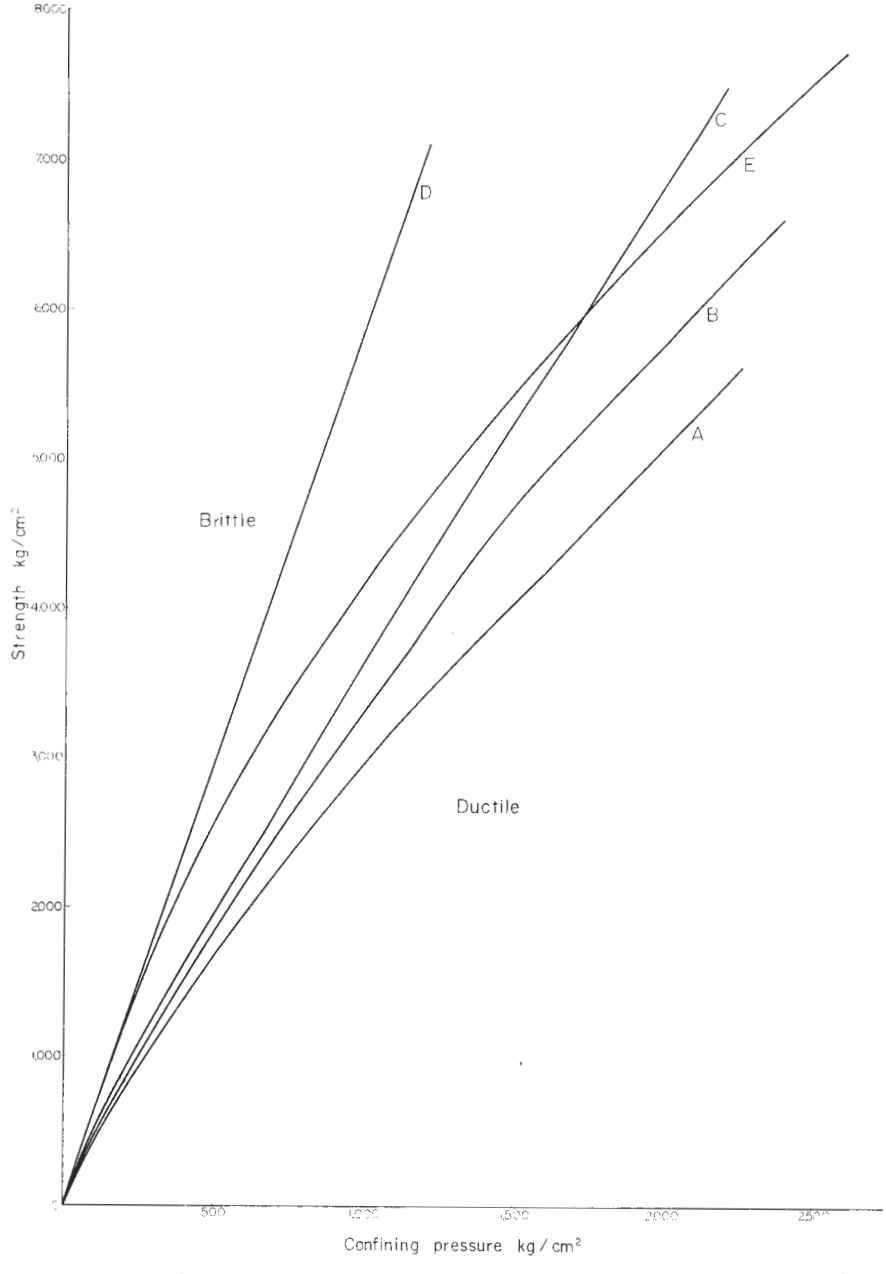

Fig. 231 The boundary lines from very brittle and brittle behaviors to transitional and ductile behaviors on confining pressure – strength co-ordinate deduced from Fig. 226. A, for argillaceous rocks; B, for arenaceous rocks; C, for volcanic rocks; D, for pyroclastic rocks. E, after BYERLEE(1968).

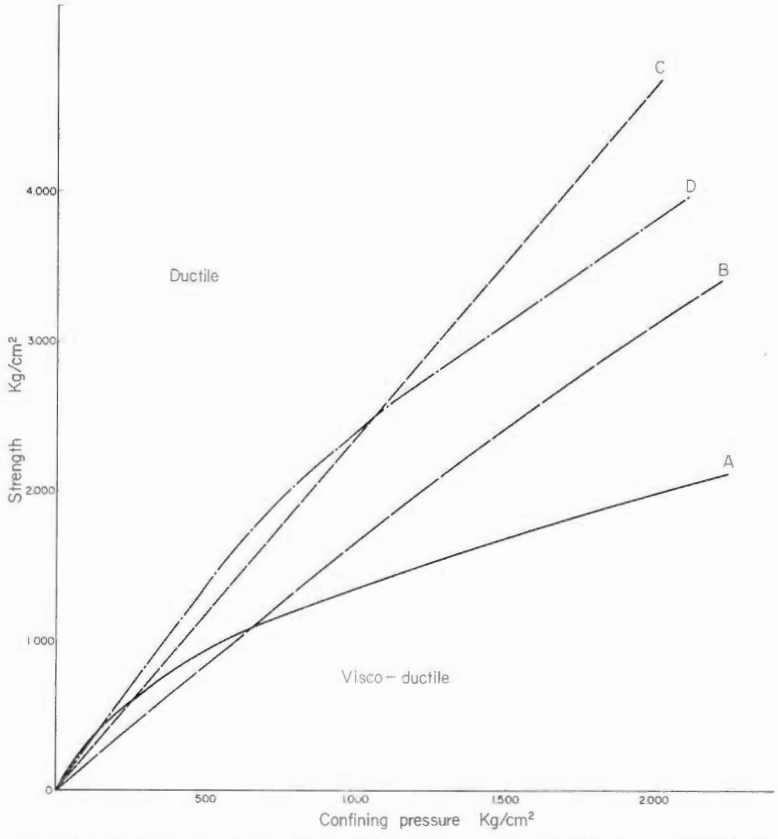

Fig. 232 The boundary lines from ductile behaviors to visco-ductile behavior for each kind of rocks. A, for argillaceous rocks; B, for arenaceous rocks; C, for volcanic rocks; and D, for pyroclastic rocks.

V. 2 Angle of fractures

In Fig. 233, value of observed 2θ for argillaceous rocks is plotted at the respective points on the $\sigma-\tau$ co-ordinate as Fig. 222. It is indicated that the value increases in regular arrangement towards right-lower direction. The contour lines for 30, 40, 50, 60, and 70 degrees were drawn on the chart as Fig. 234. In the same way, those for arenaceous, pyroclastic, and volcanic rocks were drawn as Figs. 235, 236, and 237. Fig. 238 is for all rocks tested.

In these figures, thin lines are determined by the following formula:

$$\mu=\tau/\sigma=\cot 2\theta \cdots\cdots\cdots\cdots (5.3)$$

We see that both thick and thin lines are almost the same between 30 to 40 degrees, but the difference tends to increase as the angle increases.

The observed angle is smaller than that given by the formula (5.3). It is expressed empirically as follows:

$$\mu = \cot (2\theta-\Delta) \cdots\cdots\cdots\cdots (5.4)$$

Here, Δ is the difference. For argillaceous rocks, both lines are nearly parallel between 30 and 40 degrees, but the difference amounts about 8 or 12 degrees for 60 or 70 degrees of 2θ. For arenaceous rocks, the difference is larger than for argillaceous rocks. Even at 40 degrees, the difference is counted about 6 degrees and, at 60 or 70 degrees, it is about 14 or 17 degrees. Most specimens, that were deformed at atmospheric pressure, show wedge type fracture pattern. In this case, the angle of fractures shows different values ranging 0 to around 20 or 30 degrees, and here the maximum value was measured and noted as in Table 4. Therefore, the lines from the observation around low pressure are exceptionally larger than that from the formula.

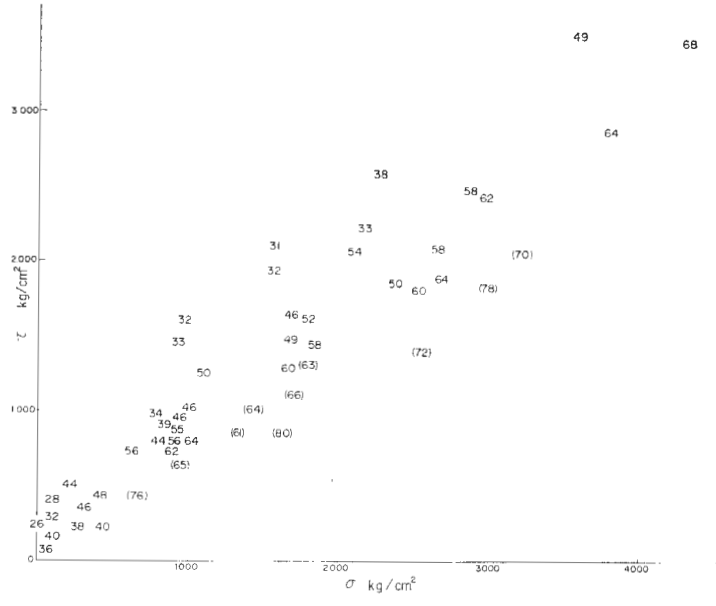

Fig. 233 Angle of fractures for argillaceous rocks plotted on $\sigma-\tau$ co-ordinate.

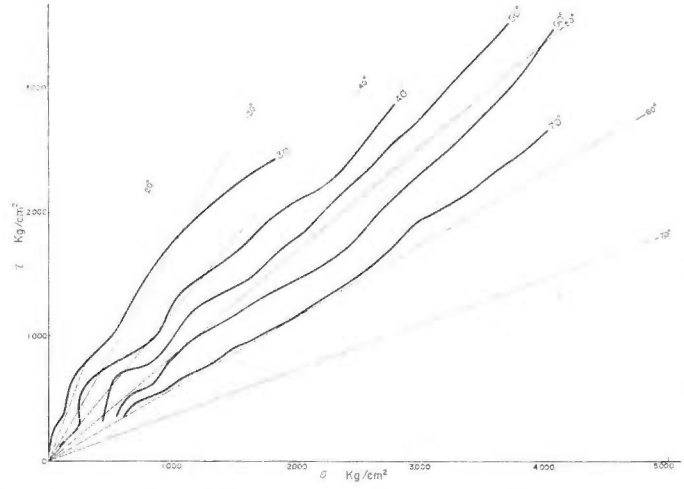

Fig. 234 Angle of fractures for argillaceous rocks on $\sigma-\tau$ co-ordinate, shown in contour lines (thick lines). Thin dotted lines show those determined by formula (5.3).

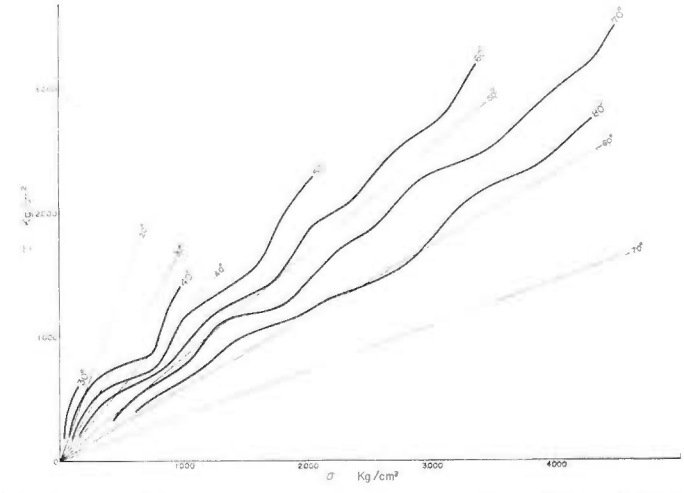

Fig. 235 Angle of fractures for arenaceous rocks on $\sigma-\tau$ co-ordinate. Thick lines are from measured angle, and thin dotted lines are from formula (5.3).

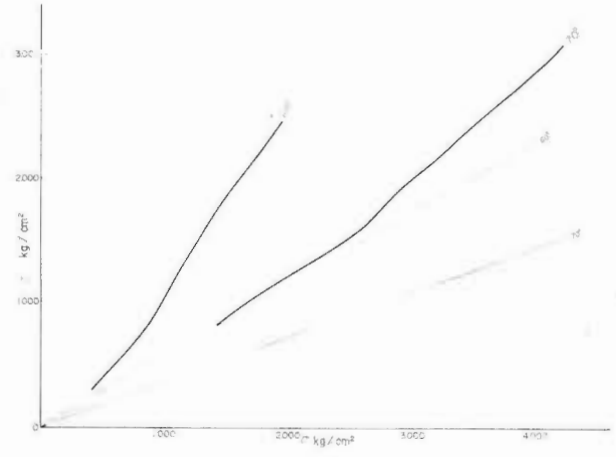

Fig. 236 Angle of fractures for pyroclastic rocks on σ–τ co-ordinate.

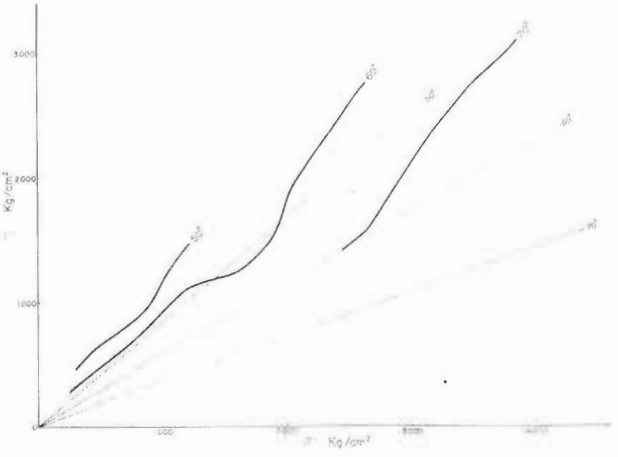

Fig. 237 Angle of fractures for volcanic rocks on σ–τ co-ordinate.

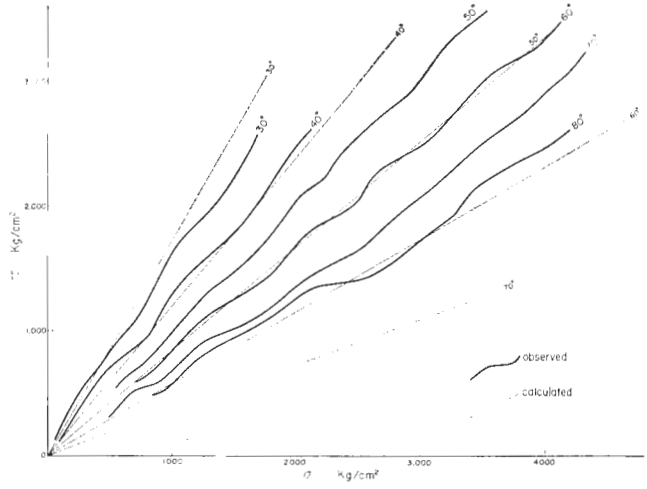

Fig. 238 Angle of fractures for all rocks tested. Thick lines are from measured angle, and thin dotted lines are from formula (5.3).

V. 3 Strain at fracturing

There is a comparatively regular relation between friction and strain at fracturing. The relation is plotted on diagrams, in which the strain ε and the ratio $\mu=\tau/\sigma$ are shown on abscissa and on ordinate, respectively. The diagrams were drawn for argillaceous, arenaceous, pyroclastic, and volcanic rocks in Figs. 239, 240, 241, and 242, respectively. It is indicated that the ratio μ decreases rapidly as the strain increases. In case of argillaceous and arenaceous rocks, comparatively more data were available. It seems that the points are arranged on a simple curve within a narrow zone except a few points. We obtain an empirical formula as follows to express the curves.

$$\mu=\cot\ (a-\beta)\cdots\cdots\cdots\cdots(5.5)$$

where "a" is a constant that is determined empirically for a kind of rock, and $\varepsilon=\cot\beta$. The thick lines in Figs. 239 and 240 are represented by the above formula, in which the values of "a" are determined 66°00′ and 67°53′, respectively, for argillaceous and arenaceous rocks. For pyroclastic and volcanic rocks, data were not enough to decide the relation. The values of "a" for the thick lines in Figs. 243 and 244 are 63°26′ and 65°46′, respectively.

If formula (5.5) is valid, the strain may be expressed on the $\sigma-\tau$ co-ordinate as in case of the angle of fractures. In Figs. 243, 244, 245 and 246, the strain at fracturing was plotted on the $\sigma-\tau$ co-ordinate for argillaceous, arenaceous, pyroclastic, and volcanic rocks, respectively. We, again, find regular arrangement of the strain, which increases towards right-lower corner direction. In Figs. 247 and 248, the contour lines were drawn for argillaceous and arenaceous rocks. In both figures, the lines deduced from the equation (5.5) were shown as thin lines. We see the both lines are approximately parallel. Figs. 249 and 250 show the relation between angle of fracture 2θ and strain. Most points are found in a zone decided

by thin dotted lines. Here, from formulas (5.3) and (5.5),

$$2\theta = a - \beta \cdots\cdots\cdots (5.6)$$

The thin lines in both figures show this relation. As it is shown in the figures, the curves are not agreeable with observed data. However, if we correct it by empirical relation of formula (5.4), the curves run through the middle of the zone decided by the thin dotted lines.

Thus, $2\theta = a - \beta + \Delta \cdots\cdots\cdots (5.7)$

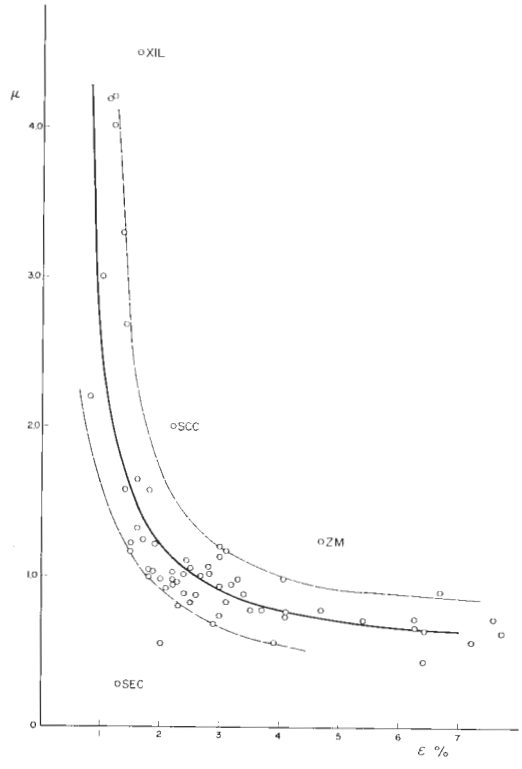

Fig. 239 Relation between the calculated internal friction μ, and the measured strain at the fracturing ε, for argillaceous rocks. The thick line shows an empirical formula, $\mu = \cot(66° - \beta)$, $\varepsilon = \cot\beta$.

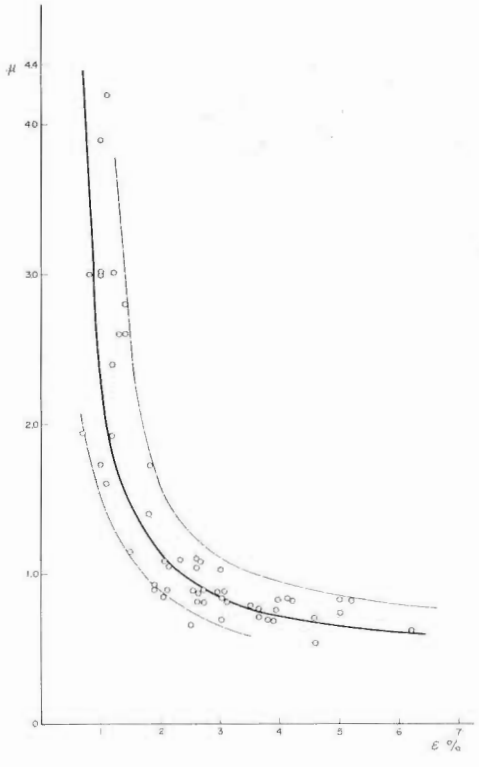

Fig. 240 Relation between μ and ε for arenaceous rocks. The thick line shows an empirical formula, $\mu=\cot(67°53'-\beta)$.

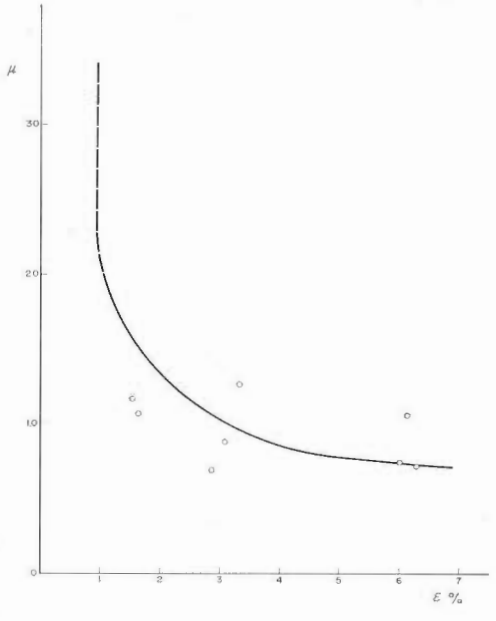

Fig. 241 Relation between μ and ε for pyroclastic rocks. The thick line shows an empirical formula, $\mu=\cot(63°26'-\beta)$.

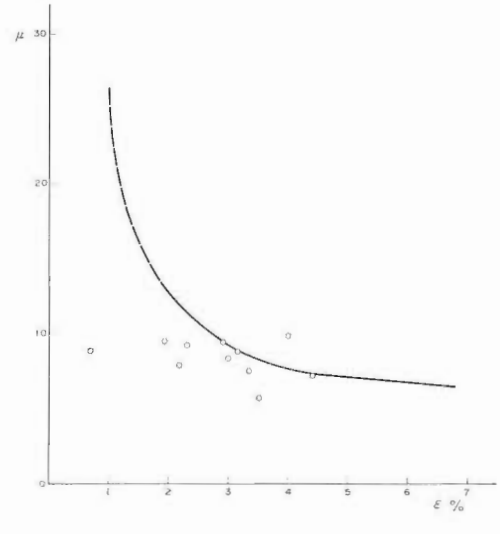

Fig. 242 Relation between μ and ε for volcanic rocks. The thick line shows an empirical formula, $\mu=\cot(65°46'-\beta)$.

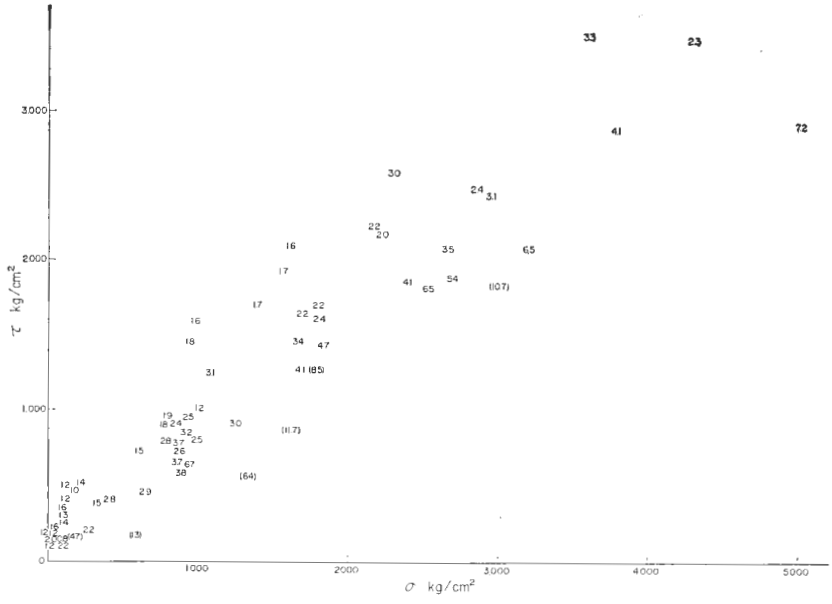

Fig. 243 Strain at fracturing for argillaceous rocks on σ–τ co-ordinate.

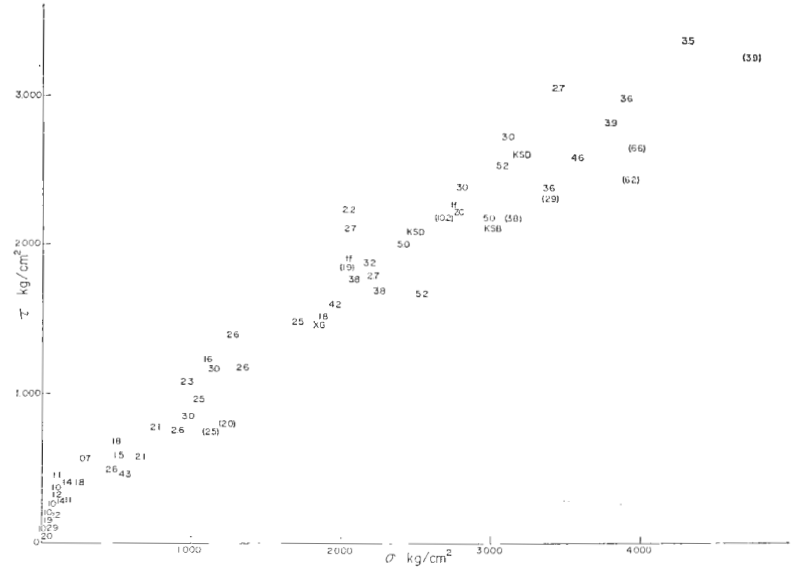

Fig. 244 Strain at fracturing for arenaceous rocks on σ–τ co-ordinate.

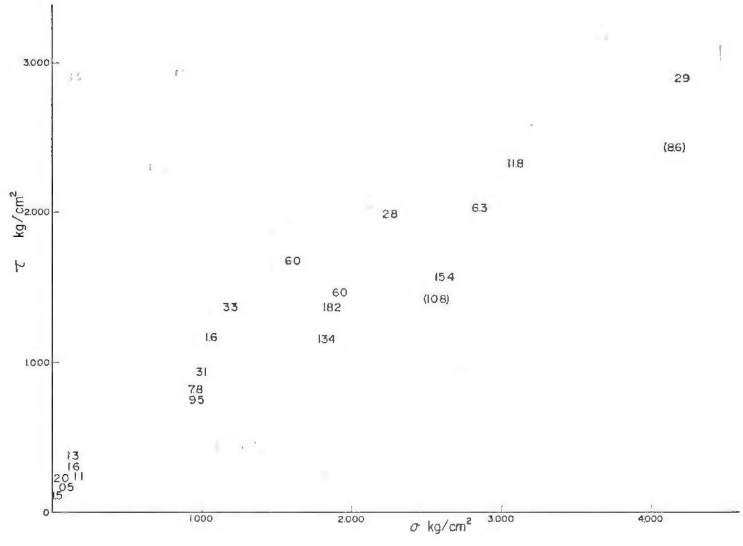

Fig. 245 Strain at fracturing for pyroclastic rocks on σ–τ co-ordinate.

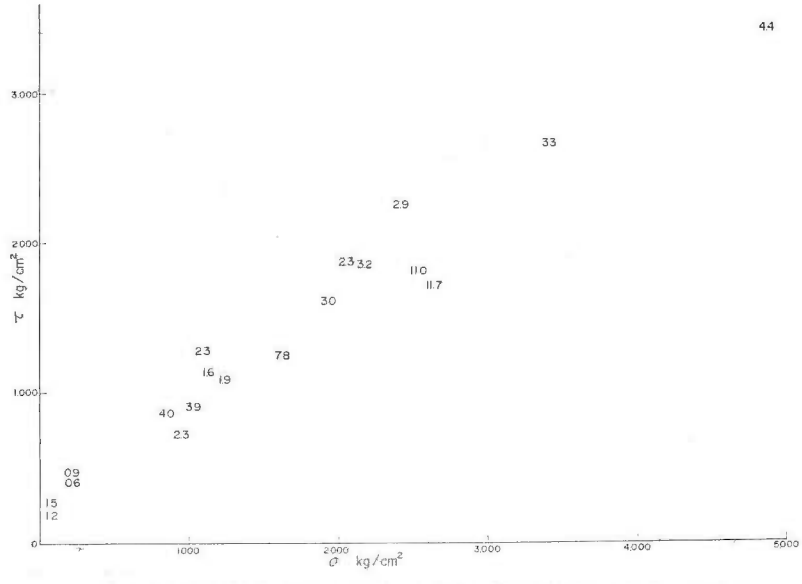

Fig. 246 Strain at fracturing for volcanic rocks on σ–τ co-ordinate.

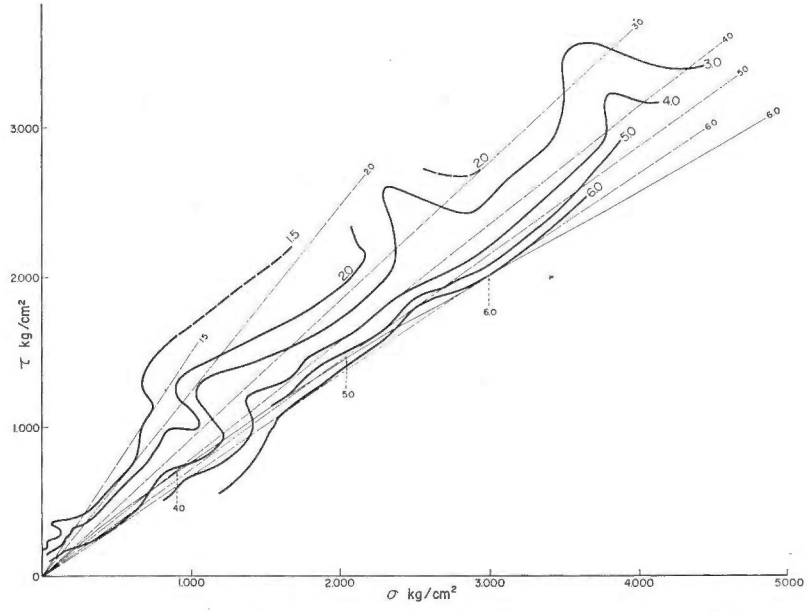

Fig. 247 Thick lines are contours for strain at fracturing drawn from observed data, and thin dotted lines are calculated from the formula in Fig. 241 for argillaceous rocks.

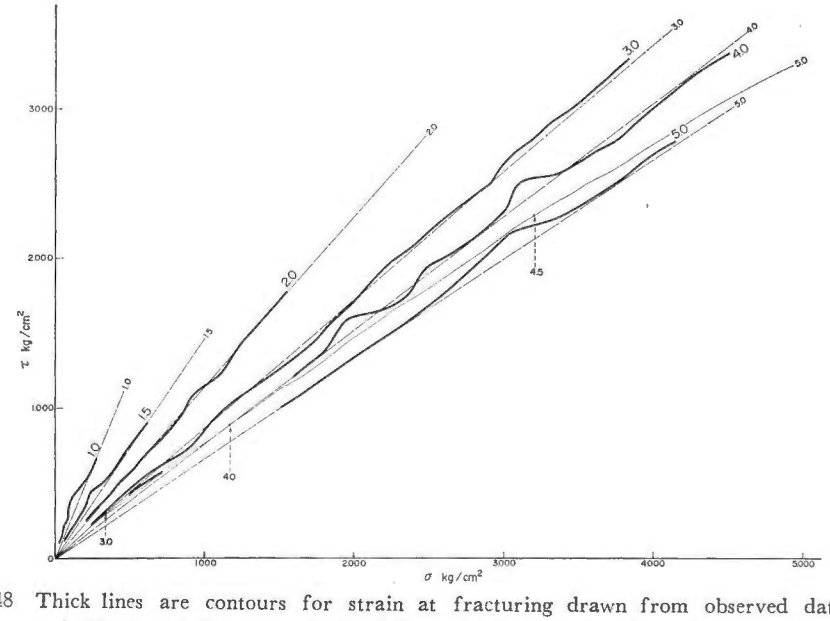

Fig. 248 Thick lines are contours for strain at fracturing drawn from observed data, and thin dotted lines are calculated from the formula in Fig. 242 for arenaceous rocks.

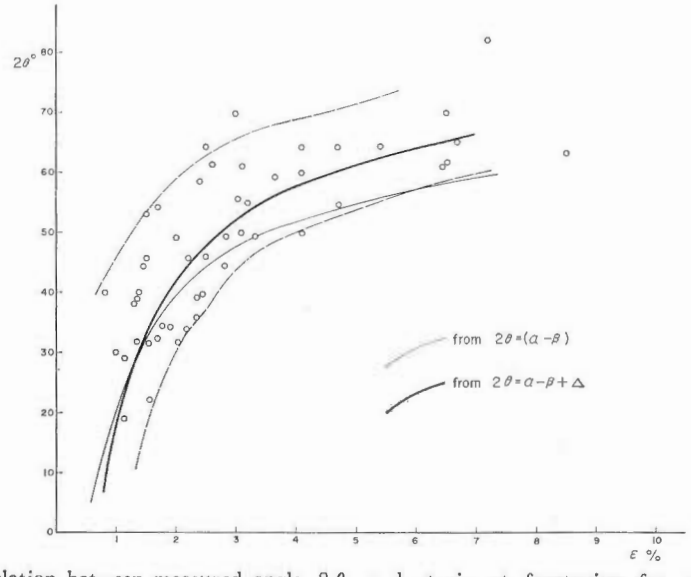

Fig. 249 Relation between measured angle 2θ, and strain at fracturing for argillaceous rocks. Thick line was calculated from formula (5.7).

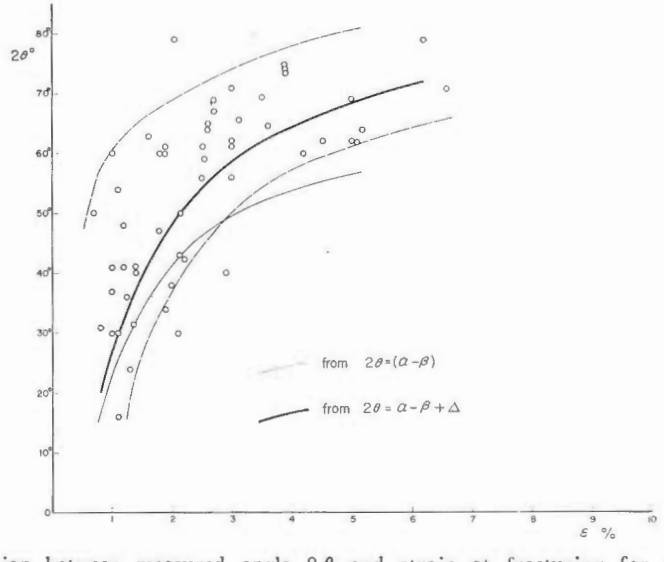

Fig. 250 Relation between measured angle 2θ and strain at fracturing for arenaceous rocks. Thick line was calculated from formula (5.7).

V. 4 Failure type

It has been shown that the mode of deformation changes under a certain relation from brittle to ductile, and from ductile to visco-ductile as a function of confining pressure. Here, we describe how failure type changes with deformational behavior.

Fig. 255 shows the frequency of failure type in each mode of deformation in cases of argillaceous, arenaceous, pyroclastic, and volcanic rocks. In very brittle behavior, the most frequent failure type is wedge, which attains to 52.1%, 48.3%, 88.2%, and 83.3% in cases of argillaceous, arenaceous, pyroclastic, and volcanic rocks, respectively. In cases of argillaceous and arenaceous rocks, a single shear type occupies most of the rest part, that is, 47.9%, or 48.3%. In case of pyroclastic rocks, the rest 11.8% is shared with a single shear type. In case of volcanic rocks, the rest 16.7% is occupied with network type. In general, more than about 85% is either wedge or single shear type for very brittle deformation. Most of wedge type are observed in the tests at atmospheric confining pressure. We observed 66 cases of wedge type fractures, of which 65 cases were from the tests at atmospheric pressure, only one was observed for SCC (S30) at 200 kg/cm^2 pressure, (Figs. 260–263).

In brittle behavior, single shear type prevails, wedge type is still next predominant, and network type appears a little. Single shear type is counted 65.9 %, 70.3%, 57.1%, and 36.4% in cases of argillaceous, arenaceous, pyroclastic, and volcanic rocks, respectively. Wedge type is 27.3%, 10.8%, 28.6%, and 9.1% in cases of argillaceous, arenaceous, pyroclastic, and volcanic rocks, respectively. The rest is occupied with network type. In case of volcanic rocks, 54.5% is network fractures. Even in brittle deformation, more than 80% are either single shear or wedge type fractures, except volcanic rocks.

Transitional deformation is an intermediate state between brittle and ductile deformation. Failure types, too, are of intermediate character in transitional deformation. The composition of the failure types is, however, quite different for each kind of rocks. In cases of argillaceous and arenaceous rocks, about 85% consists of either network or flow type. In case of argillaceous rocks, flow type is 45.5%, network type is 39.4%, and the rest 15.2% is single shear type. In case of arenaceous rocks, 80.6% is flow, 6.5% is network, and 12.9% is single shear. Pyroclastic rocks have 42.9% of single shear, the rest half is composed of 28.6% of flow and 28.6% of network. The volcanic rocks of this deformational behavior are only 4, all of which belong to network type. In transitional behavior, type of failure of argillaceous and arenaceous rocks seems to be near to ductile characteristics while that of pyroclastic and volcanic rocks are rather of brittle characteristics.

In ductile deformation, most are of flow type in all kinds of rocks. Exception is three cases of argillaceous rocks. One is seen on JN(S7) at 100 kg/cm^2 test, and the other two are on SBA (S24) at 1000 and 1500 kg/cm^2 tests. The observed fractures in these cases are of single shear type. Macroscopically, the nature of fractures are not so much different from others. These two rocks are very porous claystone. JN (S7) has a porosity of 63.9%, and SBA (S24) has that of 60.5%. These values are the highest among all rocks tested. Except these three, 22 argillaceous rocks, 14 arenaceous rocks, and four pyroclastic rocks are all of flow type.

In visco-ductile behavior, failure type becomes completely into flow type. Flow type is shown in all cases of 55 argillaceous, 18 arenaceous, 13 pyroclastic, and two volcanic rocks.

It is concluded that, in very brittle and brittle behaviors, wedge and single shear types are the most predominant, and that, in ductile and visco-ductile behaviors, nearly 100% is flow type. The failure type in transitional behavior is more similar to that of ductile behavior in argillaceous and arenaceous rocks but simi lar to that of brittle behavior in pyroclastic rocks. Volcanic rocks deform in a different manner with the predominant development of network type in brittle and ductile behaviors.

The distinction between single shear and network types seems not to be essential. The single shear in macroscopic observation is often found rather to be of network pattern, when it is examined carefully on thin section with a microscope. Under repeating load near the yielding point, it is observed that network fractures become apparent. Wedge type is formed under compression tests at extremely low confining pressure. Microscopically, the network fracture pattern is common in every deformational behavior.

HANDIN (1966) and GRIGGS and HANDIN (1960) defined ductility as the ability of the material to undergo large permanent deformation without fracture. Figs. 256, 257, 258 and 259 show the change of deformational behavior in connection with the strain at fracturing (that is, ductility) and confining pressure in argillaceous, arenaceous, pyroclastic, and volcanic rocks, respectively. Also in Figs. 260, 261, 262 and 263, the changes of failure type are shown. In these Figures, thin dotted lines are the transition boundaries between brittle and transitional in Figs. 222~225, and 243~248.

In case of argillaceous rocks (Figs. 256 and 260); on the strain at fracturing less than 3.5%, the deformational behavior is completely very brittle or brittle, and failure type is wedge and single shear; on the strain at fracturing more than 6%, the deformational behavior is transitional without any exception, but failure is a combination of single shear, network, and flow; between 3.5 and 6.0%, they are mixtures of transitional and brittle, and of wedge, single shear, network, and flow. In case of arenaceous rocks (Figs. 257 and 261), on the strain at fracturing less than 4.0%, deformational behavior is mostly very brittle or brittle, but failure type is not so simple; on the strain at fracturing more than 4.9%, deformational behavior is almost transitional, and failure type is flow with a few exception of single shear type; between 4.0 and 4.9%, they are mixtures of brittle and transitional and of single shear, network, and flow types. In case of pyroclastic rocks (Figs. 258 and 262), the diagrams are simpler than the above two. On the strain at fracturing less than 3.5%, deformtional behavior is very brittle and brittle, while more than 3.5% strain at fracturing is a transitional region. But failure type is something complex. On the strain at fracturing less than 3.5%, most are wedge type, and on more than 3.5%, failure type is a combination of single shear, network, and flow. In case of volcanic rocks (Figs. 259 and 263), on the strain at fracturing less than 3.0%, deformational behavior is very brittle and brittle. Failure type consists of wedge, single shear, and network. On the strain more than 4.4%, deformational behavior is transitional and failure type is network; between 3.0 and 4.4%, they are of very brittle, brittle, and transitional in behavior and single shear, and network in failure type.

The above results are quite consistent with the results shown in Fig. 255. The transition of deformational behavior seems to be in good accordance with the change of the strain at fracturing, while the change of failure type is more complex. A possible reason is that the change of failure type is continuous in essentials, but is affected more by the lithology of specimens. On the other hand, the fracture angle increases in accordance with the strain at fracturing. It is interesting for better understanding of the mechanism of brittle fracturing.

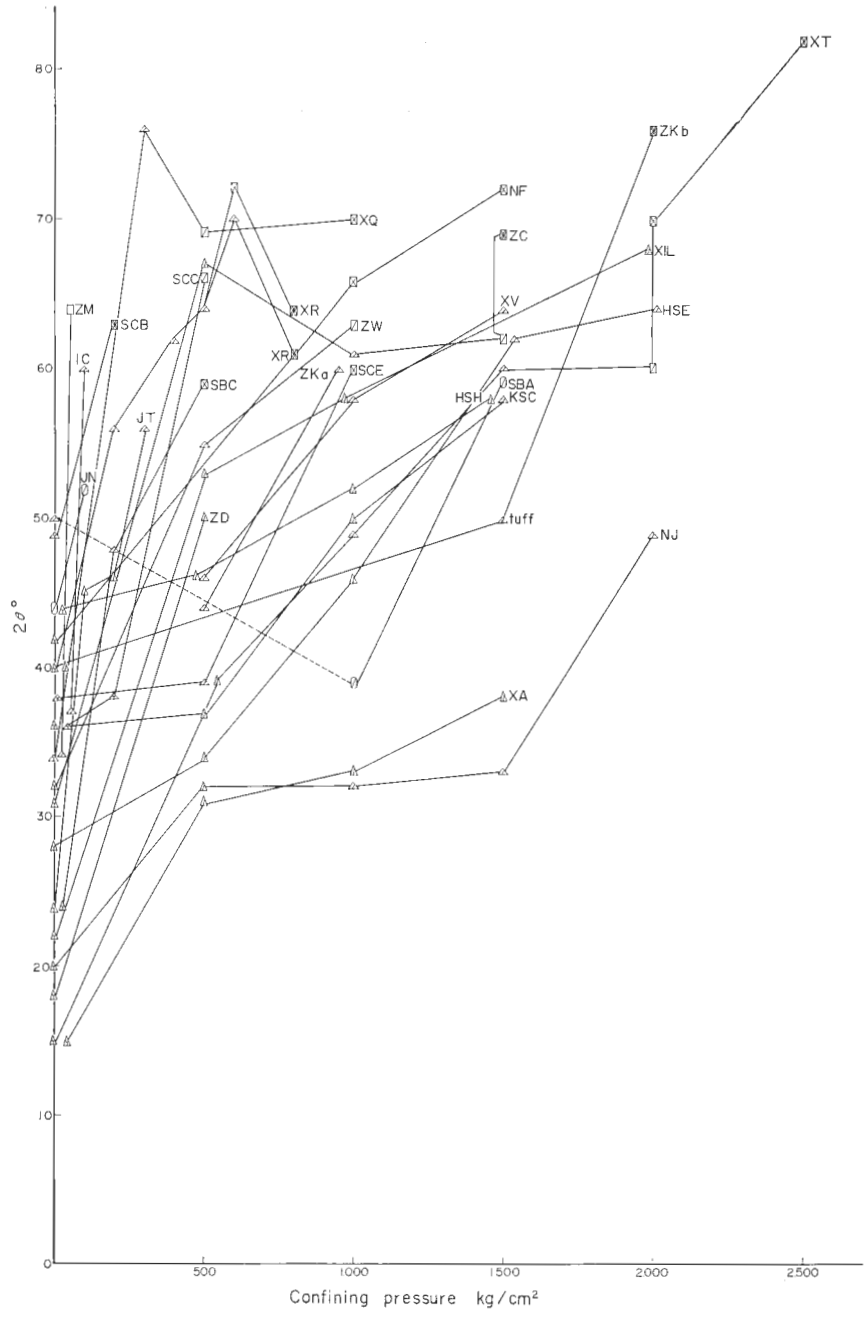

Fig. 251 Angle of fractures versus confining pressure for argillaceous rocks. The marks are the same as Fig. 222.

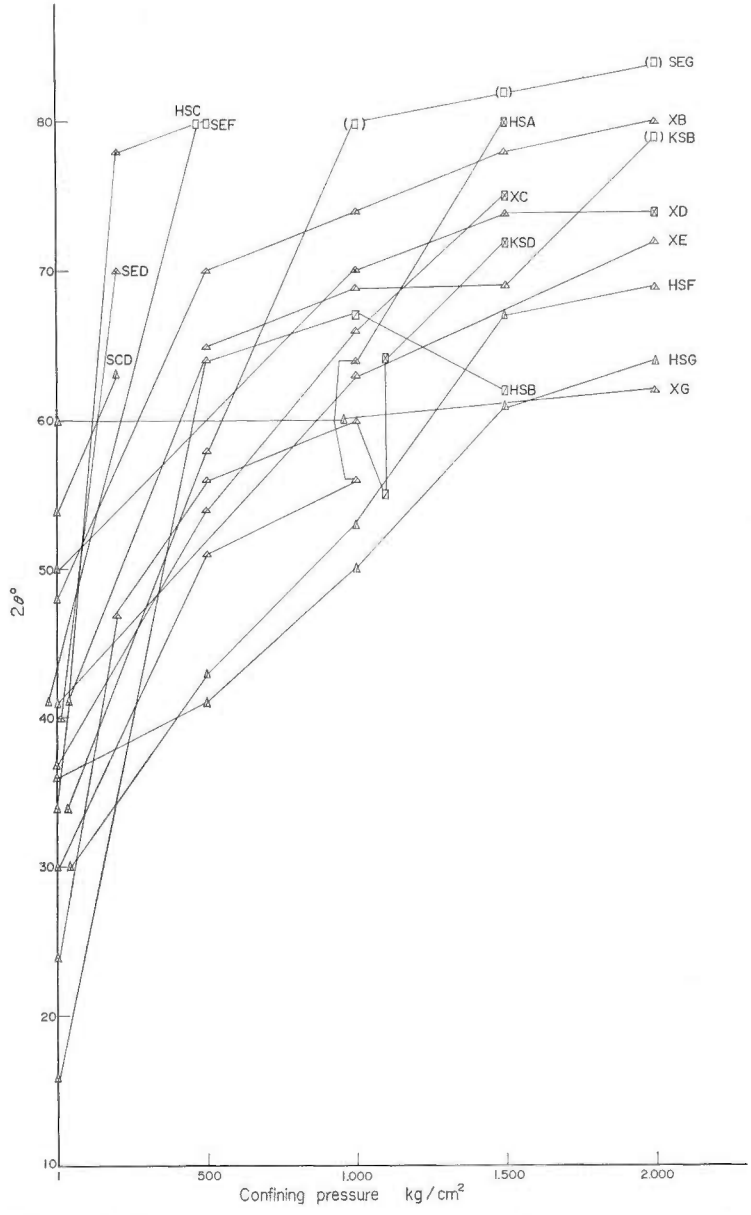

Fig. 252 Angle of fractures versus confining pressure for arenaceous rocks. The marks are the same as Fig. 222.

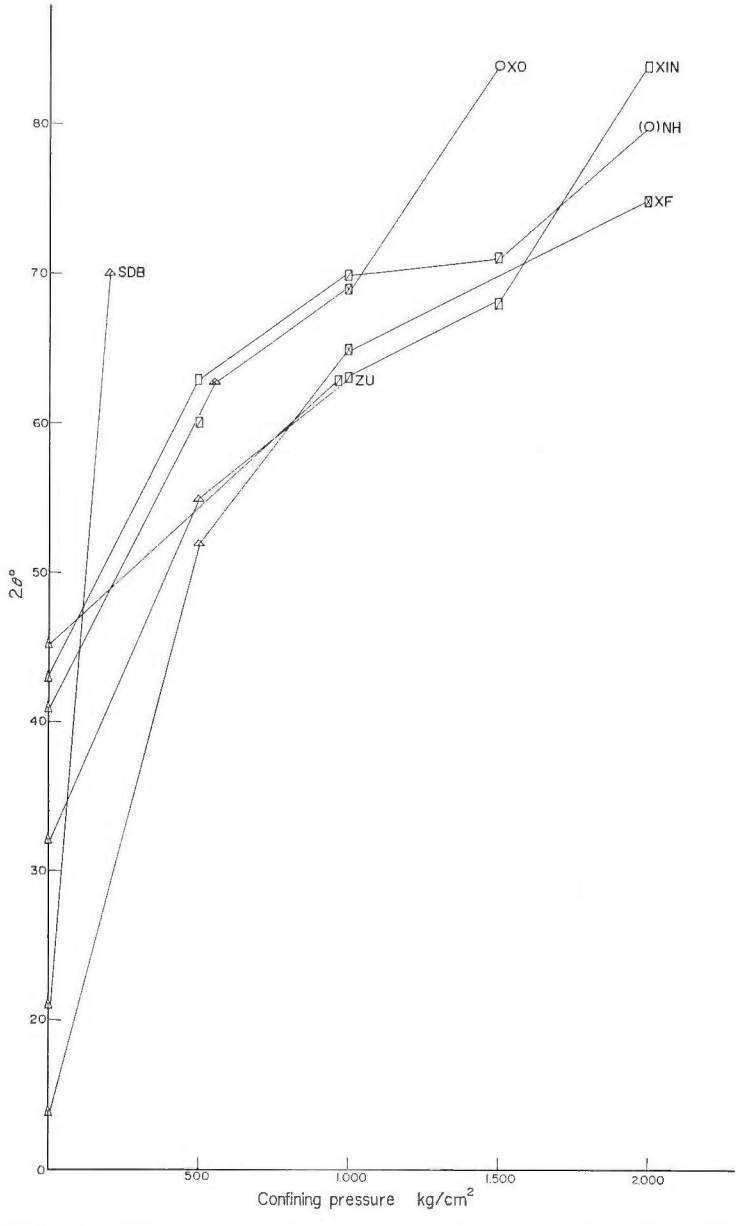

Fig. 253 Angle of fractures versus confining pressure for pyroclastic rocks. The marks are the same as Fig. 222.

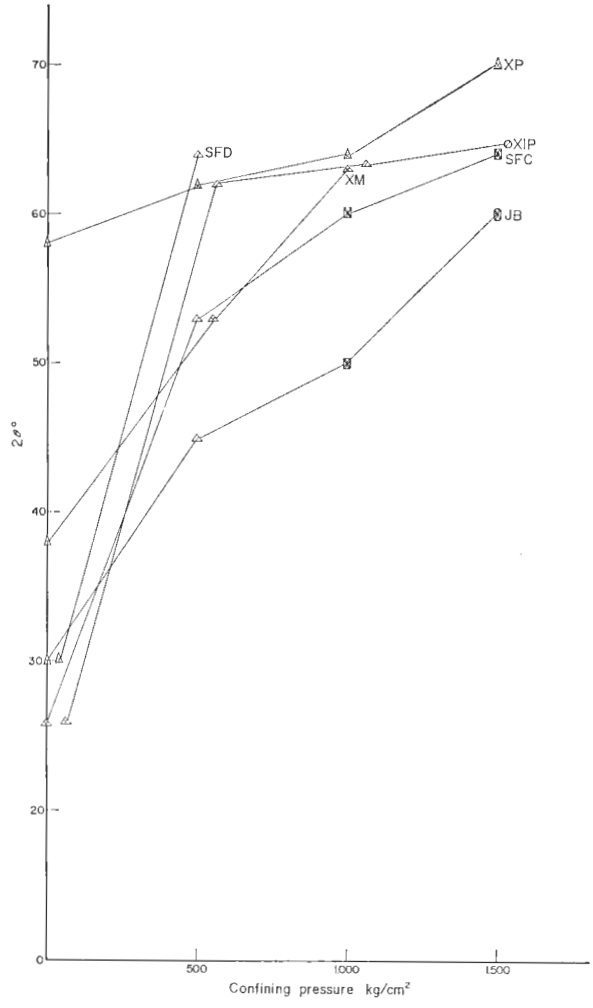

Fig. 254 Angle of fractures versus confining pressure for volcanic rocks. The marks are the same as Fig. 222.

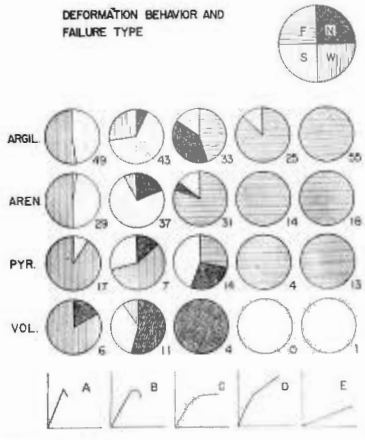

Fig. 255 Relation between failure types and deformational behaviors. W: Wedge type, S: Single shear, N: network, F: flow. The number of measurement is shown in right-below. A: Very brittle, B: Brittle, C: Transitional, D: Ductile, E: Visco-ductile behaviors.

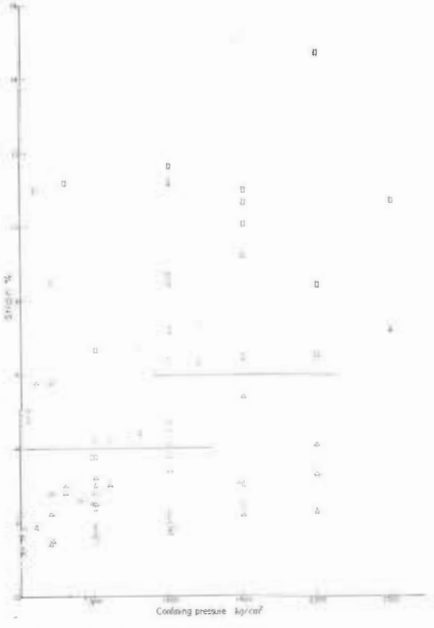

Fig. 256 Strain at fracturing versus confining pressure for argillaceous rocks. △, △, □, □, and ○ show very brittle, brittle, transitional, ductile, and visco-ductile behaviors.

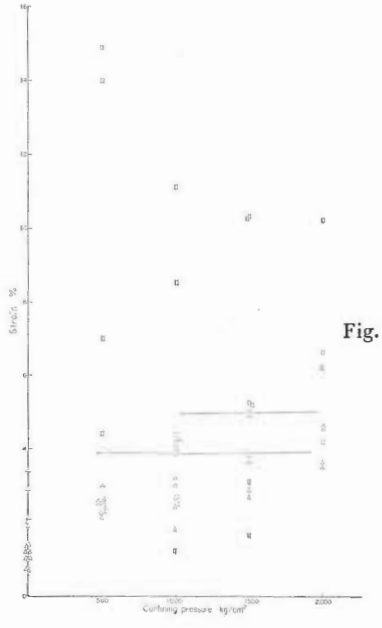

Fig. 257 Strain at fracturing versus confining pressure for arenaceous rocks. The marks are the same as Fig. 256.

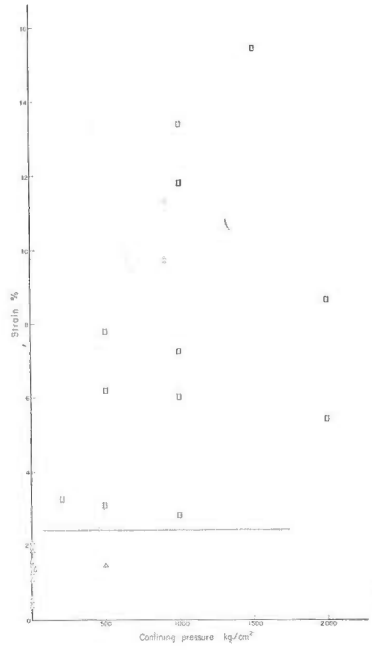

Fig. 258 Strain at fracturing versus confining pressure for pyroclastic rocks. The marks are the same as Fig. 256.

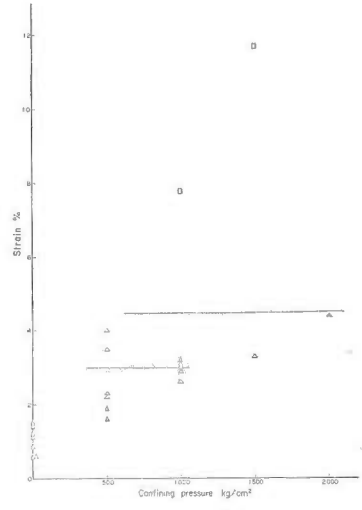

Fig. 259 Strain at fracturing versus confining pressure for volcanic rocks. The marks are the same as Fig. 256.

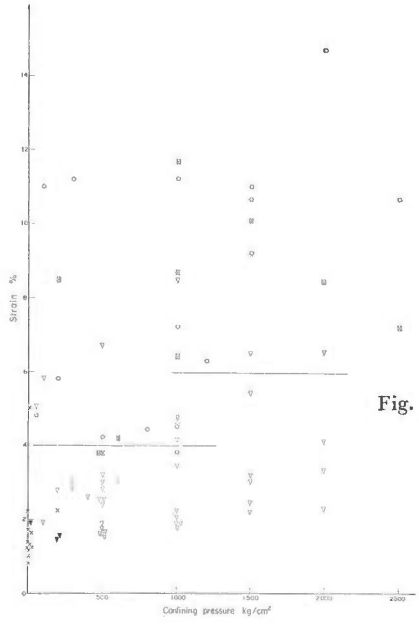

Fig. 260 Strain at fracturing versus confining pressure for argillaceous rocks. The marks, ×, ▽, ⊠, ○ show wedge, single shear, network, and flow types of failure.

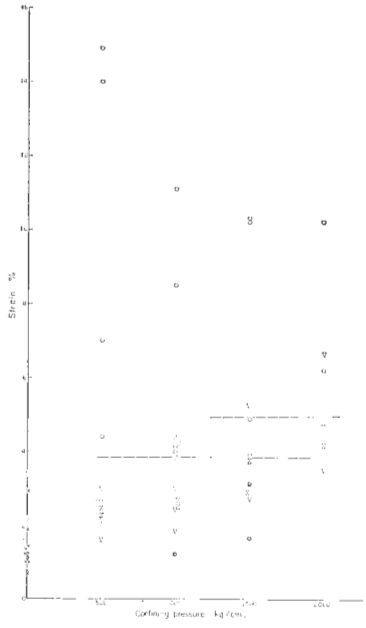

Fig. 261 Strain at fracturing versus confining pressure for arenaceous rocks. The marks are the same as Fig. 260.

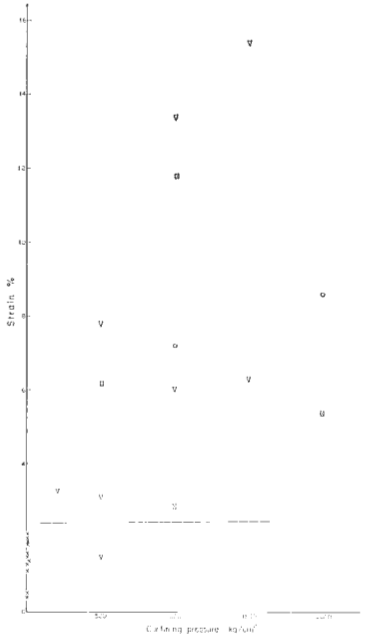

Fig. 262 Strain at fracturing versus confining pressure for pyroclastic rocks. The marks are the same as Fig. 260.

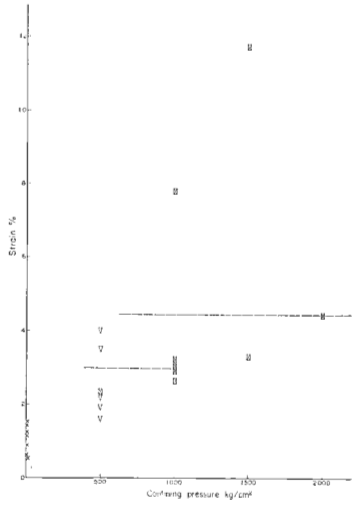

Fig. 263 Strain at fracturing versus confining pressure for volcanic rocks. The marks are the same as Fig. 260.

V. 5 Porosity and strength

Porosity has close connection with the strength of sedimentary rocks. However, the effect of porosity is different in each kind of rocks.

In Figs. 264~267, the relation between porosity and strength at 1, 500, 1000, and 1500 kg/cm^2 confining pressures on argillaceous rocks are shown. Ultimate strength is shown on very brittle and brittle behaviors, and for comparison, 10% differential stresses are used for transitional, ductile and visco-ductile behaviors. In 1 kgcm^2 confining pressure test, there is approximately a linear relationship on semi-logarithm diagram between the porosity and strength (Figs. 264 and 268). However, as confining pressure increases, the relation becomes more complicated, but still keeps a systematic relation. At more than 500 kg/cm^2, the rocks less than 20% in porosity behave very brittle or brittle behavior and exhibit one linear relation, while those more than 30% behave visco-ductile behavior and hold another linear relation. In geological age, the former belongs to from upper Oligocene to upper Miocene, while the latter from upper Miocene to lower Pliocene. This differentiation on porosity-strength relation is possibly a reflection of compaction process of argillaceous rocks.

In arenaceous rocks, a linear relation exists on semi-logarithm diagram as shown in Figs. 272 and 273, if we take the similar specimens from well stratified sequence of geologically same area.

In Fig. 274, the relation among strength, porosity, and grain size of pyroclastic rocks is shown. The strength is affected by both porosity and grain size.

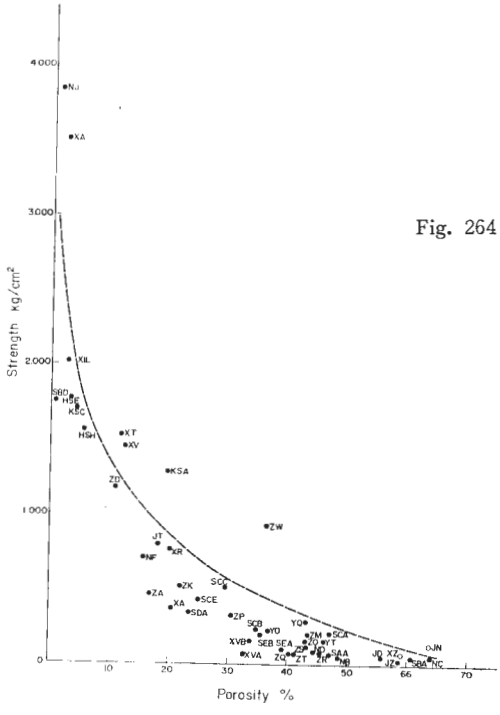

Fig. 264 Porosity versus strength for argillaceous rocks at atmospheric pressure. Strength is ultimate or 10% strength.

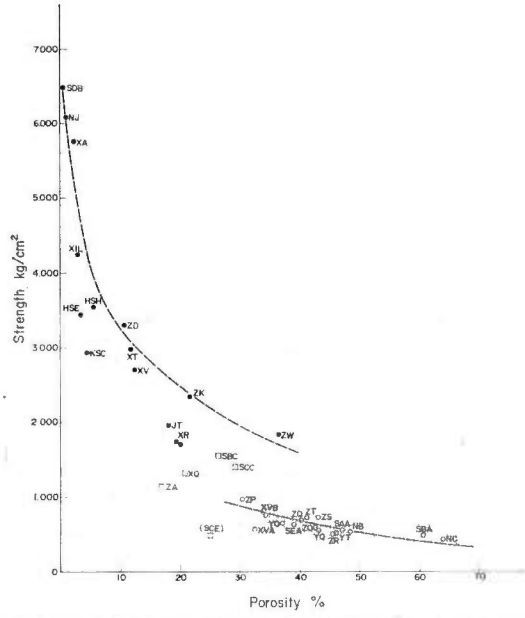

Fig. 265 Porosity versus strength for argillaceous rocks at 500 kg/cm² confining pressure. ●, ○, and □ show very brittle and brittle; visco-ductile; and transitional and ductile behaviors, respectively.

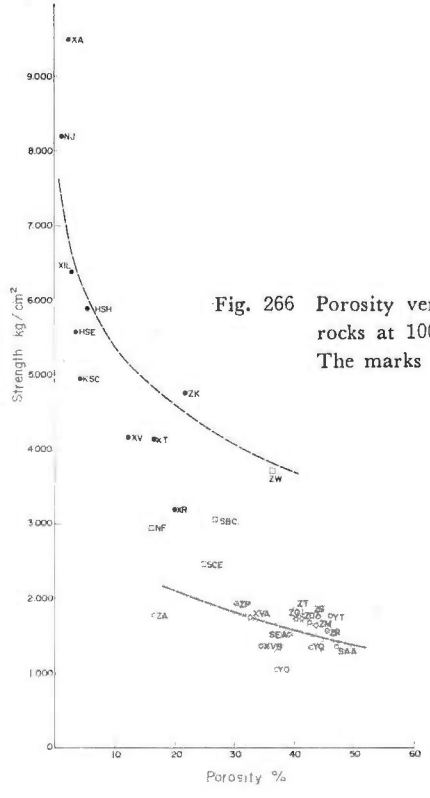

Fig. 266 Porosity versus strength for argillaceous rocks at 1000 kg/cm² confining pressure. The marks are the same as Fig. 265.

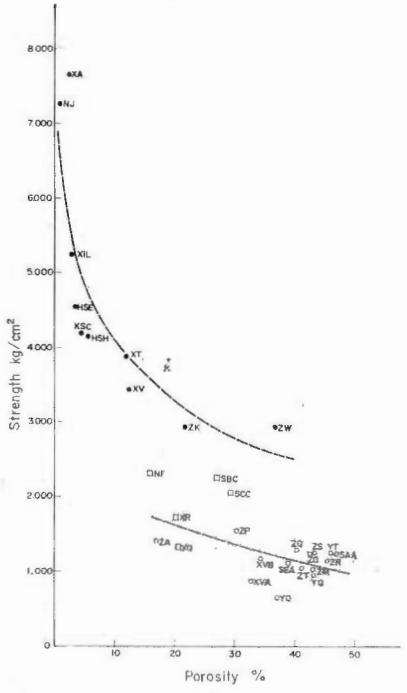

Fig. 267 Porosity versus strength for argillaceous rocks at 1500 kg/cm² confining pressure. The marks are the same as Fig. 265.

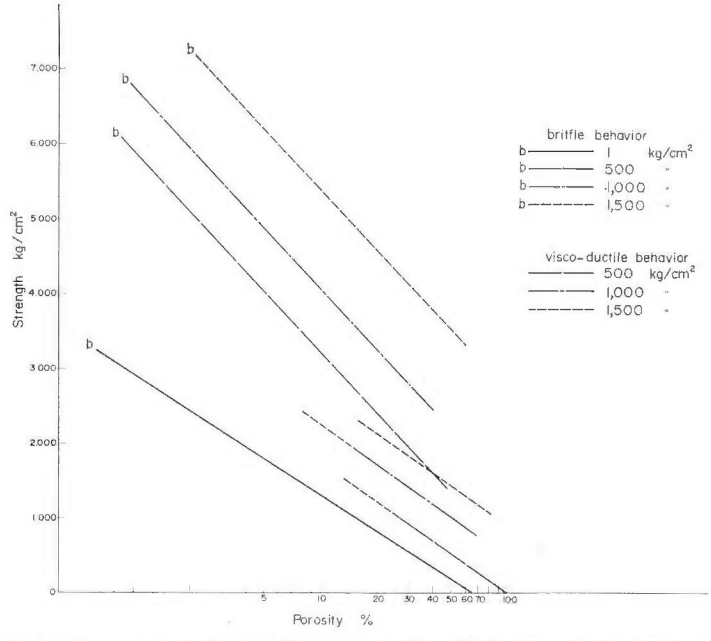

Fig. 268 Porosity versus strength for argillaceous rocks. Each line is drawn from thick dotted curves in Figs. 264 to 267.

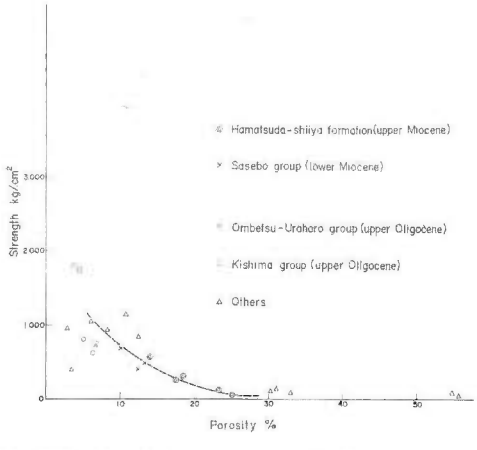

Fig. 269 Porosity versus strength for arenaceous rocks at atmospheric pressure.

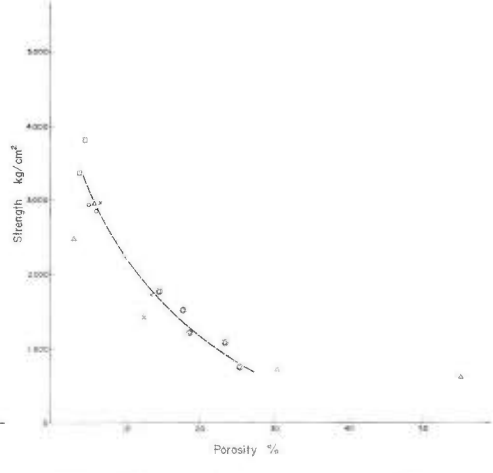

Fig. 270 Porosity versus strength for arenaceous rocks at 500 kg/cm². The marks are the same as Fig. 269.

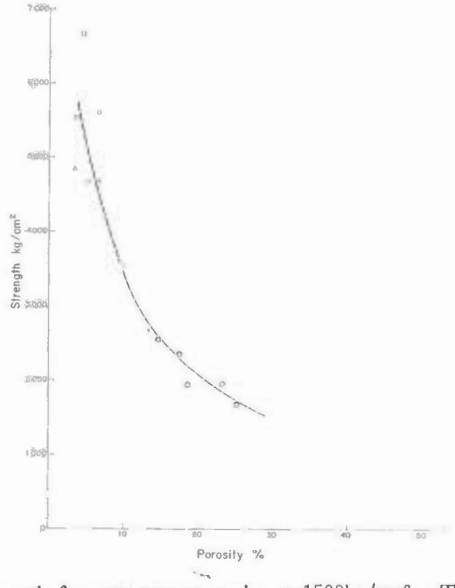

Fig. 271 Porosity versus strength for arenaceous rocks at 1500kg/cm². The marks are the same as Fig. 269.

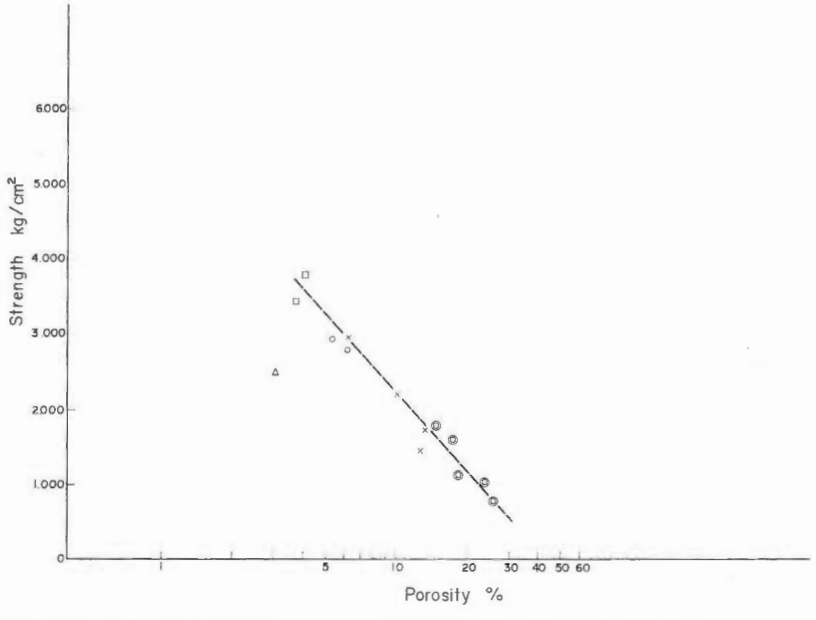

Fig. 272 Porosity versus strength for arenaceous rocks at 500kg/cm². The marks are the same as Fig. 269.

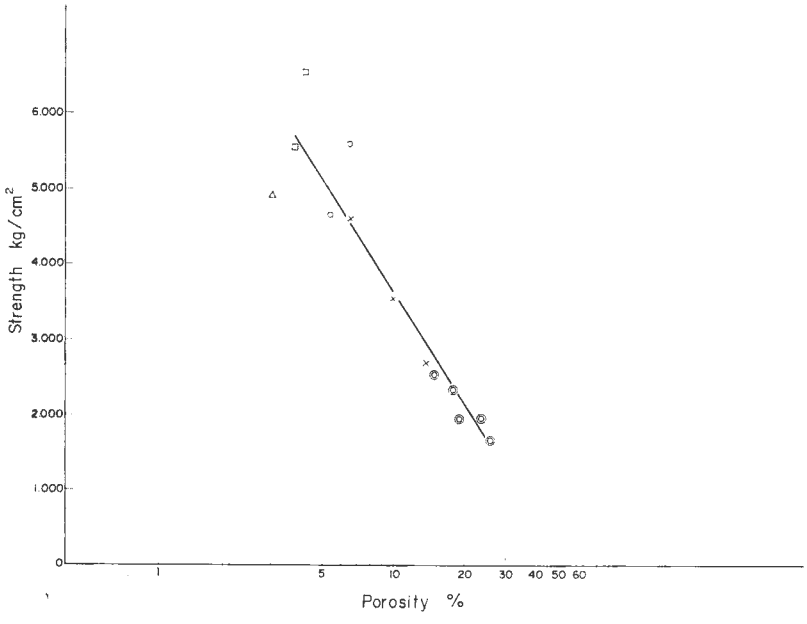

Fig. 273 Porosity versus strength for arenaceous rocks at 1500 kg/cm². The marks are the same as Fig. 269.

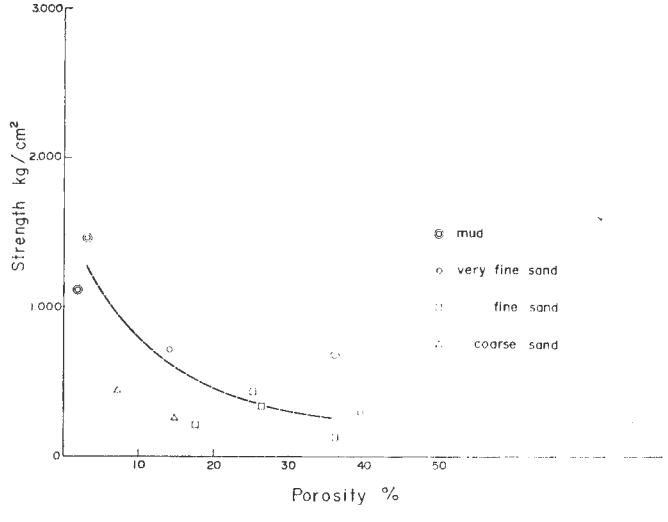

Fig. 274 Porosity versus strength for pyroclastic rocks at atmospheric pressure.

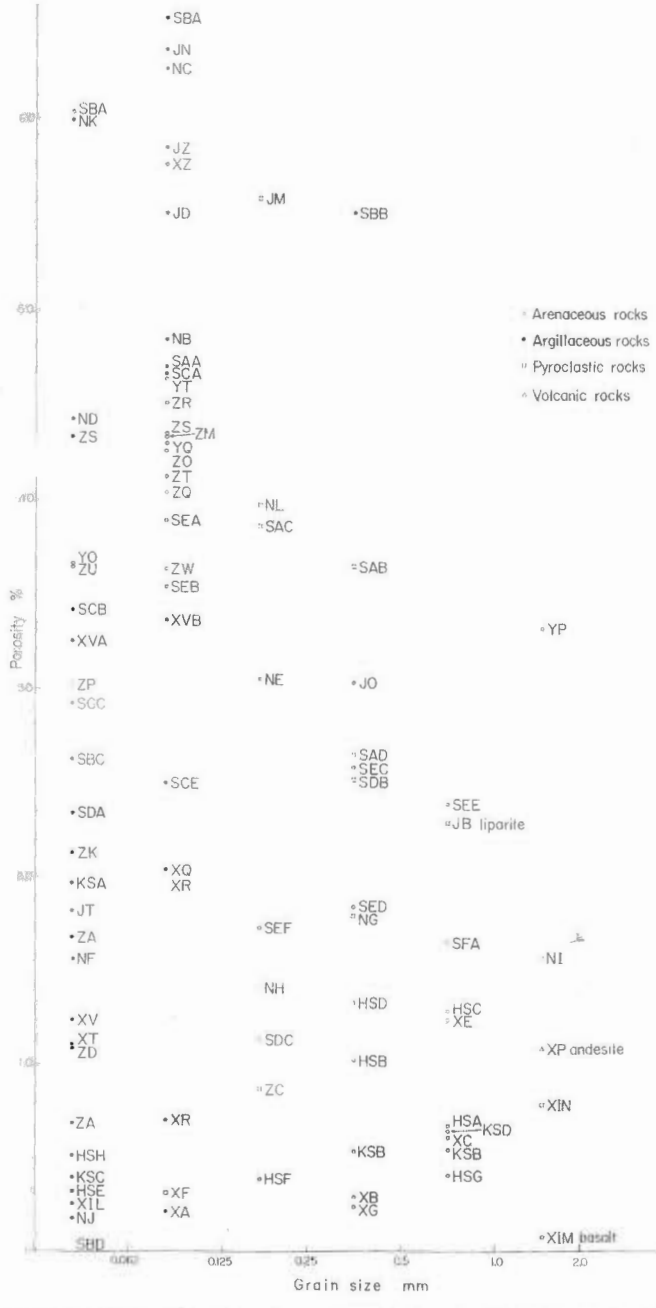

Fig. 275 A diagram showing porosity – grain size relation of the tested rocks.

V. 6 Porosity and axial shortening

In Figs. 276~278, the relations between axial shortening at each hydrostatic pressure and porosity for argillaceous, arenaceous, pyroclastic, and volcanic rocks are shown.

In case of argillaceous rocks, some specimens are low in axial shortening, comparing with their porosity. In general, however there is a tendency that axial shortening increases as porosity increases.

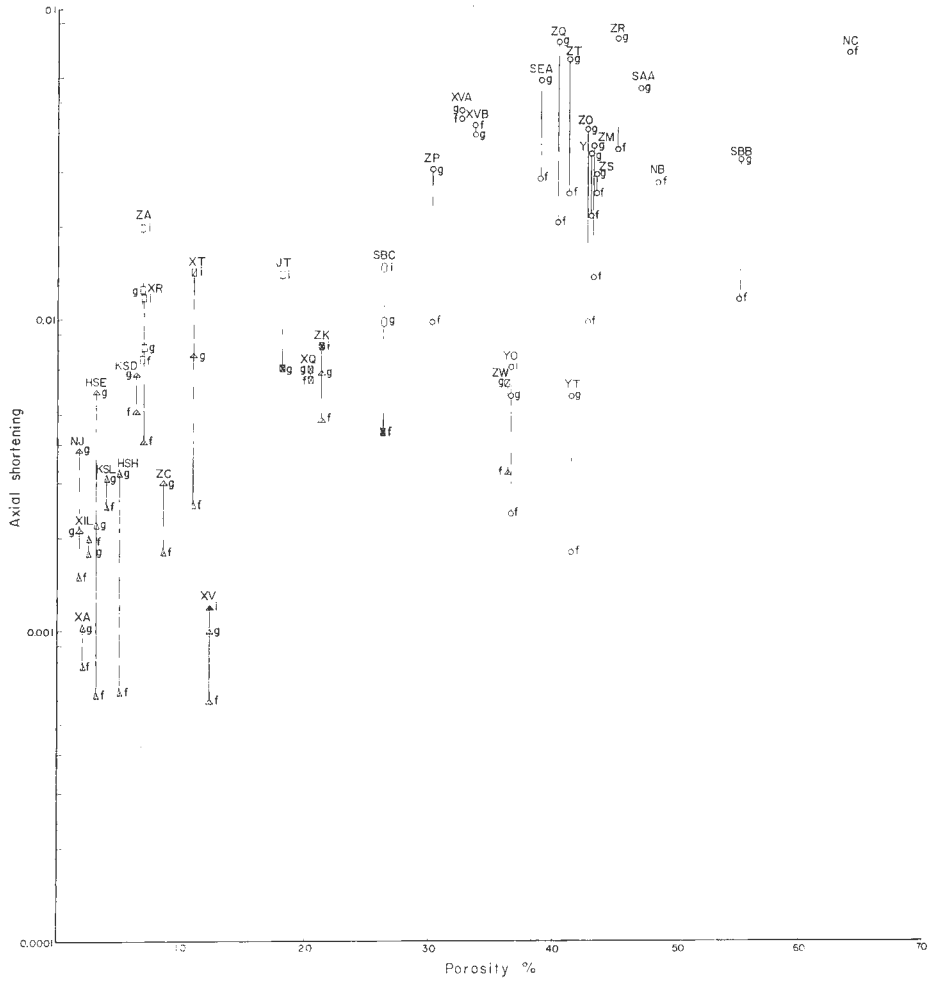

Fig. 276 Axial shortening versus porosity for argillaceous rocks.
The alphabets in the figure indicate the confining pressures; a : 1, b : 50, c : 100, d : 200, e : 300, f : 500, g : 1000, h : 1500, i : 2000, j : 2500kg/cm².

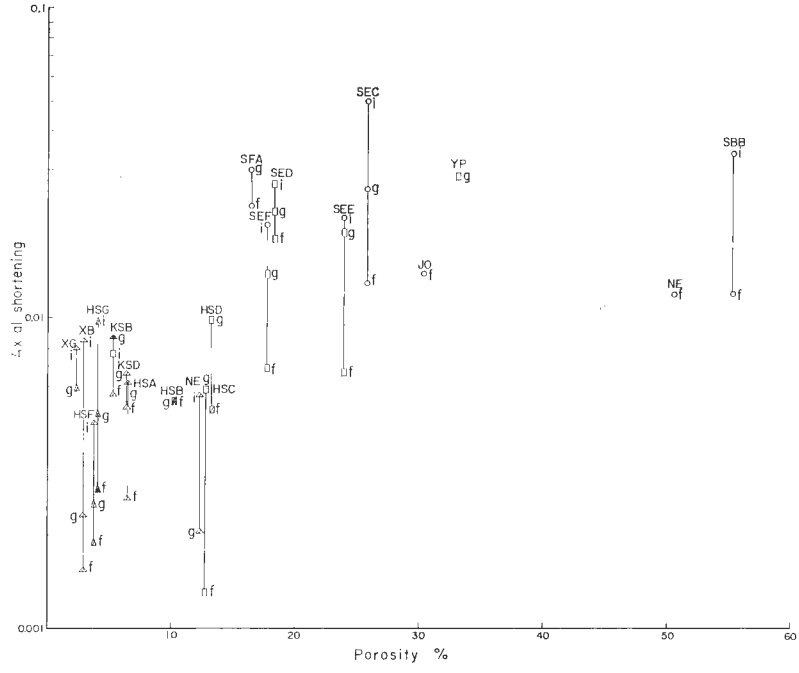

Fig. 277 Axial shortening versus porosity for arenaceous rocks. The marks are the same as Fig. 276.

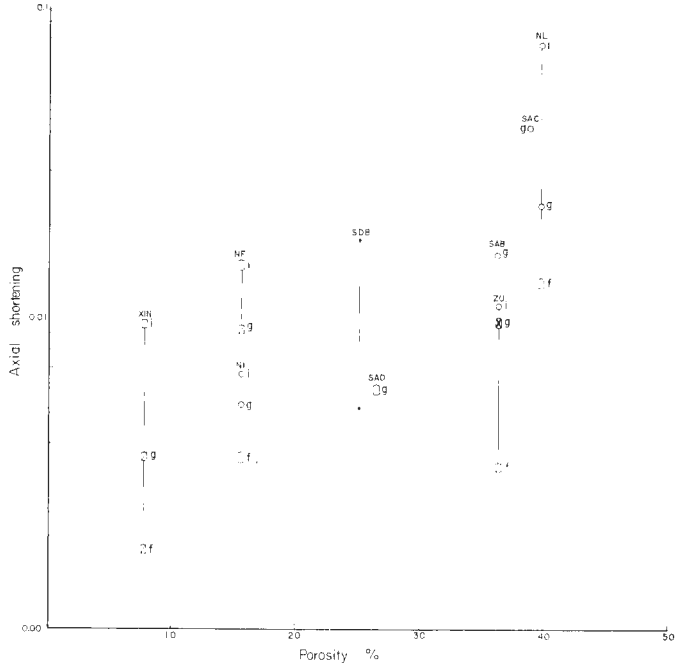

Fig. 278 Axial shortening versus porosity for pyroclastic rocks. The marks are the same as Fig. 276.

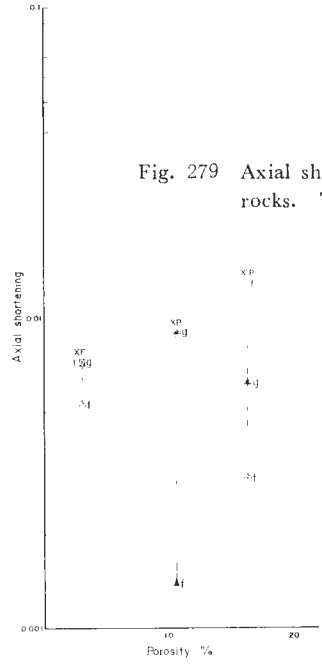

Fig. 279 Axial shortening versus porosity for volcanic rocks. The marks are the same as Fig. 276.

V. 7 Depth of well core samples and strength

It has been shown that, for the mudstone of well cores, there is nearly linear relationship between log ϕ and depth z, (ATHY, 1930; HUBBERT and RUBEY, 1959; NAGUMO, 1965). Here, ϕ is porosity. It is estimated that the depth z and strength S comes in a linear relation because of the linear relationship between log ϕ and strength S in some argillaceous and arenaceous rocks (cf. 5.5). Some of our specimens were collected from the wells for oil exploration. In Figs. 280~287, the relations between depth of samples and strength are plotted. We see the linear relation between them for some examples. The linear relation should be examined on the same kind of rock at different depths in a well. In Fig. 287, a linear relation is found on XQ (S62), XR (S63), and XT (S64) (argillaceous rocks in upper Miocene) of Kambara GS-1 well. The linear relation is observed at 1, 500, and 1000 kg/cm^2 confining pressure strength. Another case for argillaceous rocks is seen of Sawame-oki well, where SCB, SCC, and SCD may be aligned on a line in Fig. 280. Of Noshiro GS-1, Fig. 281, we see non-linear relation between XVA(S17), XVB(S18), and XV(S19). The former two are lower Pliocene, and the third is upper Miocene. This is possibly due to structural discontinuity between them.

In case of arenaceous rocks, we see a good result on Shimoigarashi well, where SEC(S53), SED(S54), SEE(S55), SEF(S56), and SEG(S57) tend to be aligned on a line at 1, 500, and 1000 kg/cm^2 confining pressure tests (Figs. 285 and 298).

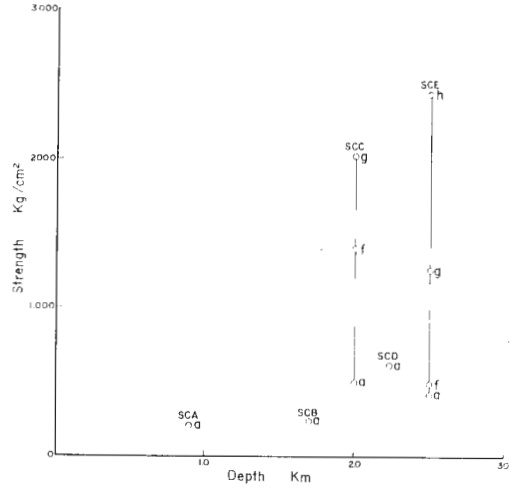

Fig. 280 Strength versus depth in Sawame-oki well. The alphabets in the figure indicate the confining pressures; a : 1, b : 50, c : 100, d : 200, e : 300, f : 500, g : 1000, h : 1500, i : 2000, j : 2500kg/cm^2. ○, claystone ×, tuff △, sandstone

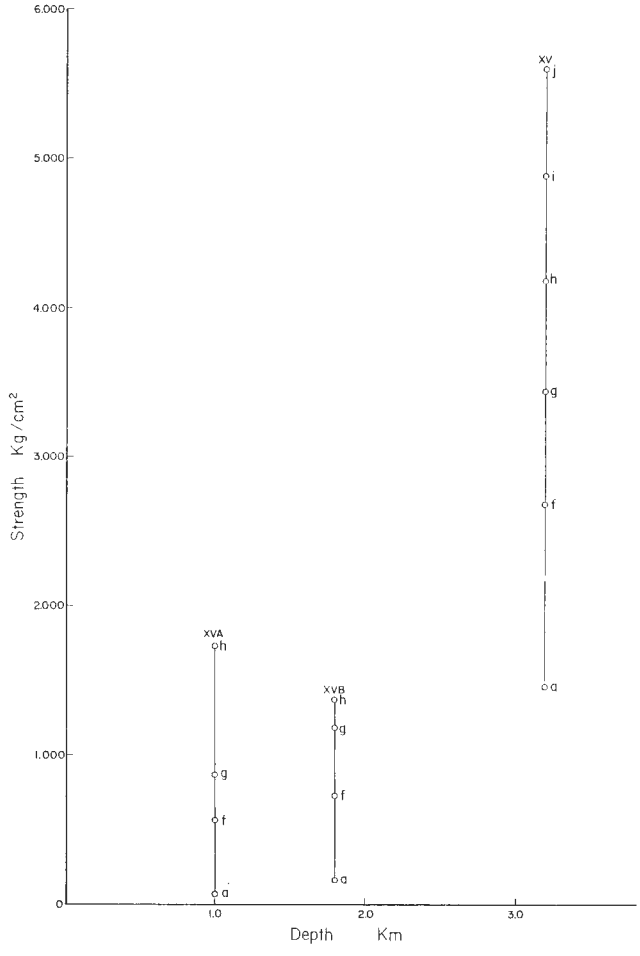

Fig. 281 Strength versus depth in Noshiro GS-1 well. The marks are the same as Fig. 280.

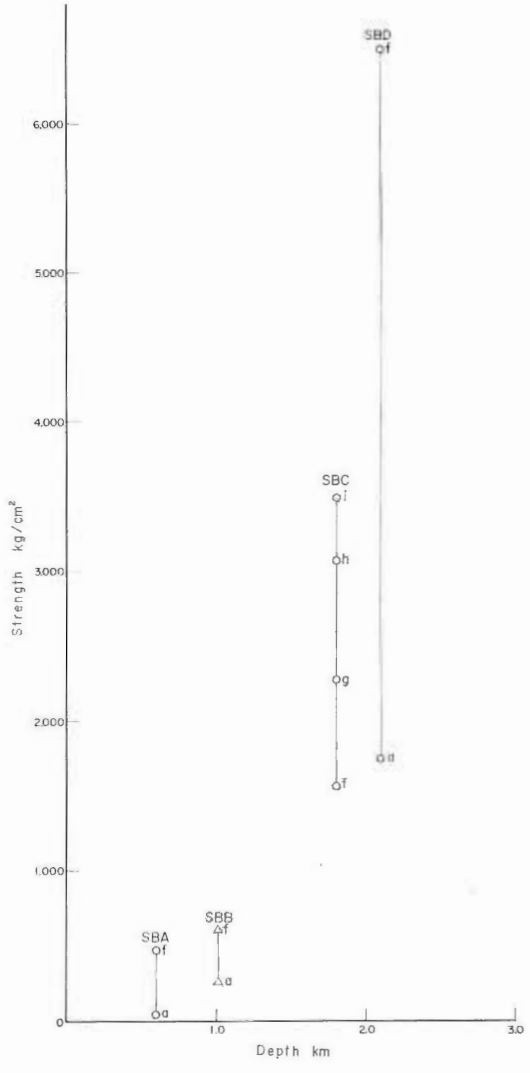

Fig. 282 Strength versus depth in Noishi-oki well. The marks are the same as Fig. 280.

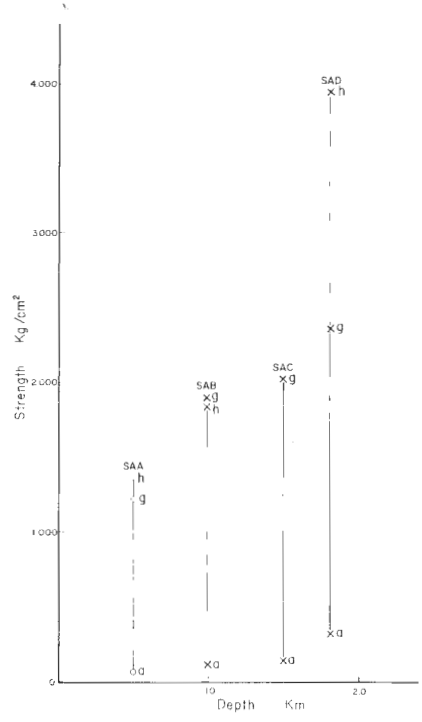

Fig. 283 Strength versus depth in Nishime-oki well. The marks are the same as Fig. 280.

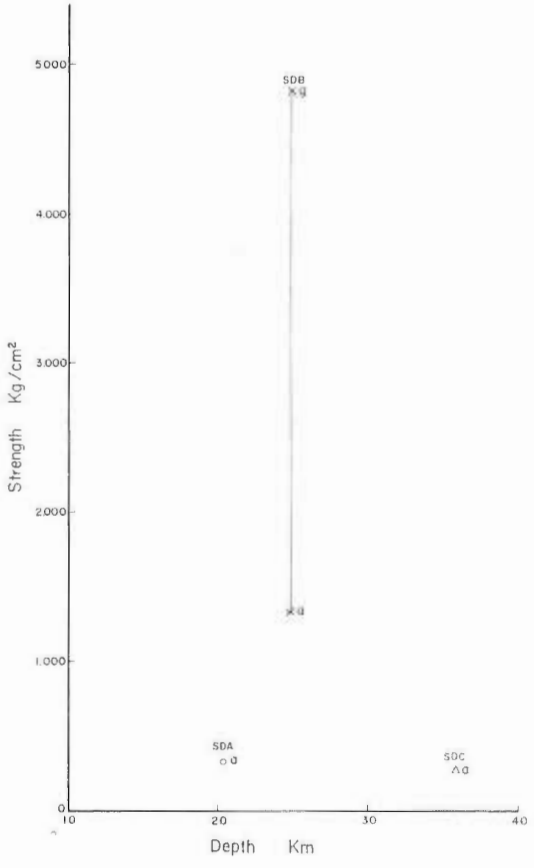

Fig. 284 Strength versus depth in Ohbuchi well. The marks are the same as Fig. 280.

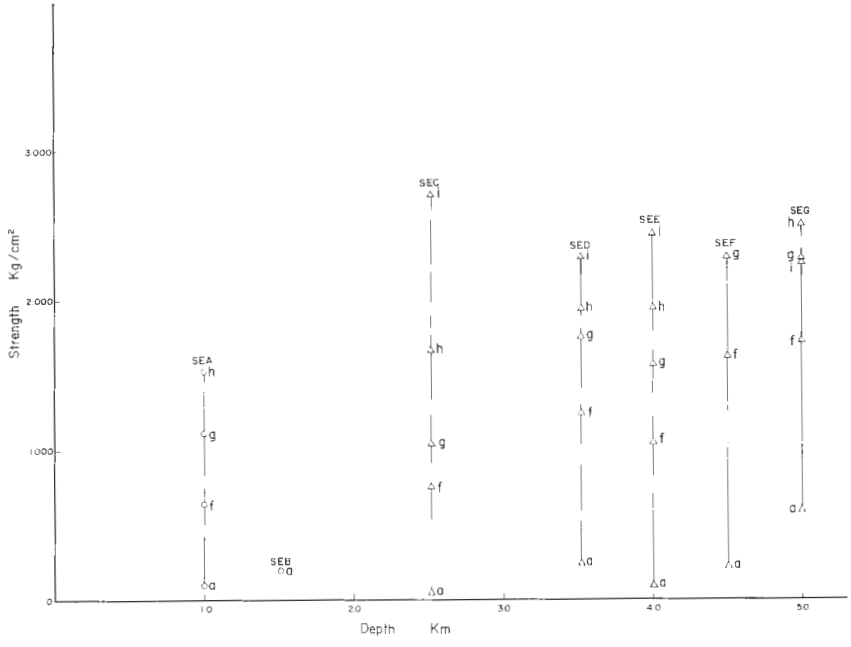

Fig. 285 Strength versus depth in Shimoigarashi well. The marks are the same as Fig. 280.

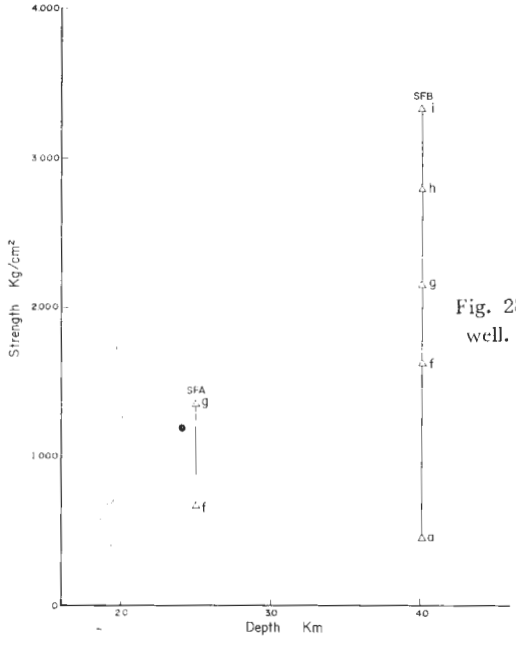

Fig. 286 Strength versus depth in Masugata well. The marks are the same as Fig. 280.

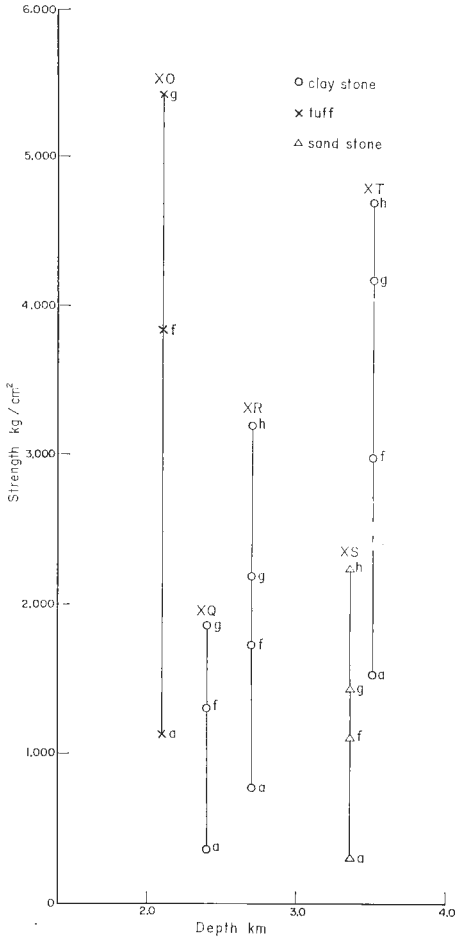

Fig. 287 Strength versus depth in Kambara GS-1 well. The marks are the same as Fig. 280.

V. 8 Elastic wave velocity and strength

In Figs. 288~291, the relation between elastic wave velocity (compressive) and strength is shown for cases of argillaceous, arenaceous, pyroclastic, and volcanic rocks. In general, strength increases in proportion to the elastic wave velocity.

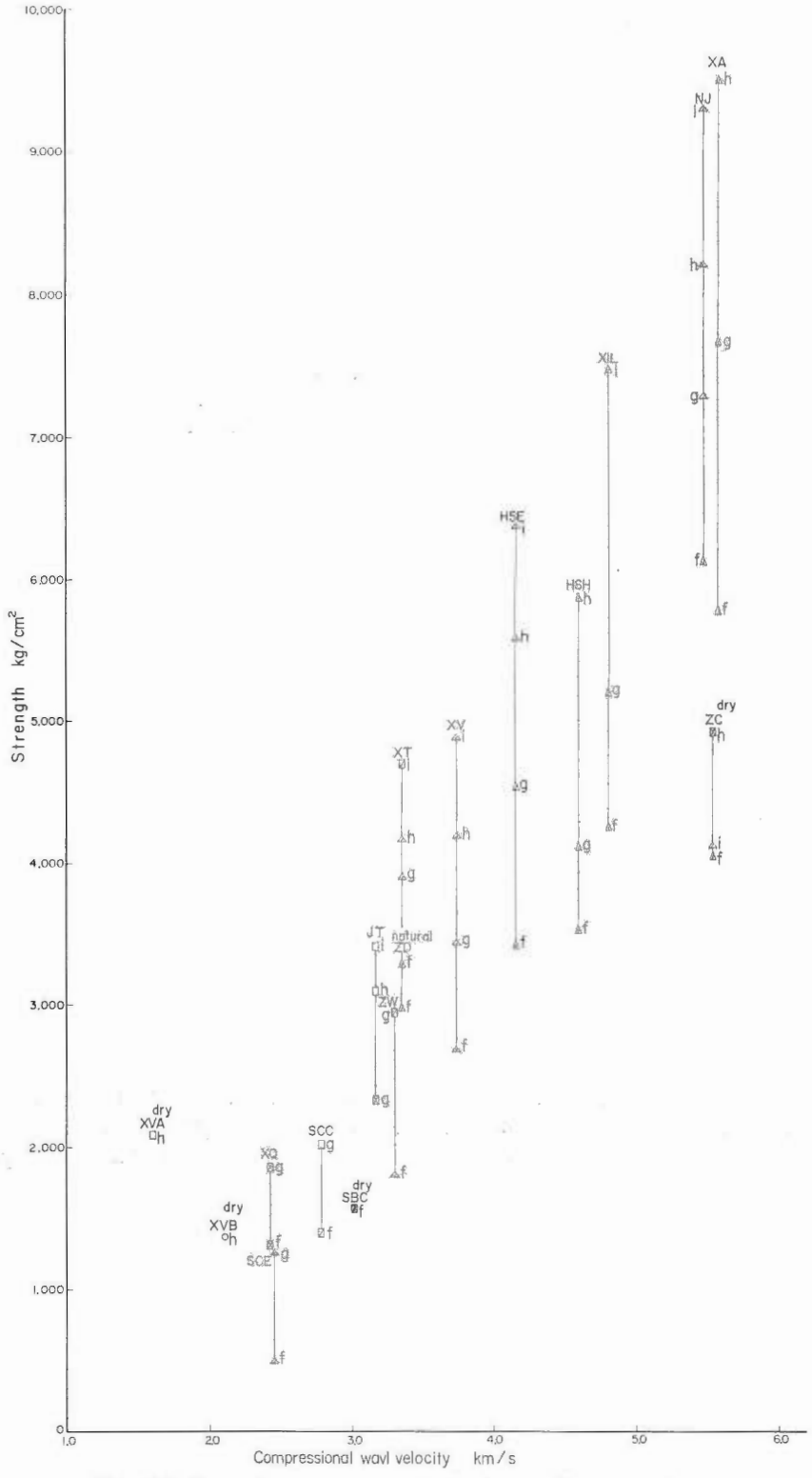

Fig. 288 Strength versus wave velocity for argillaceous rocks.

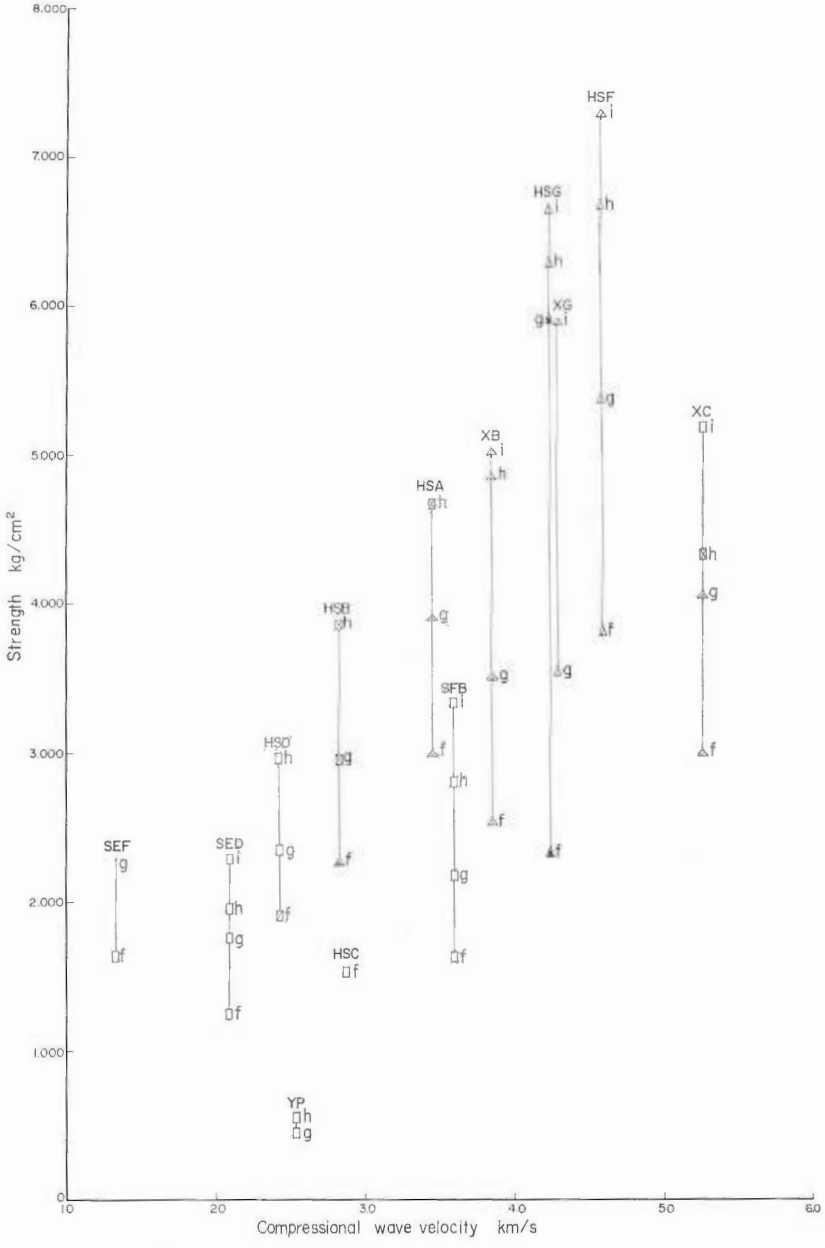

Fig. 289 Strength versus wave velocity for arenaceous rocks.

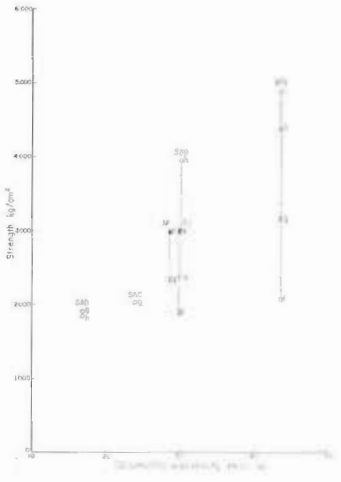

Fig. 290 Strength versus wave velocity for pyroclastic rocks.

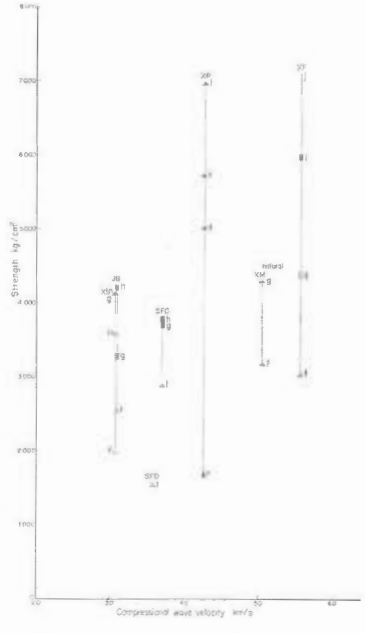

Fig. 291 Strength versus wave velocity for volcanic rocks.

V. 9 Visco-ductile deformation

In experiments, soft and porous rocks are observed to flow under very low differential stress. This mode of deformation is called "visco-ductile" in this report (cf. 4.1). The visco-ductile behavior occurs at higher confining pressure than ductile behavior.

Fig. 292 denotes the confining pressure of ductile-visco-ductile transition versus the sampled depth of well cores. The tests were carried out at a few kinds of confining pressure. The transition pressure was determined only in the wide range indicated by the thick lines in Fig. 292. Some samples become visco-ductile at high confining pressure and some hard rocks were not observed to be visco-ductile. The range of transition pressure for most of soft rocks, however, is near to the straight line B, which denotes the overburden pressure in case that the density of rocks is uniformly 2.5. The rocks in shallow place are usually porous and lighter than 2.5. The probable overburden pressure is very near to the curve A which connects smoothly the range of transition pressure.

The framework of rock can support the hydrostatic pressure under which the rock was compacted during a sufficient time. The fragile framework may be crushed by the higher hydrostatic pressure than formerly applied to the rock. It is considered that the pressure of ductile-visco-ductile transition indicates the maximum pressure formerly applied to the rock over the duration enough for consolidation.

The older rocks, generally, experienced the higher pressure because of overburden pressure and tectonic stress. The contour lines in Fig. 293 suggests the maximum pressure formerly applied to the rocks of some ages in various districts. Hard rocks are eliminated from this figure because visco-ductile behavior is not apparent. Fig. 293 suggests that the applied maximum pressures is the lowest in the Joban district and lower in the Miura district than in the other districts.

It is considered that the overburden pressure and tectonic compressive stress were low in the Joban and Miura districts.

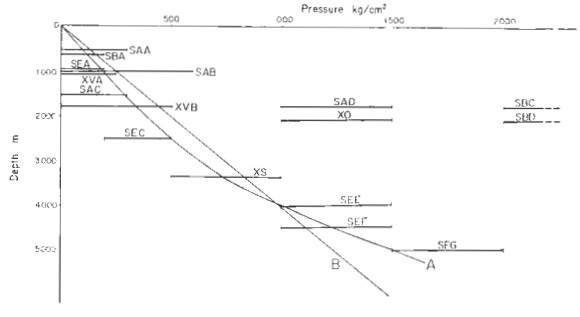

Fig. 292 Confining pressure of ductile-visco-ductile transition versus sampled depth of well log cores. The mode of deformation becomes visco-ductile at higher confining pressure than a certain pressure in the range indicated by thick lines. The straight line B denotes the overburden pressure calculated under the assumption that the density of rocks is uniformly 2.5. The curve A is the rock pressure which is estimated from the transition pressure.

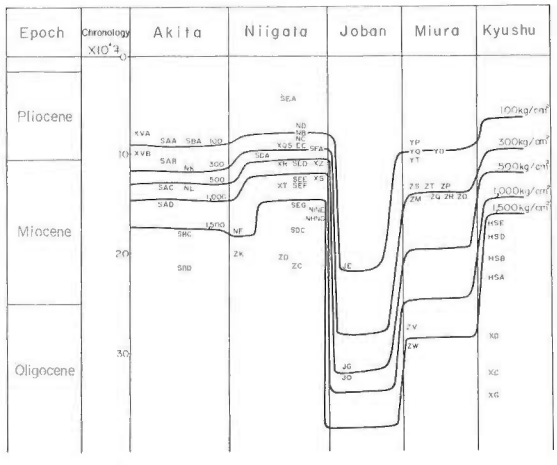

Fig. 293 The maximum pressure formerly applied to the rocks (contour lines). It is estimated from pressure of ductile–visco-ductile transition.

V. 10 Stratigraphic level

In Figs. 294, 295 and 296, schematic diagrams show confining pressures, at which the rocks become brittle from ductile (including transitional), or ductile from visco-ductile, in connection with the depth of well cores which are sampled in Akita and Niigata. Fig. 294 was made on argillaceous rocks from four wells near to Akita city (Fig. 301), and Fig. 295 from four wells in the middle plain of Niigata Prefecture (Fig. 302). Thick lines are contours of the confining pressure, at which the deformational behavior of the rocks changes, and thin lines are the stratigraphic boundary. The lines of transition of deformational behavior and that of stratigraphic sequence are almost similar, especially in Akita area. In Noishi-oki and Sawame-oki wells, the rocks are more brittle, in other words, the transitional lines are more upward than Noshiro GS-1 well. The stratigraphic levels are also more upward in the former two wells than the latter. For instance, the base of Tentokuji formation of Noishi-oki well and Sawame-oki well is respectively 2200 m and 2000 m higher than, that of Noshiro GS-1 well, while the transition line from ductile to brittle for 50 kg/cm^2 is about 1000 m higher in Sawame-oki than Noshiro GS-1, and the line for 1500 kg/cm^2 is about 1000 m higher in Noishi-oki than in Noshiro GS-1. Only local "abnormal" is seen on SCE(S32), claystone in Nishikurozawa formation. The Nishikurozawa formation consists of mainly pyroclastic and volcanic rocks, and SCE (S32) is derived from thin bed within these rocks. The similarity between the transitional lines and stratigraphic level is found for ductile–visco-ductile transition, too. One hundred kg/cm^2 transition line runs nearly parallel to the top of Tentokuji formation. In Niigata area, such concordant relation is not so clear, because of lack of sufficient data, although there is no much contradiction as far as available data is concerned. The concordant relation in Niigata area is seen for arenaceous rocks better than argillaceous rocks.

In Fig. 296, the transition line of deformational behavior offset about 500 m between the deep part of Masugata and Shimoigarashi wells, while the top of Shiiya formation offsets in the same direction about 500 m. For the depth around 2000 or 3000 m, good concordance is seen for 50 kg/cm^2 transition line and top of Nishiyama and Shiiya formations in Kambara GS-1, Masugata, and Obuchi wells.

In Fig. 297, porosity-depth relation is shown for argillaceous rocks of Kambara GS-1 and Noshiro GS-1 and for arenaceous rocks of Shimoigarashi. Also, standard porosity depth relation for argillaceous rocks in Akita and Niigata areas are shown. The relation for Kambara GS-1, and Noshiro GS-1 are quite near to the standard curve in respective area. Therefore, porosity-depth relation for both wells can be considered to represent approximate standard compaction process in the sedimentary basin in Akita or Niigata. In Fig. 298, strength-depth relation for argillaceous rocks for Kambara GS-1 and Noshiro GS-1 is again reviewed. The open circle, closed circle and square show visco-ductile, brittle, and transitional pattern, respectively, as in Fig. 268.

It is indicated that strength and deformational behavior of the clastic sedimentary rocks are related not only to either porosity or depth but to the tectonics of the sedimentary basin. The accumulative lithostatic and tectonic stresses are the most responsible for the strength and deformational behavior.

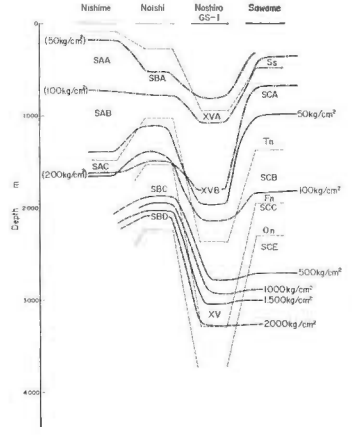

Fig. 294 Depth of transition among deformational behaviors at each confining pressure for argillaceous rocks (Akita district). Thick solid lines, thick dotted lines, and thin dotted lines indicate the boundary for transition from ductile (including transitional) to brittle, from visco-ductile to ductile, and stratigraphic boundary, respectively.

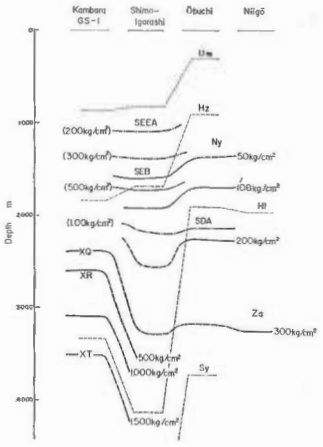

Fig. 295 Depth of transition among deformational behaviors at each confining pressure for argillaceous rocks (Niigata district).

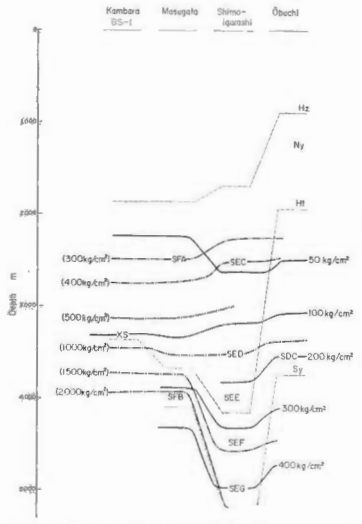

Fig. 296 The depth transition among deformational behaviors for each confining pressure for arenaceous rocks.

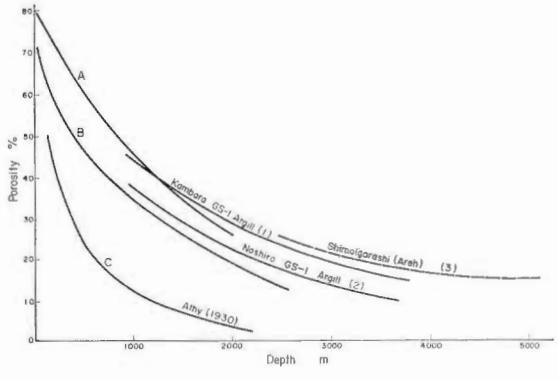

Fig. 297 Porosity versus depth for argillaceous and arenaceous rocks in representative wells in Akita and Niigata. A, standard relation in Niigata by MATSUZAWA (1961); B, standard relation in Akita by MIYAZAKI(1965); C, Pennsylvanian-Permian, North-central Oklahoma by ATHY(1930).

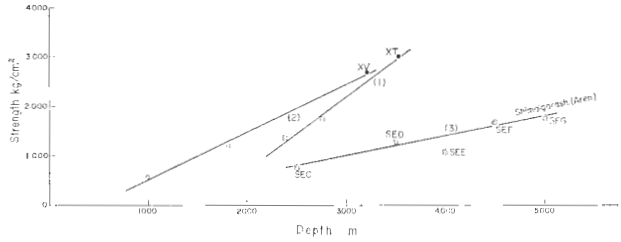

Fig. 298 Strength versus depth for representative wells. (1) is Kambara GS-1, (2) Noshiro GS-1, and (3) Shimoigarashi wells. The marks, ●, ○, and □ show brittle (including very brittle), visco-ductile and transitional (including ductile) behaviors, respectively for argillaceous rocks, and ◎ shows arenaceous rocks.

V. 11 Tectonic environment

In Figs. 299 and 300, the transition among deformational behaviors is shown in each area studied. In Fig. 299, a schematic relation with geologic age is shown for argillaceous rocks. A contrast between one group: Kyushu, Kushiro, Niigata and Akita and the other group: Miura and Joban, is very remarkable. In the former areas, transition from ductile to brittle at 500, 1000, and 2000 kg/cm² is placed in lower Miocene, while, in the latter areas, the transition is placed in upper Oligocene. The difference is larger in the transition from visco-ductile to ductile. The 100 kg/cm² line is found at the top of Pliocene in Niigata, in lower Pliocene in Akita, in upper Miocene in Miura, and in middle Miocene in Joban. The same relation is also seen for arenaceous rocks, in Fig. 300, and the contrast between both areas is more obvious. The transition lines from ductile to brittle at 500, 1000 and 1500 kg/cm² exist in lower Miocene or upper Oligocene in the former areas, while, in the latter areas, it can be found in the age concerned. The 100 kg/cm² line exists in lower Pliocene or upper Miocene in the former areas, and it is found in the lower part of Oligocene in the latter areas. The rocks in the Joban area are so much ductile. The transition from ductile to brittle is almost the same pressure (20 or 70 kg/cm²) through upper Miocene to upper Oligocene. This indicates that the depth of sedimentation had been quite shallow through these geological ages in the Joban area. 200 kg/cm² line is placed in lower Pliocene or upper Miocene in both areas.

Distribution of Tertiary System in Japan is divided into 12 areas as shown in Fig. 1, (Geological Survey of Japan, 1960). However, this is not exact expression in terms of tectonic classification. According to MATSUDA, NAKAMURA and SUGIMURA (1966), the Japanese islands, in late Cenozoic age, which includes Miocene, Pliocene and Pleistocene, are divided tectonically into two island arc systems; the east Japan island arc system and the west Japan island arc system. The boundary between two groups is the western margin of Fossa Magna, Itoigawa-Shizuoka tectonic line. The east Japan arc system has undergone a series of tectonic movements, and has three tectonic arcs; Kurile, northeast Honshu, and Izu-Mariana arcs. The west Japan arc system, on the other hand, has been tectonically stabler than the east system, and has two arcs; southwest Honshu,

and Ryukyu arcs. Among them, northeast Honshu and Izu-Mariana arcs contain the thickest sedimentary basins, and experienced the most violent deformation since Miocene. The southwest Honshu arc is probably older than the northeast Honshu arc. During Early Tertiary time, two geosynclines existed; the Hidaka geosyncline trending approximately north to south in central Hokkaido, and Shimanto geosyncline on the Pacific side of southeast Japan.

Among 12 areas in Fig. 1, Akita (7), and Niigata (9) belong to the northeast Honshu arc; northern Kyushu (12) belongs to the southwest Honshu arc. Kushiro, Hokkaido (6) is located south of the Kurile arc. Miura (4) is east of the Izu-Mariana arc. In the studied areas, Akita and Niigata were an area of thick sedimentation and violent deformation in later Cenozoic. Kushiro and northern Kyushu were off the violent mobile belts in later Cenozoic, and less active in tectonic deformation than Akita and Niigata. However, Oligocene sedimentary rocks in Kushiro experienced considerable deformation by an influence of Hidaka orogeny in early Cenozoic (HOSHINO, 1963). Also, northern Kyushu area was subjected to tectonic stress through early and later Cenozoic time (HOSHINO, 1967). Miura Peninsula is near to Izu-Mariana and is considered as an area subjected to considerable sedimentation and vertical displacement in later Cenozoic. Joban area was the stablest area among the areas studied. The area has undergone little folding although it is faulted with lots of normal faults, (HOSHINO, 1965).

The above comparison indicates that there is a good agreement between the results of laboratory work and tectonic environment for each area except only one case: Miura Peninsula.

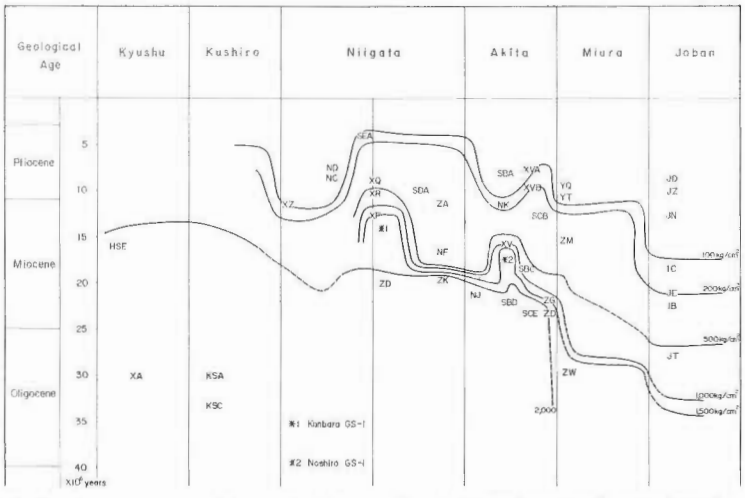

Fig. 299 Relation between transition of deformational behaviors and stratigraphic units for argillaceous rocks. Thick solid and thick dotted lines show pressures for transition from ductile (including transitional) to brittle (including very brittle) and that from plastic to ductile, respectively. The marks, *, † show peak pattern in Kambara GS-1 and Noshiro GS-1 respectively.

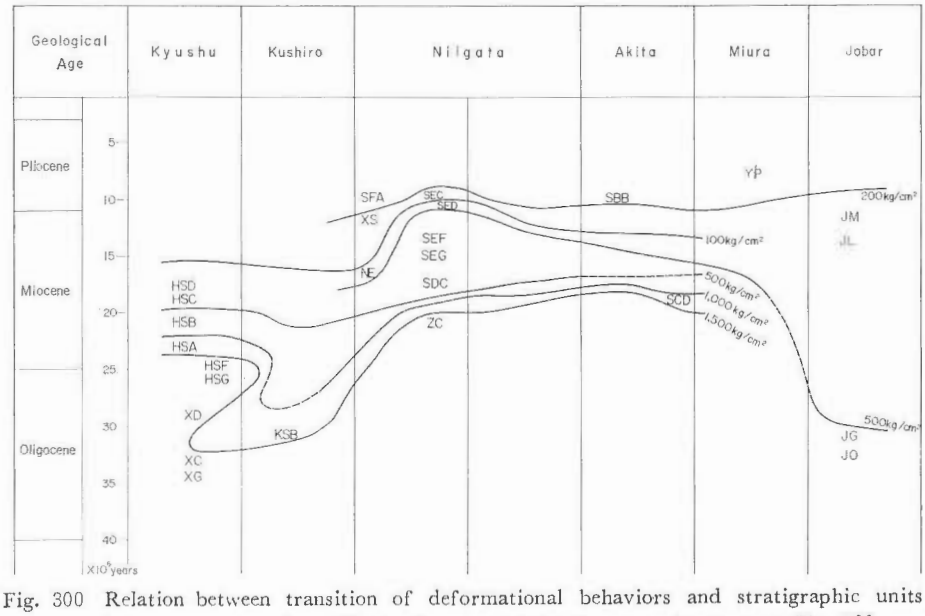

Fig. 300 Relation between transition of deformational behaviors and stratigraphic units for arenaceous rocks. The explanation of the lines are the same as Fig. 299.

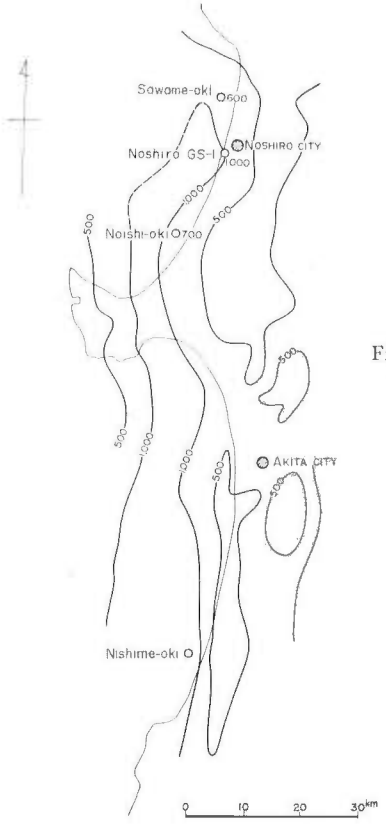

Fig. 301 Map showing localities of boring wells in Akita. The contour lines are isopachs of Funagawa formation.

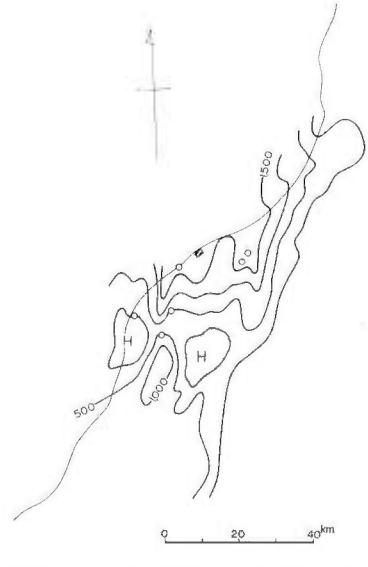

Fig. 302 Map showing localities of boring wells in Niigata. The contour lines are isopachs of Shiiya formation.

V. 12 Geologic age and strength

The relation between strength and the geologic age of studied areas is shown in diagrams. For argillaceous rocks, the relation in northern Kyushu, Niigata, Akita, Miura, and Joban, is shown in Figs. 303~310. For northern Kyushu (Fig. 306), shales from the Kishima group, HSH (S100), upper Oligocene, and from the Sasebo group, HSE (S97), upper Miocene, show nearly the same strength, whereas a shale from the Nishisonogi group, XA (S85), upper Oligocene shows much larger strength. Fig. 307 for Niigata shows rather complex pattern, which may be caused by low strength of ZA (S40), and ZK (S36), or in other words, by high strength of XQ (S62), XR (S63), XT (S64). Kambara GS-1 well, from which XQ, XR, and XT are brought, is considered to represent the thickest sequence in the sedimentary basin of Niigata. Fig. 308 for Akita is also not so simple because of weakness of SCC(S30), Onnagawa shale and SCE(S32), Nishikurozawa claystone from Sawame-oki well. On the other hand, NJ (S33), Onnagawa shale from Onnagawa, Oga Peninsula, shows extremely high strength. SCE(S32) is taken from stratigraphically abnormal position as already mentioned. Figs. 309 and 310 from Miura and Joban show rather simple pattern than those for Akita and Niigata. The value of strength at respective age is nearly similar in both areas. The low inclined lines of Joban and Miura show possibly a representative relation in comparatively stable sedimentation areas. In Fig. 317, a summary diagram of relation between strength at 500 kg/cm^2 and geologic age is presented. It is interesting that the strengths in Akita are very near to those in Miura up to 12 or 13×10^6 years or, at least, up to Tentokuji and Katsura formations.

The argillaceous rocks are divided into two groups; one group of gentle inclination (dotted line) in stable sedimentation and mild compaction, and the other of steep inclination (solid line) in thick sedimentation and, probably under tectonic compression. This line is the nearly same as that presented by one of the authors previously, (HOSHINO, 1967 a, b).

In Figs. 311~314, the relation for arenaceous rocks in northern Kyushu, Niigata, Miura, and Joban is shown. Fig. 311, for northern Kyushu, covers the age ranging from middle Oligocene to middle Miocene. The rocks from the Kishima group show larger strength than the Nishisonogi group rocks, which is older than Kishima group. Since there is no much difference between the porosities of both groups, this might be attributed to difference in the tectonic deformation. Fig. 312 for Niigata shows rather complex relation. NE (S39) is collected from an outcrop located near to the top of anticline, and it is considered to have been affected by bending. Fig. 313 shows the very simple relation in Miura. In Fig. 314 for Joban, the relation is simple, and the results are almost same as that from Miura. In Fig. 318, a summary diagram of relation between strength at 500 kg/cm^2 and geologic age of arenaceous rocks is presented. The data from Niigata covers the scope from lower Pliocene to upper Miocene and that from Kyushu covers from middle Miocene to middle Oligocene. The curves would show a representative relation between strength and age for arenaceous rocks in Japan. On the other hand, those from Miura possibly indicate another representative relation that might be applicable for rather stable area in Japan.

Fig. 315 shows strength-age relation of pyroclactic rocks in Niigata. It is indicated that there is no definite relation in this case. It was indicated in

previous pages that, for pyroclastic rocks, porosity, as well as grain size, is an important factor to determine strength. Fig. 316 shows the relation in Akita. For this case, a simple relation is indicated because three rocks, SAB, SAC, and SAD, are collected from one boring well, Nishime-oki, and nearly same in grain size.

The inclination of solid line is greater in argillaceous rocks (Fig. 317) than in arenaceous rocks. In the stable basin of Joban, too, argillaceous rocks are more affected by age than arenaceous rocks (Fig. 310, and Fig. 314). The degree of strengthening of rocks with geologic age, is the greatest in argillaceous rocks, greater in arenaceous rocks and less in pyroclastic rocks.

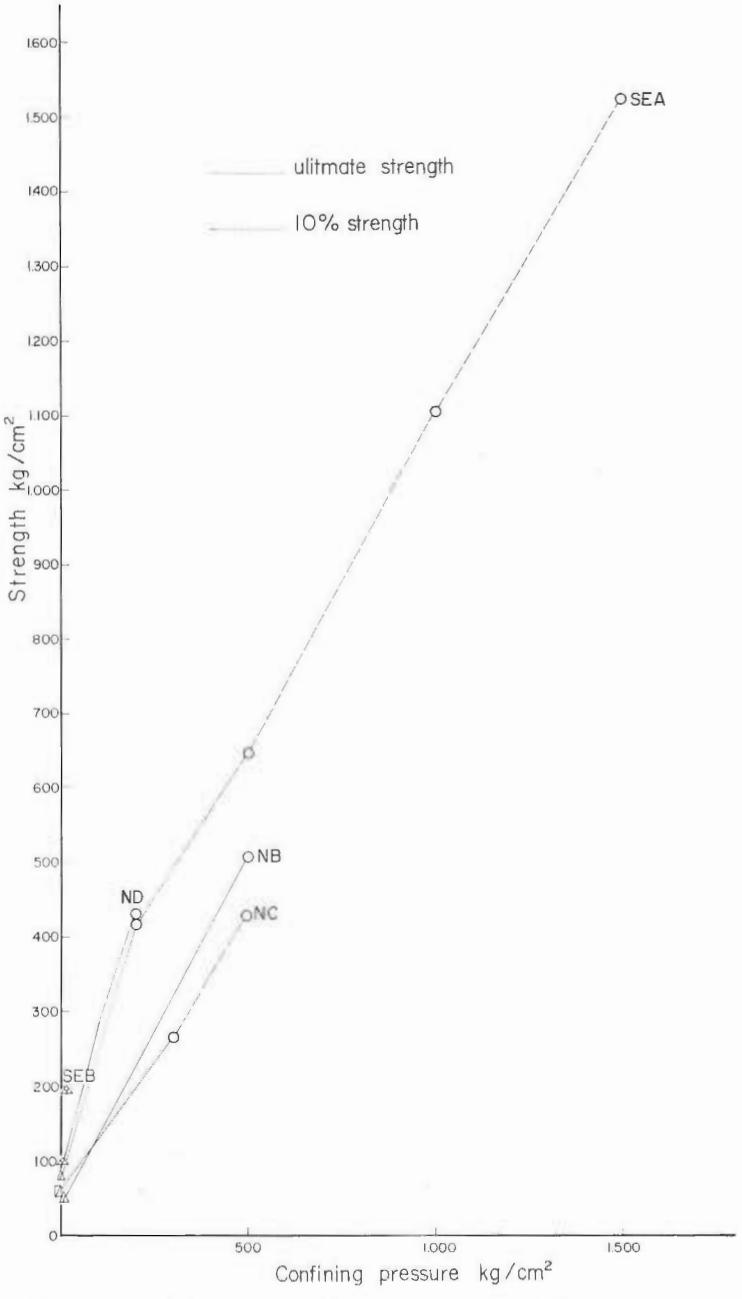

Fig. 303 Strength versus confining pressure for younger rocks in Niigata.
The marks, ▲, △, ▯, ◯, and ○ show very brittle, brittle, transitional, ductile, and visco-ductile behaviors.

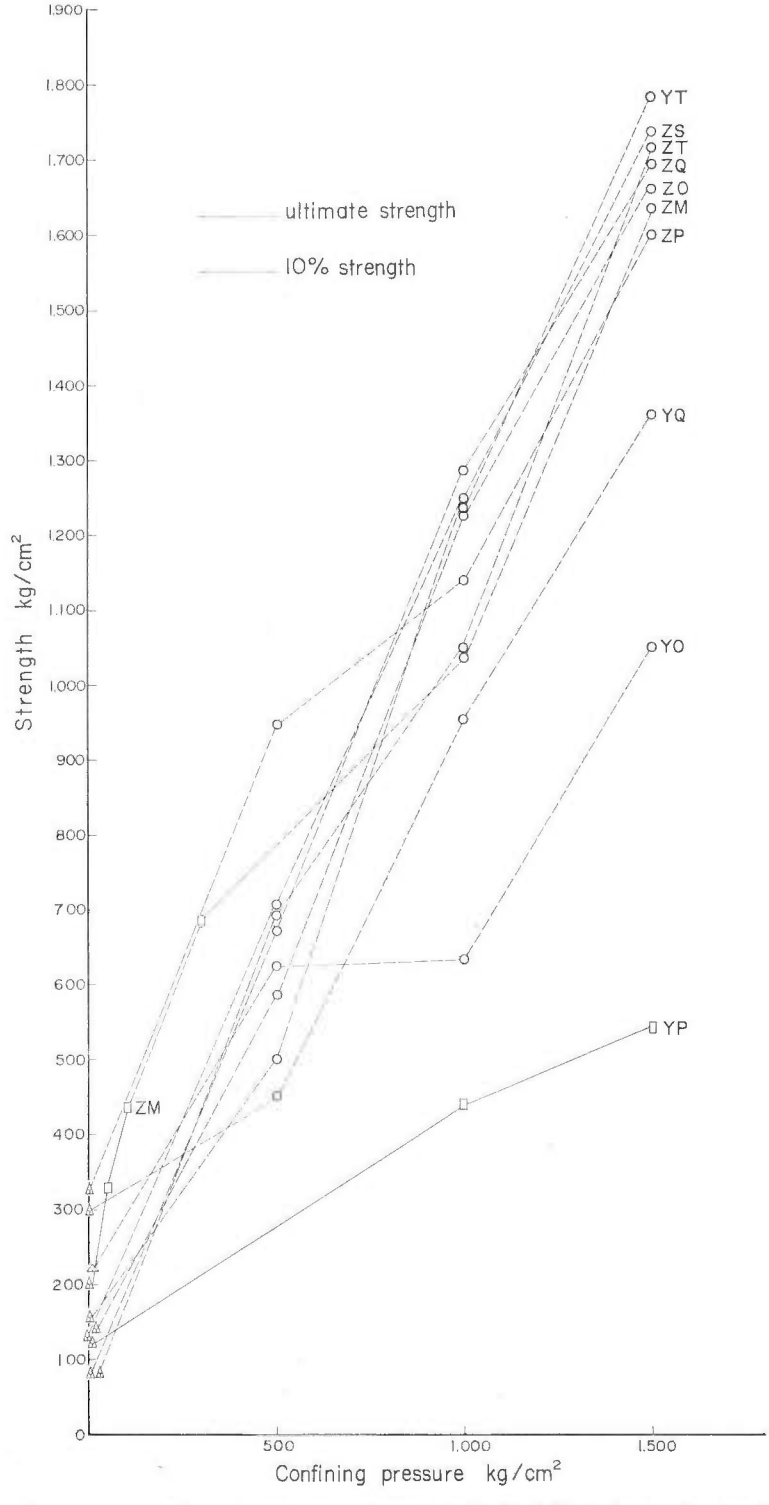

Fig. 304 Strength versus confining pressure for younger rocks in Miura Peninsula, southern Kwanto.

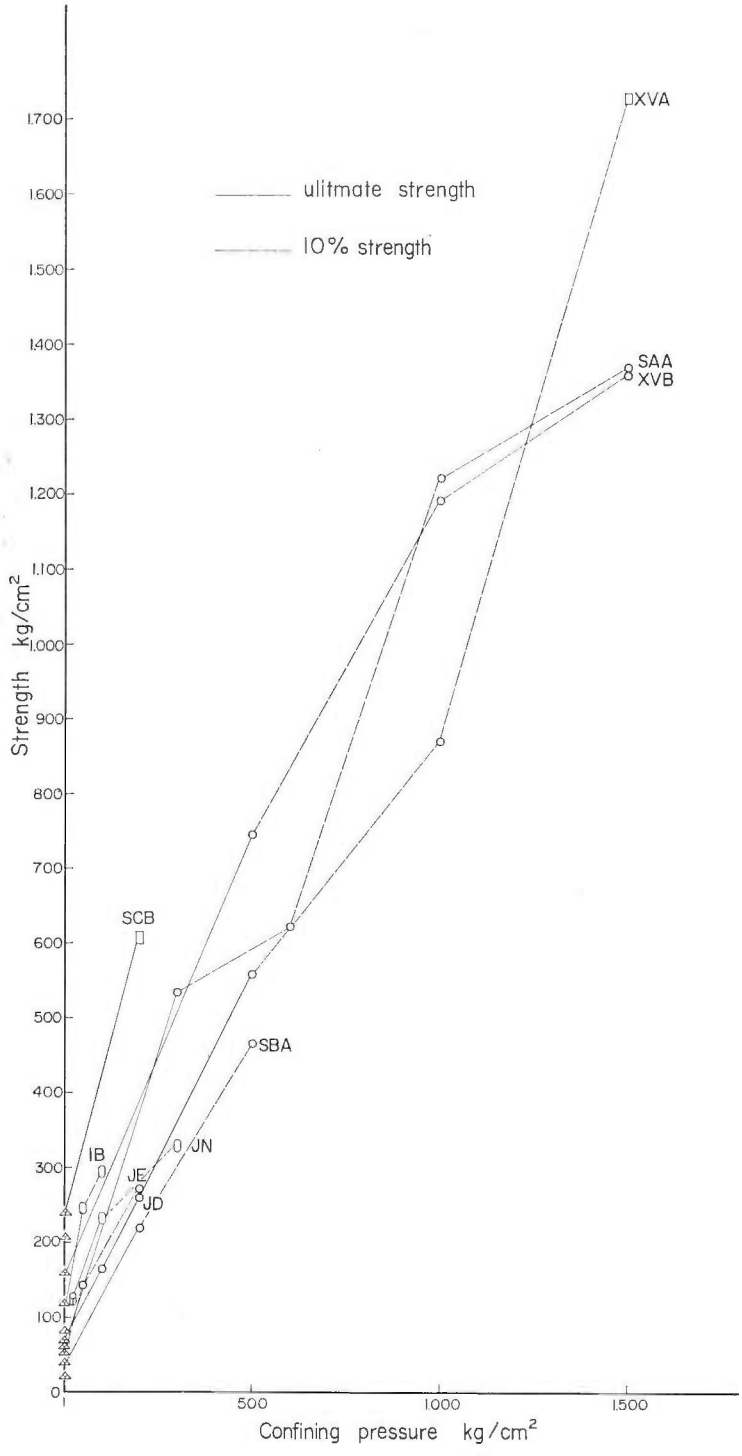

Fig. 305 Strength versus confining pressure for younger rocks in Akita and Joban.

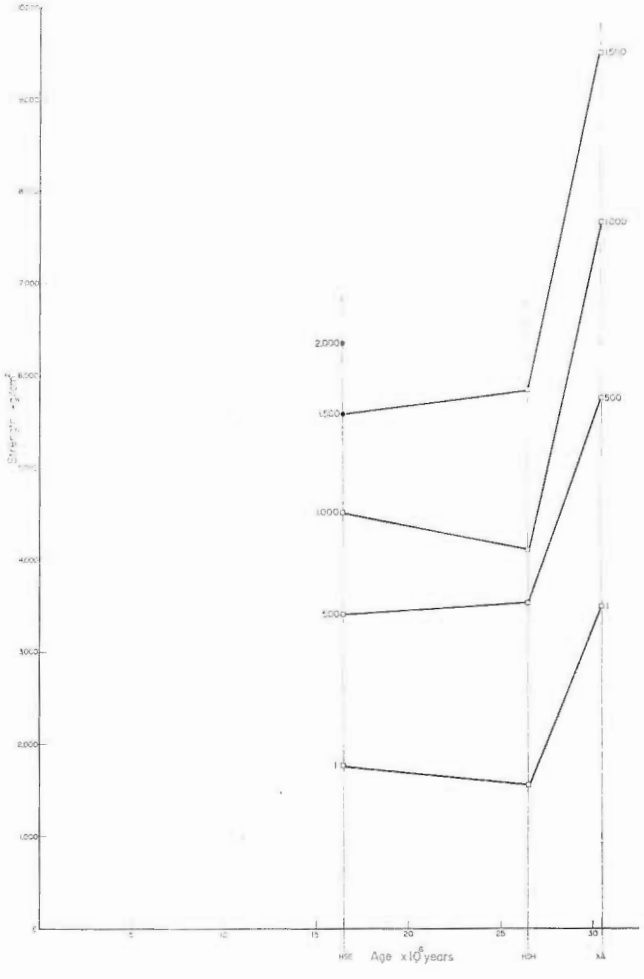

Fig. 306 Strength versus geological age for argillaceous rocks in northern Kyushu.

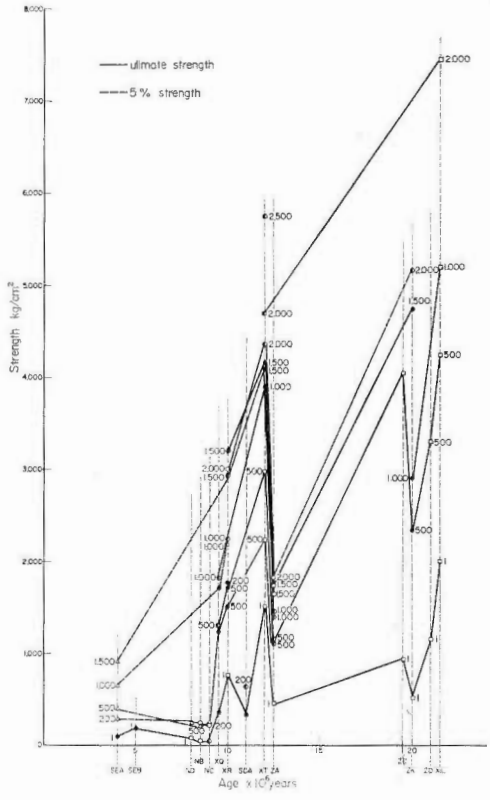

Fig. 307 Strength versus geological age for argillaceous rocks in Niigata. Ultimate and 5 % strength. Thick solid lines are ultimate strength, thin dotted lines are 5 % strength.

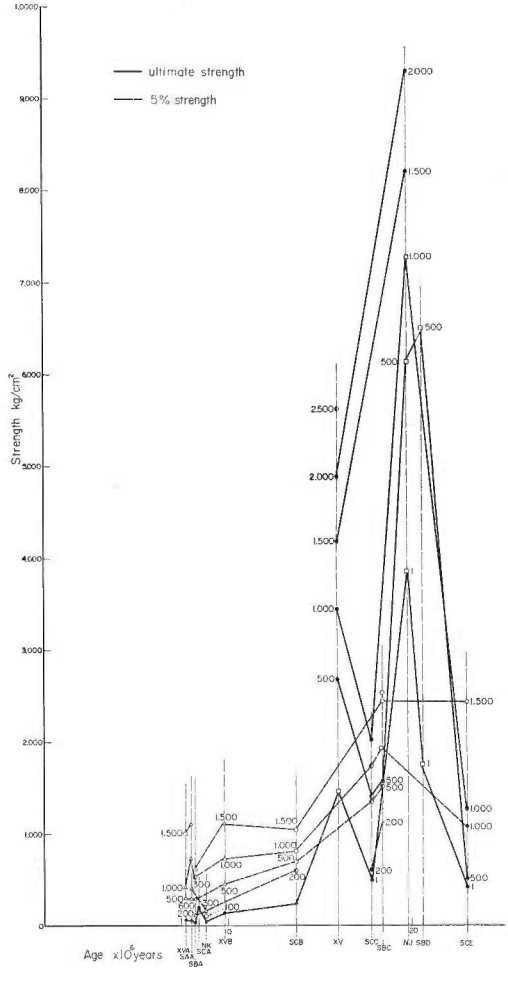

Fig. 308 Strength versus geological age for argillaceous rocks in Akita.

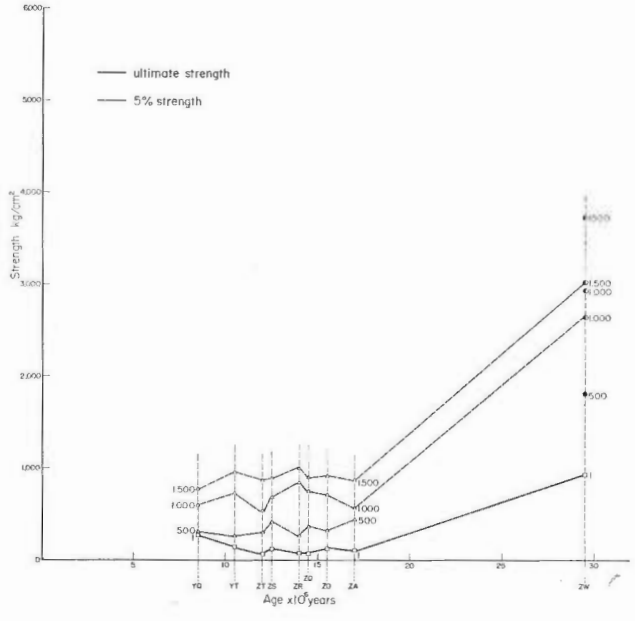

Fig. 309 Strength versus geological age for argillaceous rocks in Miura Peninsula.

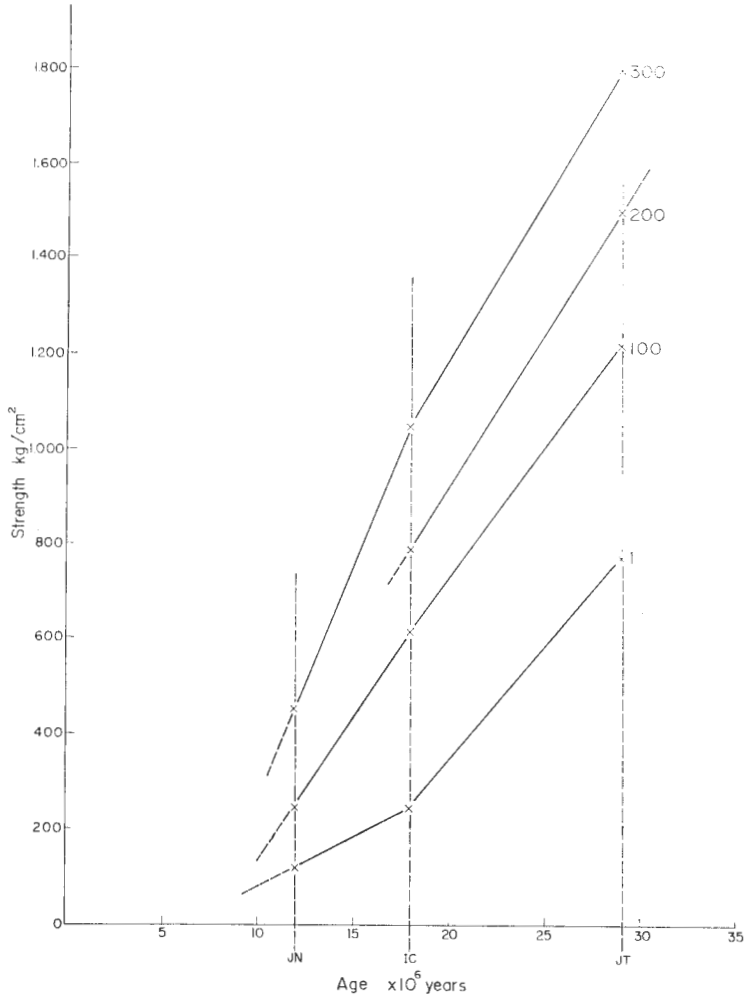

Fig. 310 Strength versus geological age for argillaceous rocks in Joban.

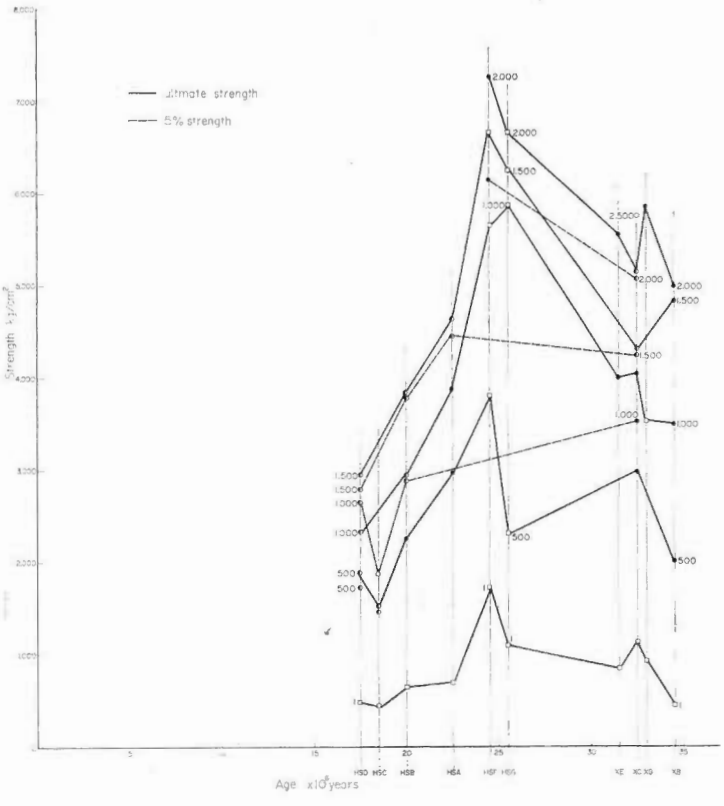

Fig. 311 Strength versus geological age for arenaceous rocks in northern Kyushu.

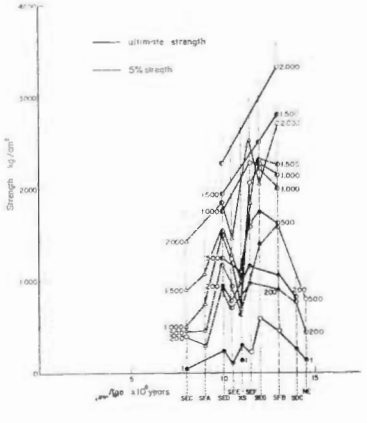

Fig. 312 Strength versus geological age for arenaceous rocks in Niigata.

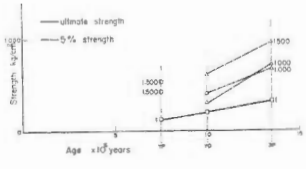

Fig. 313 Strength versus geological age for arenaceous rocks in Miura Peninsula.

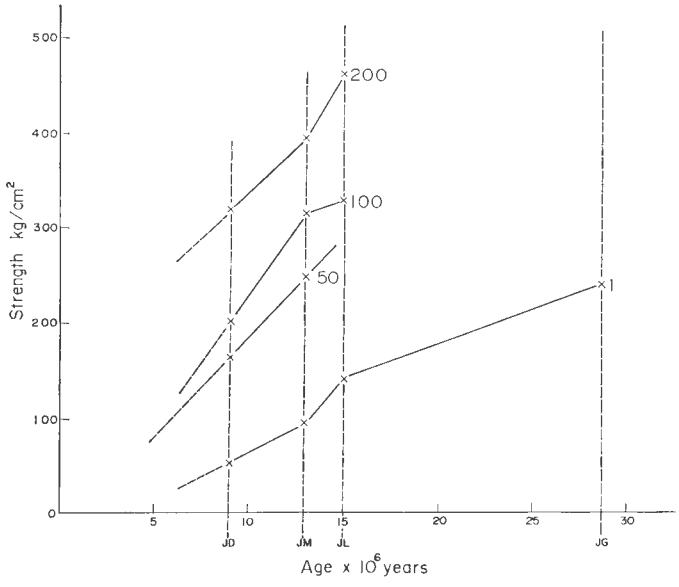

Fig. 314 Strength versus geological age for arenaceous rocks in Joban.

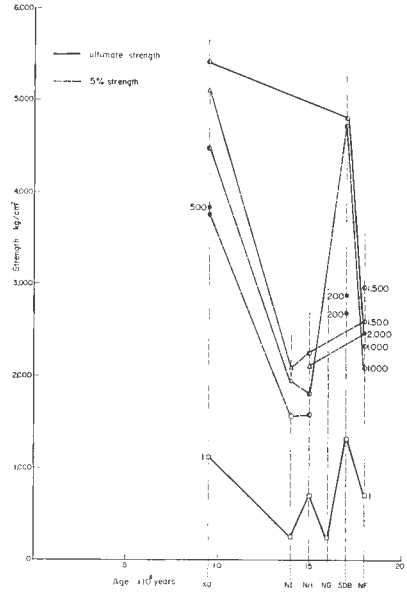

Fig. 315 Strength versus geological age for pyroclastic rocks in Niigata.

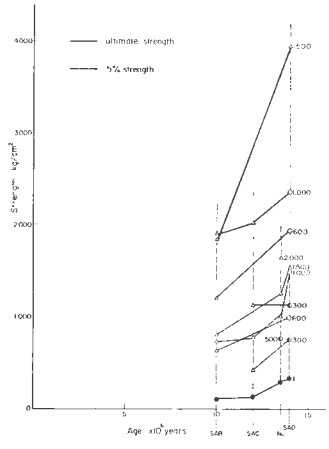

Fig. 316 Strength versus geological age for pyroclastic rocks in Akita.

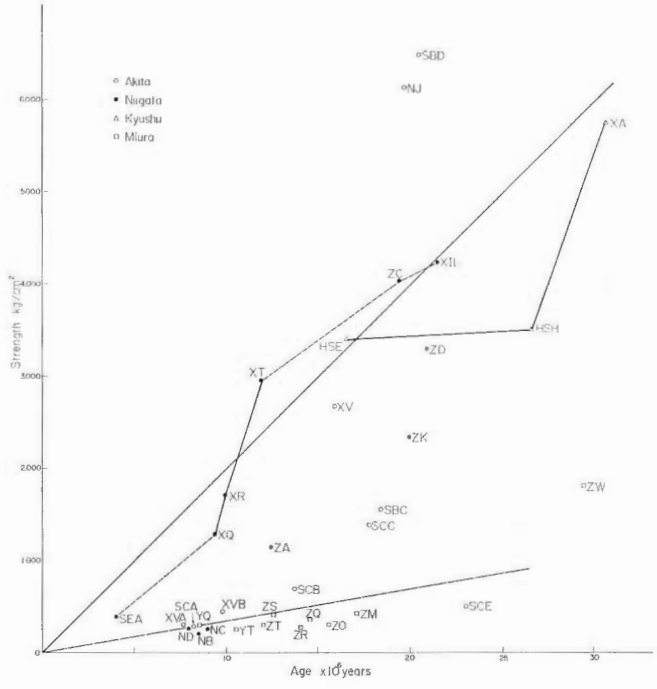

Fig. 317 Schematic relation between strength (ultimate or 5% strength at 500 kg/cm²) and geological age for argillaceous rocks. Solid line shows a representative relation for unstable sedimentary basins with thick sedimentation and tectonic compression, and dotted line for stable sedimentary basins.

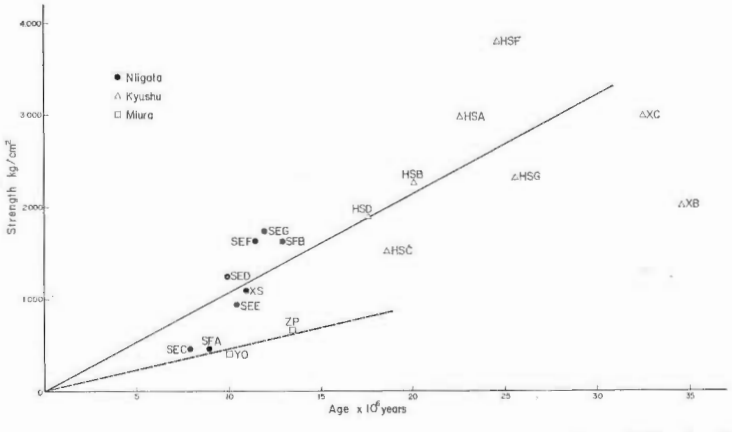

Fig. 318 Schematic relation between strength (ultimate and 5% strength at 500kg/cm²) and geological age for arenaceous rocks. Solid line is an average for unstable sedimentary basins and dotted line is for stable basins.

VI. Conclusion

One hundred dry sedimentary rocks, most of which are argillaceous and arenaceous rocks, ranging Pliocene to Oligocene in age, collected from representative Tertiary sedimentary basins in Japan, were tested at confining pressures up to 2500 kg/cm^2 at room temperature, mostly in a strain rate 10^{-5}/sec for the linear stress-strain part, and 10^{-4}/sec for part after the yield point. The results of experiments were summarized in Table 4. The mechanical properties of sedimentary rocks have a wide range of value and are influenced by many factors. We tried to study relations among the strength, confining pressure, deformational behavior, angle of fracture, strain at fracturing, failure type, porosity, grain size, axial shortening, sampled depth, elastic wave velocity, geologic age, stratigraphic level, and tectonic environment.

The deformational behavior was classified on a basis of the pattern of stress-strain curves; very brittle, brittle, transitional, ductile, and visco-ductile. Transition from brittle to ductile (including transitional) is shown as a simple curve on normal stress–shearing stress co-ordinate, where normal and shearing stresses are calculated from the measured angle of the plane of macroscopic fractures of the deformed specimens. However, the transitional curves are different among argillaceous, arenaceous, pyroclastic, and volcanic rocks. The ratio of shearing stress to normal stress to the fracture plane ($\mu = \tau/\sigma$) decreases as the angle of fracture and strain at the fracturing increase (Eq. 5.4 and Eq. 5.5).

The mode of failure was divided into wedge, single shear, and network shear and flow types on a basis of observed mode of appearance. Failure types change generally in this order as deformational behavior changes from brittle to ductile. In very brittle and brittle behaviors, wedge and single shear are most predominant, while, in ductile and visco-ductile behaviors, nearly all are flow. In transitional behavior, the failure type is more similar to that in ductile behavior in argillaceous and arenaceous rocks and to that in brittle behavior in pyroclastic rocks.

It was indicated that the transition of deformational behavior seems in good accordance with the change of the strain at fracturing, while the change of failure type is more complex. The change among the types of failure is continuous in essentials.

The strength increases with reduction of porosity caused by compaction. The strength of pyroclastic rocks are affected by both porosity and grain size. Deformational behavior is also closely related to porosity. The porous rocks flow under very low differential stress at high confining pressure ("visco-ductile" behavior). The confining pressure of ductile–visco-ductile transition increases with sampled depth and seems to suggest the formerly applied maximum pressure. The compaction (consolidation) strengthens the sedimentary rocks remarkably. The sedimentary rocks are strengthened with the geologic age. The degree of strengthening with the geologic age is the greatest in argillaceous rocks and less in pyroclastic rocks.

Among the six areas studied, there exists an interesting contrast in deformational behavior and strength. The rocks in Joban and Miura are much more ductile and weaker than those in the other areas. The confining pressure of

ductile–visco-ductile transition and degree of strengthening with geologic age suggest that lower compressive stress has been applied on the rocks in Joban and Miura than in the other areas. Ductile character of the rocks from Joban probably attributed to sedimentation in the shallow sea through late Cenozoic time. These experimental results are quite agreeable with structural setting of the six areas except Miura Peninsula, which has been considered as structurally considerably deformed area.

List of locality maps.

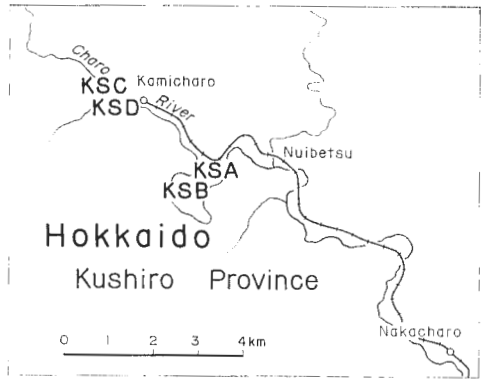

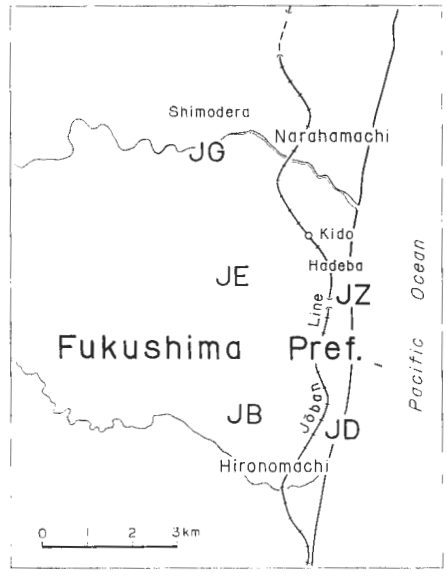

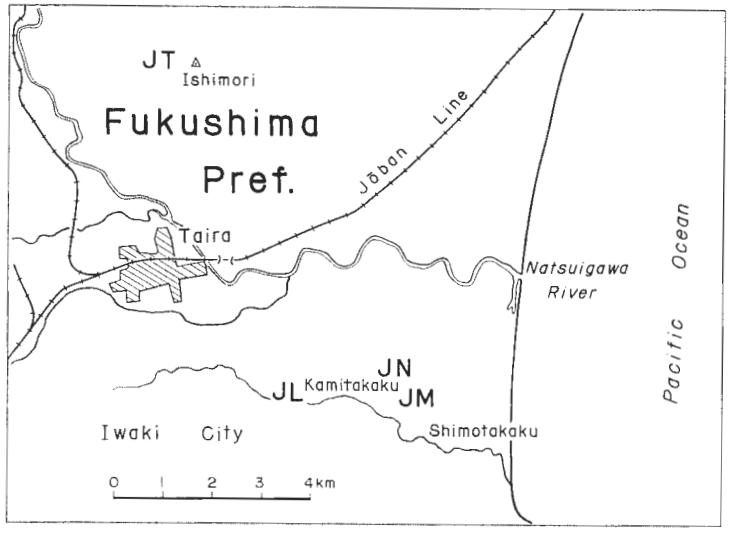

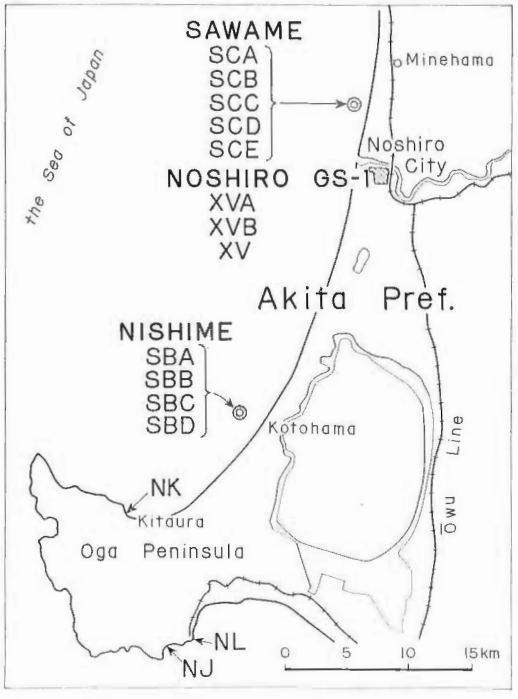
SAWAME
SCA
SCB
SCC
SCD
SCE
Minehama
Noshiro City
NOSHIRO GS-1
XVA
XVB
XV
the Sea of Japan
Akita Pref.
NISHIME
SBA
SBB
SBC
SBD
Kotohama
Ou Line
NK
Kitaura
Oga Peninsula
NL
NJ
0 5 10 15km

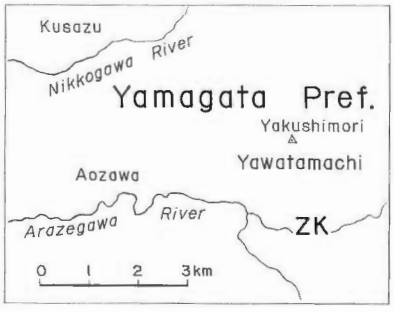
Kusazu
Nikkogawa River
Yamagata Pref.
Yakushimori
Yawatamachi
Aozawa
Arazegawa River
ZK
0 1 2 3km

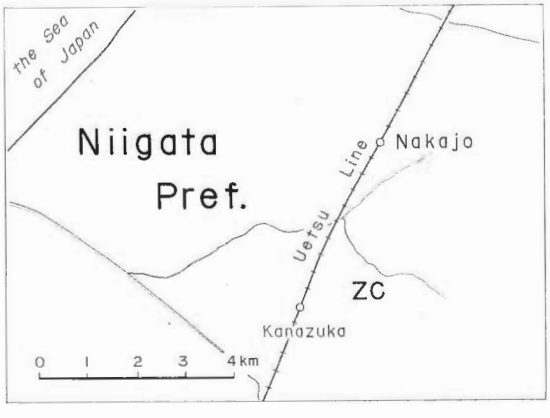
the Sea of Japan
Niigata Pref.
Nakajo
Uetsu Line
ZC
Kanazuka
0 1 2 3 4km

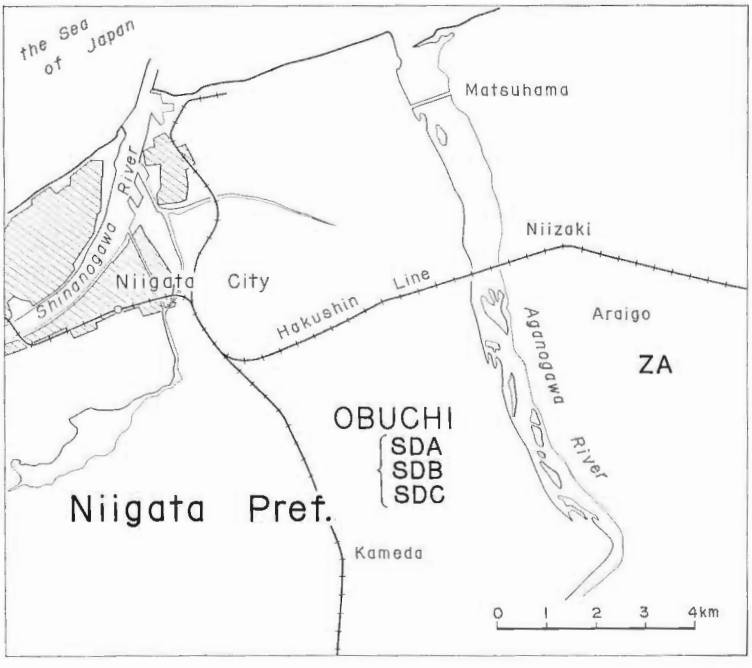
the Sea of Japan
Matsuhama
Shinanogawa River
Niigata City
Niizaki
Hakushin Line
Araigo
ZA
Aganogawa River
OBUCHI
SDA
SDB
SDC
Niigata Pref.
Kameda
0 1 2 3 4km

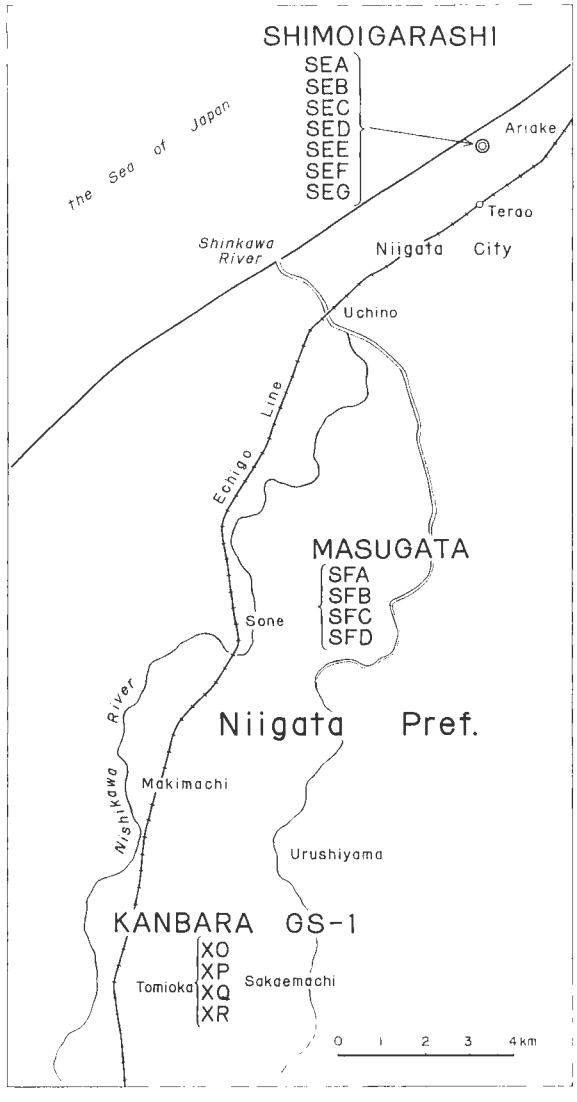
SHIMOIGARASHI
SEA
SEB
SEC
SED
SEE
SEF
SEG
the Sea of Japan
Ariake
Terao
Shinkawa River
Niigata City
Uchino
Echigo Line
MASUGATA
SFA
SFB
SFC
SFD
Sone
Niigata Pref.
Nishikawa River
Makimachi
Urushiyama
KANBARA GS-1
XO
XP
XQ
XR
Tomioka
Sakaemachi
0 1 2 3 4km

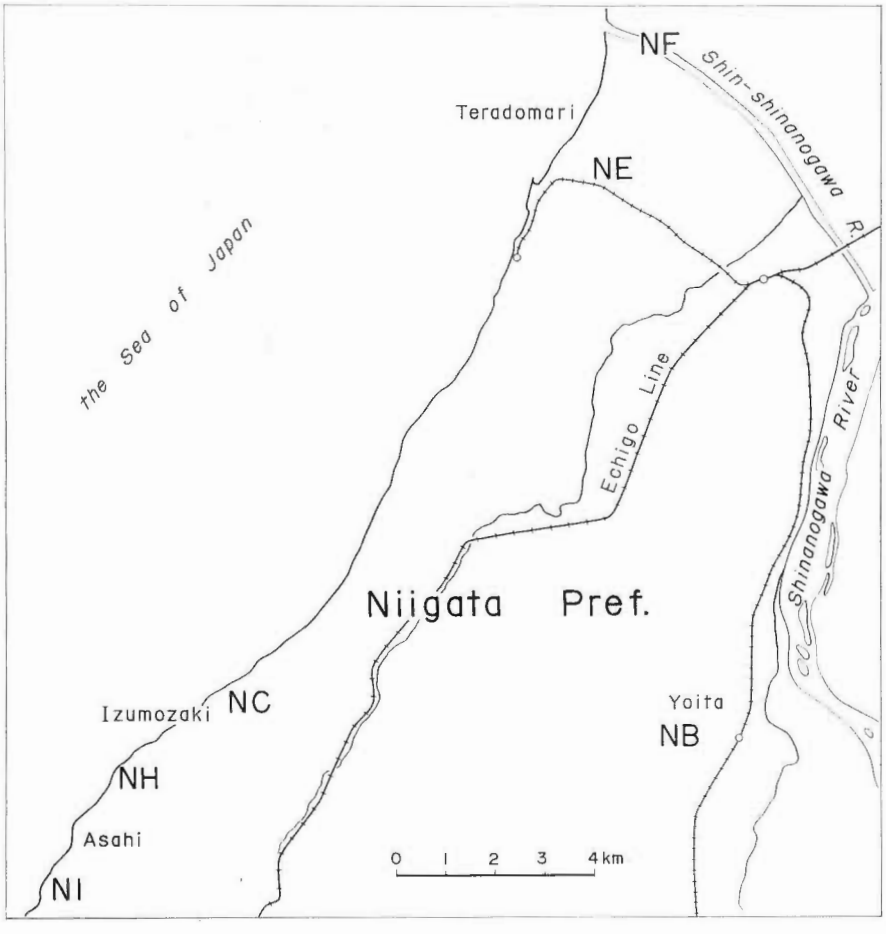
NF
Shin-shinanogawa R.
Teradomari
NE
the Sea of Japan
Echigo Line
Shinanogawa River
Niigata Pref.
Izumozaki
NC
Yoita
NB
NH
Asahi
NI
0 1 2 3 4km

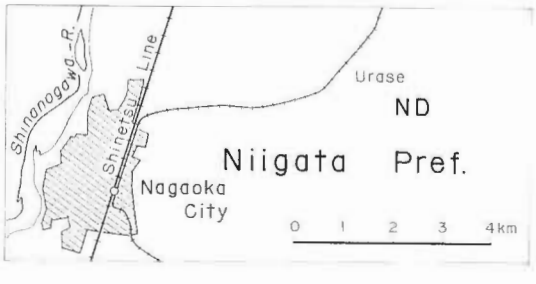
Shinanogawa R.
Shinetsu Line
Urase
ND
Niigata Pref.
Nagaoka City
0 1 2 3 4km

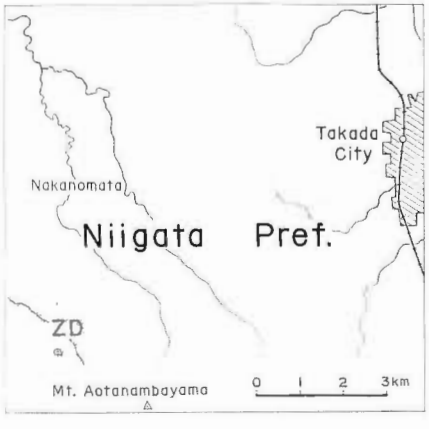
Takada City
Nakanomata
Niigata Pref.
ZD
Mt. Aotanambayama
0 1 2 3km

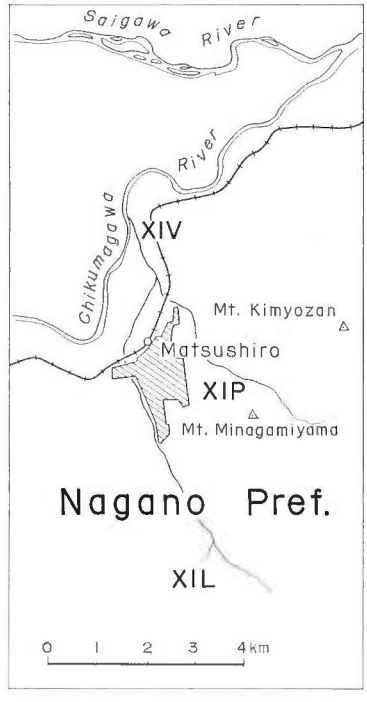
Saigawa River
Chikumagawa River
XIV
Mt. Kimyozan
Matsushiro
XIP
Mt. Minagamiyama
Nagano Pref.
XIL
0 1 2 3 4km

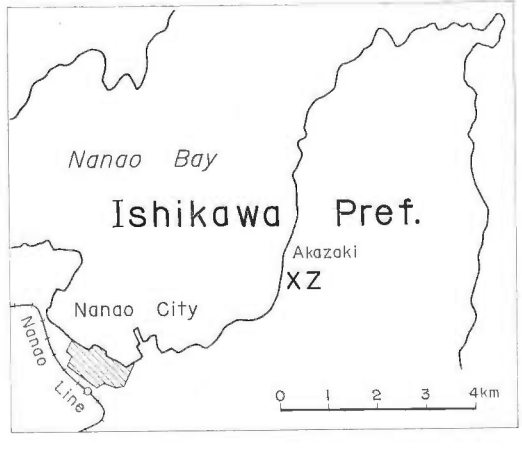
Nanao Bay
Ishikawa Pref.
Akazaki
XZ
Nanao City
Nanao Line
0 1 2 3 4km

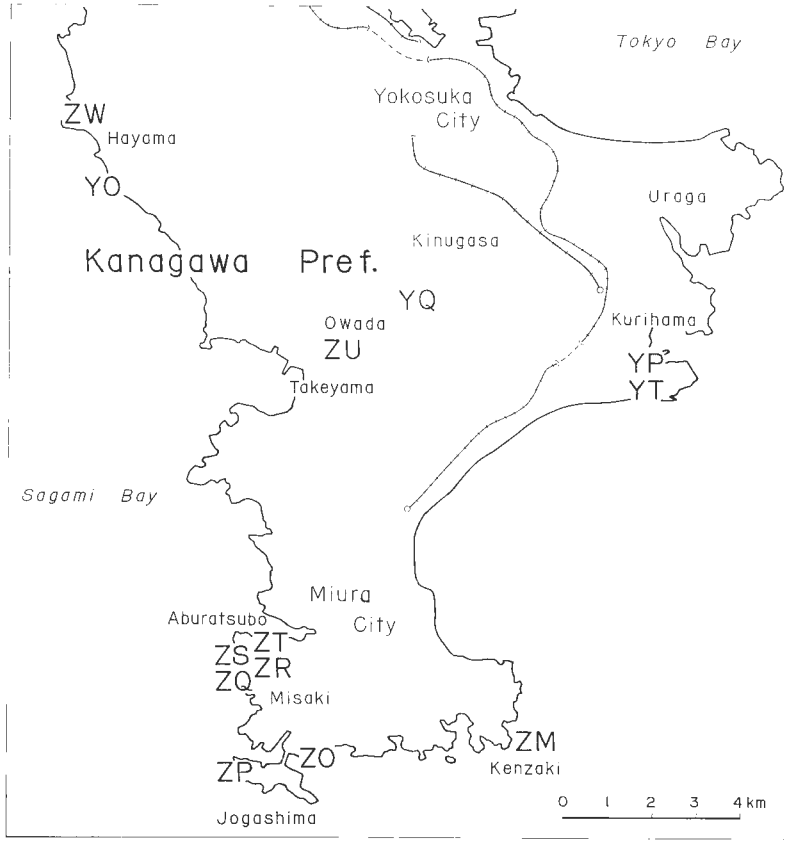
Tokyo Bay
Yokosuka City
ZW
Hayama
YO
Kanagawa Pref.
Kinugasa
YQ
Owada
ZU
Takeyama
Uraga
Kurihama
YP
YT
Sagami Bay
Miura City
Aburatsubo
ZS
ZT
ZQ
ZR
Misaki
ZM
Kenzaki
ZP
ZO
Jogashima
0 1 2 3 4km

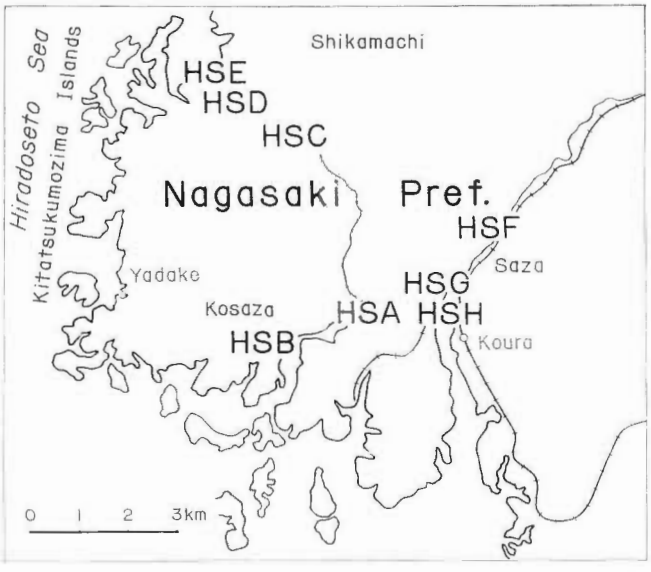
Hiradoseto Sea
Kitatsukumozima Islands
Shikamachi
HSE
HSD
HSC
Nagasaki Pref.
HSF
Saza
Yadake
HSG
Kosaza
HSA HSH
HSB
Koura
0 1 2 3km

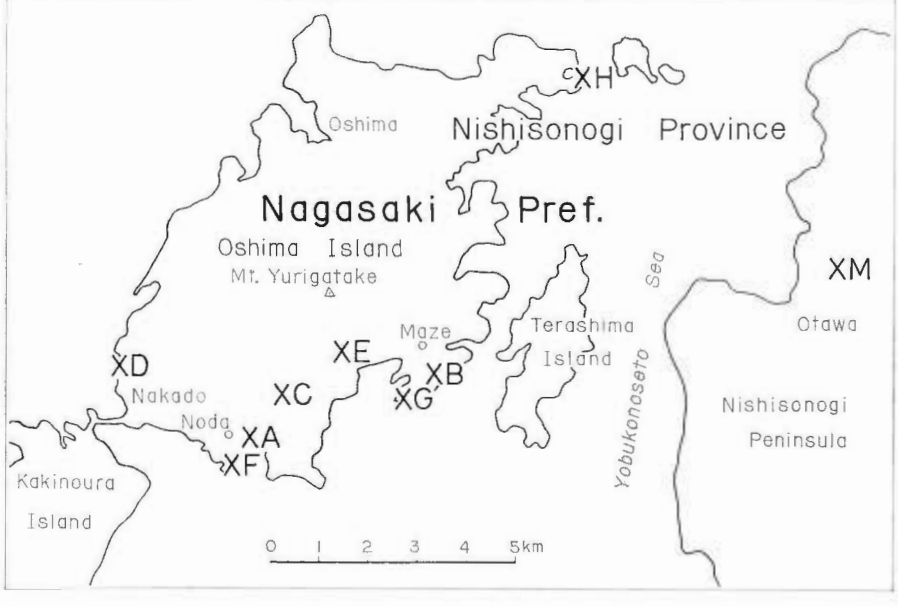
XH
Oshima
Nishisonogi Province
Nagasaki Pref.
Oshima Island
Mt. Yurigatake
Sea
XM
Otawa
Maze
Terashima Island
XE
XB
XD
Nakado
XC
XG
Noda
XA
XF
Yobukonoseto
Nishisonogi Peninsula
Kakinoura Island
0 1 2 3 4 5km

Appendix: Description of pyroclastic and volcanic rocks

1. JB(S13): This specimen was collected from liparite or liparitic tuff beds in Taki coal bearing formation, the base bed of Yunagaya group in the Joban coal field. The ground-mass is wholly glassy, and the phenocrysts consist of quartz, orthoclase, and biotite. The phenocrysts occupy about 10% of the observed area, and range between 0.5 and 1.0 mm in size.
2. SAB(S21): This is collected at a depth of 994 m of Nishime-oki exploratory well, seated in lower Tentokuji formation. In microscopic observation, most are amorphous matrix, with pumices of quartz and feldspar, less than 0.05mm in size.
3. SAC(S22): This was collected from a depth of 1506 m of Nishime-oki well. Stratigraphically it belongs to upper Funakawa formation. It is quite similar to SAB(S21) in petrofabric.
4. SAD(S23): This was collected from 1811 m deep, Funakawa formation of Nishime-oki well. It is whitish grey, acidic tuff. Pumice size is a little bigger than SAB(S21) and SAC(S23). The matrix exhibits lamination structure, partly amorphous and partly microcrystalline. The pumices consist of angular quartz, feldspar, and biotite.
5. NL(S35): This is called Nampeizawa tuff, found in Funakawa formation. It is acidic, white, medium grained tuff. Most parts of the ground-mass are amorphous. The pumice content is a little, consists of quartz, orthoclase, and a little augite.
6. NG(S44): This is also found in the upper part of Teradomari formation, known as Hozumi tuff. It is medium grained pumice tuff. The pumices occupy about 30% in area, and consist of quartz and feldspar, from 0.2 to 0.1 mm in size. The matrix is amorphous, and exhibits somewhat lamination structure.
7. NH(S45): This is known as Katsumi tuff, seated in the upper part of Teradomari formation. It is white-coloured, rather fine grained acidic tuff. The phenocrysts, less than 0.5 mm in size, include quartz, orthoclase and plagioclase. Most of the phenocrysts are granular. The ground-mass is mostly amorphous, and partly changes to sericite.
8. NI(S46): This is stratigraphically found between Shiiya and Teradomari formations and known as Gomoto or Betsuyama tuff. It contains coarse grained pumice, which consists of feldspar and quartz, 1.0 to 2.0 mm in size. The matrix, 20% in area are amorphous.
9. SDB(S49): Acidic tuff from a depth of 2485 m of Obuchi exploratory well. It belongs to Shiiya formation. It is white, fine grained pumice tuff, consists of mostly quartz and feldspar.
10. SFC(S60): This was collected from Nanatani formation of Masugata exploratory well at a depth of 4510 m. In this case, the Nanatani formation consists of mostly greenish grey or whitish grey liparite or liparitic tuff for several hundreds meters in thickness. This specimen is whitish grey liparite, which contains much plagioclase.
11. SFD(S61): This was collected from so-called Green Tuff beds, Tsugawa formation of Masugata well at a depth of 5000 m. This rock of Tsugawa

formation consists of altered basalt, basaltic tuff, of tuff breccia. This specimen is rather andesitic including orthoclase.

12. XO(S66) : This was collected from Nishiyama formation of Kambara GS-1 exploratory well at a depth of 2097 m. It is white, liparitic tuff. The ground-mass is amorphous, and contains fragments of quartz and zeolitized feldspar. The size of the fragments is approximately 0.1 mm or less.
13. XP(S67) : This was collected from Nishiyama formation of Kambara GS-1 well, too. It is hornblende andesite bearing biotite. The size of phenocrysts is from 3 to 5 mm. The ground-mass is microcrystalline.
14. XIN(S70) : This is known as Kimyozan tuff in Matsushiro, Nagano Prefecture. It is hypersthene-augite andesite. The size of phenocryst ranges between 0.2 and 2.0 mm, mostly about 1.0 mm. The ground-mass is microcrystalline. It was dated as 5.4 million years ago by K-Ar method.
15. XIP(S71) : This is the specimen from Minagami-yama in Matsushiro. Minagami-yama andesite is hornblende andesite, bearing augite and hypersthene. Minagami-yama mountain is lava dome, Pleistocene in age.
16. ZU(S83) : This is white acidic tuff from Hayama group. It contains ashes of quartz and feldspar in amorphous matrix.
17. XF(S90) : This was collected from Uridake formation of Nishisonogi formation. It is greenish grey acidic tuff. The matrix exhibits lamination structure with flakes of opaque minerals. The ashes are aggregates of quartz, orthoclase, and plagioclase, about 0.1 mm in size. In the specimen XF(S90), 4/5 length of the middle is tuff, and both ends are of common mudstone.
18. XM(S92) : Hypersthene olivine basalt from Nishisonogi, Nagasaki Prefecture. This basalt is a part of the basaltic rocks that develop over northwestern Kyushu. The specimen contains phenocrysts of plagioclase, olivine, and hypersthene, most of which are 0.5 to 1.0 mm in size. The ground-mass exhibits ophitic structure.

References

ATHY, L. F. (1930) : Geological aspects of abnormal reservoir pressures in Gulf Coast Louisiana, *Amer. Assoc. Petrol. Geol. Bull.*, vol. 14, p. 1—24.

BIRCH, F. (1966) : Compressibility; elastic constants, *Handbook of Physical Constants, rev. ed., Geol. Soc. Amer. Memoir 97*, p. 97—173.

BORG, I. et al. (1960) : Experimental deformation of St. Peter Sand: a study of cataclastic flow, *Geol. Soc. Amer. Memoir 79, Rock Deformation*, p. 133—192.

BORG, I. and HANDIN, J. (1966) : Experimental deformation of crystalline rocks, *Tectonophysics*, vol. 3, no. 4.

BRACE, W. F. (1964) : Brittle fracture of rocks, *State of stress in the Earth's crust*, Elsevier Co., p.111—180.

BRIDGMAN, P. W. (1952) : *Large plastic flow and fracture*, McGraw-Hill Book Co., New York.

BYERLEE, J. D. (1967) : Frictional characteristics of granite under high confining pressure, *Jour. Geophys. Res.*, vol. 72, p. 3639—3648.

BYERLEE, J. D. (1968) : Brittle-ductile transition in rocks, *Jour. Geophys. Res.*, vol. 73, p. 4741—4750.

CHINZEI, K. (1967) : An tentative plan for absolute age for Japanese Neogene System, *Jour. Geol. Soc. Japan*, vol. 73, p. 220—221.

DONATH, F. A. (1961) : Experimental study of shear failure in anisotropic rocks, *Bull. Geol. Soc. Amer.*, vol. 72, p. 985—990.

—— (1964) : Strength variation and deformational behavior in anisotropic rock, *State of stress in the Earth's crust*, Elsevier Co., p. 281—300.

—— and FAILL, R. T. (1963) : Ductile faulting in experimentally deformed rocks (Abstract), *Amer. Geophys. Union Trans.*, vol. 44, p. 102—103.

——, —— and TOBIN, D. G. (1971) : Deformation mode fields in experimentally deformed rock, *Geol. Soc. Amer. Bull.*, vol. 82, p. 1441—1462.

GRIGGS, D. T. (1942) : Strength and plasticity, *Handbook of Physical Constants*, *Geol. Soc. Amer.*, p. 107—130.

—— and HANDIN, J. (1960) : Observation on fracture and a hypothesis of earthquakes, *Geol. Soc. Amer. Memoir 79*, *Rock Deformation*, p. 347—364.

HANDIN, J. and HAGER, R. V., Jr. (1957) : Experimental deformation of sedimentary rocks under confininig pressure: Tests at room temperature, *Amer. Assoc. Petrol. Geol. Bull.*, vol. 41, p. 1—50.

—— and —— (1958) : Experimental deformation of sedimentary rocks under confining pressure: Tests at high temperature, *Amer. Assoc. Petrol. Geol. Bull.*, vol. 42, p. 2892—2934.

——, —— and FRIEDMAN, M. (1963) : Experimental deformation of sedimentary rocks under confining pressure: pore pressure tests, *Amer. Assoc. Petrol. Geol. Bull.*, vol. 47, p. 717—755.

—— (1966) : Strength and ductility, *Handbook of physical constants, rev. ed., Geol. Soc. Amer. Memoir 97*, p. 223—289.

—— (1969) : On the Coulomb-Mohr failure criterion, *Jour. Geophy. Res.*, vol. 74, p. 5343—5350.

HEARD, H. C. (1960) : Transition from brittle fracture to ductile flow in Solenhofen limestone as a function of temperature, confining pressure, and interstitial fluid pressure, *Geol. Soc. Amer., Memoir 79*, *Rock Deformation*, p. 196—226.

—— (1963) : Effect of large changes in strain rate in the experimental deformation of Yule marble, *Jour. Geol.*, vol. 71, p. 162—195.

HOSHINO, K. (1965) : *Fracture system and natural gas occurrence in the Joban coal field*, Rept. Geol. Surv. Japan, no. 210.

—— (1963) : Joint system of the Kushiro coal field, *Jour. Jap. Assoc. Petrol. Techn.*, vol. 28, p. 238—245.

—— (1967 a) : *Fracture system of Oshima Island, Kyushu: a study of jointing in brittle sedimentary rocks*, Rept. Geol. Surv. Japan, no. 222.

—— (1967 b) : Mechanical properties of some Japanese sedimentary rocks under confining pressure (1), *Applied Geology*, vol. 8, no. 3, p. 151—164.

—— and KOIDE, H. (1970 a) : Process of deformation of the sedimentary rocks, *Proc. of the 2nd Cong. of International Society for Rock Mechanics*, Beograd.

HOSHINO, K. and KOIDE, H. (1970 b) : Process of yieldings and the macroscopic fractures in the rocks, *Rock Mechanics in Japan*, vol. 1, p. 41—43.

HUBBERT, M. K. (1959) : Mechanics of fluid-filled porous solids and its application to overthrust faulting, *Bull. Geol. Soc. Amer.*, vol. 70, p. 115—166.

IKEBE, Y. et al. (1966) : Tertiary formations and hydrocarbon deposits in northeast Japan, *Memorial papers of Prof. Matsushita*, Kyoto, p. 191—202.

KOIDE, H. (1971) : Fractures aligned en échelon and fracture patterns, *Soc. Mining Geol. Japan*, Spec. Issue 3, p. 107—114.

——— and HOSHINO, K. (1967) : Development of microfractures in experimentally deformed rocks (preliminary report), *Jour. Seis. Soc. Japan*, vol. 20, p. 85—97.

———, ——— and NAGUMO, S. (1967) : Process of fracturing of rocks under triaxial compression, *Proc. of the 2nd Symposium on Rock Mechanics*, Japan, p. 51—56.

———, ——— and ——— (1970) : Microscopic mechanism of the development of rock failure, *Rock Mechanics in Japan*, vol. 1, p. 62—64.

———, ———, INAMI, K., IWAMURA, S. and MITSUI, S. (1971) : Variation of mechanical properties of Tertiary sedimentary rocks in Japan, *Jour. Geol. Soc. Japan*, vol. 77, p. 327—334.

MATSUDA, T., NAKAMURA, K. and SUGIMURA, A. (1967) : Late Cenozoic orogeny in Japan, *Tectonophysics*, vol. 4, p. 349—366.

MATSUSHIMA, S. (1960) : On the flow and fracture of igneous rocks, *Disaster Prevent. Res. Inst., Kyoto Univ., Bull.*, no. 36, p. 1—9.

MATSUZAWA, A. (1961 and 1962) : Density of the sedimentary rocks and geologic structure, *Butsuri Tanko*, vol. 14, p. 195—203, and vol. 15, p. 1—13.

MIYAZAKI, H. (1965) : Study on gravitational compaction of muddy sediments, in Akita oil field, *Jour. Geol. Soc. Japan*, vol. 71, p. 401—412.

MOGI, K. (1964) : Deformation and fracture of rocks under confining pressure (1), compression tests on dry sample, *Bull. Earthquake Res. Inst.*, vol. 43, p. 491—514.

——— (1965) : Deformation and fracture of rocks under confining pressure (2), elasticity and plasticity of some rocks., *Bull. Earthquake Res. Inst.*, vol. 43, p. 349—379.

——— (1966) : Pressure dependence of rock strength and transition from brittle fracture to ductile flow., *Bull. Earthquake Res. Inst.*, vol. 44, p. 215—232.

NAGUMO, S. and HOSHINO, K. (1967) : Occurrence of micro-fracturing shocks during deformation with a special reference to activity of earthquake swarms, *Bull., Earthquake Res. Inst.*, vol. 45, p. 1295—1311.

PATERSON, M. S.(1958) : Experimental deformation and faulting in wombeyan marble, *Geol. Soc. Amer. Bull.*, vol. 69, p. 465—476.

PATERSON, M. S. and WEISS, L. E. (1968 a) : Experimental deformation and folding in phyllite, *Geol. Soc. Amer. Bull.*, vol. 77, p. 343—373.

——— and ——— (1968 b) : Folding and boudinage of quartz-rich layers in experimentally deformed phyllite, *Geol. Soc. Amer. Bull.*, vol. 79, p. 795—812.

ROBERTSON, E. C. (1955) : Experimental study of the strength of rocks, *Bull. Geol. Soc. Amer.*, vol. 66, p. 1275—1314.

SERDENGECTI, S. and BOOZER, G. D. (1961): The effects of strain rate and temperature on the behavior of rocks subjected to triaxial compression, *the 4th Symposium on Rock Mechanics, Penn. State Univ.*, p. 83—97.

(Manuscript received September 1, 1970, rearranged August 14, 1971)

日本産第三系堆積岩の高圧物性

星野一男・小出　仁・井波和夫・岩村茂男・三井　忍

要　旨

高圧下における岩石の力学的性質の実験的研究は多数おこなわれている。それらのデータは J. HANDIN により「Handbook of Physical Constants」改訂版中にまとめられている。日本においても高圧下の岩石の力学的性質の実験的研究がさかんになっているが，日本産岩石の力学的性質のデータはまだ十分ではない。各種岩石の力学的性質に関するデータを系統的に集積することは，岩石力学の基礎資料として地質学や地球物理学に，また防災や土木工学・鉱山学への応用のためにも重要である。

地質調査所に岩石岩盤物性の研究グループが生まれたのは1962年であるが，1965年に高圧岩石変形試験機が装備されて以来，各種岩石の高圧物性に関するデータの集積につとめてきた。まず，第三系堆積岩の系統的な試料採取と実験を行ない，ようやく不満足ながらデータ集としてまとめることができた。第三系堆積岩を最初に選んだのは，力学的性質の変化が大きく，地域・年代によってまったく異なるためである。堆積岩の年代・地域による高圧物性の相異とその原因の究明は，地質学的にも非常に興味のある問題である。第三系以後の堆積岩は軟弱で変化が大きいために，建造物の基礎や山くずれ・地盤沈下・斜面の安定・地下構造物の維持等，防災面・工学面でも問題になることが多い。

実験した岩石は，泥質岩51，砂質岩31，火山砕屑岩12，火山岩 6 で（Table 3），釧路・常磐・三浦半島・秋田・新潟等の各第三系堆積盆地から系統的に採取した。当実験室内では岩石試料ごとに便宜的な記号（XC, SEG等）を用いている。この報告にも便宜上この記号を使用した。同記号の岩石試料はなるべく均質な岩石のブロックから作製したものである。Table 2 に岩石試料の記号・岩種・地層・時代・採取場所・孔げき率・密度・弾性波速度を記した。その年代的な関係は Table 1 に示した。岩石試料のうち37は試錐コアで，他は地表の露頭から採取した。

実験装置は圧力容器・プレス・側圧発生装置および測定装置からなる。岩石試料は長さ 39.0mm，直径 19.5mmφ の円柱状で，1/500 の精度で仕上げる。実験時は，円柱状試料の上下にあて板・ピストン・アンビルをとりつけ，試料周辺をうすい銅チューブでおおい，ピストン・アンビルと銅チューブの間にOリングを入れて試料内に油が流入しないようにする。これらを，圧力容器中にそう入して，ニューマチック・ポンプあるいはハンドポンプにより圧力容器内に圧入された灯油によって，銅チューブの外側から側圧を加える。側圧の大きさはハイゼ圧力計によって測定した。圧力の変動は 1 %以内に押えた。軸圧はピストンを通して試料に加えられる。軸圧を加える速度はほぼ一定であるが，試料の変形速度はその抵抗の大きさによって多少異なる。通常の変形速度は 10^{-4}/sec 程度であるが，ギアによって速さを変えることもできる。ピストンの変位からピストンの変形量を補正して，試料の

変形量をもとめた。圧力容器の外に出ているピストンの頭部にかかる荷重を測定し，試料の断面積で割って軸圧とした。断面積の変形による変化は，試料が差圧により体積変化をおこさないと仮定してもとめた。

Table 4 に実験した全試料の試料記号・試料番号・側圧・静水圧による軸方向の縮み・1％・2％・5％および10％歪み時の差応力の大きさ，最大強度・延性度（最大強度に達した時の歪み）・最大歪み・残留歪み・変形速度・破壊形態・剪断面角・変形様式を記載した。同一岩石ごとに応力—歪み線図とモーアの包絡線図を付した（Figure 10～219）。モーアの応力円は最大強度によって描いたが，最大強度を知ることができない試料は10％，5％，2％歪み時の差応力をもとにして応力円を描いた。

堆積岩の力学的性質はきわめて多様で，いろいろなファクターに影響されていると思われる。実験結果から，強度・側圧・変形様式・剪断面角・延性度・破壊形態・孔げき率・粒度・静水圧による縮み・試料の採取深度・弾性波速度・地質年代・層準・地質環境等の関係を調べた。

変形様式は応力—歪み線図の形から，極ぜい性・ぜい性・中間性・延性・粘延性に分類した。強度をたて軸，側圧をよこ軸にとって強度—側圧関係図をつくると，ぜい性（極ぜい性）・延性（中間性）・粘延性の領域は簡単な曲線でわけられる。この境界線は岩質によって異なる。生じた巨視的割れ目の角度から，割れ目にかかった垂直応力と剪断応力をもとめて図にプロットすると，ぜい性領域と延性領域とに簡単な境界線でわけられる。剪断面角および延性度が増大すると，割れ目面に対する剪断応力と垂直応力の比は減少する（Eq. 5.4, 5.5）。

破壊形態はくさび状・単一剪断割れ目・網目状・流動（巨視的割れ目なし）に分類した。破壊形態はほぼ変形様式にともなって変化し，極ぜい性・ぜい性ではくさび状ないし単一剪断が多く，延性・粘延性ではほとんど流動である。中間性では，砂質岩と泥質岩では破壊形態は延性に近く，火山砕屑岩ではぜい性に近い。変形様式は延性度にともなって変化するが，破壊形態と延性度との関係はより複雑である。破壊形態の変化が連続的で，本質的な変化ではないためであろう。

強度は圧密による孔げき率の減少にともなって増大する。しかし，火山砕屑岩では粒度の影響が見られる。変形様式もまた孔げき率にともなって変化する。やわらかい岩石では高側圧下できわめて低い差圧でも流動的になることがある。これを粘延性と名づけた。延性から粘延性に変化する側圧の大きさは，試料の採取深度とともに増大する。転移する側圧は試料に加わった最大岩圧を表わすと思われる。圧密のために，堆積岩の年代が古くなると強度が増し，ぜい性的になる。泥質岩がもっとも年代による強化が著しく，砂質岩でも変化が大きいが，火山砕屑岩ではやや不明りょうである。

調べられた主な6つの地域中で，常磐および三浦半島地域の岩石は他より強度が低く，延性的である。延性—粘延性転移側圧の大きさや年代による強化の程度をくらべても，常磐および三浦半島の岩石は，他の地域の同年代の岩石と比較して，高い圧力をうけていないことがわかる。常磐地域では，後期新生代を通じて浅い海に静かな堆積がつづけられたためであろう。構造的には相当変形をうけたと思われる三浦半島地域をのぞいては，実験結果は地質環境とよく一致している。

PLATES
AND
EXPLANATIONS

(With 23 Plates)

All specimens are cylinders of about 39.0 mm in length and 19.5 mm in diameter befoe deformation.

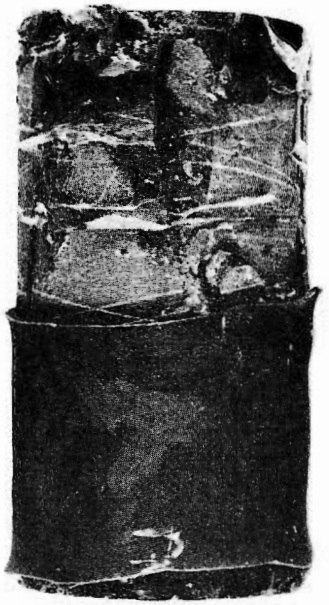

KSC 3, deformed at 1 kg/cm² covered with the copper jacket in the lower part. Wedge type failure.

KSC 9, deformed at 500 kg/cm². It seems there is a wedging effect with the spacer at the right of the lower side, which made the angle of fracture larger near of the lower end. However, in the middle, the angle is independent from the effect of the wedging.

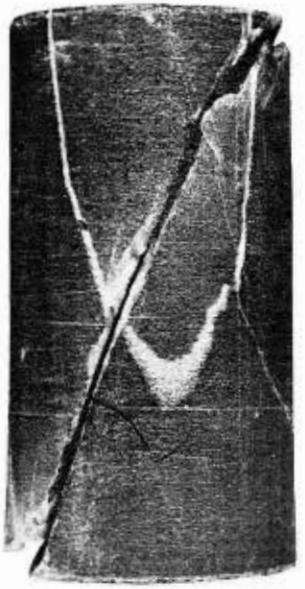

KSC 10, deformed at 1000 kg/cm². The single shear fracture has a little larger angle than KSC 9.

KSC 1, deformed at 1500 kg/cm². A sharp single shear fracture. Note that "crushed zone" along the shear fracture is wide.

Plate 1 Shakubetsu shale, KSC(S3).

JT 5, deformed at 1 kg/cm^2. A good example of wedge type failure.

JT 3,deformed at 100kg/cm^2. A transitional pattern from wedge type to single shear type failure.

JT 4,deformed at 200kg/cm^2. A single shear fracture. An effect of wedging at one end of specimen is observed. However, for the other end there seems no effect of the wedging.

JT 2,deformed at 300kg/cm^2. A single shear fracture, with "crushed zone" of about 1 mm wide.

Plate 2 Shirasaka shale, JT(S14).

ZW 1, deformed at 1 kg/cm². Wedge type failure.

ZW 2, deformed at 500 kg/cm². A sharp single shear fracture.

ZW 3, deformed at 1000 kg/cm². Microscopic fractures are formed in two white bands. These white bands are termed "deformation bands" (HOSHINO and KOIDE, 1970a).

ZW 4, deformed at 1500 kg/cm². No visible fracture. The specimen bulges in upper half.

Plate 3 Hayama group siltstone, ZW(S84).

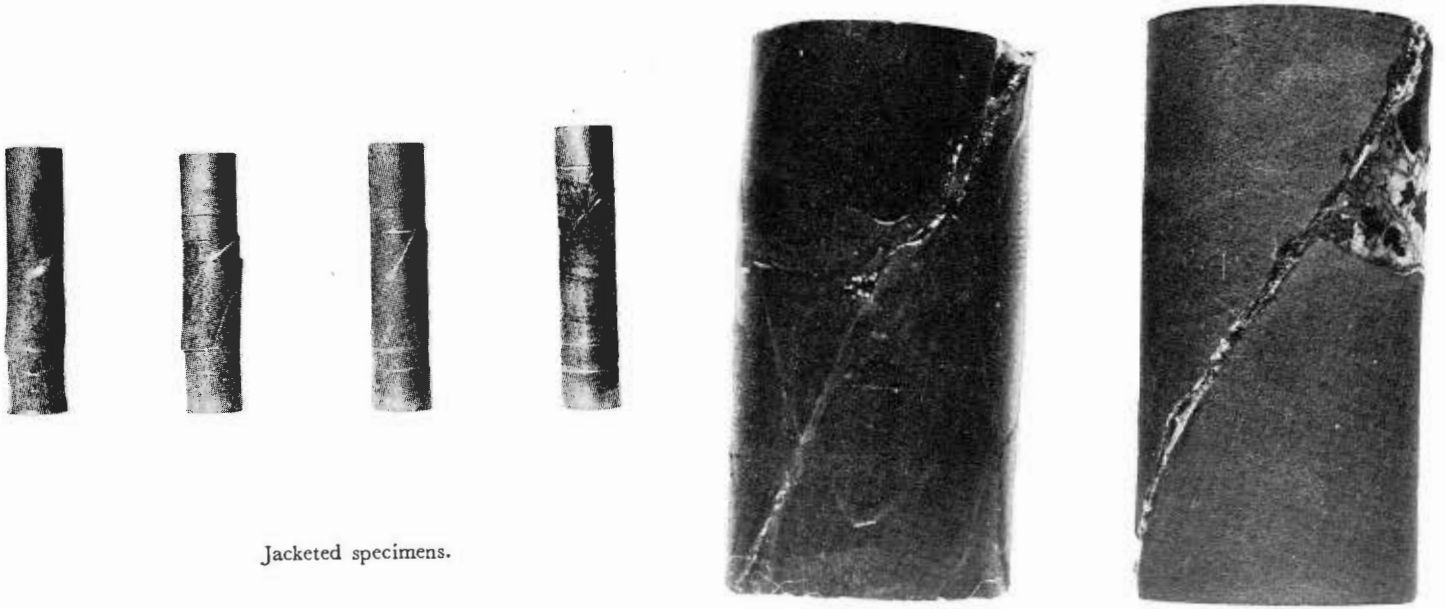

Jacketed specimens.

XIL 10, deformed at 1000 kg/cm². There is a comparatively strong line of shear fracture, accompanied by a lot of shear and extension fractures.
XIL 7, deformed at 2000 kg/cm². A sharp single shear fracture. Every specimen was cemented with a paste in order to prevent from separating in pieces after the experiments.

Plate 4 Bessho shale, XIL(S69).

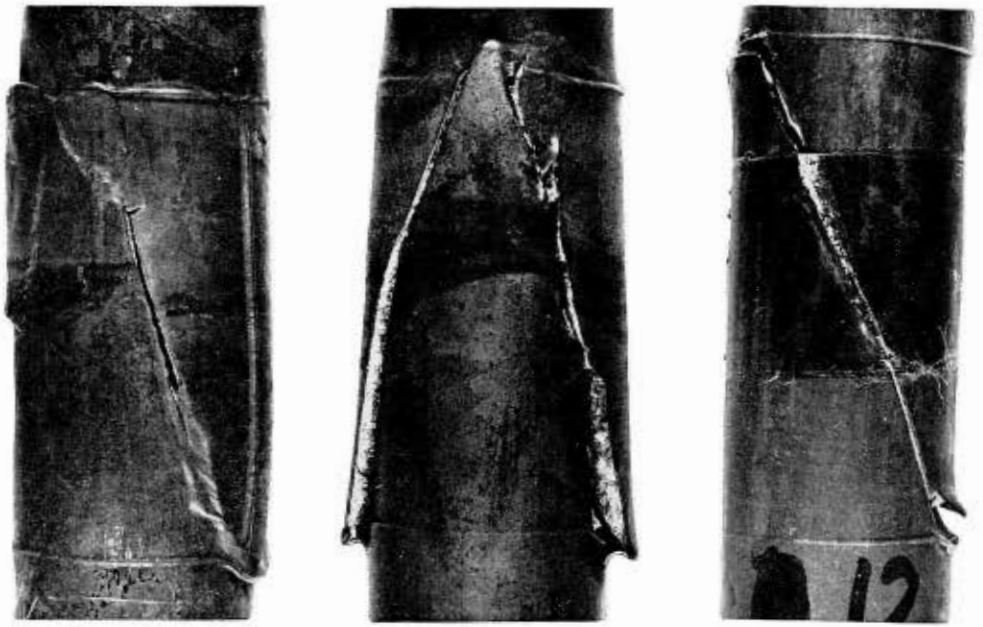

NJ 3, deformed at 500 kg/cm². A single shear fracture of extremely small angle (16°), and extension fractures at the one end.

NJ 6, deformed at 1000 kg/cm². Two strong shear fractures. The both have small angle of about 16 degrees.

NJ 12, deformed at 2000 kg/cm². A sharp single shear fracture.

Plate 5 Onnagawa shale (1), NJ(S33). All are jacket-unremoved specimens.

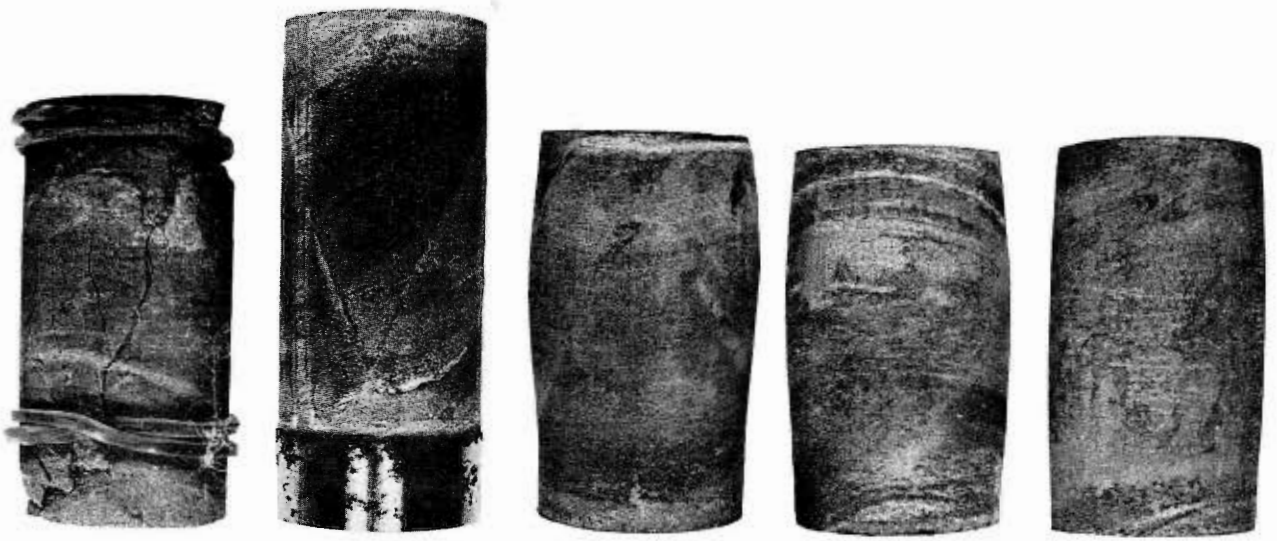

SBC 1, deformed at 1 kg/cm². Wedge type failure consists of shear and extension fractures.

SBC 2, deformed at 200 kg/cm². Conjugate shear fractures.

SBC 3, deformed at 500 kg/cm². Bulge and network deformation bands in the half part.

SBC 4, deformed at 1000 kg/cm². No experimentally formed fracture. There are some irregular cracks that might be caused by dehydration after the experiment.

SBC 5, deformed at 1500 kg/cm². No experimentally-derived fracture, too, but the cracks of dehydration mechanism after the experiment.

Plate 6 Onnagawa shale (2), SBC(S26).

ZK_a 2, deformed at 500 kg/cm². A clear cut single shear fracture.

ZK_a 4, deformed at 1000 kg/cm². Shear fractures along both boundaries of deformation band.

ZK_a 5, deformed at 2500 kg/cm². Bulging without fracture.

ZK_b 1, deformed at 1 kg/cm², containing tuffaceous content in the half part. Shear and extension fractures.

ZK_b 3, deformed at 1500 kg/cm², tuffaceous content in the half. A strong single shear. In the tuffaceous part, there are network of deformation bands. Note that the rock becomes white along the strong shear fracture, indicating deformation band.

ZK_b 6, deformed at 2000 kg/cm², tuffaceous content in the half. There is a bulge and network pattern in tuffaceous part with apparently open fractures, which exhibit en échelon arrangement.

Plate 7 Aosawa shale, ZK(S36).

NF 1, deformed at 1 kg/cm². Wedge type failure.

NF 5, deformed at 1000 kg/cm². There is bulge and network pattern of deformation bands in the part including fine-grained pumices.

NF 6, deformed at 1500 kg/cm². There is a faintly observed network pattern in the part including pumice, and a bulge in the middle.

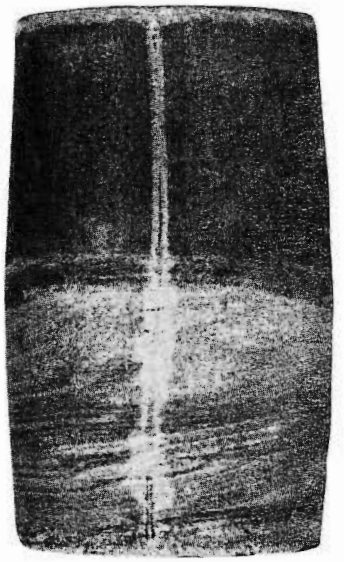

NF 7, deformed at 2000 kg/cm². There is no fracture in either shale or the part including pumice.

Plate 8 Teradomari formation shale, NF(S38).

ZM 1, deformed at 1 kg/cm². The fractures are those that are possibly resulted by connecting extension fractures. Near the end of the specimen there are seemingly an effect of end-wedging.

ZM 6, deformed at 20 kg/cm². There are extension-like fracture on one side and shear-like fractures that connect with the extension-like fracture in the middle.

ZT 1, deformed at 1 kg/cm². A typical extension fracture develops in finer-grained part, while in coarser-grained part, the fractures show shear fracture-like nature.

ZT 2, deformed at 1000 kg /cm². No fracture.

Plate 9 Misaki formation siltstones, ZM(S76) and ZT(S82).

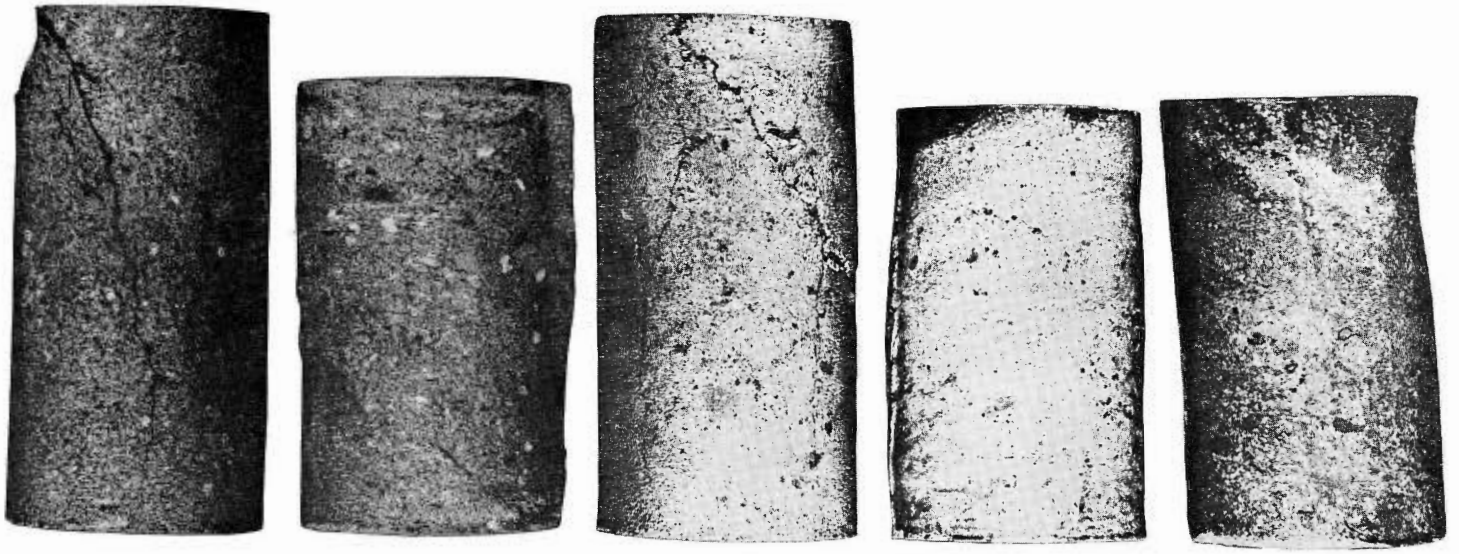

JM 3, deformed at 1 kg /cm². A shear fracture at a corner becomes into an extension fracture in the middle part of specimen.

JM 6, deformed at 50 kg /cm². No fracture.

YT 1, deformed at 1 kg /cm². Wedge type, combination of extension and shear fractures.

YT 5, deformed at 500 kg /cm².

YT 4, deformed at 1000 kg/cm². No fracture.

Plate 10 Numanouchi sandstone, JM(S8) and Ikego formation siltstone (2), YT(S75).

NK 10, deformed at 1 kg/cm². A strong fracture seems to be a kind of shear fracture. However, an extension-like fracture that extends from a curving point of the shear fracture might be very interesting for the understanding of fracturing mechanism of this specimen.

NK 2, deformed at 100 kg /cm². No fracture.

SEA 1, deformed at 1 kg /cm². The failure pattern at one end indicates end-wedging effect for the fracturing clearly.

SEA 2, deformed at 200 kg /cm². No fracture.

Plate 11 Tentokuji siltstone (1), NK(S34) and Haizume formation siltstone (1), SEA(S51).

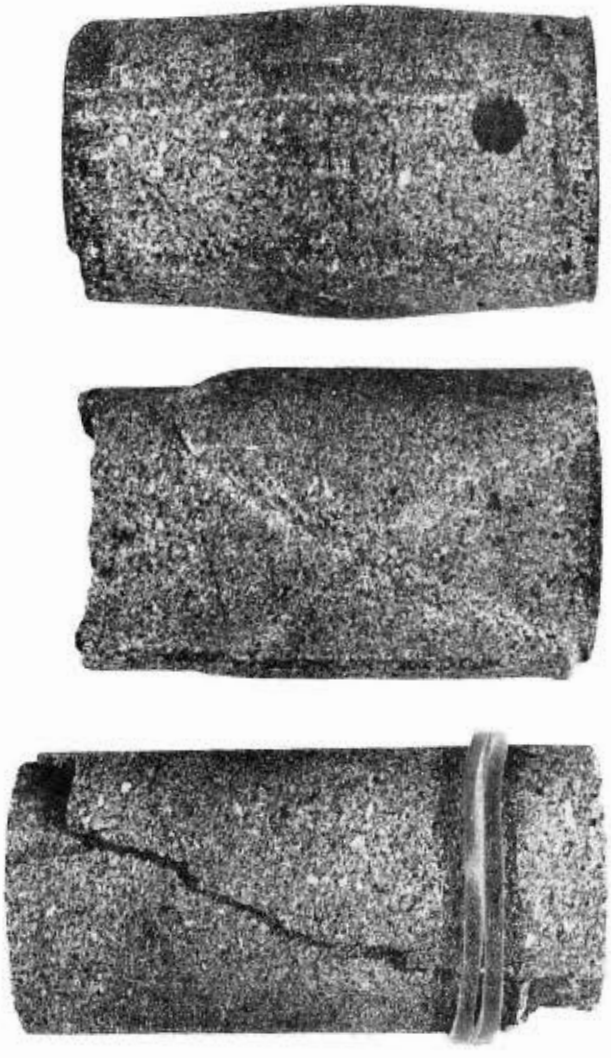

SED 1, deformed at 1 kg /cm². It looks like a shear fracture. An wedging effect at the ends and extension-like parts, however, indicate wedge failure type.

SED 2, deformed at 200 kg /cm². Conjugate deformation bands.

SED 3, deformed at 500 kg /cm². A bulge in the middle part.

Plate 12 Hamatsuda sandstone, SED(S54).

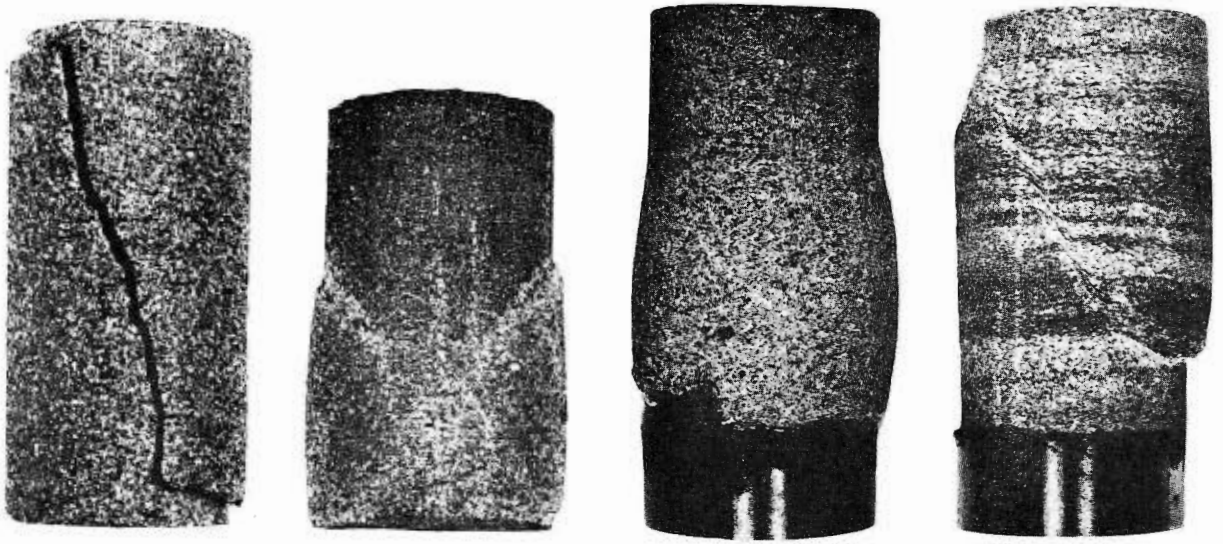

SEF 1, deformed at 1 kg/cm². Extension fracture.

SEF 2, deformed at 200 kg/cm². Conjugate deformation bands.

SEF 3, deformed at 500 kg /cm². No microscopic fracture. A bulge is observed in a half part.

SEG 3, deformed at 500 kg/cm². Thin layers are kinked in a deformation band.

Plate 13 Shiiya sandstones, SEF(S56) and SEG(S57).

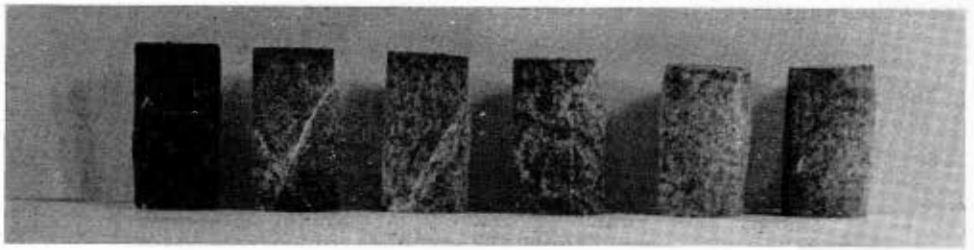

From left to right: deformed at 1(XC 6), 500(XC 1), 1000(XC 3), 1500(XC 4), 2000(XC 55), and 2500 kg/cm^2(XC 7). XC 6 showed wedge type failure and was cemented to prevent from separation. XC 1 and 3 show single shear type, and XC 4 network pattern. XC 55 and 7 show no-fracture type.

Plate 14 A Maze sandstone (3), XC(S87).

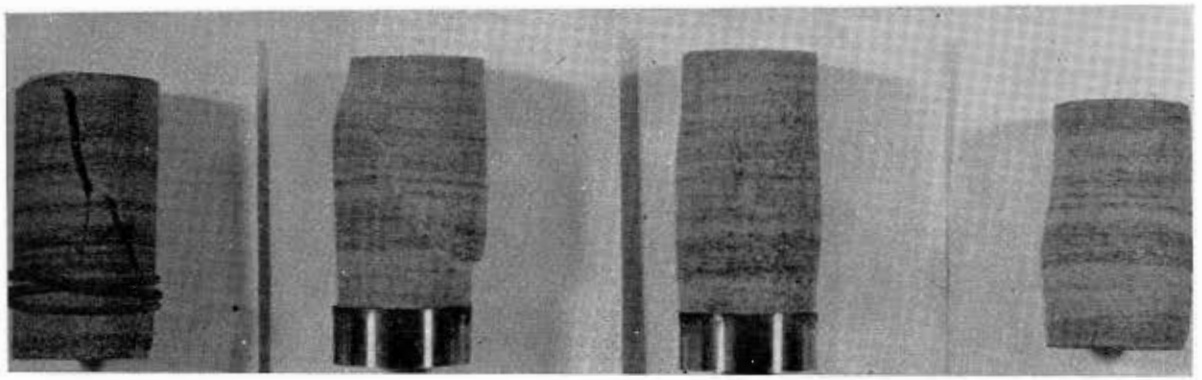

From left to right: deformed at 1(SEG 1), 500(SEG 3), 1000(SEG 4), and 2000 kg/cm^2 (SEG 6). SEG 1 shows shear-like fracture with an effect of wedging. SEG 3 shows single deformation band. SEG 4 and 6 show no-fracture failure, however, non-symmetric deformation of the specimens indicates development of ductile faulting.

Plate 14 B Shiiya sandstone, SEG(S57).

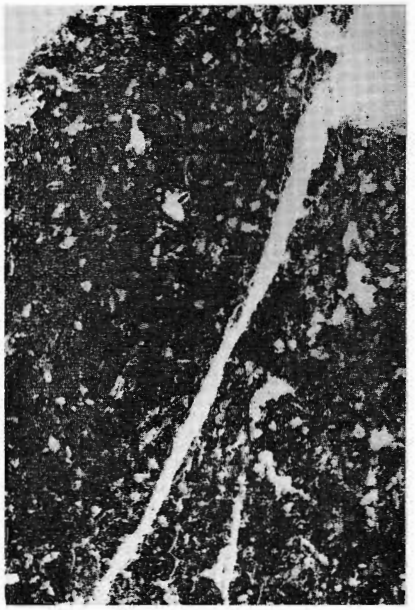

XC 26, deformed at 500kg/cm². The specimen was deformed up to 1.5% at strain rate 3.5×10^{-6}/sec. The deformational stage is similar to XC 1. A single shear fracture develops in the middle.

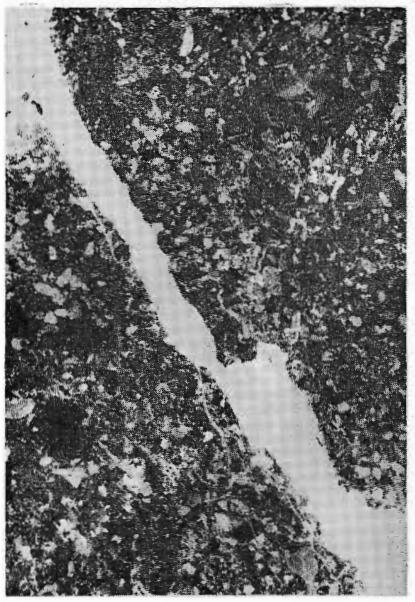

XC 9, deformed at 1000 kg/cm². This is deformed up to 2.5% at strain rate 2.8×10^{-5}/sec. The deformational stage is similar to XC 3. Also, a single shear fracture runs in the middle, accompanied with micro-fractures along the main fracture.

XC 4, deformed at 1500 kg/cm². The specimen is the same as shown in Plate 14A. Macroscopically, the specimen shows conjugate failure type. In microscopic feature,we see network pattern consists of a lots of microfractures.

Plate 15 Microscopic photographs of Maze sandstone, XC(S87).

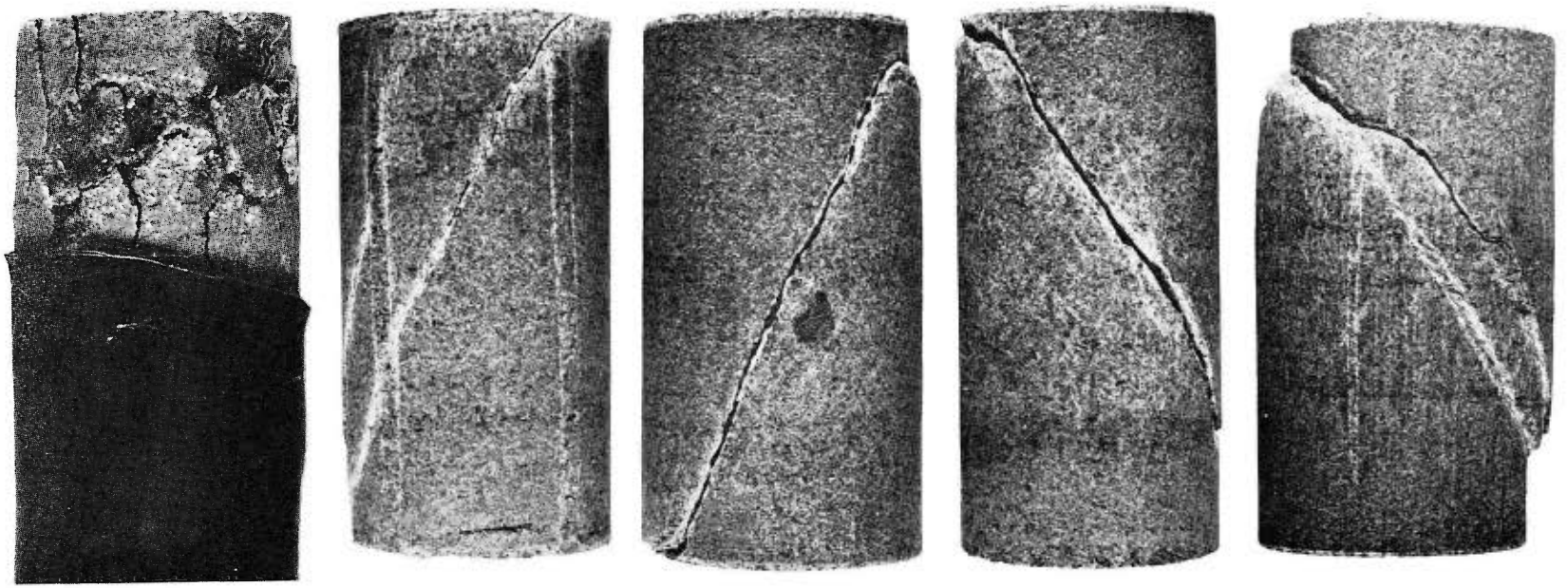

HSF 1, deformed at 1 kg/cm². Wedge type failure.

HSF 2, deformed at 500 kg /cm². A single shear fracture in the middle, and the other fracture with less angle on the side.

HSF 3, deformed at 1000 kg /cm². Very simple single shear fracture. However, notice that the colour turns white in the middle, which indicates the development of microscopic network deformation bands pattern inside the specimen.

HSF 4, deformed at 1500 kg /cm². Single shear fracture with network deformation bands inside the specimen.

HSF 5, deformed at 2000 kg /cm². Deformation bands and shear fractures.

Plate 16 Furukawa sandstone, Kishima group, HSF(S98).

HSA 3, deformed at 500 kg/cm². Conjugate deformation bands.

HSA 4, deformed at 1000 kg/cm². Conjugate deformation bands.

HSA 5, deformed at 1500 kg/cm². Conjugate deformation bands. One shear fracture occurs along a deformation band.

Plate 17 Ainoura formation sandstone, Sasebo group, HSA(S93).

SDC 1, deformed at 1kg/cm². Wedge type failure.

SDC 2, deformed at 200 kg /cm². Single deformation band.

SFB 1, deformed at 1 kg/cm². Wedge type failure.

SFB 2, deformed at 200 kg /cm². A single deformation band.

SFB 3, deformed at 500 kg /cm². No macroscopic fracture. It appears bulge in the middle.

Plate 18 Shiiya sandstone (1), SDC(S50) and Shiiya sandstone (4), SFB(S59).

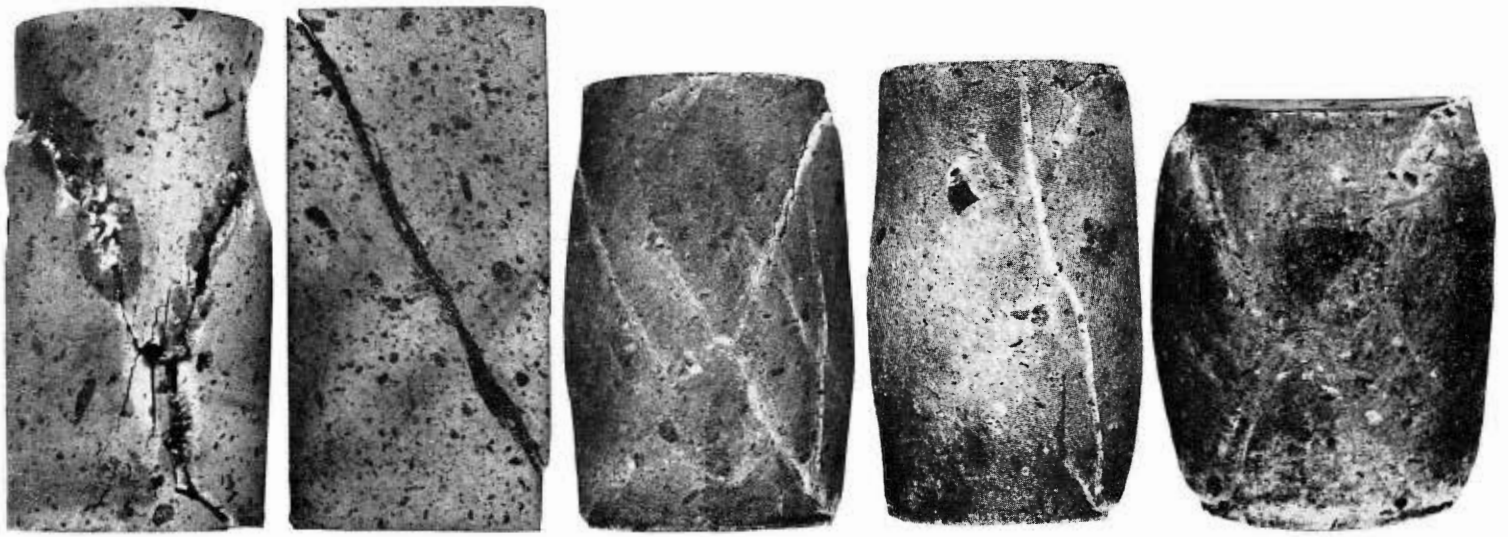

JB 1, deformed at 1 kg /cm². Wedge type failure.

JB 2, deformed at 500 kg /cm². A single shear fracture.

JB 3, deformed at 1000 kg/cm². Network pattern of shear fractures and deformation bands.

JB 4, deformed at 1500 kg/cm². Obscure deformation bands.

JB 5, deformed at 2000kg/cm². Conjugate deformation bands pattern with microscopic network pattern.

Plate 19 Taki formation liparite, JB(S13).

XM 3, deformed at 1 kg/cm². Wedge type failure.

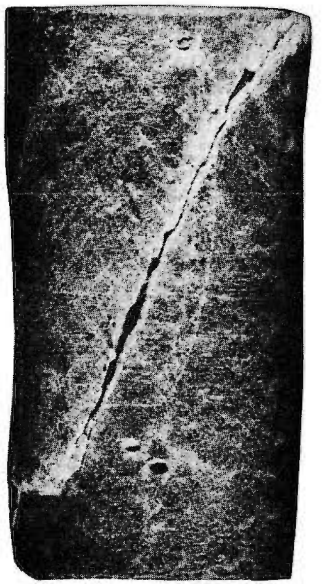

XM 5, deformed at 500 kg /cm². A single shear fracture. Network of deformation bands are observed on the surface of the specimen.

XM 6, deformed at 1000 kg /cm². Network failure pattern is clear than XM 5. One fracture is visible.

Plate 20 Ohtawa basalt, XM(S92).

NH 1, deformed at 1 kg/cm². Single shear fracture with a short extension fracture.

NH 2, deformed at 500 kg /cm². Non symmetric shape indicates that a deformation band will be developed soon, as NH 3.

NH 3, deformed at 1000 kg /cm². A bulge and deformation band in the middle.

NH 4, deformed at 1500 kg /cm². A weak deformation band is seen on the side.

NH 5, deformed at 2000 kg /cm². No macroscopic fracture.

Plate 21 Katsumi tuff, NH(S45).

XO 1, deformed at 1 kg/cm². Wedge type fracture. Combination of shear-like and extension fractures.

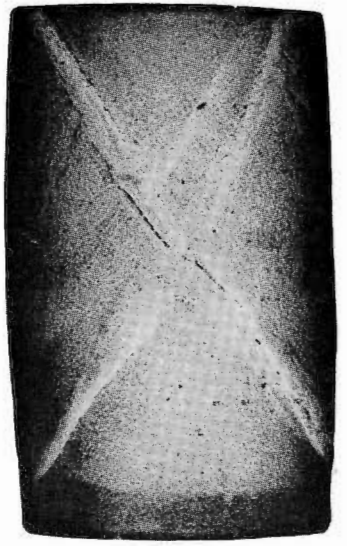

XO 2, deformed at 500 kg/cm². Network deformation band pattern. One fracture opens along a deformation band.

XO 3, deformed at 1000 kg /cm². No macroscopic fracture.

Plate 22 Nishiyama formation tuff, XO(S66).

ZU 1, deformed at 1 kg/cm². Wedge type fractures. Combination of shear-like and extension fractures.

ZU 2, deformed at 500kg/cm². A deformation band, in which fractures are arranged en échelons.

ZU 3, deformed at 1000 kg /cm². Network of deformation bands.

ZU 4, deformed at 1500 kg /cm². No macroscopic fractures.

Plate 23 Hayama group tuff, ZU(S83).

地質調査所報告は１報文について報告１冊を原則とし，その分類の便宜のために，次のようにアルファベットによる略号をつける。

A. 地質およびその基礎科学に関するもの
- a．地　質
- b．岩石・鉱物
- c．古生物
- d．火山・温泉
- e．地球物理
- f．地球化学

B. 応用地質に関するもの
- a．鉱　床
- b．石　炭
- c．石油・天然ガス
- d．地下水
- e．農林地質・土木地質
- f．物理探鉱・化学探鉱および試錐

C. そ の 他

D. 事業報告

As a general rule, each issue of the Report, Geological Survey of Japan will have one number, and for convenience's sake, the following classification according to the field of interest will be indicated on each Report.

A. Geological & allied sciences
- a. Geology
- b. Petrology and Mineralogy
- c. Paleontology
- d. Volcanology and Hot spring
- e. Geophysics
- f. Geochemistry

B. Applied geology
- a. Ore deposits
- b. Coal
- c. Petroleum and Natural gas
- d. Underground water
- e. Agricultural geology and Engineering geology
- f. Physical prospecting, Chemical prospecting and Boring

C. Miscellaneous

D. Annual Report of Progress

地 質 調 査 所 報 告

第 239 号

石原舜三：日本の主要モリブデン鉱床および関連する花崗岩質岩類，1971

第 240 号

岸　和男：石川県手取川扇状地における水収支の研究，1971

第 241 号

尾上　亨：宮崎県えびの市産の更新世植物群，1971

第 242 号

TANAKA, K. : Trace fossils from the Cretaceous flysch of the Ikushumbetsu area, Hokkaido, Japan, 1971

第 243 号

KAWADA, K. : Geology and petrology of the Nōhi rhyolites, with special reference to those along the Hida river, 1971

REPORT, GEOLOGICAL SURVEY OF JAPAN

No. 239

ISHIHARA, S. : Major molybdenum deposits and related granitic rocks in Japan, 1971 (in Japanese with English abstract)

No. 240

KISHI, K. : Study on the water balance of ground-water reservoir in the Tetori river fan, Ishikawa Prefecture, 1971 (in Japanese with English abstract)

No. 241

ONOE, T. : A Pleistocene flora from Ebino City, Miyazaki Prefecture, Japan, 1971 (in Japanese with English abstract)

No. 242

TANAKA, K. : Trace fossils from the Cretaceous flysch of the Ikushumbetsu area, Hokkaido, Japan, 1971 (in English)

No. 243

KAWADA, K. : Geology and petrology of the Nōhi rhyolites, with special reference to those along the Hida river, 1971 (in English)

Mechanical Properties of Japanese Tertiary Sedimentary Rocks under High Confining Pressures

Kazuo HOSHINO, Hitoshi KOIDE, Kazuo INAMI,
Shigeo IWAMURA & Shinobu MITSUI

Report, Geological Survey of Japan, no. 244, p. 1～200, 1972
334 illus., 23pl., 4 tab.

One hundred Tertiary sedimentary rocks in Japan were experimentally deformed under confining pressures (up to 2,500kg/cm^2)at room temperature in a strain rate of 10^{-4} to 10^{-6}/sec. The results of experiments are summarized in tables, stress-strain curves and Mohr's diagrams. The authors discuss relations among strength, confining pressure, deformational behavior, angle of fracture, strain at fracturing, failure type, porosity, grain size, axial shortening, sampled depth, wave velocity, geological age, stratigraphic level and tectonic environment. The Tertiary sedimentary rocks are compacted with geologic age and depth, although the degree of compaction is different in sedimentary basins.

552.5 : 551.78 : 53(52)

昭和 47 年 3 月 8 日　印　刷
昭和 47 年 3 月 13 日　発　行

工業技術院地質調査所

印刷者　小林銀二
印刷所　泰成印刷株式会社
東京都墨田区両国 3 — 1 —12

地 質 調 報
Rept. Geol. Surv. J.
No. 244, 1972